

NEW APPROACHES FOR THE STUDY AND TREATMENT OF AGGRESSIVE CANCERS

Emma Polonio Alcalá

ADVERTIMENT. L'accés als continguts d'aquesta tesi doctoral i la seva utilització ha de respectar els drets de la persona autora. Pot ser utilitzada per a consulta o estudi personal, així com en activitats o materials d'investigació i docència en els termes establerts a l'art. 32 del Text Refós de la Llei de Propietat Intel·lectual (RDL 1/1996). Per altres utilitzacions es requereix l'autorització prèvia i expressa de la persona autora. En qualsevol cas, en la utilització dels seus continguts caldrà indicar de forma clara el nom i cognoms de la persona autora i el títol de la tesi doctoral. No s'autoritza la seva reproducció o altres formes d'explotació efectuades amb finalitats de lucre ni la seva comunicació pública des d'un lloc aliè al servei TDX. Tampoc s'autoritza la presentació del seu contingut en una finestra o marc aliè a TDX (framing). Aquesta reserva de drets afecta tant als continguts de la tesi com als seus resums i índexs.

ADVERTENCIA. El acceso a los contenidos de esta tesis doctoral y su utilización debe respetar los derechos de la persona autora. Puede ser utilizada para consulta o estudio personal, así como en actividades o materiales de investigación y docencia en los términos establecidos en el art. 32 del Texto Refundido de la Ley de Propiedad Intelectual (RDL 1/1996). Para otros usos se requiere la autorización previa y expresa de la persona autora. En cualquier caso, en la utilización de sus contenidos se deberá indicar de forma clara el nombre y apellidos de la persona autora y el título de la tesis doctoral. No se autoriza su reproducción u otras formas de explotación efectuadas con fines lucrativos ni su comunicación pública desde un sitio ajeno al servicio TDR. Tampoco se autoriza la presentación de su contenido en una ventana o marco ajeno a TDR (framing). Esta reserva de derechos afecta tanto al contenido de la tesis como a sus resúmenes e índices.

WARNING. Access to the contents of this doctoral thesis and its use must respect the rights of the author. It can be used for reference or private study, as well as research and learning activities or materials in the terms established by the 32nd article of the Spanish Consolidated Copyright Act (RDL 1/1996). Express and previous authorization of the author is required for any other uses. In any case, when using its content, full name of the author and title of the thesis must be clearly indicated. Reproduction or other forms of for profit use or public communication from outside TDX service is not allowed. Presentation of its content in a window or frame external to TDX (framing) is not authorized either. These rights affect both the content of the thesis and its abstracts and indexes.



DOCTORAL THESIS

**NEW APPROACHES FOR THE STUDY AND
TREATMENT OF AGGRESSIVE CANCERS**

Emma Polonio Alcalá

2023





DOCTORAL THESIS

**NEW APPROACHES FOR THE STUDY AND
TREATMENT OF AGGRESSIVE CANCERS**

Emma Polonio Alcalá

2023



DOCTORAL THESIS

NEW APPROACHES FOR THE STUDY AND TREATMENT OF AGGRESSIVE CANCERS

Emma Polonio Alcalá

2023

Doctoral Program in Molecular Biology, Biomedicine and Health

Advised by Dr. Joaquim de Ciurana Gay and Dr. Teresa Puig Miquel

Thesis submitted in fulfillment of the requirement to obtain the doctoral
degree from the University of Girona



Dr. Joaquim de Ciurana Gay, Full Professor at the Department of Mechanical Engineering and Industrial Construction of the University of Girona, and Dr. Teresa Puig Miquel, Full Professor at the Department of Medical Sciences of the University of Girona,

CERTIFY:

That the thesis entitled *New Approaches for the Study and Treatment of Aggressive Cancers*, presented by Emma Polonio Alcalá to obtain a doctoral degree has been completed under our supervision.

For all intents and purposes, we hereby sign this document.

Dr. Joaquim de Ciurana Gay

Dr. Teresa Puig Miquel

“I am among those who think that science has great beauty.”

– Marie Curie

Acknowledgements

Abans de finalitzar aquesta etapa de la meua vida, no puc evitar mirar enrere, veure tot el camí recorregut i sentir-me afortunada i agraïda.

En primer lloc, m'agradaria donar les gràcies als meus directors. Teresa i Quim, gràcies per l'oportunitat de realitzar la tesi sota la vostra supervisió, pels consells que m'heu donant al llarg d'aquests anys, tant a nivell professional com personal, i sobretot, per la confiança cap a mi. Amb vosaltres, he sentit la llibertat de fer tots els experiments que volgut i de portar a terme totes les idees pensades. He après moltíssim. Teresa, gràcies per donar-me la oportunitat i obrir-me les portes del laboratori. Mai hagués pensat que aquell correu electrònic demanant si podia realitzar el TFG m'hauria portat a aquest moment sis anys després, amb un TFG, TFM i una tesi doctoral fets a TargetsLab. Amb tu, les bromes i els riures sempre estan assegurats. Quim, gràcies per obrir-me les portes del taller. Tal i com et va dir en Marc, has sigut un "pare científic": ens aconselles i ens dius aquelles coses que no volem escoltar, però que son tant necessàries. Mil gràcies per tot.

També m'agradaria donar-li les gràcies als post-docs que hi va haver al grup, Santi i Sònia. Vaig aprendre moltíssim de vosaltres, a nivell científic. Gràcies per la paciència, per escoltar-me i aconsellar-me sobre els experiments i els seus *intrínquilis*. Sònia, gràcies també per tot el viscut juntes. Ets una persona excepcional. Gràcies per escoltar-me quan més ho he necessitat i per donar-me tants i tants de consells. Has estat la meua germana gran del lab. Totes les coses bones que et passin, son poques.

Irene, la meua estimada Irene. La meua novia del lab. Conèixer-te ha sigut una de les coses per les quals ha valgut la pena fer el doctorat. Tot i passar juntes 12 hores al dia, no eren suficients, sempre hi havia alguna cosa més a parlar. Gràcies per la teua sinceritat, honestedat, humilitat, autenticitat, per ser la millor amiga que es pot tenir, per cuidar-me, per escoltar-me, per oferir el teu pis com a camp base de Girona, pels riures, les bromes, les penes, els vermutos, els sopars, les festes, els cafès, les infusions, els caramels, les fotos d'imprevist, els *stickers*,... En definitiva, gràcies per tot el viscut, que no ha sigut poc, però que mai és suficient. La vida al teu costat és molt millor. Sé que la nostra amistat serà per tota la vida, i que sempre ens tindrem una a l'altra. T'estimo molt.

Marc, mi *bebido*. Gràcies per tant... Tot va començar amb tu essent el meu germà gran del món dels *scaffolds* i el 3D, i va continuar amb les tardes de *kit-kat*, les sessions de karaoke a cultius, els riures, les bromes, els vermutos i els *bailoteos*. Gràcies per ser tant bon company i tant bon amic, per escoltar-me, per donar-me tants de consells, per introduir-me al vocabulari LGTBIQ+ i a *Only Masc*. Et trobo molt a faltar amic, però encara ens queden mil aventures i viatges junts. PD: en unes altres condicions, jo t'hagués dit que sí!

Anna, ets el meu gran descobriment. Tant de bo haguéssim compartit espai i més temps juntes. Ets una persona tan bona, meravellosa, pura i amorosa. El món és un lloc millor gràcies a que hi ha persones com tu en ell. Gràcies per tot. Pels vermutos, sopars, Canet Rocks, Londres... Que sàpigues que tenir una amiga com tu al costat, no té preu. Vals or. Espero viure molts més moments juntes.

Enric, mi *partner in the crime*. Estic agraïda de que apareguessis pel laboratori en el moment que més necessitava un xute d'energia. I de que diguessis que sí a les idees que se'm van passar pel cap, i que va resultar dos anys després en un article molt maco. Gràcies per la teva positivitat i alegria. I sobretot, pel *salseo* i *contenido* aportat durant aquests anys!

Tess, la incorporació més recent a *Targets*. Gràcies per escoltar els meus drames i aportar una visió completament diferents de les coses. Sempre em fas reflexionar. I també gràcies pel viscut juntes (vermutos, sopars, festes, excursions,...). I pel *salseo*, que tal i com fas amb els teus *tuppers*, has aportat sal extra.

Maria, tot i que la nostra experiència juntes serà fugaç, m'ha agradat molt conèixer-te i espero que seguim tenint contacte. Tant de bo haguessis nascut realment a l'any que et tocava (és a dir, el 1994), i haguéssim pogut fer la tesi juntes, amb les nostres vides paral·leles. Et desitjo molta sort en els teus futurs projectes i tot el millor.

També voldria agrair a la resta de persones que han passat per *TargetsLab/GREP* per la seva ajuda: Anna, Antonio, David, Xavier, Andreu, Maria del Mar, les Paules, Ander, Sabina, Nil, Adrià, Andrea, Lúcia, Pere, Marta, Aniol, etc.

També m'agradaria donar-li les gràcies a la Dra. Rut Porta. Gràcies per ensenyar-me la part de pacients i treballar-la juntes. He après molt.

I sortint de Girona i del laboratori i aterrant al meu estimat Alt Empordà, també volia agrair a la gent de Castelló (Estefania, Clara, Cristina, Núria, Sandra, Mireia, Maria, Beth, Aleix, Montero, Costa, Mancilla, Simon, etc.), als amics de sempre, amb la gent que he crescut, i als que sempre vaig a buscar quan vull tornar a la meva zona de confort i evadir-me de tot, que sempre hi son per rebre'm. En especial, volia donar les gràcies a l'Estefania. Gràcies per recolzar-me i estar sempre al meu costat, de forma incondicional. Ets una amiga excepcional i et mereixes el millor. Moltes gràcies. T'estimo mil.

Corall, *mi pelirroja favorita*. Gràcies per escoltar els meus drames de la tesi i de la carrera professional, per trobar els nostres moments per esmorzar, caminar per Canyelles i l'Almadrava, els berenars a la Cairó, els estius a la platja i els Carnivals. Andrea, la nostra història també va començar a la Universitat de Girona, i casi una dècada després continuem trobant els moments per fer el cafè i posar-nos al dia. Us estimo mil.

I finalment, però no menys important, a la meva família i a la meva parella, els que realment m'han aguantat el cansament, mal humor i cares llargues tots aquests anys. Mama, gracias por cuidarme, por escuchar mis dramas de tesis, y por darme toques de atención cuando trabajaba más de la cuenta. Sandra, mi hermana mayor, gracias por escucharme y aconsejarme, y por los partidos de pádel, a los que siempre llego tarde. Os quiero mucho. Als meus sogres, Fina i Vicenç, per tractar-me com una més de la vostra família, i per cuidar-me sempre com una filla. I finalment a tu amor, el meu estimat Adrià. Ens vam conèixer al principi d'aquest camí i l'he acabat al teu costat. Gràcies per estimar-me tant i tant bé, per escoltar-me sempre i aconsellar-me quan ho he necessitat, i per cuidar-me quan la tesi m'ha demandat més. Gràcies per la confiança, el respecte i la complicitat. Ets únic amor. Estic impacient per les pròximes aventures que viurem junts. T'estimo infinit.

Funding and Technical Support

This work has been supported by grants from Fundació Ramón Areces (X3_0700_E32_14_07_01), Instituto de Salud Carlos III and co-funded by European Union (ERDF/ESF, “A way to make Europe”/“Investing in your future”) (PI14/00329; PI19/00372), Ministerio de Economía y Competividad (DPI2016-77156-R), Universitat de Girona (MPCUdG2016/036), AstraZeneca (NCR-18-13804), and the Catalanian Government (2017SGR00385), Secretaria d'Universitats i Recerca de la Generalitat de Catalunya, and the European Social Fund. Financial support was also provided by Fundació Oncolliga and RadikalSwim (OncoSwim).

The author was the beneficiary of a pre-doctoral grant from the Catalanian Government (2019FI_B01011).

The author thanks TechnoSperm and Research Technical Services (University of Girona) for their technical support; R. Rosell and M. A. Molina from laboratory of Pangaea Oncology (Barcelona, Spain) for kindly provided PC9 models; AstraZeneca (London, UK) for supplying gefitinib and osimertinib; Maria Buxó for their statistical analysis support of patients' samples; Maria López and the Clinical Trial Unit of Catalan Institute of Oncology for the help provided in the identification of patients treated with EGFR-TKI; and Glòria Oliveres for the help provided in samples identification and management. The author wants to particularly acknowledge the patients and the IDIBGI Biobank for their collaboration.



Publications Resulted from This Thesis

This thesis is presented as a compendium of manuscripts. Papers published during PhD enrolment are represented in the following publications.

Title	Screening of Additive Manufactured Scaffolds Designs for Triple Negative Breast Cancer 3D Cell Culture and Stem-Like Expansion
Authors	Emma Polonio-Alcalá, Marc Rabionet, Antonio J. Guerra, Marc Yeste, Joaquim Ciurana*, and Teresa Puig*
Journal	International Journal of Molecular Sciences
Publication Year	2018
Impact Factor 2018	4.183 (Q2 in Biochemistry & Molecular Biology; Position 78 of 299)
DOI	10.3390/ijms19103148
Title	PLA Electrospun Scaffolds for Three-Dimensional Triple-Negative Breast Cancer Cell Culture
Authors	Emma Polonio-Alcalá†, Marc Rabionet†, Xavier Gallardo, David Angelats, Joaquim Ciurana, Santiago Ruiz-Martínez*, and Teresa Puig*
Journal	Polymers
Publication Year	2019
Impact Factor 2019	3.426 (Q1 in Polymer Science; Position 16 of 89)
DOI	10.3390/polym11050916
Title	Fatty Acid Synthase Inhibitor G28 Shows Anticancer Activity in EGFR Tyrosine Kinase Inhibitor Resistant Lung Adenocarcinoma Models
Authors	Emma Polonio-Alcalá†, Sònia Palomerast†, Daniel Torres-Oteros, Joana Relat, Marta Planas, Lidia Feliu, Joaquim Ciurana, Santiago Ruiz-Martínez*, and Teresa Puig*
Journal	Cancers
Publication Year	2020
Impact Factor 2020	6.639 (Q1 in Oncology; Position 51 of 242)

Title Polycaprolactone Electrospun Scaffolds Produce an Enrichment of Lung Cancer Stem Cells in Sensitive and Resistant EGFRm Lung Adenocarcinoma

Authors Emma Polonio-Alcalá, Marc Rabionet, Santiago Ruiz-Martínez, Sònia Palomeras, Rut Porta, Carmen Vásquez-Dongo, Joaquim Bosch-Barrera, Teresa Puig*, and Joaquim Ciurana*

Journal Cancers

Publication Year 2021

Impact Factor ²⁰²¹ 6.575 (Q1 in Oncology; Position 60 of 245)

DOI 10.3390/cancers13215320

Title AZ12756122, a Novel Fatty Acid Synthase Inhibitor, Decreases Resistance Features in EGFR-TKI Resistant EGFR mutated NSCLC Cell Models

Authors Emma Polonio-Alcalá, Rut Porta, Santiago Ruiz-Martínez, Carmen Vásquez-Dongo, Joana Relat, Joaquim Bosch-Barrera, Joaquim Ciurana*, and Teresa Puig*

Journal Biomedicine & Pharmacotherapy

Publication Year 2022

Impact Factor ²⁰²¹ 7.419 (Q1 in Pharmacology & Pharmacy; Position 26 of 279)

DOI 10.1016/j.biopha.2022.113942

* Corresponding author

† These authors contributed equally to this manuscript

Additional unrelated studies performed during PhD enrolment will not be presented in this thesis and are represented in the following publications.

Title Three-dimensional manufactured supports for breast cancer stem cell population characterization

Authors Emma Polonio-Alcalá†, Marc Rabionet†, Santiago Ruiz-Martínez, Joaquim Ciurana*, and Teresa Puig*

Journal Current Drug Targets

Publication Year 2019

Impact Factor ²⁰¹⁹ 2.632 (Q3 in Pharmacology & Pharmacy; Position 145 of 271)

DOI 10.2174/1389450120666181122113300

Title Fatty acid synthase as a novel biomarker for triple negative breast cancer stem cell subpopulation cultured on electrospun scaffolds

Authors Marc Rabionet, Emma Polonio-Alcalá, Joana Relat, Marc Yeste, Jennifer Sims-Mourtada, April M. Kloxin, Marta Planas, Lidia Feliu, Joaquim Ciurana*, Teresa Puig*

Journal Materials Today Bio

Publication Year 2021

Impact Factor ²⁰²¹ 10.761 (Q1 in Biomedical Engineering; Position 11 of 98)

DOI 10.1016/j.mtbio.2021.100155

Title ABTL0812 enhances antitumor effect of paclitaxel and reverts chemoresistance in triple-negative breast cancer models

Authors Emma Polonio-Alcalá, Sònia Solé-Sánchez, Pau Muñoz-Guardiola, Elisabet Megías-Roda, Héctor Perez-Montoyo, Marc Yeste-Velasco, Jose Alfón, Jose Miguel Lizcano, Carles Domènech, Santiago Ruiz-Martínez*, Teresa Puig*

Journal Cancer Communications

Publication Year 2022

Impact Factor ²⁰²¹ 15.283 (Q1 in Oncology; Position 16 of 245)

DOI 10.1002/cac2.12282

Title	The solvent chosen for the manufacturing of electrospun polycaprolactone scaffolds influences cell behavior of lung cancer cells
Authors	Emma Polonio-Alcalá†, Enric Casanova-Batlle†, Teresa Puig*, Joaquim Ciurana*
Journal	Scientific Reports
Publication Year	2022
Impact Factor <small>2021</small>	4.997 (Q2 in Multidisciplinary Sciences; Position 19 of 74)
DOI	10.1038/s41598-022-23655-2

* Corresponding author

† These authors contributed equally to this manuscript

Abbreviations

#

2D, Two-Dimensional

3D, Three-Dimensional

3R, Replacement, Reduction, and Refinement

A

ACACA, Acetyl-CoA Carboxylase

ACP, Acyl-Carrier Protein

ACYL, ATP-Citrate Lyase

AKT, Protein Kinase B

ALDH, Aldehyde Dehydrogenase

AM, Additive Manufacturing

ATP, Adenosine Triphosphate

B

BCSC, Breast Cancer Stem Cell

C

C797, Cysteine at position 797

C797S, Substitution of Cysteine for Serine at position 797

CAD, Computer-Aided Design

CAR-T, Chimeric Antigen Receptor T Cell

CD, Cluster of Differentiation

ChREBP, Carbohydrate-Activated Transcription Factor Response Element Binding Protein

CK5/6, Cytokeratins 5/6

CLSM, Confocal Laser Scanning Microscope

CSC, Cancer Stem Cell

D

DH, β -Hydroxyacyl Dehydratase

DMA, Dynamic Mechanical Analysis

DSC, Differential Scanning Calorimetry

E

ECM, Extracellular Matrix'

EGCG, (-)-Epigallocatechin-3-Gallate

EGFR, Epidermal Growth Factor Receptor

EGFRins20, Insertion in Eexon 20 of *EGFR*

EGFRm, EGFR-Mutated

ER, Enoyl Reductase

ERe, Estrogen Receptor

ES, Electrospinning

EMT, Epithelial-to-Mesenchymal

Ex19Del, Deletion in Exon 19 of *EGFR*

F

FASN, Fatty Acid Synthase

FDA, Food and Drug Administration

FFF, Fused Filament Fabrication (FFF)

G

Gli, Glioma-Associated Oncogene

GPI, Glycosyl-Phosphatidyl-Inositol

H

HER2, Human Epidermal Growth Factor Receptor - 2

Hh, Hedgehog

HMG, High-Mobility Group

HR, Hormone Receptors

I

IHC, Immunohistochemistry

J

JAK, Janus Kinase

K

KR, β -Ketoacyl Reductase

KS, β -Ketoacyl Synthase

KFDA, Korea Food and Drug Administration

L

L858R, Missense Mutation in Exon 21 of *EGFR*

M

MAPK, Mitogen Activated Protein Kinase

MAT, Malonyl/Acetyl Transferase

MEK, MAPK/ERK Kinase

MET, Mesenchymal-to-Epithelial Transition

MFI, Mammosphere Formation Index

mPEG, Methoxypolyethylene Glycol

mTOR, Mammalian Target of Rapamycin

N

NADPH, Nicotinamide Adenine Dinucleotide Phosphate Hydrogen

NF- κ B, Ubiquitous Nuclear Transcription Factor κ B

NMPA, China National Medical Products Administration

NSCLC, Non-Small Cell Lung Cancer

O

Oct3/4, Octamer-Binding Transcription Factor β

ORR, Objective Response Rate

OS, Overall Survival

P

PARP, Poly (ADP-Ribose) Polymerase

PBLG, Poly(γ -Benzyl L-Glutamate)

PCL, Polycaprolactone

PCP, Planar Cell Polarity

PD-L1, Programmed Cell Death-Ligand 1

PFS, Progression-Free Survival

PI3K, Phosphoinositide 3-Kinase

PLA, Poly(Lactic Acid)

PLGA, Poly(Lactic-Co-Glycolic Acid)

PR, Progesterone Receptor

PTCH, Patched

R

RAS, Rat Sarcoma

S

SCLC, Small Cell Lung Cancer

SCC, Squamous Cell Lung Carcinoma

SEM, Scanning Electron Microscopy

Shh, Sonic Hedgehog

Smo, Smoothened

SOX, SRY-HMG-box

SRY, Sex-Determining Region on the Y Chromosome

SREBP-1c, Sterol Regulatory Element Binding Protein-1c

STAT, Activation of Signal Transducer and Activator of Transcription

STAT3, Activation of Signal Transducer and Activator of Transcription 3

T

T90M, Substitution of Methionine for Threonine at Position 790

TCA, Tricarboxylic Acid

TE, Thioesterase

T_g , Glass Transition Temperature

TGA, Thermogravimetric Analysis

TIPS, Thermally Induced Phase Separation

TK, Tyrosine Kinase

TKI, TK Inhibitor

T_m , Melting Temperature

TNBC, Triple Negative Breast Cancer

V

VEGF, Vascular Endothelial Growth Factor

W

WHO, World Health Organization

Index

Acknowledgements	i
Publications Resulted from This Thesis	vii
Abbreviations	xiii
Index	xxi
Index of Figures and Tables	xxv
Summary	1
Introduction	15
1. Cancer.....	17
2. Lung Cancer	19
2.1. Lung Cancer Classification	20
2.1.1 Histological Classification of Lung Cancer	20
2.1.2. TNM Classification of Lung Cancer	21
2.1.3. ECOG Performance Status Scale	23
2.2. EGFR-mutated NSCLC	24
2.2.1. Epidermal Growth Factor Receptor	24
2.2.2. <i>EGFR</i> Mutations	25
2.2.3. EGFR Tyrosine Kinase Inhibitors.....	26
2.2.4. Resistance Mechanisms to EGFR-TKIs.....	29
2.2.5. Novel Therapies to Overcome Resistance to EGFR-TKIs	31
3. Breast Cancer	32
3.1. Breast Cancer Classification	33
3.2. Triple Negative Breast Cancer: Characteristics, Prognosis, and Treatment	35
4. Cancer Stem Cells	37
4.1. Origin of Cancer Stem Cells.....	38
4.2. Cancer Stem Cells Identification	39
4.2.1. Surface Markers	39
4.2.2. Aldehyde Dehydrogenase (ALDH)	40
4.2.3. Epithelial-to-Mesenchymal Transition (EMT)	40
4.2.4. Stemness Markers	42
4.2.5. Wnt, Notch & Hedgehog.....	43
4.3. Novel Therapies Against Cancer Stem Cells.....	44
5. Three-Dimensional (3D) Cell Culture	45
5.1. Origin and Development of Cell Culture	45

5.2. 3D Cell Culture	46
5.3. Additive Manufacturing Techniques for the Fabrication of a Polymeric Scaffolds	47
5.3.1. Fused Filament Fabrication	47
5.3.2. Electrospinning	49
5.4. Materials Used to Manufacture Scaffolds	50
5.4.1. Polycaprolactone	51
5.4.2. Poly(Lactic Acid)	51
5.5. The Study of Cancer Stem Cell Population Using 3D Cell Culture	53
6. Fatty Acid Synthase	54
6.1. Lipid Metabolism in Cancer	54
6.2. Fatty Acid Synthase Function	55
6.3. Fatty Acid Synthase Regulation	57
6.4. Fatty Acid Synthase Inhibition	58
Hypothesis and Objectives	61
Results I. Evaluation of PLA scaffolds for 3D cell culture of BCSCs	67
Results II. Evaluation of PCL scaffolds manufactured by ES technology for 3D cell culture of LCSCs	105
Results III. Inhibition of FASN as a new therapeutic strategy for the treatment of EGFRm NSCLC	141
Discussion	177
1. Evaluation of poly(lactic acid) (PLA) scaffolds for 3D cell culture of breast CSC (BCSC)	179
2. Evaluation of polycaprolactone (PCL) scaffolds manufactured by ES technology for 3D cell culture of lung CSCs (LCSC)	184
3. Inhibition of FASN as a new therapeutic strategy for the treatment of EGFRm NSCLC.....	189
4. Concluding remarks	194
5. Limitations of the study	196
6. Future perspectives	197
Conclusions	199
References	205

Index of Figures and Tables

Index of Figures

Figure 1.	Hallmarks of cancer. Schematic representation of the ten hallmarks of cancer and the four enabling characteristics	18
Figure 2.	Epidermal growth factor receptor (EGFR) and its downstream signaling pathways	24
Figure 3.	Mutations in the <i>EGFR</i> gene.....	26
Figure 4.	Timeline of approval of EGFR-TKIs in EGFR-mutated NSCLC.....	27
Figure 5.	Clinical classification of breast cancer.....	34
Figure 6.	Diagram of the differential features of CSCs that allow their identification	40
Figure 7.	Schematic representation about the role of epithelial-to-mesenchymal transition (EMT) and mesenchymal-to-epithelial transition (MET) in metastasis	41
Figure 8.	Schematic representation of fused filament fabrication (FFF) process	48
Figure 9.	Schematic representation of a typical electrospinning (ES) machine	49
Figure 10.	Linear structure of fatty acid synthase (FASN) domains	55
Figure 11.	Role of each domain of fatty acid synthase (FASN) during the synthesis of fatty acids	56

Index of Tables

Table 1. Categories and descriptors of T, N, and M components.....	22
Table 2. Stage Groups of Lung Cancer.	23
Table 3. ECOG Performance Status Scale.	23
Table 4. Different characteristics of polycaprolactone (PCL) and poly(lactic acid) (PLA)..	52

Summary

Resum

Les cèl·lules mare del càncer (*cancer stem cell*, CSC) són una petita població que forma part del tumor i que es caracteritza per les seves capacitats d'autorenovació, pluripotència i resistència a les teràpies anticàncer. A més, aquest subgrup de cèl·lules és responsable de l'inici, recurrència, progressió i metàstasis del tumor. Per tant, es requereix l'eliminació de les CSCs per aconseguir un tractament efectiu contra el càncer.

El càncer de mama triple negatiu (*triple negative breast cancer*, TNBC) no disposa d'una diana terapèutica, de forma que l'únic tractament disponible és la quimioteràpia. Tot i que hi ha una bona resposta al tractament, la taxa de recurrència és d'aproximadament el 30%. A més, aquest subtipus de càncer de mama és molt agressiu i presenta un mal pronòstic. D'altra banda, el càncer de pulmó de cèl·lula no petita (*non-small cell lung cancer*, NSCLC) representa al voltant del 85% de tots els casos de càncer de pulmó. Tot i que la identificació de les mutacions en el receptor del factor de creixement epidèrmic (*epidermal growth factor receptor*, EGFR) va permetre el desenvolupament dels inhibidors de tirosina quinasa d'EGFR (*EGFR tyrosine kinase inhibitors*, EGFR-TKIs), la majoria de pacients desenvolupa resistència a aquesta teràpia. Així mateix, els pacients amb NSCLC solen ser diagnosticats en un estat avançat de la malaltia, quan el tractament ja no és eficaç. Per tant, les CSCs són una potencial diana terapèutica pel TNBC i el NSCLC amb *EGFR* mutat (*EGFR-mutated NSCLC*, EGFRm NSCLC). Desafortunadament, no existeix una teràpia disponible aprovada per les agències estatals contra aquesta població maligna.

Adicionalment, l'estudi de les CSCs es troba limitat a causa de la seva baixa representació dintre dels tumors o línies cel·lulars. A més, el cultiu cel·lular en dues dimensions (2D) modifica el comportament de les cèl·lules i la seva expressió gènica i/o proteica, que resulta en la inducció de la diferenciació de les CSCs, convertint-les en cèl·lules normals de càncer. Llavors, es requereixen nous sistemes de cultiu cel·lular que permetin l'estudi d'aquesta població maligna, de manera que els investigadors puguin trobar noves teràpies contra les CSCs. Amb aquest propòsit, s'han desenvolupat diferents sistemes de cultiu cel·lular en tres dimensions (3D). Un dels sistemes de cultiu cel·lular 3D que existeix són les estructures polimèriques fabricades per diferents tècniques, destacant la fabricació per filament fos (*fused filament fabrication*, FFF) i l'electrofilat (*electrospinning*, ES).

Per tant, el primer objectiu d'aquesta tesi va ser avaluar l'àcid polilàctic (*poly(lactic acid)*, PLA) com a material per a la fabricació de suports 3D mitjançant FFF i ES. Els *scaffolds* ("bastides", traduït directament) resultants van ser testats com a sistema de cultiu cel·lular 3D per a l'expansió de les CSCs de mama (*breast cancer stem cell*, BCSC), sembrant la línia cel·lular de TNBC MDA-MB-231. Referent als PLA-FFF *scaffolds*, es va realitzar un cribratge de diferents paràmetres de fabricació de l'aparell de FFF que va permetre la creació d'un *scaffold* anomenat SS1. El SS1 presentava la proliferació cel·lular més gran aconseguida amb aquest tipus de suports 3D, aproximadament un 24% en comparació al 2D, i també, un augment significatiu de la població ALDH+, relacionada amb les BCSCs en comparació al 2D en temps curts de cultiu. Referent als PLA-ES *scaffolds*, les cèl·lules MDA-MB-231 sembrades en aquests suports presentaven una proliferació cel·lular molt elevada, d'aproximadament un 70% en comparació al 2D. No obstant això, en tots els marcadors de BCSCs analitzats, només augmentava l'expressió gènica de *SOX2* després de 3 dies de cultiu. En definitiva, el cultiu cel·lular mitjançant els *scaffolds* de PLA no mostrava un enriquiment significatiu de les BCSCs.

Estudis anteriors van demostrar que les cèl·lules MDA-MB-231 sembrades en els ES *scaffolds* de policaprolactona (PCL), un altre material polimèric, augmentaven significament la seva població de BCSCs. Així doncs, el segon objectiu d'aquesta tesi va ser l'avaluació dels PCL-ES *scaffolds* com a sistema de cultiu cel·lular 3D per a l'expansió de les CSC de pulmó (*lung cancer stem cells*, LCSC) utilitzant models cel·lulars sensibles i resistents amb EGFRm NSCLC, les PC9 i les PC9-GR3. La microarquitectura dels PCL-ES *scaffolds* va permetre una adhesió i proliferació cel·lular adequades i una major elongació cel·lular. Així mateix, les cèl·lules PC9 i PC9-GR3 sembrades en els PCL-ES *scaffolds* van mostrar un increment significatiu de múltiples marcadors de LCSCs, com una major resistència als EGFR-TKIs i un augment de l'expressió de gens i proteïnes relacionades amb el procés d'EMT, *stemness*, marcadors de superfície i l'activació de la via de senyalització de Hedgehog. A més, es va analitzar l'expressió tumoral de dos marcadors de LCSCs, CD133 i vimentina, en mostres provinents de biòpsies de pacients i els resultats obtinguts van validar la utilització dels PCL-ES *scaffolds* com a plataforma 3D. D'aquesta manera, les cèl·lules es comporten de forma més fisiològica

i, per tant, els resultats assolits utilitzant aquestes estructures 3D, sigui provant un nou fàrmac o descobrint nous biomarcadors, seran més fiables.

A més de tot això, la sintasa d'àcids grassos (*fatty acid synthase*, FASN) és un enzim fonamental en la lipogènesis *de novo*, i les cèl·lules canceroses el solen sobreexpressar i/o sobreactivar com a mecanisme de resistència a les teràpies anticàncer. Recentment, FASN ha sigut descrita com a mecanisme essencial per a la supervivència de les cèl·lules amb EGFRm NSCLC resistents als EGFR-TKIs. Així mateix, la sobreexpressió d'aquest enzim s'ha relacionat amb les CSCs. Per tant, el tercer objectiu d'aquesta tesi va ser l'avaluació de la inhibició de FASN com a estratègia terapèutica pel tractament de cèl·lules sensibles i resistents amb EGFRm NSCLC i per l'eliminació de les LCSCs. El tractament amb els inhibidors de FASN (EGCG, G28 i AZ12756122) va produir un efecte citotòxic similar en tots els models cel·lulars, independentment de la seva resistència als EGFR-TKIs. No obstant això, només el G28 i l'AZ12756122 inhibia l'activitat de l'enzim, de manera que els efectes citotòxics del EGCG eren independents a la inhibició de FASN. Així mateix, la combinació del G28 o l'AZ12756122 amb els EGFR-TKIs en cèl·lules resistents va resultar en una interacció sinèrgica, superant la resistència als EGFR-TKIs, i inhibint la via de senyalització EGFR/AKT/mTOR. Finalment, la inhibició de l'enzim va provocar la reducció de les LCSCs. Curiosament, els resultats obtinguts *in vitro* i derivats de l'expressió tumoral de FASN en pacients van revelar que els tumors amb NSCLC i mutacions sensibilitzadores d'*EGFR* i amb expressió de FASN van mostrar una millor resposta als EGFR-TKI de primera generació, com el gefitinib.

En resum, aquesta investigació demostra que els PCL-ES *scaffolds* són un òptim sistema de cultiu cel·lular que permet l'expansió de les LCSCs, i consegüentment, facilita el seu estudi *in vitro*, per així poder trobar noves teràpies dirigides contra aquesta població. En paral·lel, també s'ha provat que la inhibició de FASN és una teràpia prometedora pels tumors sensibles i resistents amb EGFRm NSCLC, així com per a l'eliminació de les LCSCs. A més, la combinació de la inhibició de FASN i EGFR sembla ser una interessant estratègia terapèutica per superar la resistència als EGFR-TKIs.

Resumen

Las células madre del cáncer (*cancer stem cell*, CSC) son una pequeña población que forma parte del tumor y que se caracteriza por sus capacidades de autorrenovación, pluripotencia y resistencia a las terapias anticáncer. Además, este subgrupo de células es responsable del inicio, recurrencia, progresión y metástasis del tumor. Por lo tanto, se requiere de la eliminación de las CSCs para conseguir un tratamiento efectivo contra el cáncer.

El cáncer de mama triple negativo (*triple negative breast cancer*, TNBC) no dispone de una diana terapéutica, de forma que el único tratamiento disponible es la quimioterapia. Aunque hay una buena respuesta al tratamiento, la tasa de recurrencia es de aproximadamente el 30%. Además, este subtipo de cáncer de mama es muy agresivo y presenta un mal pronóstico. Por otro lado, el cáncer de pulmón de célula no pequeña (*non-small cell lung cancer*, NSCLC) representa alrededor del 85% de todos los casos de cáncer de pulmón. A pesar de que la identificación de las mutaciones en el receptor del factor de crecimiento epidérmico (*epidermal growth factor receptor*, EGFR) permitió el desarrollo de los inhibidores de tirosina quinasa de EGFR (*EGFR tyrosine kinase inhibitors*, EGFR-TKIs), la mayoría de pacientes desarrollan resistencia a esta terapia. Asimismo, los pacientes con NSCLC suelen ser diagnosticados en un estado avanzado de la enfermedad, cuando el tratamiento ya no es eficaz. Por lo tanto, las CSCs son una potencial diana terapéutica para el TNBC y el NSCLC con *EGFR* mutado (*EGFR-mutated NSCLC*, EGFRm NSCLC). Desafortunadamente, no existe una terapia disponible aprobada por las agencias estatales contra esta población maligna.

Adicionalmente, el estudio de las CSCs se encuentra limitado debido a su baja representación dentro de los tumores o líneas celulares. Además, el cultivo celular en dos dimensiones (2D) modifica el comportamiento de las células y su expresión génica y/o proteica, que resulta en la inducción de la diferenciación de las CSCs, convirtiéndolas en células normales de cáncer. Entonces, se requieren nuevos sistemas de cultivo celular que permitan el estudio de esta población maligna, de manera que los investigadores pueden encontrar nuevas terapias contra las CSCs. Con este propósito, se han desarrollado diferentes sistemas de cultivo celular en tres dimensiones (3D). Uno de los sistemas de cultivo 3D que existe son las estructuras poliméricas fabricadas por distintas técnicas,

destacando la fabricación por filamento fundido (*fused filament fabrication*, FFF) y el electrohilado (*electrospinning*, ES).

Por tanto, el primer objetivo de esta tesis fue evaluar el ácido poliláctico (*poly(lactic acid)*, PLA) como material para la fabricación de soportes 3D mediante FFF y ES. Los *scaffolds* (“andamios”, traducido directamente) resultantes fueron testados como sistema de cultivo celular 3D para la expansión de las CSCs de mama (*breast cancer stem cell*, BCSC), sembrando la línea celular de TNBC MDA-MB-231. En referencia a los PLA-FFF *scaffolds*, se realizó un cribado de diferentes parámetros de fabricación del aparato de FFF, que permitió la creación de un *scaffold* llamado SS1. El SS1 presentaba la mayor proliferación celular conseguida con este tipo de soportes 3D, aproximadamente un 24% en comparación al 2D, y también, un aumento significativo de la población ALDH+, relacionada con las BCSCs en comparación al 2D en tiempos cortos de cultivo. En referencia a los PLA-ES *scaffolds*, las células MDA-MB-231 sembradas en estos soportes presentaban una proliferación celular muy elevada, de aproximadamente un 70% en comparación al 2D. No obstante, de todos los marcadores de BCSCs analizados, solamente aumentaba la expresión génica de *SOX2* después de 3 días de cultivo. En definitiva, el cultivo celular mediante los *scaffolds* de PLA no mostraba un enriquecimiento significativo de las BCSCs.

Estudios anteriores demostraron que las células MDA-MB-231 sembradas en los ES *scaffolds* de policaprolactona (PCL), otro material polimérico, aumentaban significativamente su población de BCSCs. Por ende, el segundo objetivo de esta tesis fue la evaluación de los PCL-ES *scaffolds* como sistema de cultivo celular 3D para la expansión de las CSC de pulmón (*lung cancer stem cells*, LCSC) utilizando modelos celulares sensibles y resistentes de EGFRm NSCLC, las PC9 y las PC9-GR3. La microarquitectura de los PCL-ES *scaffolds* permitía una adhesión y proliferación celular adecuadas y una mayor elongación celular. Asimismo, las células PC9 y PC9-GR3 sembradas en los PCL-ES *scaffolds* mostraron un incremento significativo de múltiples marcadores de LCSCs, como una mayor resistencia a los EGFR-TKIs y un aumento de la expresión de genes y proteínas relacionadas con el proceso de EMT, *stemness*, marcadores de superficie y la activación de la vía de señalización de Hedgehog. Además, se analizó la expresión tumoral de dos marcadores de LCSCs, CD133 y vimentina, en muestras provenientes de biopsias de pacientes y los resultados obtenidos validaron la

utilización de los PCL-ES *scaffolds* como plataforma 3D. De esta manera, las células se comportan de forma más fisiológica y, por tanto, los resultados obtenidos utilizando estas estructuras 3D, ya sea probando un nuevo medicamento o descubriendo nuevos biomarcadores, serán más fiables.

Además de todo esto, la sintasa de ácidos grasos (*fatty acid synthase*, FASN) es una enzima fundamental en la lipogénesis *de novo*, y las células cancerosas la suelen sobreexpresar y/o sobreactivar como mecanismo de resistencia a las terapias anticáncer. Recientemente, FASN ha sido descrita como mecanismo esencial para la supervivencia de las células de EGFRm NSCLC resistentes a los EGFR-TKIs. Así mismo, la sobreexpresión de esta enzima se ha relacionado con las CSCs. Por lo tanto, el tercer objetivo de esta tesis fue la evaluación de la inhibición de FASN como estrategia terapéutica para el tratamiento de células sensibles y resistentes de EGFRm NSCLC y para la eliminación de las LCSCs. El tratamiento con los inhibidores de FASN (EGCG, G28 y AZ12756122) produjo un efecto citotóxico similar en todos los modelos celulares, independientemente de su resistencia a los EGFR-TKIs. Sin embargo, solamente el G28 y el AZ12756122 inhibía la actividad de la enzima, de manera que los efectos citotóxicos del EGCG eran independientes a la inhibición de FASN. Asimismo, la combinación del G28 o el AZ12756122 con los EGFR-TKIs en células resistentes resultó en una interacción sinérgica, superando la resistencia a los EGFR-TKIs, e inhibiendo la vía de señalización EGFR/AKT/mTOR. Finalmente, la inhibición de la enzima provocó la reducción de las LCSCs. Curiosamente, los resultados obtenidos *in vitro* y derivados de la expresión tumoral de FASN en pacientes revelaron que los tumores NSCLC con mutaciones sensibilizadoras de *EGFR* y con expresión de FASN mostraban una mejor respuesta a los EGFR-TKI de primera generación, como el gefitinib.

En resumen, esta investigación demuestra que los PCL-ES *scaffolds* son un óptimo sistema de cultivo celular que permite la expansión de las LCSCs, y, por consiguiente, facilita su estudio *in vitro*, para así poder encontrar nuevas terapias dirigidas contra esta población. En paralelo, también se ha probado que la inhibición de FASN es una terapia prometedora para los tumores sensibles y resistentes de EGFRm NSCLC, así como para la eliminación de las LCSCs. Además, la combinación de la inhibición de FASN y EGFR parece ser una interesante estrategia terapéutica para superar la resistencia a los EGFR-TKIs.

Summary

Cancer stem cells (CSCs) are a small population that is part of the tumor and is characterized by their features, such as self-renewal, pluripotency, and resistance to anti-cancer therapies. Additionally, this subgroup of cells is responsible for tumor initiation, recurrence, progression, and metastasis. Therefore, the elimination of CSCs is required for effective cancer treatment.

Triple negative breast cancer (TNBC) does not have a therapeutic target; hence, chemotherapy is the only available treatment. Although there is a good response to treatment, the recurrence rate is approximately 30%. Furthermore, it is very aggressive and has a poor prognosis. Non-small cell lung cancer (NSCLC) accounts for around 85% of all lung cancer cases. Although the identification of mutations in the epidermal growth factor receptor (EGFR) allowed the development of EGFR tyrosine kinase inhibitors (EGFR-TKIs), most patients develop resistance to this therapy. Patients with NSCLC are also frequently diagnosed at an advanced stage when treatment is no longer effective. Therefore, CSCs are a potential therapeutic target for TNBC and NSCLC with EGFR-mutated (EGFRm NSCLC). Unfortunately, there are no available therapies approved by state agencies for this malignant population.

In addition, the study of CSCs is limited because of their low representation within tumors or cell lines. Moreover, two-dimensional (2D) cell culture modifies the behavior of the cells and their gene and/or protein expression, which results in the induction of CSCs differentiation, converting them into normal cancer cells. Thus, new cell culture systems are required to study this malignant population to find new therapies against CSCs. Different three-dimensional (3D) cell culture systems have been developed for this purpose. One of the existing 3D culture systems is polymeric structures fabricated by different techniques, notably fused filament fabrication (FFF) and electrospinning (ES).

Therefore, the first objective of this thesis was to evaluate poly(lactic acid) (PLA) as a material for the fabrication of 3D supports by FFF and ES. The resulting scaffolds were tested as a 3D cell culture system for expanding breast CSCs (BCSCs) by seeding the TNBC cell line MDA-MB-231. Regarding the PLA-FFF structures, different manufacturing parameters of the FFF apparatus were screened, which allowed the creation of a scaffold named SS1. SS1

exhibited the highest cell proliferation achieved with this type of 3D support, about 24% compared to 2D-cultured cells, and a significant increase in the ALDH+ population, related to BCSCs compared to 2D at short culture times. Concerning the PLA-ES platforms, MDA-MB-231 cells seeded on these supports showed a very high cell proliferation of approximately 70% compared to 2D-cultured cells. However, of all the BCSCs markers analyzed, only *SOX2* gene expression increased after 3 days of culture. Ultimately, cell culture using PLA scaffolds did not demonstrate significant enrichment of BCSCs.

Previous studies proved that MDA-MB-231 cells cultured on ES scaffolds manufactured using polycaprolactone (PCL), another polymeric material, significantly enriched the BCSC population. Hence, the second objective of this thesis was the evaluation of PCL-ES scaffolds as a 3D cell culture system for lung cancer stem cell (LCSC) expansion using EGFRm NSCLC sensitive and resistant cell models, PC9 and PC9-GR3. The microarchitecture of the PCL-ES scaffolds enabled proper cell adhesion, proliferation, and higher cell elongation. Additionally, PC9 and PC9-GR3 cells seeded on PCL-ES scaffolds showed a significant enhancement of multiple LCSC markers, such as higher resistance to EGFR-TKIs and elevated expression of genes and proteins related to the EMT process, stemness, surface markers, and activation of the Hedgehog signaling pathway. Tumor expression of two LCSC markers, CD133 and vimentin, was also analyzed in samples from patient biopsies, and the results obtained validated the use of PCL-ES scaffolds as a 3D platform. Cells cultured on these 3D supports behave more physiologically; therefore, the results obtained, whether testing a new drug or discovering new biomarkers, will be more reliable.

In addition, fatty acid synthase (FASN) is a key enzyme in *de novo* lipogenesis. Its overexpression and/or hyperactivation are often observed in cancer cells as a mechanism of resistance to anti-cancer therapies. Recently, FASN was described as an essential mechanism for the survival of EGFR-TKI-resistant EGFRm NSCLC cells. The overexpression of this enzyme has also been associated with CSCs. Thus, the third objective of this thesis was the evaluation of FASN inhibition as a therapeutic strategy for the treatment of sensitive and resistant EGFRm NSCLC cells and the removal of LCSCs. Treatment with FASN inhibitors (EGCG, G28, and AZ12756122) produced similar cytotoxic effects in all cell models, regardless of their resistance to EGFR-TKIs. However, only G28 and AZ12756122 inhibited enzyme activity;

hence, the cytotoxic effects of EGCG were independent of FASN inhibition. The combination of G28 or AZ12756122 with EGFR-TKIs in resistant cells resulted in a synergistic interaction, overcoming resistance to EGFR-TKIs, and inhibiting the EGFR/AKT/mTOR signaling pathway. Finally, the inhibition of the enzyme resulted in a reduction in LCSCs. Interestingly, results obtained *in vitro* and derived from FASN tumor expression in patients revealed that NSCLC tumors with EGFR-sensitizing mutations and FASN expression showed a better response to first-generation EGFR-TKIs, such as gefitinib.

In summary, this research demonstrates that PCL-ES scaffolds are an optimal cell culture system that allows the expansion of LCSCs and facilitates their study *in vitro* to find new therapies directed against this population. In parallel, FASN inhibition has also proven to be a promising therapy for sensitive and resistant EGFRm NSCLC tumors as well as for the elimination of LCSCs. Furthermore, the combination of FASN and EGFR inhibition is an interesting therapeutic strategy for overcoming resistance to EGFR-TKIs.

Introduction

1. Cancer

According to the World Health Organization (WHO), cancer is a group of diseases that can originate in any organ or tissue of the body when abnormal cells proliferate uncontrollably, invade adjacent tissues, and/or spread to other organs through a process named metastasis [1]. When normal cells are damaged or aged and not replaced, the expansion of abnormal cells results in the appearance of a tumor [2]. Cancer development is caused by genetic changes (both inherited and spontaneous errors during cell division) and by physical, chemical, and biological carcinogens [1,2]. Risk factors for cancer include age, alcohol consumption, tobacco smoking, unhealthy diet, physical inactivity, obesity, ultraviolet radiation, and air pollution [1,2].

Cancer is a leading cause of death on a global scale. The rapid increase in cancer incidence and mortality is associated with aging, population growth, and socioeconomic development [3]. In 2020, there were an estimated 19.3 million new cases diagnosed and 10 million cancer-related deaths worldwide [3]. In Spain, there were an estimated 282,421 new cases diagnosed and 113,054 cancer-related deaths [4].

In 2000, Hanahan and Weinberg summarized a set of essential acquired capabilities that govern the multistep transformation of normal cells into tumor cells. The authors proposed six hallmarks of cancer: sustaining proliferative signaling, evading growth suppressors, activating invasion and metastasis, enabling replicative immortality, inducing angiogenesis, and resisting cell death [5]. In 2011, Hanahan and Weinberg added two additional hallmarks: reprogramming of cellular metabolism and avoiding immune destruction. The authors also introduced the term “enabling characteristics”. These molecular and cellular mechanisms allow tumor cells to adopt the hallmarks. Tumor-promoting inflammation and genome instability and mutation were proposed as enabling characteristics. Furthermore, the tumor microenvironment plays an integral role in tumorigenesis and the development of malignancy [6]. Recently, Hanahan has reviewed and added two new emerging hallmarks — unlocking phenotypic plasticity and senescent cells — and two new enabling characteristics — non-mutational epigenetic reprogramming and polymorphic microbiomes —, as shown in Figure 1 [7].

Introduction

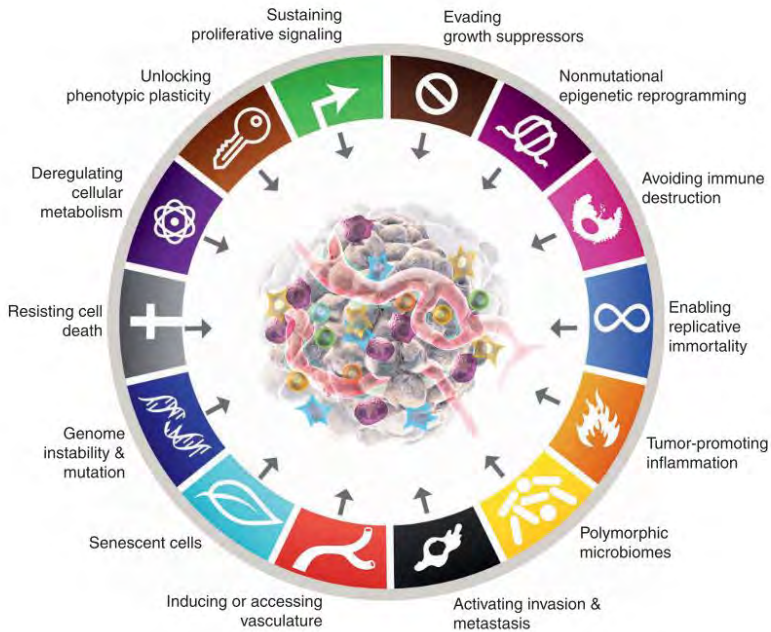


Figure 1. Hallmarks of cancer. Schematic representation of the ten hallmarks of cancer and the four enabling characteristics. Adapted from Hanahan, 2022 [7].

There are over 100 types of cancer, often named for the tissues or organs where tumors develop, for instance, breast cancer or lung cancer. Cancer is also classified based on the type of cell that forms it [2]:

- **Carcinoma.** It begins in the epithelial cells.
- **Sarcoma.** It originates in the bone and the soft tissues.
- **Leukemia.** It starts in the blood-forming tissue of the bone marrow.
- **Lymphoma.** It originates in the lymphocytes.
- **Myeloma.** It begins in the plasma cells.
- **Melanoma.** It starts in the melanocytes.
- **Brain and spinal cord tumors.** They begin in the central nervous system (CNS).

2. Lung Cancer

Lung cancer is the second most diagnosed cancer and the first cause of cancer-related mortality worldwide, with an estimated 2.2 million (11.4%) new cases and 1.8 million (18%) deaths [3,4]. In Spain, lung cancer is the fourth most diagnosed cancer, with 29,188 new cases (10.3%), and is the leading cause of cancer-related mortality, with 22,930 deaths (20.3%) [4]. Lung cancer is more frequent in men and women aged 70 and over [8]. Additionally, African-American men exhibit the largest incidence and mortality rates, while Hispanic women show the lowest [9].

The 5-year relative survival rate for lung cancer is 22%, which is strongly influenced by the stage at diagnosis (60% in the localized stage, 33% in the regional stage, and 6% in the distant stage) [8]. Moreover, the proportion of individuals living at least 3 years after diagnosis rose from 19% in 2001 to 31% in 2017 [8]. Although lung cancer survival has increased over the years, this improvement is limited to non-small cell lung cancer owing to the advances in diagnostic and surgical procedures, the development of targeted therapies against the most common driver mutations (for example, epidermal growth factor receptor (EGFR) tyrosine kinase inhibitors), and the recent introduction of immunotherapy as a treatment for this disease [10–13].

Tobacco smoking is the most important risk factor for lung cancer, with 81% of male and 72% of female patients between 20 and 49 years of age being smokers or former smokers [14]. Thus, the vast majority of lung cancer cases can be prevented by tobacco prevention and cessation [15]. Nevertheless, more than 25% of lung cancer patients worldwide are non-smokers, with men accounting for 15% of the cases and women accounting for 53% [15]. Other risk factors associated with lung cancer have been described, such as air pollution, chronic lung diseases, asbestos exposure, a high-fat diet, or a sedentary lifestyle [15].

2.1. Lung Cancer Classification

2.1.1 Histological Classification of Lung Cancer

Lung cancer is classified into two categories: non-small cell lung cancer (NSCLC) and small cell lung cancer (SCLC) [16,17].

NSCLC is the most common subtype representing 80-85% of all lung cancer cases [16,17]. It can be managed if detected and treated early [18]. Nevertheless, most patients with NSCLC are diagnosed at an advanced stage of the disease when therapies are ineffective [19]. NSCLC is susceptible to drug resistance, toxicity, and malignant migration [20]. Several treatments have been used to treat NSCLC, such as platinum-based chemotherapy, targeted therapy, and immunotherapy [18], but the 5-year survival rate is less than 15% [19]. Additionally, the nature of the disease and its tendency to metastasize are the main causes of death in NSCLC and are already present at the time of diagnosis and treatment [21]. Thus, therapeutic strategies against NSCLC must continue to be investigated to achieve reliable and safe treatments without causing resistance.

The three predominant histological types of NSCLC are adenocarcinoma, squamous cell carcinoma, and large cell carcinoma. These three types, which arise from distinct types of lung cells, are classified together as NSCLC because their behavior, response to treatment, and prognoses are frequently similar [16,17].

- **Adenocarcinoma.** Adenocarcinoma is the most frequent histological type, representing approximately 40% of all lung cancer cases in both sexes [22,23]. It originates from mucus-producing gland cells lining the airways. This subtype is usually detected in the outer regions of the lungs before dissemination [16,17]. Moreover, around 54% of patients with lung adenocarcinoma exhibit genetic mutations [24]. Comprehensive molecular profiling of lung adenocarcinoma revealed that 62% of these patients harbor activating mutations in known driver oncogenes, for instance, *EGFR* (14%), *KRAS* (33%), or *BRAF* (10%) [25].
- **Squamous cell carcinoma.** Squamous cell lung carcinoma (SCC) is the second most frequent subtype, accounting for roughly 20% of all primary lung neoplasms [22]. It grows in flat cells lining the airways. Generally, this cancer develops in the center

of the lungs and is associated with a smoking history [16,17,26]. Genetic mutations usually found in this subtype of lung cancer differ from those observed in adenocarcinoma [26]. Some genes that are frequently mutated in squamous cell carcinoma are *PIK3CA* (16%), *CDKN2A* (15%), *PTEN* (%), and *NOTCH1* (8%) [24,27].

- **Large cell carcinoma.** Large cell carcinoma represents 15% of all lung cancer cases [28]. This uncommon subtype, with large and rounded cells, can develop in any region of the lungs [16,17]. It also shows a poorly differentiated morphology and lacks cytological, architectural, and immunohistochemical markers [29,30]. Large cell carcinomas proliferate and spread aggressively, exhibiting resistance to treatment [16,17]. Although most cases show known genetic alterations (e.g., *EGFR* or *KRAS*), about 40% of the patients do not exhibit any genetic alteration. However, these patients usually show a high expression of programmed death ligand-1 (PD-L1) [29,30].

Approximately 15-20% of all lung cancer cases are identified as SCLC. These patients often show metastasis at diagnosis; thus, this subtype has a poor prognosis and a low 5-year survival rate. Patients with SCLC usually exhibit a good initial response to therapy. Unfortunately, drug resistance and aggressive relapses are observed in SCLC cases a few months later. Despite the identification of different potentially actionable mutations, no targeted treatments for SCLC have been authorized [31].

2.1.2. TNM Classification of Lung Cancer

The classification of tumor stage is a tool routinely used by physicians to determine the anatomic extent of the disease, which is characterized by three components: (1) the T component, which describes the extension of the primary tumor; (2) the N component, which explains the involvement of lymph nodes; and (3) the M component, which defines the presence of distant metastases [32]. Furthermore, each component is classified into various groups, which are defined by several features known as descriptors (Table 1).

Introduction

Table 1. Categories and descriptors of T, N, and M components. Modified from [32]

T component (Extension of Primary Tumor)	
T0	No primary tumor
Tis	Carcinoma <i>in situ</i> (squamous or adenocarcinoma)
T1	Tumor ≥ 3 cm
T1a	Minimally invasive adenocarcinoma, superficial spreading tumor in central airways, and tumor ≤ 1 cm
T1b	Tumor >1 but ≤ 2 cm
T1c	Tumor >2 but ≤ 3 cm
T2	Tumor >3 but ≤ 5 cm or tumor involving visceral pleura or main bronchus (not carina), atelectasis to hilum.
T2a	Tumor >3 but ≤ 4 cm
T2b	Tumor >4 but ≤ 5 cm
T3	Tumor >5 but ≤ 7 cm, or invading chest wall, pericardium, phrenic nerve, or separate tumor nodule(s) in the same lobe
T4	Tumor >7 cm, or tumor invading mediastinum, diaphragm, heart, great vessels, recurrent laryngeal nerve, carina, trachea, esophagus, spine; or tumor nodule(s) in a different ipsilateral lobe
N component (Regional Lymph Nodes)	
N0	No regional node metastasis
N1	Metastasis in ipsilateral pulmonary or hilar nodes
N2	Metastasis in ipsilateral mediastinal/subcarinal nodes
N3	Metastasis in contralateral mediastinal/hilar, or supraclavicular nodes
M component (Distant Metastasis)	
M0	No distant metastasis
M1a	Malignant pleural/pericardial effusion, or pleural/pericardial nodules, or separate tumor nodule(s) in a contralateral lobe
M1b	Single extrathoracic metastasis
M1c	Multiple extrathoracic metastases (1 or >1 organ)

The combination of T, N, and M components is grouped into four stages (Table 2). Staging is essential for choosing the initial treatment at the moment of diagnosis, and it is the most significant prognostic indicator after tumor resection [10,32]. For example, patients with stage I, II, and some cases of stage IIIA tumors undergo surgical resection, while patients with stage IV tumors receive chemotherapy, targeted therapy, and/or immunotherapy [33].

Table 2. Stage Groups of Lung Cancer. Modified from [32]

T/M	N0	N1	N2	N3
T1a	IA1	IIB	IIIA	IIIB
T1b	IA2			
T1c	IA3			
T2a	IB	IIB	IIIA	IIIB
T2b	IIA			
T3	IIB	IIIA	IIIB	IIIC
T4	IIIA	IIIA	IIIB	IIIC
M1a	IVA			
M1b				
M1c	IVB			

2.1.3. ECOG Performance Status Scale

The ECOG Performance Status is a standard criterion for determining how an illness affects a patient's daily living capacities, also known as the patient's performance status. This scale represents a patient's degree of functioning in terms of self-care, daily activities, and physical capabilities (e.g., walking, working). The ECOG Functional Status Scale (Table 3) is employed in clinical trials to both identify the patient population to be evaluated and to assess changes in patient functioning as a result of treatment during the investigation [34].

Table 3. ECOG Performance Status Scale. Modified from [34].

Grade	ECOG
0	Totally active, capable of performing all pre-disease functions without limitation
1	Limited in physically intense activities but ambulatory and capable of performing light or sedentary labor, e.g., light housework, office work
2	Ambulatory and able to self-care but unable to do any job tasks; awake for more than 50% of waking hours
3	Only able to minimal self-care; confined to chair or bed for more than 50% of waking hours
4	Completely physically disabled; incapable of self-care; confined to a chair or bed
5	Dead

2.2. EGFR-mutated NSCLC

2.2.1. Epidermal Growth Factor Receptor

The EGFR is a receptor with tyrosine kinase (TK) activity and is part of the ErbB family. It is located on the cell membrane and has three domains: extracellular, transmembrane, and cytoplasmic. Under normal conditions, receptor activation requires ligand binding to the extracellular domain, which causes a conformational change that facilitates dimerization and phosphorylation of the cytoplasmic or TK domain. This phosphorylation results in the activation of downstream signaling pathways, such as rat sarcoma (RAS)/ MAPK/ERK kinase (MEK)/ mitogen activated protein kinase (MAPK), phosphoinositide 3-kinase (PI3K)/ protein kinase B (AKT), and janus kinase (JAK)/ signal transducer and activator of transcription (STAT), as well as self-regulation (Figure 2) [35,36].

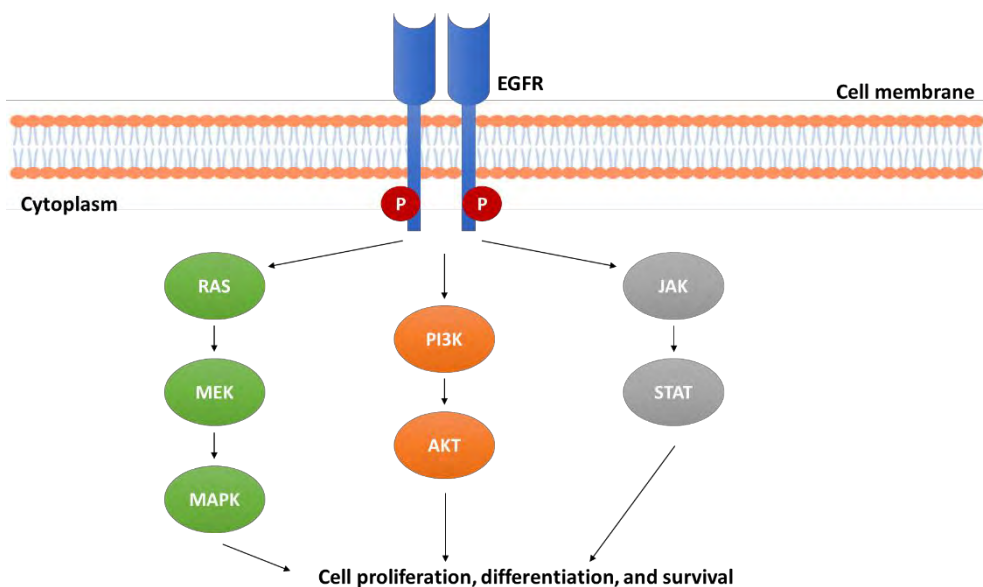


Figure 2. Epidermal growth factor receptor (EGFR) and its downstream signaling pathways (RAS, Rat sarcoma; MEK, MAPK/ERK kinase; MAPK, Mitogen activated protein kinase; PI3K, Phosphoinositide 3-kinase; AKT, Protein kinase B; JAK, Janus kinase; STAT, signal transducer and activator of transcription).

This receptor is encoded by the *EGFR* gene, which is located on the short arm of chromosome 7 at position 11.2 (7p11.2) and contains 28 exons [37]. EGFR regulates cell proliferation, differentiation, and survival. Thus, *EGFR* is an oncogenic driver in several types of cancer, including NSCLC [38].

2.2.2. *EGFR* Mutations

EGFR mutations are commonly found in adenocarcinomas, young women, and never-smokers [39]. Their incidence varies significantly by ethnicity, with rates of 17% reported in the Caucasian population [40], 26% in Latin Americans [41], and 62% in Asians [42].

The most prevalent *EGFR* mutations are the deletion in exon 19 (Ex19Del) and the missense mutation in exon 21 (L858R) (Figure 3). Approximately 80-90% of EGFR-mutated (EGFRm) NSCLC cases exhibit one of these activating or sensitizing mutations, which are susceptible to treatment using TK inhibitors (TKIs) [43]. Hence, EGFR-TKIs have been used as first-line therapy for patients with EGFRm NSCLC since the approval of gefitinib in 2010.

Another important mutation is the substitution of methionine for threonine at position 790 (T790M) in exon 20 of *EGFR* (Figure 3), which results in decreased affinity for first- and second-generation EGFR-TKIs. Hence, it is responsible for around 50% of the acquired resistance cases [44–46].

It also should be noted that approximately 10% of *EGFR*-activating mutations correspond to insertion in exon 20 of *EGFR* (EGFRins20) (Figure 3). Nonetheless, the first EGFR-TKIs developed did not have the same sensitivity to this mutation as Ex19Del and L858R. The US Food and Drug Administration (FDA) recently approved amivantamab as a therapy for patients with EGFRins20 mutation [47]. Additionally, patients with rare *EGFR* mutations have been reported, such as G719X, S768I, and L861Q (Figure 3), and have been treated with osimertinib, a third-generation EGFR-TKI [48].

Introduction

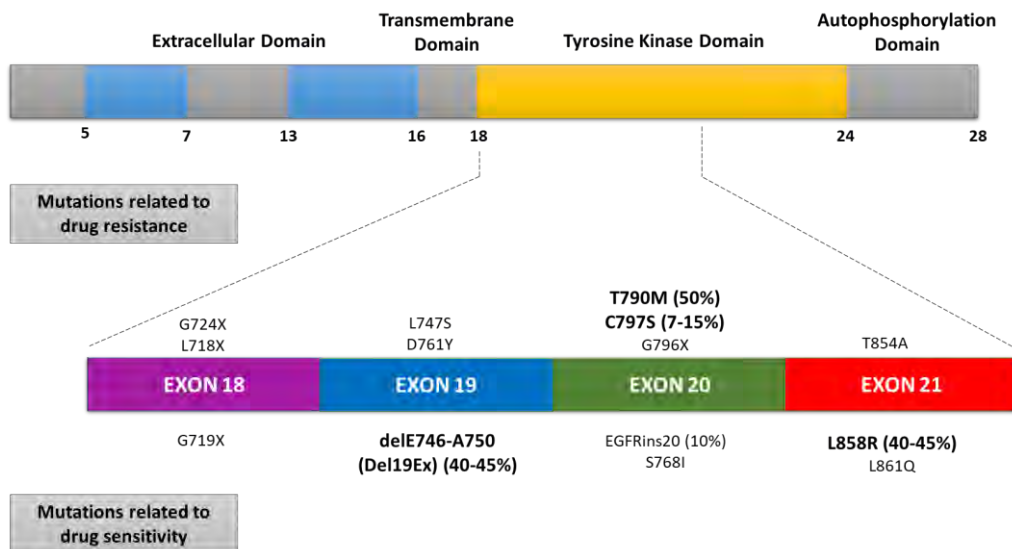


Figure 3. Mutations in the *EGFR* gene. Mutations associated with drug resistance are indicated above and mutations associated with drug sensitivity are indicated at the bottom. The most frequent mutations are highlighted in bold.

2.2.3. EGFR Tyrosine Kinase Inhibitors

The identification of specific genetic mutations in *EGFR* has resulted in substantial advances in the management of patients with lung cancer in recent years since it has allowed the development of targeted therapies. EGFR-TKIs are the standard treatment for most patients with EGFRm NSCLC. Additionally, patients can be treated with multiple EGFR-TKIs before requiring chemotherapy, because several drugs are available. Currently, three generations of EGFR-TKIs are authorized to treat patients with EGFRm NSCLC (Figure 4).

Gefitinib was the first EGFR-TKI used. It competitively and reversibly binds to the adenosine triphosphate (ATP)-binding site in the TK domain of EGFR, inhibiting its activity [49]. The results obtained from clinical trials showed that patients harboring *EGFR*-sensitizing mutations treated with gefitinib had a significantly longer progression-free survival (PFS) than those treated with standard chemotherapy [50,51]. In 2010, gefitinib received FDA approval as first-line therapy for patients with EGFRm NSCLC. In addition to gefitinib, there are two more first-generation EGFR-TKIs: erlotinib and icotinib. Patients who received

treatment with any of these drugs significantly improved PFS compared to those in the chemotherapy group [52,53]. Although patients treated with first-generation EGFR-TKIs often experience rash and diarrhea, as drugs also inhibit wild-type EGFR, all three inhibitors had a safer profile and greater efficacy as first-line treatment than standard chemotherapy in patients with EGFRm NSCLC. Nevertheless, the therapeutic effectiveness was limited because the majority of patients develop acquired resistance, primarily the secondary T790M mutation, within 9–14 months during or after EGFR-TKI treatment [54]. Hence, second-generation EGFR-TKIs were used to address acquired resistance to first-generation EGFR-TKIs.

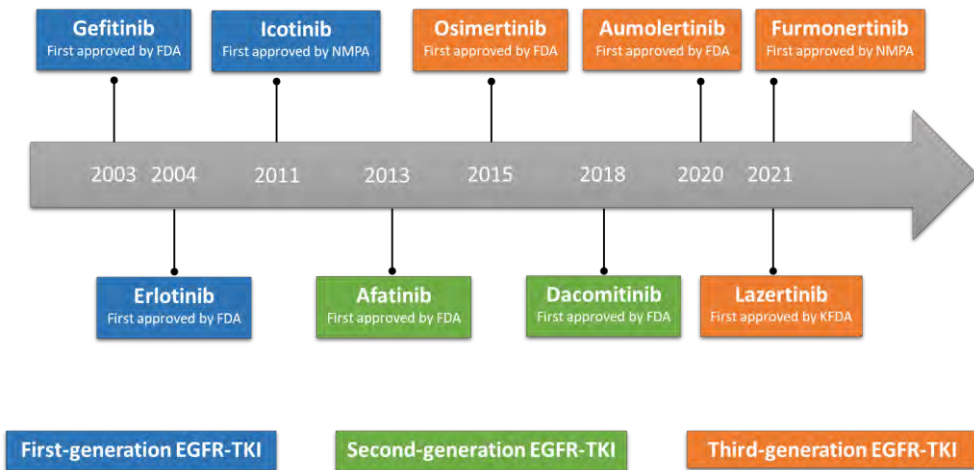


Figure 4. Timeline of approval of EGFR-TKIs in EGFR-mutated NSCLC (FDA, US Food and Drug Administration; NMPA, China National Medical Products Administration; KFDA, Korea Food and Drug Administration).

Second-generation EGFR-TKIs irreversibly inhibit the TK domain of EGFR. Various clinical trials have demonstrated that patients treated with afatinib have longer PFS than those treated with standard chemotherapy [55,56]. It was also observed that patients with the L858R mutation may be less sensitive to the afatinib therapy than those with the Ex19Del mutation [57]. Furthermore, afatinib showed a prolonged time to treatment failure and a

Introduction

longer objective response rate (ORR) and PFS, and dacomitinib had a higher PFS and overall survival (OS) as first-line treatment than gefitinib [58–61]. However, no clinical effectiveness of second-generation EGFR-TKIs was found in patients with the T790M mutation. More importantly, these drugs also caused this secondary mutation in the tumor, acquiring resistance to treatment, and have a higher incidence of treatment-related adverse effects than first-generation TKIs. Therefore, the success of the treatment is limited using first- and second-generation EGFR-TKIs.

The first third-generation EGFR-TKI authorized for the treatment of patients with metastatic NSCLC with the T790M mutation was **osimertinib**. This drug irreversibly binds to the ATP-binding site (concretely, the cysteine at position 797 (C797)) of the TK domain of EGFR. Osimertinib has high selectivity and reduced toxicity. Specifically, the drugs target *EGFR*-activating mutations and the T790M mutation while avoiding wild-type EGFR. It also has an enhanced capacity to cross the blood-brain barrier and is potentially effective against central nervous system metastases [62]. The superior effectiveness of osimertinib compared to chemotherapy and first-generation EGFR-TKIs was demonstrated in the AURA3 and FLAURA trials in patients with the T790M mutation as second-line therapy and in patients with *EGFR*-sensitizing mutations as first-line treatment, respectively [63,64]. Additionally, osimertinib treatment did not cause the development of the T790M mutation [65]. It was also revealed that afatinib demonstrated more benefit in OS compared to osimertinib in NSCLC patients with the L858R mutation [66]. In 2020, the FDA approved osimertinib as an adjuvant therapy for patients with EGFRm NSCLC after resection [67]. Recent results from the ADAURA study support osimertinib as an adjuvant treatment for these patients, with or without previous adjuvant chemotherapy [68]. Other third-generation EGFR-TKIs are effective against the acquired mutation T790M: aumolertinib, furmonertinib, and lazertinib [69–71].

Regrettably, the acquisition of osimertinib resistance has also been described through several mechanisms [72]. At this point, the most common therapeutic option for patients is chemotherapy because other approved treatments, such as immune checkpoint inhibitors are ineffective in these patients [73] and there is no fourth-generation EGFR-TKI authorized for the treatment of these patients.

2.2.4. Resistance Mechanisms to EGFR-TKIs

Resistance usually emerges after patients are treated with EGFR-TKI. Consequently, resistant clones can flourish again in the same tumor and/or other locations in the patient's body [18]. There are several mechanisms by which tumors acquire resistance to EGFR-TKIs, that can be broadly divided into EGFR-dependent or EGFR-independent.

Acquisition of additional EGFR mutations is the most common EGFR-dependent mechanism. These mutations are characterized by variations in amino acid residues that modify the ATP-binding site of the TK domain of the receptor, interfering with drug action, and consequently, causing resistance.

The most frequently acquired mutation due to the treatment using first- and second-generation EGFR-TKIs is the **T790M point mutation**. More than 50% of patients with EGFRm NSCLC who received a first- or second-generation EGFR-TKI as initial treatment developed resistance because of the acquisition of this secondary mutation in exon 20 [44–46]. It has been observed that the T790M mutation is more common in patients with Ex19Del than the L858R mutation [74]. Other uncommon secondary mutations involved in gefitinib or erlotinib resistance have been documented, including L747S [75], D761Y [45], and T854A [76] (Figure 3).

Regarding treatment using third-generation EGFR-TKIs, specifically osimertinib, the most recurrent mutation is the substitution of cysteine for serine at position 797 (**C797S) point mutation** in exon 20 (Figure 3). The incidence of this mutation varies between 7-15% depending on whether osimertinib is administered as first-line or second-line therapy, respectively [77,78]. It has also been observed that approximately half of the patients had **T790M loss** [79], which may be related to intratumor heterogeneity, selection pressure, and clonal expansion. Researchers have reported the acquisition of other *EGFR* mutations that allow for the development of resistance to osimertinib, such as G796X, G724X [79], L972X, or L718X [80] (Figure 3).

Other EGFR-dependent resistance mechanisms to EGFR-TKIs are the amplification of wild-type EGFR (which has a lower affinity to EGFR-TKI drugs) [81], EGFR ligand overexpression [82], and tertiary EGFR mutations [83].

Introduction

Different mechanisms of EGFR-independent resistance have been identified. Some of these are detailed below.

- ***MET* amplification.** This oncogene encodes c-Met, a TK receptor responsible for cell migration, proliferation, and apoptosis. c-Met is able to activate EGFR downstream signaling pathways by bypassing [84]. This mechanism has been reported in 5-20% of patients resistant to EGFR-TKIs [77,78,85–87].
- ***HER2* amplification.** HER2 is a TK receptor that also belongs to the ErbB receptor family. HER2 directly activates EGFR downstream signaling, such as RAS/MEK/MAPK, PI3K/AKT, or JAK/STAT, as they share downstream signaling pathways. Thus, it mediates resistance to EGFR-TKIs [88]. HER2 amplification was detected in 2-13% of patients who acquired resistance to EGFR-TKIs [77,78,89].
- ***PIK3CA* mutations.** These mutations lead to continuous activation of the PI3K/AKT pathway, which promotes carcinogenesis, cell migration, invasion, and proliferation [90]. Approximately 1-17% of patients who developed resistance to EGFR-TKIs carried these mutations [78,86,91].
- ***STAT3* activation.** The activation of STAT3 is involved in cell proliferation, differentiation, apoptosis, angiogenesis, and the immune response [92–94]. In addition, it has been reported as a resistance mechanism for EGR-TKI treatment [95]. In patients, STAT3 activation is associated with poorly differentiated tumors, an advanced clinical stage, and metastasis [96,97]. Neither gefitinib nor osimertinib can block STAT3 activation [98,99].
- **Histological transformation.** Among the patients who failed to respond to EGFR-TKI therapy, 3-14% had tumors that exhibited histologic transition from NSCLC to SCLC [86,89,91]. Recently, some cases have also documented the transformation from NSCLC to SCC [100]. Furthermore, the epithelial-to-mesenchymal transition is another histologic alteration proposed as a mechanism of resistance to EGFR-TKIs [101].

In addition, other mechanisms of resistance to EGFR-TKIs have been described, such as *KRAS* (1-4%) and *BRAF* (1-4%) mutations [78,91,102], Axl and IGF1R overexpression [103,104],

PTEN loss [105], changes in proteins related to apoptosis, such as BIM and Bcl-2 [106], or EphA2 activation [107].

2.2.5. Novel Therapies to Overcome Resistance to EGFR-TKIs

Tumor heterogeneity promotes the variety and complexity of molecular resistance mechanisms. Furthermore, the changes and the coexistence of different resistance mechanisms complicate the development of efficient therapies, resulting in unsatisfactory results.

Recently, the advancement of fourth-generation EGFR-TKIs has been emphasized, with many drugs showing promising outcomes in clinical studies. The first fourth-generation EGFR-TKI is EAI045. However, preclinical results determined that it had no effect as a single agent [108]. Consequently, this new EGFR-TKI was modified and improved to obtain JBJ-04-12502, a novel allosteric inhibitor with better effectiveness, reduced toxicity, and efficacy against L858R/T790M/C797 EGFR mutations [109]. Although still in the research stage, this drug has a more potent beneficial effect when combined with osimertinib [110]. Another fourth-generation EGFR-TKI is TQB3804. It not only overcomes osimertinib resistance associated with EGFR-activating mutations/T790M/C797S, but is also effective against the double mutation implicated in the resistance to first- and second-generation EGFR-TKIs [111]. This drug is currently being studied in patients with advanced malignant tumors (NCT04128085).

Amivantamab is a bispecific antibody against EGFR and MET. This drug has also been defined as a fourth-generation EGFR-TKI. After acquiring osimertinib resistance, amivantamab was found to be effective against tumors harboring the C797S mutation and MET amplification. Moreover, the combination of amivantamab and lazertinib successfully overcame osimertinib resistance, since the disease control rate was 60% with a median follow-up time of 4 months [112,113].

Other drugs with the potential to address resistance to osimertinib are antibody-drug conjugates. U3-1402, for example, combines patritumab, which acts on HER3 antibodies,

Introduction

with the topoisomerase inhibitor DX-8951. U3-1402 is effective against several resistance mechanisms derived from EGFR-TKI treatment and has shown tolerable safety in the phase I ongoing trial (NCT03260491) in patients with advanced or unresectable NSCLC [114].

Several studies have focused on the treatment using bevacizumab, an antibody against the vascular endothelial growth factor (VEGF). Cui *et al.* reported the effectiveness and safety of osimertinib with bevacizumab vs. chemotherapy with bevacizumab in patients with osimertinib resistance. Both PFS and OS significantly improved in the osimertinib-bevacizumab group [115]. Lu *et al.* studied the combination of sintilimab (PD-1 inhibitor)-bevacizumab-chemotherapy vs. standard chemotherapy alone in patients with T790M loss after the treatment with third-generation EGFR-TKI. It was observed that the PFS was longer in the triple-treatment group [116].

Another strategy being evaluated is the use of osimertinib in combination with inhibitors of EGFR downstream signaling pathways. Several clinical trials are currently ongoing to evaluate the use of osimertinib in combination with selumetinib (a MEK inhibitor) (NCT03392246), dactolisib (a dual PI3K and mTOR inhibitor) (NCT02503722), and itacitinib (a JAK1 inhibitor) (NCT02917993) to inhibit the RAS/MEK/MAPK, PI3K/AKT, and JAK/STAT pathways, respectively.

To sum up, different fourth-generation EGFR-TKIs are being developed and several combinations of approved drugs are being tested; unfortunately, there is still no standard therapy to treat many patients resistant to EGFR-TKIs. Therefore, new therapeutic strategies are needed to overcome drug resistance.

3. Breast Cancer

Breast cancer is the most diagnosed cancer and the fifth leading cause of cancer-related mortality worldwide, accounting for 2.2 million (11.7%) new cases and 658,000 (6.9%) deaths [3,4]. In Spain, it is the third most commonly diagnosed cancer, representing 34,088 (12.1%) new cases, and the fourth cause of cancer-related mortality, with 6,606 (5.8%) deaths [4]. More than 99% of patients with breast cancer are women because of anatomical

variations between genders [2]. In most countries, the incidence of this disease has increased owing to higher exposure to specific risk factors, for example, hormonal status, advanced age at first pregnancy, fewer pregnancies, shorter or no periods of breastfeeding, prolonged exposure to menstruation, and family history of breast cancer [117,118]. Nonetheless, survival has risen owing to early detection and the development of new therapeutic strategies over the last decade [119].

3.1. Breast Cancer Classification

Owing to the high diversity of the disease, different subtypes of breast cancer have been described [120]. It is commonly classified by clinicians according to the presence or absence of three cell membrane receptors: the estrogen receptor (ERe), the progesterone receptor (PR), and the human epidermal growth factor receptor 2 (HER2) (Figure 5). This classification aids in prognosis prediction and treatment selection.

- **Hormone-positive breast cancer.** It is the most common subtype, accounting for 60–70% of all breast cancer cases. Patients exhibit overexpression of ERe and/or PR and have a better prognosis than other types [121]. Selective estrogen modulators and aromatase inhibitors are targeted therapies for hormone-positive breast cancers [122,123].
- **HER2-positive breast cancer.** It represents 20–30% of patients with breast cancer and is characterized by the amplification of HER2. These patients show a high risk of metastasis and a poor prognosis [124,125]. Monoclonal antibodies and small molecule TKIs are examples of targeted therapies available against this subtype [126].
- **Triple negative breast cancer (TNBC).** It is identified by the lack of ERe, PR, and HER2 [127], and accounts for 15–20% of all breast cancer cases. Compared to the other subtypes, patients with TNBC are younger, have larger tumors, and have a higher rate of recurrence, distant metastasis, and mortality [128–130]. Hence, TNBC is highly aggressive and has a poor prognosis [128]. Chemotherapy is the only therapeutic option for these patients due to the lack of validated targeted therapies

Introduction

[131]. Although there is a good initial response to treatment, the recurrence rate within 5 years after diagnosis is approximately 30% [132].

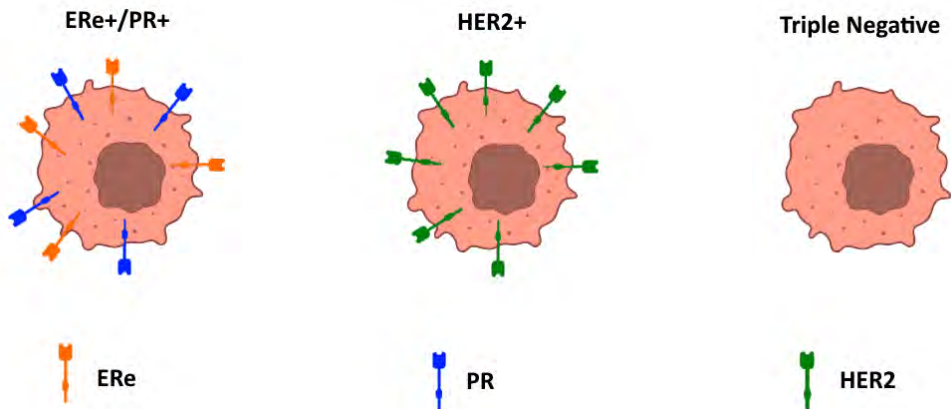


Figure 5. Clinical classification of breast cancer (ERe, Estrogen receptor; PR, Progesterone receptor; HER2, human epidermal growth factor receptor 2).

Additionally, molecular classifications have been reported to clarify breast cancer heterogeneity [133–135].

- **Luminal A.** It usually shows increased expression of ERe- and PR-regulated genes and low expression of proliferation-associated genes. Moreover, the luminal A subtype has no HER2 amplification. It corresponds to 40% of all breast tumors and has the best prognosis compared to other subtypes [134].
- **Luminal B.** It exhibits a lower expression of ERe- and PR-regulated genes and a higher expression of proliferative-associated genes. Patients may also have *HER2* amplification. The luminal B subtype represents 10% of all breast cancer cases and has an intermediate prognosis [134].
- **HER2-enriched.** The main features of this subtype are the overexpression of the *HER2* gene and/or protein levels and the low expression of ERe- and PR-regulated genes and basal-like genes. The HER2-enriched tumors account for 10% of all breast cancer patients and have a poor prognosis [136].

- **Basal-like.** It shows a low or absent expression of ERe-, PR-, and HER2-related genes, high expression of proliferative-associated genes, and the expression of a basal cluster formed by different cytokeratins and EGFR. The basal-like subtype corresponds to 75% of TNBC cases and has a poor prognosis [137,138]
- **Mesenchymal-like.** It exhibits a low expression of HER2, luminal cytokeratins, proliferative-associated genes, and cell-cell adhesion-related genes (claudin genes) [135]. The mesenchymal-like subtype is enriched in immune system responses and mesenchymal genes [135,139]. It represents 5–10% of all breast tumors and has a poor prognosis [134,140].

Although clinical subtypes can be correlated with molecular groups, the two classifications do not completely overlap [137,141,142].

3.2. Triple Negative Breast Cancer: Characteristics, Prognosis, and Treatment

As aforementioned, TNBC is characterized by the lack of expression of ERe and PR and HER2 amplification [127], representing 15-20% of all patients with breast cancer [128]. Patients with TNBC are premenopausal younger women, usually of African-American and Black ethnicity, and exhibit a higher grade, larger tumor size, and lymph node positivity [128,143]. In fact, the prognosis of younger patients with TNBC is worse than that of patients older than 70 years [144]. Other risk factors associated with developing TNBC are young age at first pregnancy, higher waist/hip ratio, and multiparity [145].

Although patients with TNBC show high chemosensitivity, there is a high probability of relapse during the first few years after surgery, and more than 45% of these patients develop distant metastasis [146,147]. The mortality rate within the first five years following diagnosis is 40% [128]. Moreover, the median survival time after metastasis is only 13.3 months and the mortality rate within three months following recurrence is more than 75% [148,149]. Thus, the risk of death is higher after the first metastatic event [146]. Usually, metastases in patients with TNBC are located in the viscera, brain, and lungs [148,149].

Introduction

At a molecular level, TNBC is classified as basal-like or mesenchymal-like, accounting for 49% and 30% of all breast cancer cases, respectively [141,142]. Because of the difficulty to identify both subtypes using immunohistochemistry (IHC), the technique used in the clinic, some markers are added in the procedure to improve breast cancer classification, for instance, cytokeratins 5/6 (CK5/6) or EGFR to identify basal-like subtype [138,150,151], or vimentin and E-cadherin to identify mesenchymal-like subtype [152,153].

Owing to the high diversity of TNBC, it is challenging to find new therapeutic biomarkers and develop targeted therapies. Therefore, TNBC has limited treatment options, including the following:

- **Surgery.** Breast-conservative surgery is the predominant treatment for patients with small tumors, whereas mastectomy and neoadjuvant chemotherapy are the chosen option for patients with larger and/or multifocal tumors [154].
- **Radiotherapy.** This therapeutic preference depends on the extent of surgery and lymph nodes. It is usually given in combination with breast-conservative surgery, resulting in better long-term outcomes. Nonetheless, some researchers reported radioresistance in TNBC tumors due to ERe-negative status [155,156]
- **Chemotherapy.** It is the only systemic therapy available for patients with TNBC. The use of neoadjuvant chemotherapy improves substantially the prognosis of patients with TNBC [132,154,157]. The tumor size is reduced by neoadjuvant treatment, allowing breast-conservative surgery. The absence of ERe expression shows a better response to chemotherapy [158,159]. TNBC is often treated with combination regimens based on taxanes [160], anthracyclines [161], cyclophosphamide [162], platinum drugs [163,164], and fluorouracil [165].

Chemotherapy is the primary treatment for metastatic relapse, but its prognosis is poorer than that of other breast cancer subtypes [132,149]. The response to chemotherapeutic treatment is unsatisfactory, resulting in the rapid progression of the disease [146]. Additionally, changes in ERe, PR, or HER2 status occur in a few patients with TNBC during metastasis, thereby increasing their therapeutic options [166].

Therefore, new targeted treatments are needed for patients with TNBC. However, their development is complicated due to the high heterogeneity of the disease. Despite this, a significant number of clinical trials are currently ongoing in which some therapeutic targets are VEGF (NCT04739670), EGFR (NCT04485013), the mammalian target of rapamycin (mTOR) (NCT02531932), poly (ADP-ribose) polymerase (PARP) (NCT05203445), or programmed cell death-ligand 1 (PD-L1) (NCT03125902).

4. Cancer Stem Cells

Cancer stem cells (CSCs) are a small population of cells within a tumor responsible for cancer initiation, progression, relapse, and metastasis. These cells, which only account for 0.1–2% of tumor cells, exhibit unlimited self-renewal and pluripotency capacities, as well as resistance to anti-cancer therapies. After treatment, CSCs are involved in tumor regrowth due to the reversibility of their quiescent state. The therapy also selectively enriches CSCs owing to the removal of sensitive non-stem cancer cells, promoting de-differentiation to produce more CSCs. This population also transdifferentiates into other multi-lineage cells to control tumorigenesis [167–170].

In 1937, Furth & Kahn were the first to describe cancer cells with stem features. The researchers implanted derived-leukemia single cells into inbred mice. Tumors with characteristics similar to those of the original clinical tumor were initiated by only 5% of these cells, demonstrating the presence of a subpopulation of cells with tumorigenic features and capable of extensive growth [171]. After several investigations in this field, the identification and purification of human acute myeloid leukemia CSCs using the specific expression of clusters of differentiation (CD) CD34+/CD38- was accomplished for the first time in 1997 [172].

CSCs can grow as spheres in suspension. This methodology was described to allow the *in vitro* propagation of stem cells due to their abilities to proliferate in anchorage-independent conditions, differentiate into other lineages, and form complex and functional three-

dimensional structures [173,174]. Additionally, CSCs can form colonies, which are used for the separation and identification of different types of tumors [175].

4.1. Origin of Cancer Stem Cells

CSCs originate from various sources [176]:

- Random mutations during DNA replication can convert normal stem cells to CSCs [177].
- Genomic instability causes cell transformation and cancer initiation at both chromosomal and molecular levels. This process occurs in stem and progenitor cells as well as in differentiated cells [178].
- Through horizontal gene transfer, normal stem cells can capture fragmented DNA, leading to genetic reprogramming and CSC generation. It is well known that cancer cells can phagocytose or capture fragmented DNA that can be transferred to recipient cancer cells [179–181].
- Microenvironmental factors play an essential role in CSC formation. For example, arsenic triggers the conversion of normal stem cells to CSCs [182].
- Cell fusion is implicated in tumor initiation and progression. For instance, leukocytes and cancer cells can fuse, starting the development of metastatic cancer cells [183].
- Metabolic reprogramming is also involved in CSC formation. Folmes *et al.* demonstrated that somatic differentiated cells changed from oxidative phosphorylation to glycolysis, reprogramming these cells into pluripotent cells [184].

4.2. Cancer Stem Cells Identification

4.2.1. Surface Markers

Identification of CSCs is essential for researchers and clinicians as it may allow for better diagnosis and treatment of patients. Differential expression of cell surface markers has entailed the identification of CSCs such as CD24, CD133, and CD166 (Figure 6).

- **CD24.** It is a glycosyl-phosphatidyl-inositol (GPI)-anchored glycoprotein expressed by various cells from the immune system [185]. As a result of the study by Al-Hajj *et al.*, which showed tumorigenesis after transplantation of CD44⁺CD24^{-/low} cells into NOD/SCID mice [186], CD24 began to be used as a marker to identify CSCs. Moreover, the ectopic expression of CD24 was associated with tumor formation, growth, and metastasis [187].
- **CD133.** It is a transmembrane glycoprotein, a member of the prominin family, that preserves the lipid content in cell membranes [188,189]. Although it was first identified in hematopoietic stem cells, it has been reported to be highly expressed in CSCs from several human cancers, such as the lung, colorectum, or pancreas [190–192]. Concretely, CD133⁺ cells have a higher tumorigenic potential, stemness, adhesion, motility, and drug efflux [193].
- **CD166.** It is a cell surface glycoprotein, structurally similar to immunoglobulin superfamily members, that was first reported in activated leukocytes [194]. Its expression is associated with different CSC features, i.e., tumorigenesis, in lung, colorectal, and head and neck cancers [195–197]. Additionally, CD166 expression is related to some biological functions, such as angiogenesis, anti-apoptosis, and cell migration [198].

4.2.2. Aldehyde Dehydrogenase (ALDH)

ALDH belongs to a family of enzymes responsible for the transformation of retinol to retinoic acid [199]. These enzymes protect organisms against harmful aldehydes and cytotoxic agents by their detoxification role and control hematopoietic stem cell differentiation [200,201]. Among the 19 members of the ALDH family, ALDH1 has been identified as a CSC

Introduction

biomarker (Figure 6), and its high activity is associated with stemness, tumorigenesis, chemoresistance, and rapid proliferation [202–204]. Additionally, ALDH1 is higher expressed in TNBC than in other breast cancer subtypes [205].

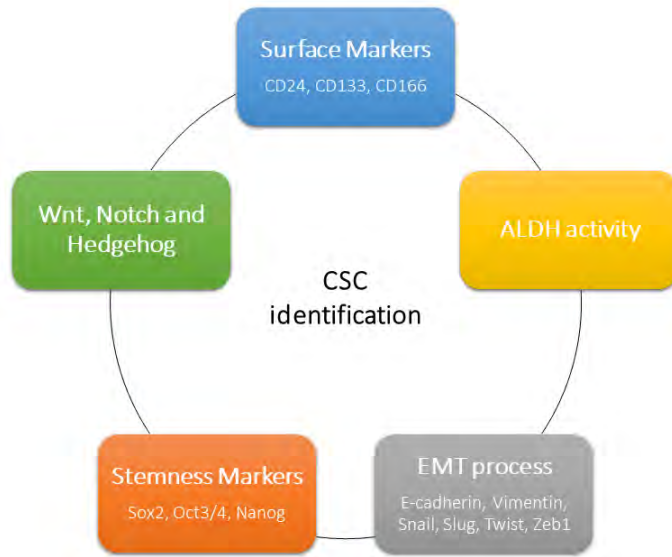


Figure 6. Diagram of the differential features of CSCs that allow their identification.

4.2.3. Epithelial-to-Mesenchymal Transition (EMT)

The epithelial-to-mesenchymal transition (EMT) is a critical biological process that allows the transformation of epithelial cells into a mesenchymal phenotype, arranging along the epithelial-mesenchymal axis [206]. Epithelial cells show epithelial cell-to-cell junctions and apical-basal polarity. In contrast, mesenchymal cells possess increased motility and invasiveness, and a spindle shape that lacks apical-basal polarity [207].

Researchers have reported that the EMT process is triggered by EMT transcription factors, including Snail, Slug, Twist, and Zeb [208,209]. These events are followed by the downregulation of the epithelial biomarker E-cadherin [210] and the enhancement of vimentin and N-cadherin, among others [211].

Under normal conditions, EMT has significant functions during embryogenesis; however, this process is abnormally activated in cancer [212]. Cancer cells use the EMT process to locally invade the main tumor site, intravasate into blood arteries, translocate via circulation, extravasate into distant tissue parenchyma, and survive as micrometastases [213]. EMT is frequently reversible, allowing cancer cells to return to more epithelial stages via mesenchymal-to-epithelial transition (MET). Through a process known as colonization, this phenotypic plasticity enables micrometastases to spread into macroscopic metastases (Figure 7) [214]. Nevertheless, cancer cells do not often lose all epithelial traits and acquire a complete spectrum of mesenchymal characteristics [206].

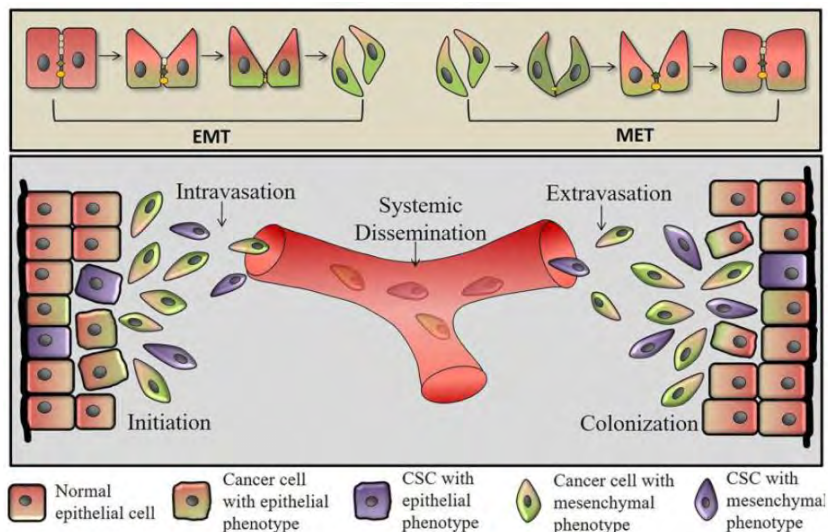


Figure 7. Schematic representation about the role of epithelial-to-mesenchymal transition (EMT) and mesenchymal-to-epithelial transition (MET) in metastasis. Extracted from Roy *et al.*, *Frontiers in Bioscience*, 2021 [211].

The activation of EMT in non-CSCs also leads to their conversion into CSCs (Figure 6). Some studies have demonstrated that non-CSC populations spontaneously acquire EMT under the right circumstances, obtaining cell surface markers comparable to CSCs, and improved potential to generate tumors. Because CSCs serve as stem cells, they have the capacity to

Introduction

differentiate into non-CSCs, presumably through MET stimulation [215,216]. Furthermore, EMT activation induces multiple drug resistance in cancer cells through different mechanisms such as slow cell growth, increased production of anti-apoptotic proteins, and upregulation of ATP-binding cassette (ABC) transporters that mediate drug efflux [217,218].

4.2.4. Stemness Markers

The transcription factors Sox2, Oct3/4, and Nanog trigger genes that are involved in self-renewal and pluripotency and repress genes related to differentiation. These transcription factors have been reported as biomarkers for CSC identification (Figure 6) [219].

- **Sox2.** It is a transcription factor from the sex-determining region of the Y chromosome (SRY)-related high-mobility group (HMG)-box (SOX) family, which plays a key role in the early development and maintenance of an undifferentiated cell phenotype [220]. A study demonstrated that upregulation of Sox2 may help to identify poorly differentiated/stem cell phenotype in TNBC [221]. Moreover, Sox2 overexpression is related to resistance to EGFR-TKIs [222] and chemotherapy [223]. Moreover, high expression of Sox2 has been reported in lung cancer cells cultured as *in vitro* spheroids [224].
- **Oct3/4.** Octamer-binding transcription factor 3/4 (Oct3/4), also called POU51, is a member of the POU homeobox gene family [225]. In 1998, it was first reported as a pluripotency regulator in a mammalian stem cell population [226]. Oct3/4 is increased in a variety of human malignancies, including TNBC [227] and NSCLC [228], and is associated with a poor differentiation degree, high pathological tumor size, a worse TNM stage, and more lymphatic metastasis. Moreover, high levels of Oct3/4 are linked to enhanced tumorigenesis and tumor progression, leading to poor prognosis in NSCLC [229].
- **Nanog.** It is a homeobox protein that promotes pluripotency and self-renewal while suppressing differentiation. Aberrant expression of this transcription factor is common in human malignancies [230]. In breast cancer, Nanog upregulation promotes EMT, contributes to metastasis, and is correlated with poor prognosis

[231]. In NSCLC, Nanog activation is associated with metastasis, self-renewal, and EMT [232].

4.2.5. Wnt, Notch & Hedgehog

CSCs share several features with embryonic or tissue stem cells, including the continuous activation of one or more highly conserved signaling pathways implicated in the development and tissue homeostasis, for instance, Wnt, Notch, and Hedgehog signaling pathways (Figure 6).

- **The Notch signaling pathway.** It plays an essential role in cell proliferation, stem cell maintenance, differentiation, and homeostasis in a multicellular organism [233]. Researchers have found that the Notch pathway is activated in various human cancers, including breast, lung, and colorectal cancers [234–236]. Induction of angiogenesis, inhibition of apoptosis, initiation of EMT, increase in drug resistance, maintenance of stem phenotype, and contribution to metastasis are the main oncogenic effects of this signaling pathway [237].
- **The Hedgehog signaling pathway.** It is associated with embryonic development, tissue patterning, homeostasis, and stem maintenance in adults. This signaling pathway also controls cell growth, survival, differentiation, and angiogenesis [238,239]. Sonic Hedgehog (Shh) is the most studied Hedgehog ligand. The binding of the ligand removes the inhibition of Patched (PTCH) on Smoothed (Smo), enhancing the expression of glioma-associated oncogene (Gli) transcription factors. Gli triggers the expression of Hedgehog target genes [240]. Activation of the Hedgehog pathway leads to tumorigenesis, progression, and metastasis in various human cancers, such as lung, breast, and ovarian cancers [241–243]. Aberrant activation could be caused by (I) mutations in some elements of the pathway resulting in Hedgehog ligand-independent activation, (II) Hedgehog protein overexpression that causes Hedgehog ligand-dependent activation, and (III) Hedgehog signaling activation via crosstalk with other signaling cascades, such as EGFR or PI3K [238,239].

- **The Wnt signaling pathway.** It plays a vital role in cell migration, differentiation, and polarization during embryonic development. Wnt ligand can activate either the canonical β -catenin dependent or two β -catenin independent pathways, the planar cell polarity (PCP) pathway and Ca^{2+} Wnt pathway [244,245]. Dysregulation of this pathway contributes to tumorigenesis, metastasis, alterations in the cell cycle, and cell migration and is strongly related to the EMT process [246–249].

4.3. Novel Therapies Against Cancer Stem Cells

Eradication of CSCs is essential for effective cancer treatment, particularly for tumors that relapse after apparently successful therapy. Hence, different therapeutic strategies have been designed against this malignant population, such as drugs targeting CSC-associated surface markers or CSC-associated signaling pathways.

Monoclonal antibodies that target CSC-specific surface markers have emerged as promising therapies. For example, CX-2009 is an antibody-drug conjugate directed against CD166 and conjugated to DM4, a potent microtubule inhibitor. A first-in-human study of CX-2009 was conducted in patients with metastatic or locally advanced unresectable solid tumors (specifically, breast cancer, NSCLC, head and neck cancer, and ovarian cancer) with high CD166 expression and microtubule inhibitor sensitivity (NCT03149549). Disease stabilization was the most observed outcome, although some patients had a partial response [250]. A phase II clinical study has been initiated in patients with advanced metastatic breast cancer that expressed hormone receptors (NCT04596150). The treatment against CSC also focuses on the Notch, Hedgehog, and Wnt signaling pathways. For instance, Sonidegib, an SMO antagonist, showed encouraging results; thus, it was approved for locally advanced basal cell carcinoma that recurred after surgery or radiotherapy [251]. In patients with SCLC, the drug exhibited sustained PFS in patients with Sox2 amplification when combined with cisplatin and etoposide in a phase I study [252].

Despite the promising findings, multiple obstacles still need to be overcome to eradicate successfully CSCs [167]. For instance, CSCs from specific types of tumors have not been well identified [253]. Another example is that the survival of CSCs is related to a specific

microenvironment, which most studies do not consider as they isolate CSCs [254]. Additionally, anti-cancer therapy must consider cell metabolism or epigenetics, for example, due to its contribution to CSCs [255,256]. Thus, the research focused on this malignant population is crucial to obtain a definitive treatment.

5. Three-Dimensional (3D) Cell Culture

5.1. Origin and Development of Cell Culture

In vitro cell culture is a fundamental methodology in cell biology research because it allows the maintenance of cells outside of a living organism. *In vitro* cell culture is widely used in laboratories worldwide, enabling the study of cell behavior and biological mechanisms [257].

At the end of the 19th century, researchers started the first experiments related to *in vitro* cell culture to maintain living tissues and cells outside the organism. For instance, in 1882, Sidney Ringer succeeded in preserving the heartbeat of frog hearts outside their bodies using Ringer's solution, an established mixture of salts [258,259]. However, these experiments were conducted for only a few days. Hence, subsequent attempts were focused on extending the duration of *in vitro* cell culture and achieving cell division. In 1907, the modern cell culture was originated when Ross G. Harrison accomplished *in vitro* cell culture of frog nerve fibers and cell growth for several weeks [260]. Subsequently, the first immortalized animal cell line, the L strain, was created in 1943 [261], and the first immortalized human cell line, HeLa cells, was established in 1951 [262]. The creation of both cell lines promoted the use of *in vitro* cell culture and the establishment of different cell culture protocols.

Two-dimensional (2D) polystyrene supports are commonly used in cell-based assays because of their simplicity, high performance, cost-effectiveness, and reproducibility [263]. However, 2D cell culture systems have several limitations, including the lack of a three-dimensional (3D) structure that simulates the extracellular matrix (ECM). Therefore, more dependable and appropriate *in vitro* cell culture platforms are needed for cell biology research.

5.2. 3D Cell Culture

Under physiological conditions, cells are surrounded by ECM, a non-cellular physical support for the organization and expansion of cells to maintain morphogenesis and provide tissue homeostasis, integrity, and elasticity. It is mostly composed of fibrous-forming proteins such as collagen, fibronectin, elastin, glycoproteins, laminins, glycosaminoglycans, and proteoglycans. ECM is also a rich reservoir of growth factors and metabolic precursors. Moreover, ECM plays an essential role in several cellular processes, such as molecular signaling, morphology, differentiation, and proliferation [264,265]. Cancer cells also influence ECM deposition, degradation, and remodeling, thereby affecting tumor progression and invasiveness [266]. Therefore, monolayer cell cultures do not properly mimic the physiological architecture or microenvironment. Flat surfaces alter nutrient and oxygen distribution, apical-basal polarity, soluble gradients, cell morphology and proliferation, cell-cell and cell-matrix interactions, and signal transduction [263,267].

Animal models have also been employed in cancer research. Although they provide a realistic environment, these models are expensive, time-consuming, and inconsistent owing to variations among species, and their use is discouraged due to the 3R principle (Replacement, Reduction, and Refinement) [268]. Additionally, only 8% of drugs tested in animals remain in clinical trials and less than 5% of anti-cancer therapies are finally approved by the regulatory agencies [268,269]. Thus, the establishment of new models is required to address the inaccuracy among monolayer cell cultures, animal models, and clinical trials

Recently, researchers have reported different 3D *in vitro* cancer models to investigate cancer pathogenesis and new biomarkers and therapies in a more realistic environment [270]. Several 3D cell culture systems have been described, including cell-line spheroids [271], patient-derived organoids [272], hydrogels [273], tumor-on-chip [274], and biopolymeric structures [275], among others. Cells cultured on 3D cell culture change their cell proliferation and viability, genetic and protein expression, cellular responses to stimuli (i.e., anti-cancer drugs), or cell-cell interactions compared to 2D cell culture [267,276]. Moreover, researchers have discovered that mechanical signals induced by cell-generated physical forces cause changes in cell morphology, alignment, adhesion, migration, and differentiation [277].

More specifically, the scientific community has focused on translating tissue engineering technologies and concepts into cancer research. That has resulted in the fabrication of 3D structures using different biopolymeric materials through several additive manufacturing (AM) techniques, thus mimicking the ECM and achieving more physiological cell behavior.

5.3. Additive Manufacturing Techniques for the Fabrication of a Polymeric Scaffolds

5.3.1. Fused Filament Fabrication

Fused Filament Fabrication (FFF) is a 3D printing technique widely used in research because of its cost-effectiveness, a significant degree of flexibility in design, user-friendly, and high efficiency compared with traditional manufacturing processes. Moreover, the machine is compact and inexpensive [257,278]. This methodology was created in the late 1980s and Stratasys Inc. began marketing in the 1990s [279].

During the FFF process, the selected material, in a filament form, is predominantly melted and extruded by a heated nozzle. Then, successive layers are printed following a software-controlled path resulting in the designed scaffold, using computer-aided design (CAD) software, after cooling and solidification [281,282] (Figure 8). The FFF technique allows the rapid fabrication of 3D scaffolds with a medium resolution and good accuracy, and post-printing treatment is not required. This process is also low polluting because no solvents are needed. However, the process has some disadvantages, such as the high temperature required, rough surfaces, high porosity, the need for the material to be in filament form, or the difficulty of scale-up. In addition, depending on the geometry, the printing of support structures is required [281,283].

Generally, the width of the printed trajectory corresponds to the nozzle diameter (which ranges from 0.2 to 0.4 mm), and its height is equal to half of the breadth. However, these values can be modified owing to the properties of the selected material and/or by adjusting different printer parameters, such as the flow or infill density. The final resolution of the

Introduction

printed 3D scaffolds will be influenced by both the nozzle diameter and layer height [281,283].

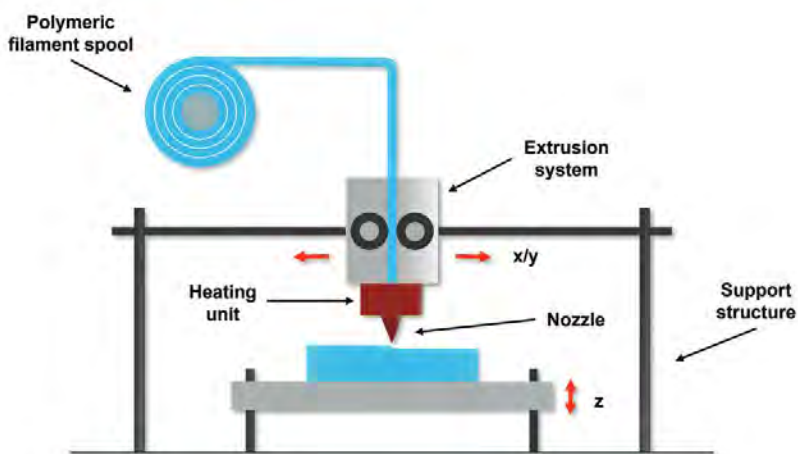


Figure 8. Schematic representation of fused filament fabrication (FFF) process. Extracted from Grivet-Branco *et al.*, *Macromol. Biosci.*, 2022 [280].

Different aspects related to this technique must be considered to avoid processing issues, such as:

- The mechanical properties of a 3D structure are correlated to the number of contours of the external wall of the scaffold and the infill pattern (e.g., linear or hexagonal) [281].
- The rheological properties of the materials (particularly viscosity, relaxation dynamics, and surface tension) influence the processability of FFF. Specifically, these properties affect the adhesion of the layer and intralayer, and consequently, the accuracy and resolution of 3D scaffolds [284,285].
- The thermal properties of materials affect the configuration of FFF parameters and are crucial for fiber reduction and deformation [284].

The most common applications of the FFF technique are tissue engineering and regenerative medicine [280], drug delivery systems in different forms (polypills, tablets, or films), medical devices [281], and the creation of 3D models for the study of several diseases, such as cancer [286].

5.3.2. Electrospinning

Electrospinning (ES) is a cost-effective, versatile, and simple technique used extensively for manufacturing micro- and nanofibers with continuous morphology, small fiber diameter, high surface area, and great flexibility [287,288]. The elements required to perform this process are a syringe pump, stainless-steel needle, high-voltage power supply (1-30 kV), and grounded collector [289,290] (Figure 9).

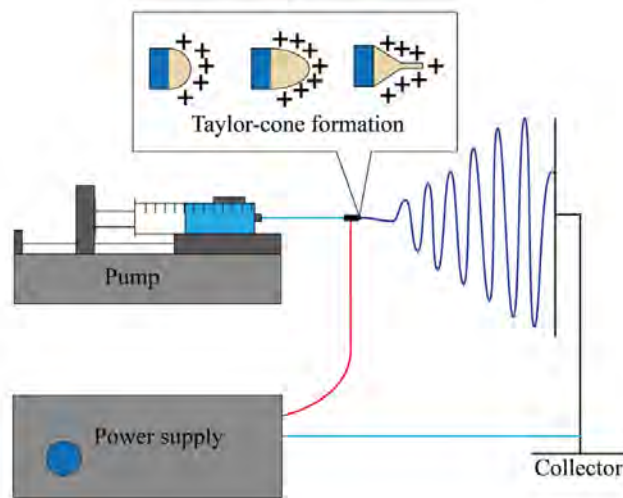


Figure 9. Schematic representation of a typical electrospinning (ES) machine. Extracted from Yan *et al.*, SN Applied Sciences, 2022 [290].

During the ES procedure, the polymer solution is expelled from the needle at a specific flow rate regulated by a syringe pump. The initially ejected solution has the shape of spherical

Introduction

droplets because of the surface tension. However, the high voltage between the metal needle and the collector generates an electrostatic repulsion that modifies the droplet from a spherical to a conical shape, forming the Taylor cone. The applied voltage has to surpass a threshold value and the fluid surface tension has to overcome by the electrostatic force. Consequently, a stable charged jet of the polymer solution is produced, and the filament is extended from the tip of the Taylor cone [289,291–293]. During this step, the charged jet rapidly solidifies and the resulting polymer fibers are deposited and collected by an electrically charged grounded collector maintained at an optimal distance. Hence, the ES technique generates 3D structures [294].

Polymer fiber's composition, properties, and structure can be customized by controlling the materials and number of variables. These variables directly affect the electrospinning process [295–299]:

- **The spinning conditions.** They involve the flow rate controlled by the pump, the distance between the emitter and collector, the intensity of the applied high voltage, and the geometry of the collector.
- **The polymer solution.** The process may be modified by the polymer concentration, selected polymer and solvent, conductivity and viscosity of the solution, surface tension, and polymer molecular weight.
- **The environmental conditions.** The temperature and humidity may also influence the electrospinning process.

Tissue engineering, wound dressing, and the study, diagnosis, and treatment of different diseases, such as cancer, are some of the applications of ES fibers, as reviewed in [290].

5.4. Materials Used to Manufacture Scaffolds

To date, more than 200 natural and synthetic materials have been employed to manufacture scaffolds. Among these, biodegradable polymers have a broad spectrum of biomedical applications in tissue engineering and regenerative medicine. Polycaprolactone (PCL) and

poly(lactic acid) (PLA) are examples of polyesters that have been used to manufacture scaffolds with both FFF and ES technologies [300].

5.4.1. Polycaprolactone

PCL is a thermoplastic polyester obtained via a polymerization method based on the ring-opening of ϵ -caprolactone monomers. Several polymerization techniques under various conditions have been described, resulting in the production of PCL with different molecular weights and polydispersity indices, which cause variations in mechanical strength and degradation behavior [301–303]. Because of the existence of amorphous regions, this non-hazardous polymer is semi-crystalline at physiological temperature and exhibits high elasticity and low tensile strength [280,300]. Regarding the solubility of PCL, it is very high in chloroform, carbon tetrachloride, or benzene, whereas it is less soluble in ethyl alcohol, acetone, or water [300,302,304].

PCL offers many advantages for its use as a biomaterial. It is biodegradable, biocompatible, and inexpensive. This synthetic polymer is also simple to produce blends, copolymers, and composites and is commercially accessible in medical grade [305–307]. The other properties and chemical structures of PCL are listed in Table 4. Its degradation is affected by several parameters, such as molecular weight, residual monomer concentration, and pH of the medium. Moreover, the degradation products of PCL do not remain in the body [306,308,309].

PCL has been previously selected in different investigations for the fabrication of scaffolds for 3D cell culture using the FFF methodology as well as the ES technique. Additionally, these PCL structures allowed the culture of different cell lines of both animal and human origin, including cancer cell models [310–315].

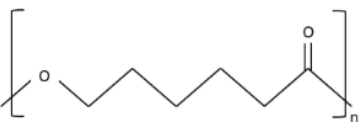
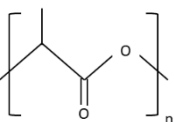
5.4.2. Poly(Lactic Acid)

PLA is an aliphatic polymer and an environmentally friendly material because it is created from renewable sources such as wheat, corn, sugars, and organic acids [316–318]. This

Introduction

thermoplastic polymer can be produced by ring-opening polymerization of cyclic lactide dimers using a catalyst or direct condensation polymerization of lactic acid monomers [319,320]. PLA has two enantiomers of lactic acid: poly(L-lactic acid) (PLLA) and poly(D-lactic acid) (PDLA). Hence, there are two pure homopolymers (PLLA and PDLA) and poly(D,L-lactic acid) (PDLLA), which have varying proportions of D and L monomers [321,322]. The mechanical properties of PLA depend on the distribution of these stereoisomers along the polymer chains and molecular weight. For example, the degree of crystallinity is higher for pure PLLA and PDLA. In contrast, PDLLA is amorphous, which directly affects the ultimate tensile strength, degradation time, and melting temperature (T_m) but not its glass transition temperature (T_g) (Table 4). Consequently, PDLLA is better processed via extrusion, molding, and casting [280,322]. Moreover, PLLA and PDLA are only soluble in benzene or dichloromethane at high temperatures, whereas PDLLA can be dissolved in several organic solvents, such as chloroform, acetone, or methylene chloride [323].

Table 4. Different characteristics of polycaprolactone (PCL) and poly(lactic acid) (PLA).

	Polycaprolactone (PCL)	Poly(lactic acid) (PLA)
Glass Transition Temperature (T_g) (°C)	-60	50 - 64
Melting Temperature (T_m) (°C)	60	130 - 250
Degradation Time (years)	2 - 3	2 - 8
General Chemical Structure		

PLA is probably the most commonly used polymer for biomedical applications (i.e., drug delivery, surgical instruments, tissue engineering, or scaffolding) because of its biodegradability, biocompatibility, safety, commercial availability of medical grade PLA, capacity to form blends and composites, and versatility. However, PLA has some

disadvantages: its price is higher than that of several non-biodegradable polymers, and it has low impact strength and toughness [320,324–326].

Although many studies have used PLA together with FFF technology for bone tissue engineering [327], to our knowledge, there is no literature regarding its use in 3D cancer cell cultures. However, FFF scaffolds have been tested using cancer cell models but manufactured using other materials [313,314]. Furthermore, PLA mixed with other materials, such as poly(γ -benzyl L-glutamate) (PBLG) or methoxypolyethylene glycol (mPEG)/poly(lactic-co-glycolic acid) PLGA, have been used to manufacture ES-scaffolds in to grow tumor-like structures with cancer cell lines [328,329].

5.5. The Study of Cancer Stem Cell Population Using 3D Cell Culture

As mentioned above, researchers have traditionally employed flat surfaces for cell culture. Monolayer culture does not adequately mimic the tumor microenvironment, as there is a lack of a matrix, resulting in changes in cell proliferation, gene and protein expression, among others [257,263,276]. 2D cell culture also causes CSC differentiation during cell propagation, losing the stemness behavior [330,331]. Additionally, this malignant population represents a very low percentage of tumors [170]. Therefore, new culture systems are required to allow the study of CSCs to identify new therapies or biomarkers. Previous studies have shown that polymeric structures are useful for the expansion of both normal and cancer stem cells. For example, Islami *et al.* demonstrated that PLLA-ES fibers coated with fibroin recreated an environment that allowed the proliferation of umbilical cord blood stem cells [332]. Sims-Mourtada *et al.* also reported the enrichment of breast CSCs using PCL/chitosan-ES fibers [331]. Furthermore, our research group previously demonstrated that PCL structures fabricated by FFF or ES techniques allowed the culture of breast CSCs and their expansion [312,314].

6. Fatty Acid Synthase

6.1. Lipid Metabolism in Cancer

Dysregulation of energy metabolism is a hallmark of cancer cells and supports their high growth and division [6]. Oncogenic events and the tumor microenvironment are responsible for these modifications in metabolic pathways [333]. Otto Warburg observed that cancer cells practically based their energy production on “aerobic glycolysis”, even in the presence of oxygen, due to the reprogramming of their glucose metabolism [334,335]. This process is energetically poor. However, it produces different glycolytic intermediates that are used in some biosynthetic pathways to generate new macromolecules and organelles required for the assembly of new cells [336,337]. Although most studies have focused on the dysregulation of carbohydrate metabolism, researchers have recently studied alterations in lipid metabolism in cancer cells.

Cancer cells obtain free fatty acids mostly via *de novo* synthesis. In the cytoplasm, excess citrate from the tricarboxylic acid (TCA) cycle is catalyzed to acetyl-CoA by ATP-citrate lyase (ACYL). Acetyl-CoA carboxylase (ACACA) then converts acetyl-CoA to malonyl-CoA. Fatty acid synthase (FASN) catalyzes the condensation of acetyl-CoA and malonyl-CoA into palmitate in a nicotinamide adenine dinucleotide phosphate hydrogen (NADPH)-dependent reaction [338]. Palmitates can be modified further to form more complex fatty acids. Generally, these lipogenic enzymes are overexpressed and/or hyperactivated in cancer cells [339].

The role of lipids in cancer is widely diverse because they are involved in cell proliferation, survival, migration, invasion, angiogenesis, tumorigenesis, tumor progression, and metastasis [340,341]. In addition to their structural function as part of the cell membrane, lipids play an essential role in the energy and redox homeostasis of cancer cells and the post-translational modification of proteins [340,341]. They also act as signaling molecules and second messengers and as specific binding sites for proteins in the cell membrane [341,342]. Lipids initiate various signal transduction pathways and are involved in autophagy, initiation of apoptosis, and growth arrest [341,343].

6.2. Fatty Acid Synthase Function

FASN is a 270 kDa multifunctional and homodimeric enzyme. Dimer formation is required for enzyme activation. FASN has seven catalytic domains: β -ketoacyl synthase (KS), malonyl/acetyl transferase (MAT), β -hydroxyacyl dehydratase (DH), enoyl reductase (ER), β -ketoacyl reductase (KR), acyl-carrier protein (ACP), and thioesterase (TE). The domains work together to generate palmitate, the final product of FASN, in an NADPH-dependent reaction [344,345] (Figure 10). FASN has three main domains: (I) contains KS, MAT, and DH; (II) includes ER, KR, and ACP; and (III) contains TE. The interdomain/core region between domains I and II is essential for dimer formation [344,345].



Figure 10. Linear structure of fatty acid synthase (FASN) domains: β -ketoacyl synthase (KS), malonyl/acetyl transferase (MAT), β -hydroxyacyl dehydratase (DH), enoyl reductase (ER), β -ketoacyl reductase (KR), acyl-carrier protein (ACP), and thioesterase (TE).

As previously mentioned, FASN catalyzes the final step of FA synthesis. Specifically, the MAT domain transfers the acetyl group (from acetyl-CoA) and malonyl group (from malonyl-CoA) to ACP, and then the KS domain generates the β -ketoacyl-ACP intermediate. Afterward, the β -carbon position is changed by the KR, DH, and ER domains to produce a saturated acyl group product with two extra carbon units, the substrate for the subsequent elongation reactions to obtain a 16-carbon fatty acid. Finally, the TE domain released fatty acids from ACP [346] (Figure 11).

Under normal conditions, fatty acids are obtained from the diet; therefore, *de novo* lipogenesis is negligible. FASN expression has been reported in neural stem cells, cerebral neurons, basket cells of the cerebellum, type II alveolar cells, adipocytes, sebaceous glands, hepatocytes, in the epithelium of the stomach, duodenum, and colon, corpus luteum,

Introduction

decidua, uroepithelium, epididymis, and hormone-sensitive cells from the breast, prostate, endometrium, anterior pituitary, adrenal cortex, seminal vesicles, and apocrine glands [347–351]. FASN expression is also essential for early embryo development and the production of milk components during lactation [352,353].

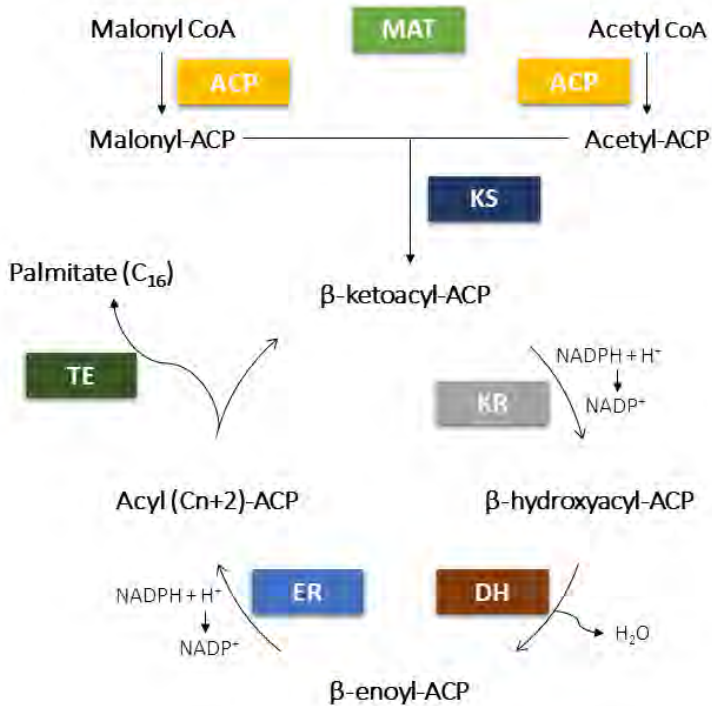


Figure 11. Role of each domain of fatty acid synthase (FASN) during the synthesis of fatty acids.

Nevertheless, cancer cells obtain fatty acids from both *de novo* lipogenesis and diet. FASN overexpression and/or hyperactivation have been frequently reported in several cancers, including lung, breast, colorectal, endometrial, and prostate cancers. It is associated with cancer progression, aggressiveness, and poor prognosis [354–359].

Focusing on lung cancer, several researchers found that FASN expression and activity were higher in tumor tissues than in normal lung tissues [360–362]. Visca *et al.* demonstrated that

FASN+ expression in stage I patients was associated with worse survival [354]. Furthermore, FASN+ expression was found in patients with vascular invasion or bone metastasis [363] and was associated with malignant grades of tumor cells [362]. However, none of these investigations considered mutations in oncogenes such as *EGFR* or *KRAS*.

6.3. Fatty Acid Synthase Regulation

The regulation of FASN expression is mainly controlled by PI3K/Akt and MAPK signaling pathways, which are triggered by growth factor receptors, such as EGFR or HER2. Moreover, the interaction between sex hormones, growth factors, and their receptors can increase FASN expression. PI3K/Akt and MAPK signaling transduction cascades activate the transcription of FASN through the expression of transcription factors such as sterol regulatory element binding protein-1c (SREBP-1c) [339,344]. Active SREBP-1c enters the nucleus and transcribes FASN by binding to the sterol regulatory elements within the FASN promoter [364].

Although the regulation of FASN expression by PI3K/Akt and MAPK signaling pathways is similar between normal and cancer cells, there are some differences. Nutritional and hormonal stimulations trigger the transcription of SREBP-1c in normal cells [365,366]. In contrast, cancer cells are insensitive to nutritional levels, and the transcription of SREBP-1c is controlled by abnormal growth factors and excessive steroid hormone signaling [344]. FASN stabilization by post-translational modifications to prevent its degradation also contributes to the high levels of FASN observed in tumors [367–369].

Other transcription factors also regulate FASN transcription in cancer, such as carbohydrate-activated transcription factor response element binding protein (ChREBP), NAC1, P300 acetyltransferase, and the ubiquitous nuclear transcription factor Y (NF-Y) [370–372].

In EGFRm NSCLC, EGFR is directly involved in the regulation of Akt/SREBP1/FASN to palmitoylate the receptor and localize it into the cell membrane in sensitive cells or the cytoplasm and nucleus in resistant cells. Moreover, EGFR palmitoylation is relevant to the growth and survival of resistant cells [373].

6.4. Fatty Acid Synthase Inhibition

Differences in the expression and activity of FASN between normal tissues and cancer cells have allowed researchers to develop different FASN inhibitors.

Several mechanisms have been proposed to identify the anti-cancer effect seen after FASN inhibition: lack of phospholipids for cell membranes, modification of lipid raft assembly impairing the proper localization and/or function of tyrosine kinase receptors (e.g., EGFR) at the cell membrane, inhibition of DNA replication, initiation of apoptosis in non-functioning p53 cancer cells, growth arrest in functioning p53 cells, accumulation of malonyl-CoA, which leads to the induction of pro-apoptotic genes, and inhibition of anti-apoptotic proteins (e.g., Akt) [374].

Cerulenin, a natural compound isolated from *Cephalosporium caerulens*, was reported as the first FASN inhibitor, binding irreversibly to the KS domain, and demonstrated effectiveness against several tumor cell lines and xenograft models [375–377]. However, cerulenin is highly reactive due to its cysteine-reactive epoxide groups and off-target activities. To address this issue, C75, a synthetic analog of cerulenin, was developed, which interacts with FASN in TE, KS, and ER domains [378]. C75 showed a great anti-cancer activity both *in vitro* and *in vivo*, but some side effects were observed, such as anorexia and severe body weight loss [379–382].

Orlistat is another FASN inhibitor widely studied. This drug is a reduced form of the natural product lipstatin, isolated from the *Actinobacterium Streptomyces toxytricini*. Although the compound was approved for the treatment of obesity, researchers found that it inhibited FASN activity by interacting with the TE domain [383,384]. Several studies have demonstrated anti-tumor activity both *in vitro* and *in vivo* [373,385]. Nevertheless, Orlistat exhibits some limitations that have hampered its progress in clinical trials, such as its instability, low solubility in water, and poor gastrointestinal absorption [386].

TVB-2640 was developed by Sagimet Biosciences. A phase I clinical trial of TVB-2640 in patients with solid tumors, including KRAS-mutated NSCLC, ovarian cancer, and breast cancer, was completed. The compound was administered as a daily oral dose and bound to FASN in the KR domain. TVB-2640 has demonstrated anti-tumor effects alone and in

combination with paclitaxel, with non-serious and reversible side effects [387]. Currently, this compound is in phase II clinical trials for metastatic HER2+ breast cancer (NCT03179904), KRAS^m NSCLC (NCT03808558), resectable colon cancer (NCT02980029), and astrocytoma (NCT03032484).

(-)-epigallocatechin-3-gallate (EGCG) is a polyphenolic compound extracted from green tea. This natural FASN inhibitor competes with NADPH for the binding to the KR domain of the enzyme [388]. Different researchers have reported its cytotoxic effect *in vitro* and *in vivo* in a wide range of cancers [381,382,389]. EGCG also exhibited synergistic effects when combined with other anti-cancer therapies [390,391]; it has activity against cancer stem cells [392,393], increased chemotherapy efficacy by changing the microenvironment and microvasculature [394], and did not show side effects, such as body weight loss [395]. Because of the low bioavailability and limited stability of EGCG under physiological conditions, several synthetic derivatives have been developed, such as G28 [396–398]. The G28 compound has been extensively investigated in both sensitive and resistant breast cancer cells. The compound demonstrated strong FASN activity inhibition, an anti-tumor effect both *in vitro* and *in vivo*, alone or in combination with other treatments, and activity against cancer stem cells [391–393,399].

Hypothesis and Objectives

Hypothesis

The generation of a 3D cell culture system using an optimal fabrication technique and materials allows cells from aggressive cancers, such as TNBC and EGFRm NSCLC, to behave more physiologically and expand the CSC population. Additionally, FASN inhibition is a new therapeutic strategy for sensitive and resistant EGFRm NSCLC cells and CSCs niche.

Objectives

The main objective of this thesis was the evaluation of various types of *in vitro* 3D cell culture for the study of the CSC population and the inhibition of FASN as different approaches for the study and treatment of aggressive cancers.

Three specific objectives were stated to achieve the main objective:

1. Evaluation of poly(lactic acid) (PLA) scaffolds for 3D cell culture of breast CSCs (BCSC)

- Determine the influence of different manufacturing parameters of FFF technology on cell adhesion and proliferation of the MDA-MB-231 TNBC cell model following the experiment design via the Taguchi method.
- Select the optimal PLA-FFF scaffold designs, verify their suitability for cell adhesion and proliferation, and analyze the capacity to enrich BCSCs using the MDA-MB-231 cell model.
- Characterize the microstructure of PLA scaffolds manufactured by ES technology and evaluate cell adhesion and proliferation of the MDA-MB-231 cell model cultured on PLA-ES scaffolds.
- Assess a possible BCSC enrichment of the MDA-MB-231 cell model cultured on PLA-ES scaffolds through mammosphere forming capacity and gene expression of BCSC-related markers.

2. Evaluation of polycaprolactone (PCL) scaffolds manufactured by ES technology for 3D cell culture of lung CSCs (LCSC)

- Perform a thermal characterization of PCL-ES scaffolds through thermogravimetric analysis (TGA), differential scanning calorimetry (DSC), and dynamic mechanical analysis (DMA).
- Characterize the microstructure of PCL-ES scaffolds by scanning electron microscopy (SEM) images.
- Study the effect of the sterilization process and medium soaking on PCL-ES scaffolds.
- Examine possible changes in cell morphology of sensitive and resistant EGFRm NSCLC cell models, PC9 and PC9-GR3 cells, cultured on PCL-ES scaffolds.
- Evaluate cell viability of EGFRm NSCLC cell models cultured on PCL-ES scaffolds.
- Determine EGFR status of EGFRm NSCLC cell models cultured on PCL-ES scaffolds.
- Assess a possible LCSC enrichment of EGFRm NSCLC cell models cultured on PCL-ES scaffolds by resistance to the treatment, and gene and protein expression of multi-drug efflux pumps, EMT and stemness markers, membrane receptors, and Hedgehog and Canonical pathways.
- Validate *in vitro* results through the evaluation of CD133 and Vimentin tumor expression of samples from patients with EGFRm NSCLC.

3. Inhibition of FASN as a new therapeutic strategy for the treatment of EGFRm NSCLC

- Determine gene and protein expression of FASN in sensitive and resistant EGFRm NSCLC cell models.
- Evaluate cytotoxic effect and the capacity to inhibit FASN activity of EGCG, a synthetic derivative of EGCG, G28, and a novel synthetic compound, AZ12756122 in sensitive and resistant EGFRm NSCLC cell models.

- Analyze the molecular effect caused by FASN inhibition on FASN, EGFR, STAT3, AKT/PRAS40, and MAPK pathways in sensitive and resistant EGFRm NSCLC cell models, alone and in combination with EGFR-TKIs.
- Assess FASN inhibition as a therapeutic strategy against LCSCs in sensitive and resistant EGFRm NSCLC cell models.
- Validate *in vitro* results through the evaluation of FASN tumor expression of samples from patients with EGFRm NSCLC.

Results I. Evaluation of PLA scaffolds for 3D cell culture of
BCSCs

This section is based on the following publications:

Title	Screening of Additive Manufactured Scaffolds Designs for Triple Negative Breast Cancer 3D Cell Culture and Stem-Like Expansion
Authors	Emma Polonio-Alcalá, Marc Rabionet, Antonio J. Guerra, Marc Yeste, Joaquim Ciurana*, and Teresa Puig*
Journal	International Journal of Molecular Sciences
Publication Year	2018
Impact Factor ²⁰¹⁸	4.183 (Q2 in Biochemistry & Molecular Biology; Position 78 of 299)
DOI	10.3390/ijms19103148

Title	PLA Electrospun Scaffolds for Three-Dimensional Triple-Negative Breast Cancer Cell Culture
Authors	Emma Polonio-Alcalá†, Marc Rabionet†, Xavier Gallardo, David Angelats, Joaquim Ciurana, Santiago Ruiz-Martínez*, and Teresa Puig*
Journal	Polymers
Publication Year	2019
Impact Factor ²⁰¹⁹	3.426 (Q1 in Polymer Science; Position 16 of 89)
DOI	10.3390/polym11050916

Abstract

This chapter aimed to evaluate PLA as a material for manufacturing scaffolds for 3D cell culture and BCSC enrichment.

First, PLA scaffolds fabricated using FFF were tested. Following the Taguchi experimental design, the effect of different fabrication parameters (*layer height, infill density, infill pattern, infill direction, and flow*) on 3D cell growth was investigated using the MDA-MB-231 TNBC cell model through the MTT assay. Moreover, the BCSC population cultured on the optimal PLA-FFF structures was determined using the ALDEFLUOR™ assay. Subsequently, PLA scaffolds fabricated using ES were assessed. Two PLA concentrations, 12 and 15%, were used for the manufacturing. The microarchitectures were characterized through SEM images. The MDA-MB-231 cell model was also used to evaluate 3D cell growth and BCSC enrichment of cells cultured on PLA-ES structures. Concretely, BCSCs were quantified by mammosphere-forming capacity and gene expression of BCSC-related markers.

Regarding the results obtained with the PLA-FFF platforms, 27 different configurations were manufactured according to the Taguchi experimental design. *Infill density* and *infill direction* significantly influence cell growth, with optimal values of 70% and 45°, respectively. Three more scaffold configurations (named SS) were designed and fabricated using these optimal parameters, differing in their infill patterns (zigzag, triangles, and grid). The SS1 scaffold exhibited the highest cell growth, confirming the findings obtained with the Taguchi experimental design. Furthermore, cells cultured on SS1 matrices showed a higher ALDH+ population at short culture times than 2D-cultured cells. This feature is directly related to BCSCs.

Regarding the results obtained with the PLA-ES scaffolds, few differences were observed in filament diameter, porosity, and pore area between both PLA-ES structures. Consequently, no differences in cell growth were observed between the 12%- and 15%-PLA-ES structures. Thus, 15%-PLA-ES scaffolds were selected for the following experiments. *EGFR* gene expression and phosphorylation levels were lower in MDA-MB-231 cells cultured in 3D culture, whereas STAT3 phosphorylation levels were upregulated. Mammosphere formation also tended to increase in 3D-cultured cells. Although no differences in EMT-related gene expression were found, there was a significant increase in *SOX2* expression after 3 days of

Results I

culture in PLA-ES scaffolds. Therefore, the 15%-PLA-ES scaffolds did not show significant enrichment of BCSCs.



Article

Screening of Additive Manufactured Scaffolds Designs for Triple Negative Breast Cancer 3D Cell Culture and Stem-Like Expansion

Emma Polonio-Alcalá^{1,2}, Marc Rabionet^{1,2}, Antonio J. Guerra², Marc Yeste³,
Joaquim Ciurana^{2,*} and Teresa Puig^{1,*}

¹ New Therapeutic Targets Laboratory (TargetsLab)—Oncology Unit, Department of Medical Sciences, Faculty of Medicine, University of Girona, Emili Grahit 77, 17003 Girona, Spain; emma.polonio@udg.edu (E.P.-A.); m.rabionet@udg.edu (M.R.)

² Product, Process and Production Engineering Research Group (GREP), Department of Mechanical Engineering and Industrial Construction, University of Girona, Maria Aurèlia Capmany 61, 17003 Girona, Spain; antonio.guerra@udg.edu

³ Biotechnology of Animal and Human Reproduction (TechnoSperm), Department of Biology, Institute of Food and Agricultural Technology, University of Girona, Pic de Peguera 15, 17003 Girona, Spain; marc.yeste@udg.edu

* Correspondence: quim.ciurana@udg.edu (J.C.); teresa.puig@udg.edu (T.P.); Tel.: +34-972-418265 (J.C.); +34-972-419628 (T.P.)

Received: 10 September 2018; Accepted: 11 October 2018; Published: 12 October 2018



Abstract: Breast cancer stem cells (BCSCs) are tumor-initiating cells responsible for metastasis and tumor reappearance, but their research is limited by the impossibility to cultivate them in a monolayer culture. Scaffolds are three-dimensional (3D) cell culture systems which avoid problems related with culturing BCSC. However, a standardized scaffold for enhancing a BCSC population is still an open issue. The main aim of this study is to establish a suitable poly (lactic acid) (PLA) scaffold which will produce BCSC enrichment, thus allowing them to be studied. Different 3D printing parameters were analyzed using Taguchi experimental design methods. Several PLA scaffold architectures were manufactured using a Fused Filament Fabrication (FFF) 3D printer. They were then evaluated by cell proliferation assay and the configurations with the highest growth rates were subjected to BCSC quantification by ALDH activity. The design SS1 (0.2 mm layer height, 70% infill density, Zigzag infill pattern, 45° infill direction, and 100% flow) obtained the highest proliferation rate and was capable of enhancing a ALDH+ cell population compared to 2D cell culture. In conclusion, the data obtained endorse the PLA porous scaffold as useful for culturing breast cancer cells in a microenvironment similar to *in vivo* and increasing the numbers of BCSCs.

Keywords: 3D printing; three-dimensional cell culture; scaffolds; PLA; TNBC; breast cancer stem cells

1. Introduction

Breast cancer is the most commonly diagnosed cancer and the second cause of cancer death among women [1]. Triple negative breast cancer (TNBC) is characterized by the lack of estrogen and progesterone receptors and no overexpression of human epidermal growth factor receptor-2 [2]. It accounts for 15–20% of the patients diagnosed with breast cancer [3]. TNBC is very aggressive and has a poor prognosis due to the young age of the patients, its high metastasis and relapse incidence and its higher mortality in comparison with the other breast cancer subtypes [4]. Cytotoxic chemotherapy is the main treatment against TNBC owing to the lack of a validated targeted therapy [5]. Cancer stem cells (CSCs) are a tumor-initiating subpopulation responsible for tumor recurrence as a result of

their resistance to the anti-cancer therapy [6–9]. They share similar features with normal stem cells, such as the ability to self-renew and generate the bulk of the tumor [10]. CSCs have the capacity to grow in suspension where they form spheres and they also have an enhanced activity of the aldehyde dehydrogenase (ALDH) enzyme [11,12]. Hence, a breast cancer stem cell (BCSC) population could become a potential target for breast cancer treatment, and in particular, the TNBC subtype.

Traditionally, cells are cultivated on two-dimensional (2D) supports, however these supports modify the shape of the cell, and consequently, gene expression and protein regulation are altered compared with cells surrounded by a physiological environment [13,14]. In vivo, the extracellular matrix (ECM), which is a three-dimensional (3D) structure composed of fibrous proteins and molecules, surrounds cells and plays a key role in cell regulation [15]. For that reason, 3D cell culture systems such as scaffolds, have emerged as an alternative to mimicking in vivo cell conduct, thus making experiment results more reliable [16]. Different methodologies exist for manufacturing these structures. For instance, fused filament fabrication (FFF) is an additive manufacturing (AM) technique where a 3D printer melts and deposits the material in successive layers [17]. The porous scaffolds obtained allow seeded cells to adopt their natural morphology and interact with their adjacent cells in a 3D tissue-like environment [16]. While a wide range of materials has been employed, it is biopolymers that are extensively used for 3D cell culture [16,18]. Poly (lactic acid) (PLA) is an ideal biopolymer for biomedical and cell culture applications thanks to its biocompatibility, safe degradation products, high strength, and good blend-compatibility with others polymers [19–21], and as such, has been used for porous scaffolds [21].

While there is considerable interest in BCSC population, its study is limited because 2D culture induces their differentiation during cell propagation, losing their stem properties [22,23], as well as their low representation within the tumor [24,25]. The environment may also influence the CSC differentiation state [22,26]. 3D culture systems, like scaffolds, offer a physical structure that mimics the in vivo environment and overcomes the problems related to BCSC culture. Moreover, researchers have demonstrated that scaffolds produce an enrichment of this malignant subpopulation, thus facilitating its investigation [23,27,28].

Despite the research that has already been carried out in this field, many concerns remain and manufacturing a 3D scaffold with the appropriate properties to achieve optimal BCSC enrichment is still an open issue. As the printing procedure involves many input parameters, this complicates the settings of all the variables. Therefore, this current work aims to analyze the most important parameters through a robust design of experiment method known as the Taguchi method. Different 3D printing parameters-layer height, infill density, infill pattern, infill direction, and material flow-were studied. Several PLA scaffold designs were fabricated with a FFF 3D printer and then evaluated through a cell proliferation assay using MDA-MB-231 triple negative breast carcinoma cells. The architectures with the highest growth rates were subjected to BCSC quantification. The data obtained supports the idea that PLA porous scaffold are useful for culturing and proliferating breast cancer cells in a microenvironment that preserves stemness and increase the BCSC subpopulation in a short timeframe.

2. Results

2.1. PLA Scaffolds Production and Characterization

To accommodate an optimal three-dimensional cell culture, the main aim was to develop a scaffold architecture which affords a high breast cancer cell proliferation rate. For this purpose, several values of the selected parameters (layer height, infill density, infill pattern, infill direction, and flow) were tested to find the optimal ones. Using the Taguchi experimental design method, twenty-seven scaffold configurations were manufactured and then analyzed (Table 1). To perform the characterization and cell proliferation assays, at least ten copies of each configuration were printed.

As shown in Figure 1, different scaffold typologies were manufactured. Some of them had a regular pattern and their pores had similar areas, for example, designs 10 or 22, while others, for example, configurations 6 or 14, had a non-regular pattern with pores of different areas.

To study the microscopic architecture of the scaffolds produced, only the top side was analyzed by optical microscopy because the first printed layer (on the bottom) was different from the rest of layers. Generally, the filament diameter was a little bigger and irregular because of flattening.

Table 1. Design and process parameters of PLA scaffold configurations resulting from Taguchi experimental design.

Configuration	Layer Height (mm)	Infill Density (%)	Infill Pattern	Infill Direction (°)	Flow (%)
1	0.10	50	Zigzag	45	80
2	0.10	50	Zigzag	45	90
3	0.10	50	Zigzag	45	100
4	0.10	60	Grid	60	80
5	0.10	60	Grid	60	90
6	0.10	60	Grid	60	100
7	0.10	70	Triangles	90	80
8	0.10	70	Triangles	90	90
9	0.10	70	Triangles	90	100
10	0.15	50	Grid	90	80
11	0.15	50	Grid	90	90
12	0.15	50	Grid	90	100
13	0.15	60	Triangles	45	80
14	0.15	60	Triangles	45	90
15	0.15	60	Triangles	45	100
16	0.15	70	Zigzag	60	80
17	0.15	70	Zigzag	60	90
18	0.15	70	Zigzag	60	100
19	0.20	50	Triangles	60	80
20	0.20	50	Triangles	60	90
21	0.20	50	Triangles	60	100
22	0.20	60	Zigzag	90	80
23	0.20	60	Zigzag	90	90
24	0.20	60	Zigzag	90	100
25	0.20	70	Grid	45	80
26	0.20	70	Grid	45	90
27	0.20	70	Grid	45	100

The results observed for PLA scaffold characterization (Table 2) were as expected. In general, the filament diameter was approximately 0.3 mm in all designs because of the 0.3 mm nozzle chosen and the very similar flow rate (80–100%). Also, it was observed when the quantity of printed material increased, the pore area decreased, while the filament diameter was enlarged.

Moreover, small pore areas were reached, with average values between 0.040 and 0.402 mm². However, some configurations showed bigger pore areas greater than 1 mm². Concrete examples of this are architectures 10, 11, and 12 (50% infill density, grid pattern, and 90° direction) and 19, 20, and 21 (50% infill density, triangles pattern, and 60° direction).

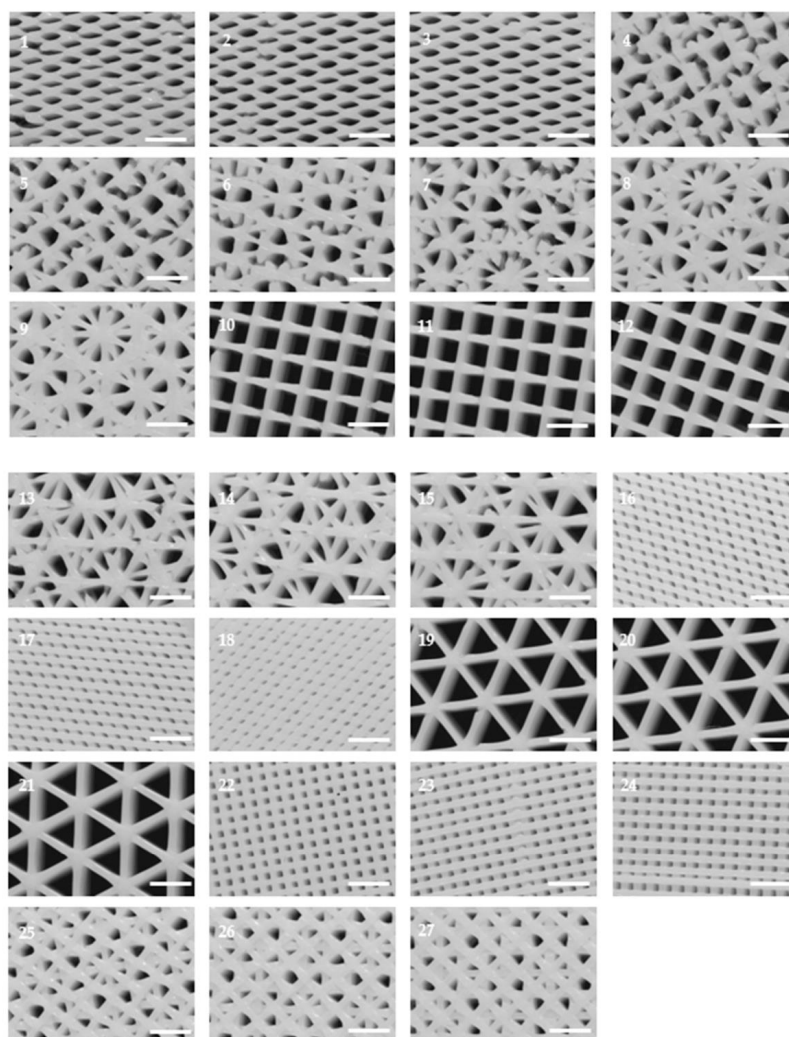


Figure 1. Microscopic characterization of PLA scaffold configurations. Top side was visualized under an optical microscope and images were used to calculate pore area and filament diameter. (Scale bar: 2 mm).

Table 2. Pore area (mm²) and filament diameter (mm) values of each PLA scaffold configuration obtained from scaffold image analyses.

Configuration	Pore Area (mm ²)	Filament Diameter (mm)
1	0.353 ± 0.010	0.243 ± 0.006
2	0.337 ± 0.009	0.301 ± 0.009
3	0.301 ± 0.006	0.331 ± 0.007
4	0.402 ± 0.025 (Irregular Pores; From 0.055 to 0.753)	0.287 ± 0.007
5	0.384 ± 0.032 (Irregular Pores; From 0.065 to 0.794)	0.294 ± 0.010
6	0.361 ± 0.031 (Irregular Pores; From 0.047 to 0.748)	0.338 ± 0.012
7	0.263 ± 0.021 (Irregular Pores; From 0.029 to 0.550)	0.348 ± 0.011
8	0.240 ± 0.017 (Irregular Pores; From 0.081 to 0.505)	0.359 ± 0.010
9	0.197 ± 0.018 (Irregular Pores; From 0.044 to 0.546)	0.367 ± 0.007
10	1.376 ± 0.013	0.298 ± 0.008
11	1.322 ± 0.009	0.341 ± 0.007
12	1.216 ± 0.010	0.378 ± 0.008
13	0.365 ± 0.034 (Irregular Pores; From 0.065 to 0.825)	0.334 ± 0.013
14	0.335 ± 0.031 (Irregular Pores; From 0.054 to 0.786)	0.354 ± 0.015
15	0.296 ± 0.032 (Irregular Pores; From 0.054 to 0.715)	0.370 ± 0.011
16	0.074 ± 0.002	0.332 ± 0.007
17	0.069 ± 0.002	0.348 ± 0.007
18	0.041 ± 0.002	0.408 ± 0.007
19	1.736 ± 0.029	0.329 ± 0.007
20	1.714 ± 0.027	0.340 ± 0.004
21	1.611 ± 0.025	0.374 ± 0.008
22	0.125 ± 0.003	0.295 ± 0.005
23	0.098 ± 0.002	0.312 ± 0.005
24	0.090 ± 0.002	0.338 ± 0.005
25	0.202 ± 0.019 (Irregular Pores; From 0.039 to 0.437)	0.364 ± 0.011
26	0.187 ± 0.018 (Irregular Pores; From 0.029 to 0.390)	0.373 ± 0.014
27	0.180 ± 0.016 (Irregular Pores; From 0.046 to 0.381)	0.394 ± 0.014

2.2. Cell Proliferation Assay

2.2.1. Selecting the Optimal Values for Each Parameter Tested

Once all the configurations had been printed, a cell proliferation assay was performed for all the architectures to select the scaffolds that provide optimal cell growth rates, as depicted in Figure 2. The cell proliferation that was obtained in 3D cell culture was then normalized to the growth rate exhibited for 2D cell culture. This characterization was required to evaluate whether scaffolds could be used for BCSC experiments or not, as having enough cells attached with which to perform these experiments is a mandatory requirement. Hence, MDA-MB-231 cells were cultured for three days on 2D adherent surfaces and on PLA scaffolds. Results were then analyzed using Quantum XL software.

As seen in Figure 2, architectures with larger pore areas obtained the lowest cell proliferation rates (for instance, 10, 11, and 12), whereas design 18, which had the smallest average pore area, presented the highest proliferation. Scaffolds with irregular pore areas also had good cell proliferation rates, for example, architectures 4 and 25.

In Figure 3, the results obtained indicated that infill density and infill direction parameters had a significant influence on cell proliferation with the optimal tested values being 70% (designs 7–9, 16–18, and 25–27) and 45° (designs 1–3, 13–15, and 25–27), respectively.

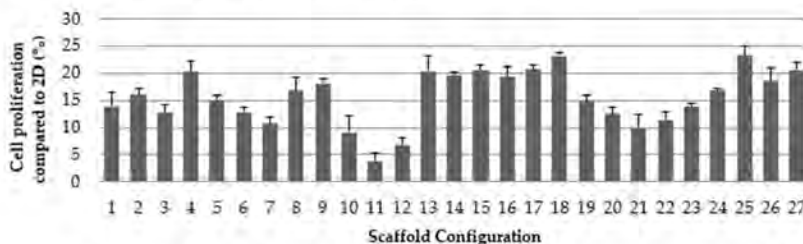


Figure 2. MDA-MB-231 cell proliferation for each PLA scaffold configuration (3D) as compared to a two-dimensional surface (2D) ($n = 3$).

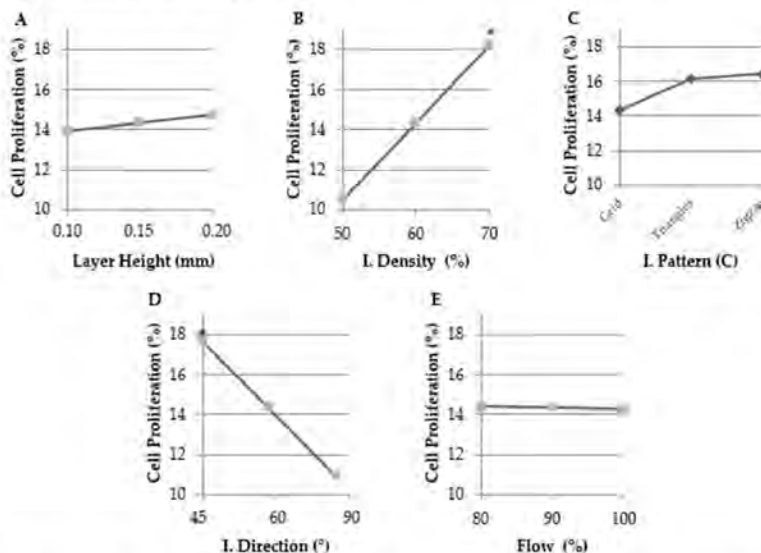

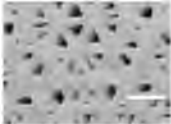


Figure 3. Main effect plots for each parameter on cell proliferation rate obtained through Quantum XL software. (A) Layer height. Samples printed with 60% infill density, grid infill pattern, 60° infill direction and 90% flow. (B) Infill density. Samples printed with 0.15 mm layer height, grid infill pattern, 60° infill direction, and 90% flow. The value of 70% significantly increased cell proliferation. (C) Infill pattern. Samples printed with 0.15 mm layer height, 60% infill density, 60° infill direction, and 90% flow. Zigzag pattern showed a light trend to obtain a higher proliferation rate. (D) Infill direction. Samples printed with 0.15 mm layer height, 60% infill density, grid infill pattern, and 90% flow. The value of 45° significantly increased cell proliferation. (E) Flow. Samples printed with 0.15 mm layer height, 60% infill density, grid infill pattern, and 60° infill direction. Significant differences are indicated as * ($p < 0.05$).

Therefore, three more scaffold configurations, called SS (selected scaffold), were designed and synthesized with the previously determined optimal value parameters but differing in pattern (see Table 3). The main aim of these new structures was to develop a scaffold with optimal value

parameters that would reach a maximum cell growth rate. The value selected for layer height was 0.2 mm thanks to its positive trend. Despite its negative tendency, the chosen flow parameter value was 100% because printing at 100% flow presented fewer difficulties than at 80%, which caused some issues like nozzle obstruction, etc. However, the SS3 scaffold design was not printed because the selected values were the same as those for configuration 27, which had already been tested.

Table 3. Scaffold configurations resulting from the Taguchi experimental design analysis. (Scale bar: 2 mm).

Configuration	Selected Values	Pore Area (mm ²)	Filament Diameter (mm)	Microscopic Image
SS1	Layer Height: 0.2 mm Infill Density: 70% Infill Pattern: Zigzag Infill Direction: 45° Flow: 100%	0.054 ± 0.002	0.483 ± 0.009	
SS2	Layer Height: 0.2 mm Infill Density: 70% Infill Pattern: Triangles Infill Direction: 45° Flow: 100%	0.224 ± 0.020 (Irregular pores: From 0.041 to 0.491)	0.387 ± 0.010	

2.2.2. Selected Value Verification and Final Selection of the Optimal Designs

At least ten copies of the new scaffold configurations SS1 and SS2 were printed and a cell proliferation assay was also performed for MDA-MB-231 cells following the same methodology as that used for the other 27 architectures.

As expected from the results for pattern, the SS1 scaffold configuration had an increased cell proliferation rate compared to SS3 (same design as 27), and significantly, to SS2. These results, shown in Figure 4, verified the Taguchi experimental design.

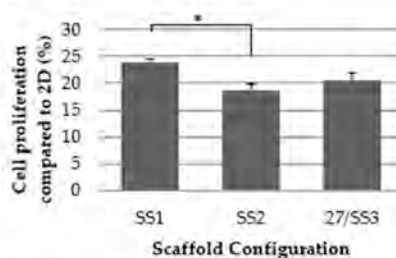


Figure 4. MDA-MB-231 cell proliferation assay of PLA scaffold configurations SS1, SS2 and 27/SS3 (3D) compared to two-dimensional surface (2D) ($n = 3$). Significant differences are indicated as * ($p < 0.05$).

The main objective here was to manufacture a scaffold that provided a high cell growth rate to further obtain BCSC enrichment. It is important to emphasize that, while a high proliferation rate does not mean a high proportion of BCSCs, the enrichment of this malignant subpopulation is required for their study. The more cells there are attached to the scaffold, the easier it will be to perform enrichment experiments. If a particular scaffold produces a good enrichment, a high absolute number of BCSCs will be collected. Consequently, those scaffold designs with an average cell proliferation rate $\geq 23\%$ and a SE $\leq 2\%$ were chosen. Following this criterion, configurations SS1, 18 and 25 were selected and

are presented in Figure 5. Cells grown on 2D surfaces were extended in contrast with the 3D-cultured cells which appeared more rounded and smaller.

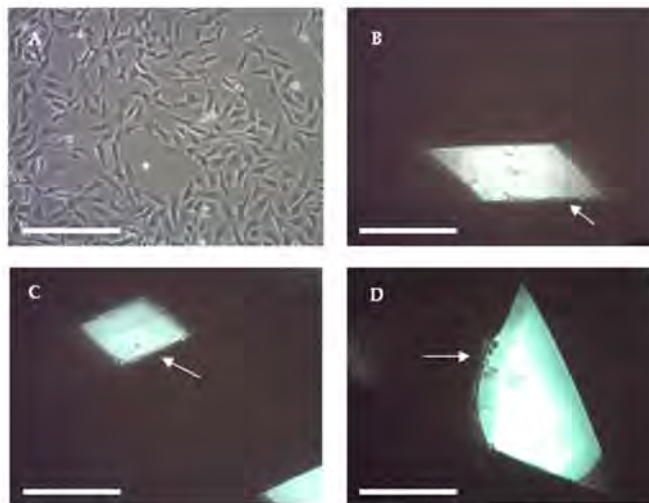


Figure 5. Optical microscope images of MDA-MB-231 cells attached to scaffold walls. (A) MDA-MB-231 cells on a 2D cell culture. (B) Cells attached to the SS1 configuration scaffold. (C) MDA-MB-231 cells attached to scaffold configuration 18. (D) Cells attached to scaffold configuration 25. White arrows indicate cells adhered to PLA filaments. Images from optical microscopy 100 \times . Scale bar: 0.25 mm.

2.3. Aldehyde Dehydrogenase Activity

Aldehyde dehydrogenases is a family of enzymes involved in aldehyde metabolism and the oxidation of exogenous and endogenous aldehydes into carboxylic acids [29]. Aldehyde dehydrogenase 1 (ALDH1) is considered to be an internal marker for stem and progenitor cells [12] and is used to isolate and identify CSCs [30]. ALDH1 is highly expressed in different types of cancer, including breast [31–33]. ALDEFLUOR™ assay is a commercial test employed to identify and isolate CSCs of different types of cancers.

MDA-MB-231 cells were cultured for 3 and 6 days on 2D adherent surfaces and on selected PLA scaffold configurations (SS1, 18, and 25). ALDEFLUOR™ assay was performed to test if 3D cell culture increased ALDH+ cell population.

As shown in Figure 6, the SS1 architecture significantly enriched the ALDH+ cell population compared to the 2D control after three days of culture. Scaffold configuration 18 exhibited a tendency to increase the ALDH+ population as compared to the 2D control, whereas design 25 presented a population reduction trend. In contrast, during six culture days, none of the architectures significantly increased the ALDH+ cell population compared to the monolayer cells. Designs 18 and 25 had a slight tendency to increase ALDH+ population, whereas SS1 decreased it. Therefore, these results show that the SS1 scaffold could be a useful tool to enrich ALDH+ populations in short culture timeframes. ALDH activity increase indicated an expansion in the BCSCs population, making the SS1 scaffold a good support for BCSCs study.

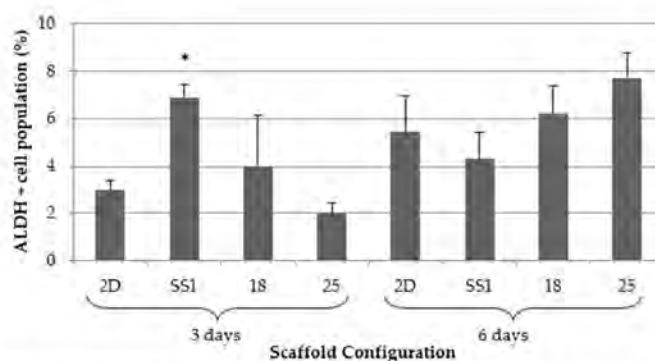


Figure 6. ALDEFLUO™ assay results for three scaffold selected architectures and 2D control for 3 and 6 days. (*) Denotes significant ($p < 0.05$) differences between scaffold culture and 2D sample ($n = 3$).

3. Discussion

BCSCs are a small population implicated in cancer recurrence, metastasis, and chemoresistance. New therapeutic approaches need to be found, but researchers have experienced difficulties in doing so because of their low representation in the tumor and traditional 2D cultures causes. Hence, 3D scaffolds appear to be a suitable alternative in which to culture and enrich this malignant subpopulation because they can mimic the physiological cell environment.

PLA porous scaffolds were used to culture MDA-MB-231 triple negative breast cancer cells. Five parameters—layer height, infill density, infill pattern, infill direction, and flow—were analyzed to obtain a scaffold design that would be able to provide high cell proliferation. Twenty-seven different configurations were manufactured with a 3D printer following the Taguchi experimental design method. Some designs obtained smaller pore areas (less than 0.1 mm^2) than other architectures with pore areas above 1 mm^2 . Besides this, some configurations had regular patterns with similar pore size, whereas others had non-regular patterns and irregular pores. Pore structure is an important characteristic to consider because it is directly related to cell growth and migration, nutrient flow, or vascularization [34].

TNBC cells were cultivated on 3D structures for three days and 2D cell culture was used as the control because the plastic dish is the main system used to cell culture in worldwide laboratories. All 3D configurations showed less cell proliferation than 2D cultures did. This is in line with previous studies [35,36]. Some investigations explained that cells can survive longer in 3D culture because of their slow growth, their migration through the pores and growth in the layers [36,37]. Ye et al. manufactured mineralized polyvinyl alcohol scaffolds and observed that MDA-MB-231 cells had higher proliferation in scaffolds with smaller pores [38]. Xiong et al. synthesized bacterial cellulose scaffolds and MDA-MB-231 cells showed a greater attachment, growth, proliferation, and spreading over those scaffolds with a diameter pore greater than $100 \mu\text{m}$ [34]. Our results have showed that the scaffold with the largest pores had a lower cell proliferation than the scaffolds with the smallest pores, which is in agreement with previous research [34,38]. Proliferation rate results were analyzed using Quantum XL software and the infill density and direction parameters that had a significant influence on cell proliferation were the optimal tested values of 70% and 45°, respectively. These results represented that proliferation was greater when cells had more available material and corners to attach to and grow on. It was described that scaffold geometry affects cell seeding and proliferation and must be optimized for each cell type [39]. Sobrat et al. demonstrated that orientation and layout of filament are significantly important for biological experiments. Moreover, they observed that cell seeding efficiency improves with stepped filament [40]. New designs with the optimal tested values

were manufactured and the highest proliferation was obtained with the SS1 configuration, followed by configurations 18 and 25. These three architectures were selected to evaluate BCSC enrichment.

It was demonstrated that 3D printed PLA scaffold enhanced ALDH activity, which is used to identify a CSC niche. After three days of 3D culture, the SS1 configuration significantly increased the ALDH+ cell population when compared to the monolayer cells. These results indicated that scaffolds avoid differentiation of BCSC population. This could be the result of a cytoskeleton reorganization because of culture cells in a 3D system [22]. Interestingly, Rabiomet et al. and Feng et al. demonstrated that poly(ϵ -caprolactone) (PCL) electrospun scaffolds also increased ALDH+ niche, but that was after six days culturing with scaffolds [28,37]. Florczyk et al. manufactured chitosan and sodium alginate scaffolds and after 15 days of 3D culture, the structures promoted CSC-like cell growth [35]. Therefore, 3D printed PLA scaffolds can enrich BCSC niche in a MDA-MB-231 cell line in less time than other types of scaffolds can. Noreikaitė et al. demonstrated that PLA electrospun scaffolds ensured a suitable environment for cell growth with mesenchymal stem cells which were capable of spreading after three days of cultivation [41].

In future investigations, it would be interesting to use PLA blends to mimic the extracellular matrix structure. PLA is very hydrophobic, but it can be modified with other polymers like collagen or hyaluronic acid [42–44]. PLA blends enhanced cell viability, endothelization, and cell morphology [45]. Archille et al. fabricated PCL electrospun scaffolds which incorporated and delivered a short RNA hairpin against the cell cycle specific protein Cdk2, decreasing their mRNA expression and cell proliferation [46]. Thus, PLA could be modified to improve the results obtained in the present study.

In conclusion, FFF PLA scaffolds could be a useful tool with which to culture and enrich BCSCs. Consequently, 3D culture would allow BCSCs to be studied.

4. Materials and Methods

4.1. Scaffolds Design and Manufacture Process

SolidWorks® (Dassault Systèmes SE, Suresnes, France) was the computer-aided design (CAD) software used to create a cylinder with 20 mm diameter and 2.4 mm height. Scaffold design was saved in a stereolithography (STL) file which was transferred to the computer-aided manufacturing (CAM) software BCN3D Cura (BCN3D Technologies®, Barcelona, Spain). Input process parameters were selected according the design of experiments.

4.2. Design of Experiment

Through Quantum XL (Digital Computations Inc., Orlando, FL, USA), Taguchi experimental design was chosen with the aim to analyze the effect of the input parameters, such as layer height, infill density, pattern, and direction and flow, on cell proliferation (Table 4). The parameter of infill density is the quantity of material founded in each layer, whereas the flow is the quantity of material that printer expelled.

Taguchi is a statistical method, also known as a robust design method, developed by Genichi Taguchi. Taguchi helps to improve the quality of manufacturing processes. This statistical method is especially useful to reduce the number of experiments in processes with many input variables as 3D Printing based on FFF is.

Table 4. Tested values of each analyzed parameter to obtain the best cellular growth rate.

Parameter	Tested Values
Layer Height	0.1, 0.15 and 0.2 mm
Infill Density	50, 60 and 70%
Infill Pattern	Grid, Triangles and Zigzag
Infill Direction	45, 60 and 90°
Flow	80, 90 and 100%

The set parameters were printing temperature of initial layer (220 °C), printing temperature (200 °C), build plate temperature (30 °C), print speed (50 mm/s), retraction speed (40 mm/s), and nozzle diameter (0.3 mm). BCN3D Cura generated a G-code file of each scaffold configuration designed with the software and they were loaded in the 3D printer BCN3D Sigma Release 2017 (BCN3D Technologies®). PLA white (BCN3D Technologies®) was the biopolymer chosen to manufacture all scaffolds.

4.3. Material

Poly (lactic acid) (PLA, BCN3D Technologies®, Barcelona, Spain) was selected as the material for the experiments (Table 5). PLA is a biodegradable thermoplastic aliphatic polyester derived from renewable resources, such as corn starch or sugarcane, and has a melting point of about 173–178 °C with a glass transition of 60–65 °C. Degradation of PLA is produced by the hydrolysis of their ester linkages in physiological conditions.

Table 5. Poly (lactic acid) properties.

Material (#)	Molecular Weight (g/mol)	Young's Modulus (MPa)	Strain at Break (%)	Degradation Time (Months)
PLA	30,000	108	3.5	≈12

4.4. Cell Line

MDA-MB-231 triple negative breast cancer cells were obtained from the American Type Culture Collection (ATCC; Rockville, MD, USA). MDA-MB-231 cells were routinely grown in Dulbecco's Modified Eagle's Medium (DMEM) supplemented with 10% fetal bovine serum (FBS) and 50 U/mL penicillin/streptomycin (Hyclone, Logan, UT, USA). Cells were kept at 37 °C and 5% CO₂ atmosphere.

4.5. Three-Dimensional Cell Culture

Scaffolds were soaked overnight in 70% ethanol/water solution. The structures were washed two times with phosphate-buffered saline (PBS) (Hyclone) and exposed to UV light for 30 min. This sterilization process were followed based on previous work to avoid changes in the material properties [47].

Sterilized scaffolds were placed in non-adherent cell culture 12-well plates (Sartstedt, Nümbrecht, Germany) and immersed in a culture medium for 30 min at 37 °C and 5% CO₂ atmosphere with the purpose to facilitate cell attachment. Then, the pertinent cell density was prepared in 50 µL of medium and the suspension was pipetted drop by drop over the scaffold centre. They were incubated for three hours at 37 °C and 5% CO₂ atmosphere to allow cell attachment. After this incubation period, 1 mL of culture medium was added covering the PLA structures.

4.6. Scaffold Dimensional Characterization

Scaffolds were analyzed through digital images captured by Optical Microscope Nikon SMZ-745T attached to a digital camera CT3 ProgRes. The images were examined using the ImageJ® Software 1.5F (National Institutes of Health, Bethesda, MD, USA) and the pore area and the filament diameter were measured.

4.7. Cell Proliferation Assay

On adherent 12-well cell culture plates (Sartstedt) and PLA scaffolds, 50,000 cells were seeded for 72 h. Scaffolds and adherent wells were washed two times with PBS and PLA structures were placed in new wells so as to ensure only attached cells would be tested. Then, 3-(4,5-dimethylthiazolyl)-2,5-diphenyltetrazolium bromide (MTT) assay was performed adding 1 mL DMEM and 100 µL MTT (Sigma-Aldrich, St. Louis, MO, USA) in each well for 150 min at 37 °C and

5% CO₂ atmosphere. Only viable cells are capable of transform MTT into formazan crystals. After incubation, formazan crystals were dissolved with 1 mL dimethyl sulfoxide (Sigma-Aldrich) for 15 min under shaking. Three 100 µL aliquots from each well were pipetted into a 96-well plate and placed into a microplate reader (Bio-Rad, Hercules, CA, USA) where absorbance was measured at 570 nm.

4.8. Aldefluor Assay

On adherent 12-well cell culture plates (Startstedt) and PLA scaffolds, 50,000 cells were seeded for three days or 25,000 cells for six days. Scaffolds and adherent wells were washed two times with PBS and PLA structures were placed in new wells. Cells were detached using trypsin-EDTA (HyClone) at 37 °C and 5% CO₂ atmosphere. A final concentration of 200,000 cells was needed to analyze the ALDH enzyme activity using the ALDEFLUOR™ kit (Stem Cell Technologies, Durham, NC, USA). Following the manufacturer indications, cells were resuspended in ALDEFLUOR™ assay buffer. There was a negative control for each sample to evaluate the background fluorescence using ALDH inhibitor ALDEFLUOR™ diethylaminobenzaldehyde (DEAB). So, ALDEFLUOR™ Reagent (BODIPY-aminoacetaldehyde; BAAA) was added to each cell suspension, and then, the half of each one was putted in other microcentrifuge tubes with DEAB, for their negative control. Samples were incubated at 37 °C for 45 min in the dark. Finally, all reagent was removed and incubated samples were resuspended in ALDEFLUOR™ assay buffer.

Cell Lab Quanta flow cytometer (Beckman Coulter Inc., Miami, FL, USA) was utilized to quantify the ALDH-positive cell population of all samples. The argon ion laser (488 nm) was used as a light source set at a power of 22 mW and the sheath rate was set at 4.17 µL/min. Green fluorescence was detected with fluorescent channel 1 (FL1) optical filter (dichroic/splitter, dichroic long-pass: 550 nm, band-pass filter: 525 nm, detection width 505 to 545 nm). Information of a minimum of 10,000 events was recorded in List-mode Data files (LMD) and analyzed using Flowing Software version 2.5.1 (Flowing Software, Turku, Finland). Data were not compensated.

First, side-scatter (SS) and electronic volume (EV) dot plots were executed and only single cells were selected, excluding aggregated and damaged cells (less than 5–10%). Then, SS and FL1 fluorescence dot plots from negative control samples were performed in order to determine background fluorescence. The ALDH-positive cells region was drafted at the rightmost plot zone and including only the 0.5% of total single cell population. BAAA samples were equally processed and ALDH-positive cells region of respective controls were adopted to identify the percentage of population with high ALDH activity for each sample.

4.9. Statistical Analysis

All results were confirmed by at least three independent experiments. Data are expressed as mean ± standard error (SE). Data were analyzed by Student *t* test. *P* value is shown in results when significance was reached (*p* < 0.05). Ten copies (*n* = 10) of each DOE configuration were printed to perform characterization and cell proliferation assays.

5. Conclusions

The results of this work indicate that MDA-MB-231 cells can be cultured on PLA 3D printed scaffolds and support PLA as being a suitable material for 3D cell culture. PLA scaffolds with smaller pores produced higher proliferation, proving to be good physical supports for TNBC cells. Moreover, these structures provide for the expansion of BCSC niche. In conclusion, PLA scaffolds may be useful to culture BCSCs, thus making their growth and cultivation possible. This can facilitate research into this malignant subpopulation.

Author Contributions: T.P. and J.C. conceived and designed the experiments; E.P., M.R., A.J.G. and M.Y. performed the experiments; E.P., T.P., J.C., M.R., A.J.G. and M.Y. analyzed the data; T.P. and J.C. contributed reagents/materials/analysis tools; E.P. wrote the paper.

Funding: This research received no external funding.

Acknowledgments: The authors acknowledge the financial support from the Ministry of Economy and Competitiveness (MINECO), Spain for the PhD scholarship and grants from DPI2016-77156-R and RYC-2014-15581, the financial support from the University of Girona (Spain) MPCUdG2016/036 and the support of the Catalan Government (2017SGR00385). This work was also partially supported by the grants from the Fundación Ramón Areces (Spain) and the Instituto de Salud Carlos III (Spain) (PI1400329).

Conflicts of Interest: The authors declare no conflict of interest. The founding sponsors had no role in the design of the study, nor the collection, analyses, or interpretation of data, nor in the writing of the manuscript, or in the decision to publish the results.

Abbreviations

2D	Two-dimensional
3D	Three-dimensional
ALDH	Aldehyde Dehydrogenase
AM	Additive Manufacturing
BCSC	Breast cancer stem cell
CAD	Computer-aided design
CAM	Computer-aided manufacturing
CSC	Cancer stem cell
DMEM	Dulbecco's modified eagle's medium
ECM	Extracellular matrix
FBS	Fetal bovine serum
FFF	Fused filament fabrication
MTT	3-(4,5-dimethylthiazolyl-2)-2,5-diphenyltetrazolium bromide
PBS	Phosphate-buffered saline
PCL	Poly(ϵ -caprolactone)
PLA	Poly (lactic acid)
SS	Selected scaffold
STL	Stereolithography
TNBC	Triple negative breast cancer

References

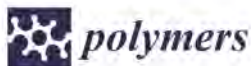
1. Siegel, R.L.; Miller, K.D.; Jemal, A. Cancer statistics. *CA Cancer J. Clin.* **2017**, *67*, 7–30. [[CrossRef](#)] [[PubMed](#)]
2. Perou, C.M.; Sorlie, T.; Eisen, M.B.; van de Rijn, M.; Jeffrey, S.S.; Rees, C.A.; Rees, C.A.; Pollack, J.R.; Ross, D.T.; Johnsen, H.; et al. Molecular portraits of human breast tumours. *Nature* **2000**, *406*, 747–752. [[CrossRef](#)] [[PubMed](#)]
3. Bauer, K.R.; Brown, M.; Cress, R.D.; Parise, C.A.; Caggiano, V. Descriptive analysis of estrogen receptor (ER)-negative, progesterone receptor (PR)-negative, and HER2-negative invasive breast cancer, the so-called triple-negative phenotype. *Cancer* **2007**, *109*, 1721–1728. [[CrossRef](#)] [[PubMed](#)]
4. Dent, R.; Trudeau, M.; Pritchard, K.I.; Hanna, W.M.; Kahn, H.K.; Sawka, C.A.; Lickley, L.A.; Rawlinson, E.; Sun, P.; Narod, S.A. Triple-negative breast cancer: Clinical features and patterns of recurrence. *Clin. Cancer Res.* **2007**, *13*, 4429–4434. [[CrossRef](#)] [[PubMed](#)]
5. Perou, C.M. Molecular Stratification of Triple-Negative Breast Cancers. *Oncologist* **2011**, *16* (Suppl. 1), 61–70. [[CrossRef](#)]
6. Matsui, W.; Wang, Q.; Barber, J.P.; Brennan, S.; Smith, B.D.; Borrello, I.; McNiece, L.; Lin, L.; Ambinder, R.F.; Peacock, C.; et al. Clonogenic multiple myeloma progenitors, stem cell properties, and drug resistance. *Cancer Res.* **2008**, *68*, 190–197. [[CrossRef](#)] [[PubMed](#)]
7. Nakamura, K.; Inuma, H.; Aoyagi, Y.; Shibuya, H.; Watanabe, T. Predictive value of cancer stem-like cells and cancer-associated genetic markers for peritoneal recurrence of colorectal cancer in patients after curative surgery. *Oncology* **2010**, *78*, 309–315. [[CrossRef](#)] [[PubMed](#)]

8. Diehn, M.; Cho, R.W.; Lobo, N.A.; Kalisky, T.; Dorie, M.J.; Kulp, A.N.; Qian, D.; Lam, J.S.; Ailles, L.E.; Wong, M.; et al. Association of reactive oxygen species levels and radioresistance in cancer stem cells. *Nature* **2009**, *458*, 780–783. [CrossRef] [PubMed]
9. Kyjáčová, L.; Hubáčková, S.; Krejčíková, K.; Strauss, R.; Hanzlíková, H.; Dzijak, R.; Imrichová, T.; Simová, J.; Reinis, M.; Bartek, J.; et al. Radiotherapy-induced plasticity of prostate cancer mobilizes stem-like non-adherent, Erk signaling-dependent cells. *Cell Death Differ.* **2015**, *22*, 898–911. [CrossRef] [PubMed]
10. Singh, S.K.; Clarke, I.D.; Terasaki, M.; Bonn, V.E.; Hawkins, C.; Squire, J.; Dirks, P.B. Identification of a cancer stem cell in human brain tumors. *Cancer Res.* **2003**, *63*, 5821–5828. [PubMed]
11. Dontu, G.; Abdallah, W.M.; Foley, J.M.; Jackson, K.W.; Clarke, M.F.; Kawamura, M.J.; Wicha, M.S. In vitro propagation and transcriptional profiling of human mammary stem/progenitor cells. *Genes Dev.* **2003**, *17*, 1253–1270. [CrossRef] [PubMed]
12. Ginestier, C.; Hur, M.H.; Charafe-Jauffret, E.; Monville, F.; Dutcher, J.; Brown, M.; Jacquemier, J.; Viens, P.; Kleer, C.G.; Liu, S.; et al. ALDH1 Is a Marker of Normal and Malignant Human Mammary Stem Cells and a Predictor of Poor Clinical Outcome. *Cell Stem Cell* **2007**, *1*, 555–567. [CrossRef] [PubMed]
13. Thomas, C.H.; Collier, J.H.; Sfeir, C.S.; Healy, K.E. Engineering gene expression and protein synthesis by modulation of nuclear shape. *Proc. Natl. Acad. Sci. USA* **2002**, *99*, 1972–1977. [CrossRef] [PubMed]
14. Vergani, L.; Grattarola, M.; Nicolini, C. Modifications of chromatin structure and gene expression following induced alterations of cellular shape. *Int. J. Biochem. Cell Biol.* **2004**, *36*, 1447–1461. [CrossRef] [PubMed]
15. Theocharis, A.D.; Skandalis, S.S.; Gialeli, C.; Karamanos, N.K. Extracellular matrix structure. *Adv. Drug Deliv. Rev.* **2016**, *97*, 4–27. [CrossRef] [PubMed]
16. Knight, E.; Przyborski, S. Advances in 3D cell culture technologies enabling tissue-like structures to be created in vitro. *J. Anat.* **2015**, *747*, 746–756. [CrossRef] [PubMed]
17. De Ciurana, J.; Serenó, L.; Vallès, E. Selecting process parameters in RepRap additive manufacturing system for PLA scaffolds manufacture. *Procedia CIRP* **2013**, *5*, 152–157. [CrossRef]
18. Mikos, A.G.; Sarakinos, G.; Leite, S.M.; Vacanti, J.P.; Langer, R. Laminated three-dimensional biodegradable foams for use in tissue engineering. *Biomaterials* **1993**, *14*, 323–330. [CrossRef]
19. Conn, R.; Kolstad, J.; Borzelleca, J.; Dixler, D.; Filer, L.J.; LaDu, B.J.; Pariza, M.W. Safety assessment of polylactide (PLA) for use as a food-contact polymer. *Food Chem. Toxicol.* **1995**, *33*, 273–283. [CrossRef]
20. Lasprilla, A.J.R.; Martinez, G.A.R.; Lunelli, B.H.; Jardini, A.L.; Filho, R.M. Poly-lactic acid synthesis for application in biomedical devices—A review. *Biotechnol. Adv.* **2012**, *30*, 321–328. [CrossRef] [PubMed]
21. Saini, P.; Arora, M.; Kumar, M.N.V.R. Poly(lactic acid) blends in biomedical applications. *Adv. Drug Deliv. Rev.* **2016**, *107*, 47–59. [CrossRef] [PubMed]
22. Tsuyada, A.; Chow, A.; Wu, J.; Somlo, G.; Chu, P.; Loera, S.; Luu, T.; Li, A.X.; Wu, X.; Ye, W.; et al. CCL2 mediates cross-talk between cancer cells and stromal fibroblasts that regulates breast cancer stem cells. *Cancer Res.* **2012**, *72*, 2768–2779. [CrossRef] [PubMed]
23. Sims-Mourtada, J.; Niamat, R.A.; Samuel, S.; Eskridge, C.; Kmiec, E.B. Enrichment of breast cancer stem-like cells by growth on electrospun polycaprolactone-chitosan nanofiber scaffolds. *Int. J. Nanomed.* **2014**, *9*, 995–1003. [CrossRef] [PubMed]
24. Al-Hajj, M.; Wicha, M.S.; Benito-Hernandez, A.; Morrison, S.J.; Clarke, M.F. Prospective identification of tumorigenic breast cancer cells. *Proc. Natl. Acad. Sci. USA* **2003**, *100*, 3983–3988. [CrossRef] [PubMed]
25. Charafe-Jauffret, E.; Ginestier, C.; Iovino, F.; Wicinski, J.; Cervera, N.; Finetti, P.; Hur, M.H.; Diebel, M.E.; Monville, F.; Dutcher, J.; et al. Breast Cancer Cell Lines Contain Functional Cancer Stem Cells with Metastatic Capacity and a Distinct Molecular Signature. *Cancer Res.* **2009**, *69*, 1302–1313. [CrossRef] [PubMed]
26. Xu, F.; Burg, K.J. Three-dimensional polymeric systems for cancer cell studies. *Cytotechnology* **2007**, *54*, 135–143. [CrossRef] [PubMed]
27. Palomerias, S.; Rabionet, M.; Ferrer, I.; Sarrats, A.; Garcia-Romeu, M.; Puig, T.; Ciurana, J. Breast Cancer Stem Cell Culture and Enrichment Using Poly(ϵ -Caprolactone) Scaffolds. *Molecules* **2016**, *21*, 537. [CrossRef] [PubMed]
28. Rabionet, M.; Yeste, M.; Puig, T.; Ciurana, J. Electrospinning PCL Scaffolds Manufacture for Three-Dimensional Breast Cancer Cell Culture. *Polymers* **2017**, *9*, 328. [CrossRef]
29. Marchitti, S.A.; Brocker, C.; Stagos, D.; Vasiliou, V. Non-P450 aldehyde oxidizing enzymes: the aldehyde dehydrogenase superfamily. *Expert. Opin. Drug Metab. Toxicol.* **2008**, *4*, 697–720. [CrossRef] [PubMed]

30. Douville, J.; Beaulieu, R.; Balicki, D. ALDH1 as a functional marker of cancer stem and progenitor cells. *Stem Cells Dev.* **2009**, *18*, 17–25. [[CrossRef](#)] [[PubMed](#)]
31. Kim, M.P.; Fleming, J.B.; Wang, H.; Abbruzzese, J.L.; Choi, W.; Kopetz, S.; McConkey, D.J.; Evans, D.B.; Gallick, G.E. ALDH activity selectively defines an enhanced tumor-initiating cell population relative to CD133 expression in human pancreatic adenocarcinoma. *PLoS ONE* **2011**, *6*, e20636. [[CrossRef](#)] [[PubMed](#)]
32. Wang, Y.-C.; Yo, Y.-T.; Lee, H.-Y.; Liao, Y.-P.; Chao, T.-K.; Su, P.-H.; Lai, H.-C. ALDH1-Bright Epithelial Ovarian Cancer Cells Are Associated with CD44 Expression, Drug Resistance, and Poor Clinical Outcome. *Am. J. Pathol.* **2012**, *180*, 1159–1169. [[CrossRef](#)] [[PubMed](#)]
33. Ricardo, S.; Vieira, A.F.; Gerhard, R.; Leitao, D.; Pinto, R.; Cameselle-Teijeiro, J.F.; Milanezi, F.; Schmitt, F.; Paredes, J. Breast cancer stem cell markers CD44, CD24 and ALDH1: expression distribution within intrinsic molecular subtype. *J. Clin. Pathol.* **2011**, *64*, 937–946. [[CrossRef](#)] [[PubMed](#)]
34. Xiong, G.; Luo, H.; Zhu, Y.; Raman, S.; Wan, Y. Creation of macropores in three-dimensional bacterial cellulose scaffold for potential cancer cell culture. *Carbohydr. Polym.* **2014**, *114*, 553–557. [[CrossRef](#)] [[PubMed](#)]
35. Florczyk, S.J.; Kievit, F.M.; Wang, K.; Erickson, A.E.; Ellenbogen, R.G.; Zhang, M. 3D Porous Chitosan-Alginate Scaffolds Promote Proliferation and Enrichment of Cancer Stem-Like Cells. *J. Mater. Chem. B* **2016**, *4*, 6326–6334. [[CrossRef](#)] [[PubMed](#)]
36. Rijal, G.; Bathula, C.; Li, W. Application of Synthetic Polymeric Scaffolds in Breast Cancer 3D Tissue Cultures and Animal Tumor Models. *Int. J. Biomater.* **2017**, *2017*, 8074890. [[CrossRef](#)] [[PubMed](#)]
37. Feng, S.; Duan, X.; Lo, P.-K.; Liu, S.; Liu, X.; Chen, H.; Wang, Q. Expansion of breast cancer stem cells with fibrous scaffolds. *Integr. Biol.* **2013**, *5*, 768. [[CrossRef](#)] [[PubMed](#)]
38. Ye, M.; Mohanty, P.; Ghosh, G. Biomimetic apatite-coated porous PVA scaffolds promote the growth of breast cancer cells. *Mater. Sci. Eng. C Mater. Biol. Appl.* **2014**, *44*, 310–316. [[CrossRef](#)] [[PubMed](#)]
39. Gleadall, A.; Visscher, D.; Yang, J.; Thomas, D.; Segal, J. Review of additive manufactured tissue engineering scaffolds: relationship between geometry and performance. *Burn Trauma* **2018**, *6*, 19. [[CrossRef](#)] [[PubMed](#)]
40. Sobral, J.M.; Caridade, S.G.; Sousa, R.A.; Mano, J.F.; Reis, R.L. Three-dimensional plotted scaffolds with controlled pore size gradients: Effect of scaffold geometry on mechanical performance and cell seeding efficiency. *Acta Biomater.* **2011**, *7*, 1009–1018. [[CrossRef](#)] [[PubMed](#)]
41. Noreikaitė, A.; Antanavičiūtė, L.; Mikalayeva, V.; Darinskas, A.; Tamulevičius, T.; Adomavičiūtė, E.; Šimatonis, L.; Akramienė, D.; Stankevičius, E. Scaffold design for artificial tissue with bone marrow stem cells. *Medicina* **2017**, *53*, 203–210. [[CrossRef](#)] [[PubMed](#)]
42. Tang, X.; Thankappan, S.K.; Lee, P.; Fard, S.E.; Harmon, M.D.; Tran, K.; Yu, X. Natural polymers in tissue engineering and regenerative medicine. In *Natural and Synthetic Biomedical Polymers*; Kumar, S.G., Laurencin, C.T., Eng, M.D., Eds.; Elsevier Science: Amsterdam, The Netherlands, 2014; pp. 352–358.
43. Nair, N.R.; Nampoothiri, K.M.; Pandey, A. Preparation of poly(L-lactide) blends and biodegradation by *Lentzea waywayandensis*. *Biotechnol. Lett.* **2012**, *34*, 2031–2035. [[CrossRef](#)] [[PubMed](#)]
44. Takayama, T.; Todo, M.; Tsuji, H. Effect of annealing on the mechanical properties of PLA/PCL and PLA/PCL/LTI polymer blends. *J. Mech. Behav. Biomed. Mater.* **2011**, *4*, 255–260. [[CrossRef](#)] [[PubMed](#)]
45. Mi, H.-Y.; Salick, M.R.; Jing, X.; Jacques, B.R.; Crone, W.C.; Peng, X.-F.; Turng, L.S. Characterization of thermoplastic polyurethane/polylactic acid (TPU/PLA) tissue engineering scaffolds fabricated by microcellular injection molding. *Mater. Sci. Eng. C Mater. Biol. Appl.* **2013**, *33*, 4767–4776. [[CrossRef](#)] [[PubMed](#)]
46. Achille, C.; Sundaresh, S.; Chu, B.; Hadjiargyrou, M. Cdk2 silencing via a DNA/PCL electrospun scaffold suppresses proliferation and increases death of breast cancer cells. *PLoS ONE* **2012**, *7*, e52356. [[CrossRef](#)] [[PubMed](#)]
47. Guerra, A.J.; Cano, P.; Rabionet, M.; Puig, T.; Ciurana, J. Effects of different sterilization processes on the properties of a novel 3D-printed polycaprolactone stent. *Polym. Adv. Technol.* **2018**, *29*, 2327–2335. [[CrossRef](#)]



© 2018 by the authors. Licensee MDPI, Basel, Switzerland. This article is an open access article distributed under the terms and conditions of the Creative Commons Attribution (CC BY) license (<http://creativecommons.org/licenses/by/4.0/>).



Article

PLA Electrospun Scaffolds for Three-Dimensional Triple-Negative Breast Cancer Cell Culture

Emma Polonio-Alcalá ^{1,2,†}, Marc Rabionet ^{1,2,†}, Xavier Gallardo ^{1,2}, David Angelats ^{1,2}, Joaquim Ciurana ², Santiago Ruiz-Martínez ^{1,*} and Teresa Puig ^{1,*}

¹ New Therapeutic Targets Laboratory (TargetsLab)—Oncology Unit, Department of Medical Sciences, Faculty of Medicine, University of Girona, Emili Grahit 77, 17003 Girona, Spain; emma.polonio@udg.edu (E.P.-A.); m.rabionet@udg.edu (M.R.); xagallardo@gmail.com (X.G.); dangelatslobo4@gmail.com (D.A.)

² Product, Process and Production Engineering Research Group (GREP), Department of Mechanical Engineering and Industrial Construction, University of Girona, Maria Aurèlia Capmany 61, 17003 Girona, Spain; quim.ciurana@udg.edu

* Correspondence: santiago.ruiz@udg.edu (S.R.-M.); teresa.puig@udg.edu (T.P.); Tel.: +34-972-419628 (S.R.-M. & T.P.)

† These authors contributed equally to this work.

Received: 29 March 2019; Accepted: 21 May 2019; Published: 23 May 2019



Abstract: Three-dimensional (3D) systems provide a suitable environment for cells cultured *in vitro* since they reproduce the physiological conditions that traditional cell culture supports lack. Electrospinning is a cost-effective technology useful to manufacture scaffolds with nanofibers that resemble the extracellular matrix that surround cells in the organism. Poly(lactic acid) (PLA) is a synthetic polymer suitable for biomedical applications. The main objective of this study is to evaluate electrospun (ES)-PLA scaffolds to be used for culturing cancer cells. Triple-negative breast cancer (TNBC) is the most aggressive breast cancer subtype with no validated targeted therapy and a high relapse rate. MDA-MB-231 TNBC cells were grown in scaffolds from two different PLA concentrations (12% and 15% *w/v*). The appropriateness of ES-PLA scaffolds was evaluated using a cell proliferation assay. EGFR and STAT3 gene expression and protein levels were compared in cells grown in 2D versus in 3D cultures. An increase in STAT3 activation was shown, which is related to self-renewal of cancer stem cells (CSCs). Therefore, the enrichment of the breast CSC (BCSC) population was tested using a mammosphere-forming assay and gene expression of BCSC-related stemness and epithelial-to-mesenchymal transition markers. Based on the results obtained, ES-PLA scaffolds are useful for 3D cultures in short culture periods with no BCSC-enrichment.

Keywords: breast cancer; triple-negative breast cancer; three-dimensional cell culture; poly(lactic acid); EGFR; STAT3

1. Introduction

Two-dimensional (2D) cell culture is a well-established system used in the vast majority of studies involving cells. However, this approach is not completely faithful to reality since in the organism, cells are surrounded by the extracellular matrix (ECM), which provides a physical support for cells; this is missing in *in vitro* flat conditions. The ECM has also been proven to exert an important role in many cellular processes, such as cell growth or differentiation [1,2]. Monolayer cell cultures hardly mimic the physiological architecture and environment [3]. Therefore, three-dimensional (3D) cell culture has become an important hotspot in worldwide research in order to fix the aforementioned issues [4].

Researchers have proved that 3D systems provide a suitable spatial distribution for cells cultured *in vitro*, allowing cell–cell and cell–matrix interactions [5]. Hence, 3D-cultured cells have a different

morphology, proliferation rate, gene expression and protein synthesis, differentiation, and drug metabolism compared to 2D culture [6–10]. Scaffold-based culture is a type of 3D culture that has been increasingly gaining importance in medical research, especially in oncology. Electrospinning and Fused Filament Fabrication (FFF) techniques are the two most used methods nowadays to manufacture these structures [11]. Using the electrospinning, a more ECM-resembling scaffold within the micrometer to nanometer fibers range may be formed [12,13]. Electrospinning has been used for a wide range of applications, including drug delivery [14] or postoperative adhesion prevention [15]. Moreover, synthetic materials come with some advantages, such as high versatility and reproducibility [16]. Among them, poly(lactic acid) (PLA), a biodegradable synthetic polymer that has been declared to be biocompatible by the United States (US) Food and Drug Administration (FDA), is used in scaffold manufacturing, mostly with bone tissue engineering purposes such as in dentistry and orthopedics [17]. Furthermore, no immune rejection or cytotoxic effects were found in patients with PLA coronary stents implanted for six months [18]. To date, however, no studies have been published using electrospun (ES)-PLA scaffolds for oncogenic purposes.

Breast cancer is the most prevalent cancer among women in US and Europe. It is also the second leading cause of cancer death in women [19,20]. Between 15–20% of breast cancer cases correspond to triple-negative breast cancer (TNBC), an aggressive subtype with no overexpression of the estrogen receptor, progesterone receptor, or epidermal growth factor receptor-2 (HER2) [21,22]. The lack of known druggability leaves cytotoxic chemotherapy as the only possible treatment option for these patients. Despite a good initial response to chemotherapy, TNBC patients present a high relapse rate leading to poor prognosis, thus more effective therapies are needed [23,24].

In the current study, we aim to test whether TNBC cells can be cultured in ES-PLA fibrous scaffolds and analyze the impact of this 3D culture on cancer cells' behaviour. In addition, stem features were assessed in order to corroborate a possible enrichment of the breast cancer stem cell (BCSC) population. Based on the results obtained, we conclude that ES-PLA scaffolds are suitable for in vitro 3D culture of the TNBC MDA-MB-231 cell line with no enlargement of BCSCs observed within the culture days tested.

2. Materials and Methods

2.1. Polymer

The polymer chosen to manufacture the scaffolds was poly(lactic acid) (PLA, BCN3D Technologies®, Barcelona, Spain), commonly used in 3D printing for bone tissue replacement. The selected solvent was chloroform (Labkem, Labbox Labware, Barcelona, Spain). PLA characteristics extracted from manufacture's indications are shown in Table 1.

Table 1. Poly(lactic acid) properties.

Molecular Weight (g/mol)	Melting Point (°C)	Glass Transition (°C)	Young's Modulus (MPa)	Strain at Break (%)	Degradation Time (Months)
30,000	173–178	60–65	108	3.5%	12

2.2. Polymer Thermal Analysis

The thermal properties of PLA samples (7.01 mg) were measured by Differential Scanning Calorimetry (DSC; TA-Q2000, Lukens Drive, New Castle, PA, USA). The melting point (T_m), glass-transition temperature (T_g), and cold crystallization was measured from 25 to 180 °C under nitrogen in aluminum capsules at heating rate of 10 °C/min.

The thermal stability of the samples (9.25 mg) was investigated with thermogravimetric analysis (TGA; Mettler-Toledo TGA/DSC 1, Schwerzenbach, Switzerland) under nitrogen from 30 to 700 °C at a heating rate of 10 °C/min.

2.3. Electrospun Scaffolds Manufacturing

Two different PLA concentrations of 12% and 15% *w/v* were dissolved with chloroform at room temperature and under stirring. Scaffolds were manufactured by an electrospinning machine (Spraybase, Dublin, Ireland) using a 24 G needle emitter with an inner diameter of 0.55 mm. A fixed voltage of 7 kV and a flow rate of 2 mL/h was established by the Syringe Pump Pro software (New Era Pump Systems, Farmingdale, NY, USA). The collector was placed at 15 cm from the emitter. The electrospinning process was performed injecting 5 mL of the desired solution. The resulting scaffolds were cut using a scalpel into squares of 2.5 cm for their use in 6-well plates or of 1.6 cm for 12-well plates.

2.4. Scaffold Physical Characterization

12-well scaffolds manufactured using 12% and 15% PLA solution were weighed by Sartorius ED224S analytical balance (Sartorius, Göttingen, Germany) and scaffold thickness was measured using Mahr Micromar 40EWW (Mahr, Göttingen, Germany). Scanning electron microscopy (SEM; Zeiss, Oberkochen, Germany) was used to characterize the microarchitecture of the ES-PLA scaffolds. To discern the fiber uniformity, different images from the top and bottom sides were taken. Fiber diameter, surface porosity, and pore area were calculated from both sides to obtain the average value. The images were processed with the ImageJ software (National Institutes of Health, Bethesda, MD, USA). At least three scaffolds were tested.

2.5. Cell Line and Culture Conditions

MDA-MB-231 human TNBC cell line was obtained from the American Type Culture Collection (ATCC; Rockville, MD, USA). Cells were grown in Duplecco's Modified Eagle's Medium (DMEM), supplemented with 10% fetal bovine serum (FBS) and 50 U/mL of penicillin/streptomycin (HyClone, Logan, UT, USA). MDA-MB-231 cells were maintained at 37 °C and 5% CO₂ atmosphere. Cells were monitored routinely and found to be mycoplasma-free.

2.6. Three-Dimensional Cell Culture

PLA scaffolds were sterilized by submersion in a solution of 70% ethanol overnight, washed two times with phosphate-buffered saline (PBS, Hyclone), and exposed to UV light for 30 min with no alteration of the properties as previously described [25].

Sterilized scaffolds were placed in non-adherent cell culture 6- or 12-well plates (Sarstedt, Nümbrecht, Germany) and soaked in DMEM for 30 min at 37 °C and 5% CO₂ humidified atmosphere prior to cell seeding with the aim to promote cell attachment. Then, the corresponding cell density was prepared into a reduced volume of medium (50 µL for 12-well scaffolds and 100 µL for 6-well ones) and pipetted drop by drop over the center of the scaffolds. Therefore, approximately the whole scaffold surface was covered with cell suspension and the scaffold remain soaked but with no cell loss over the well plate. Finally, seeded scaffolds were incubated for three hours to allow cell attachment at 37 °C and 5% CO₂ atmosphere, then DMEM was added. Bidimensional (2D) cell culture was performed as a control in adherent cell culture microplates (Sarstedt) with the same cell density used in 3D culture.

2.7. Cell Proliferation Assay

To investigate cell proliferation, MDA-MB-231 cells were seeded into adherent 12-well plates for three and six days at a density of 50,000 and 8000 cells/well, respectively. Next, scaffolds were washed two times with PBS, PLA structures were placed in new wells to ensure only scaffold-attached cells would be analyzed, and a 3-(4,5-dimethylthiazolyl)-2,5-diphenyltetrazolium bromide (MTT) assay was performed as described elsewhere [26].

2.8. Quantitative Real-Time PCR Analysis

Suspensions of 125,000 and 20,000 MDA-MB-231 cells were seeded on standard wells and 15% PLA scaffolds were placed in non-adherent 6-well plates for three and six days, respectively. Then, scaffolds were washed twice with PBS and PLA structures were placed in new wells. MDA-MB-231 cells were detached as mentioned above. Trypsinized cells from 2D or 3D cultures were suspended with 750 μ L of Qiazol (Qiagen, Hilden, Germany). The total RNA from each sample was isolated using an RNeasy Mini Kit (Qiagen) and reverse-transcribed into complementary DNA (cDNA) using the High Capacity cDNA Archive Kit (Applied Biosystems, Foster City, CA, USA). Gene expression levels were assessed using LightCycler 480 Real-Time PCR System (Roche, Basel, Switzerland) with LightCycler 480 SYBR Green I Master (Roche) as previously described [27]. Primers were designed as shown in Table 2.

Table 2. Forward and reverse sequences of analyzed genes.

Gene	Forward sequence (5'-3')	Reverse sequence (5'-3')
<i>SNAIL</i>	GCTGCAGGACTCTAATCCAGA	ATCTCCGGAGGTGGGATG
<i>SOx2</i>	AACCCCAAGATGCACAACCTC	GCTTAGCCTCGTCGATGAAC
<i>E-cadherin</i>	TGGAGGAATCTTGCCTTTC	CGCTCTCCTCCGAAGA AAC
<i>VIM</i>	TGGTCTAACGGTTTCCCTA	GACCTCGGAGGCGAGAGTG
<i>EGFR</i>	CATGTCGATGGACTCCAGA	GGGACAGCTTGGATCACACT
<i>STAT3</i>	CACCTTCAGGATGTCGGAA	ATCTGGAGATCTCTACCACITTC A
<i>GAPDH</i>	TCTTCCAGGAGCGAGATC	CAGAGATGATGCCCTTTTG

Gene expression levels were quantified by the double delta Cycle threshold (Ct) analysis method and normalized to the housekeeping gene GAPDH [28].

2.9. Protein Analysis

A suspension of 125,000 and 20,000 MDA-MB-231 cells were seeded on 15% PLA scaffolds placed in 6-well plates and in adherent 6-well plates for three and six days, respectively. Next, scaffolds were washed twice with PBS and PLA meshes were placed in new wells. Cells were detached as described above. Cell pellets were lysed in ice-cold lysis buffer (Cell Signaling Technology, Inc., Danvers, MA, USA) with 100 mg/mL of the protease inhibitor phenylmethylsulfonylfluoride (PMSF) by vortexing every 5 min for 30 min. The same protein quantity (20 μ g) was heated in lithium dodecyl sulfate (LDS) sample buffer with sample reducing agent (Invitrogen, Carlsbad, CA, USA) for 10 min at 70 $^{\circ}$ C, electrophoresed on acrylamide gels (Bio-Rad Laboratories, Inc., Hercules, CA, USA), and transferred onto nitrocellulose membranes (Thermo Fisher Scientific, Waltham, MA, USA). Transferred membranes were blocked (blocking buffer of 5% bovine serum albumin (BSA) in tris-buffered saline/TBS 0.05% Tween (TBS-T)) at room temperature for 1 h. Then, membranes were incubated overnight with the following primary antibodies: Rabbit polyclonal antibodies against pEGFR^{Y1068} (Cell Signaling Technology Inc.; #2234S; dilution 1:1000), STAT3 (Cell Signaling Technology Inc.; #4904S; dilution 1:1000), pSTAT3^{Y705} (Cell Signaling Technology Inc.; #9131S; dilution 1:1000), rabbit monoclonal antibody against EGFR (Cell Signaling Technology Inc.; #4267S; dilution 1:1000), and mouse polyclonal antibody GAPDH (Proteintech, Manchester, UK; #60004-1-IG; dilution 1:50,000). Antibodies were diluted in blocking buffer at 4 $^{\circ}$ C. Specific horseradish peroxidase (HRP)-conjugated secondary antibody was incubated for 1 h at room temperature. Immune complexes were detected using a chemiluminescent HRP substrate (ClarityTM Western ECL Substrate (Bio-Rad Laboratories, Inc.)) and a ChemiDocTM Imaging System (Bio-Rad Laboratories, Inc.). GAPDH was used as a control of protein loading. Protein analyses were repeated at least three times and the representative results are shown.

2.10. Mammosphere-Forming Assay

50,000 and 8000 cells were seeded on 15% PLA scaffolds placed in 12-well adherent cell culture plates for three and six days, respectively. Afterward, scaffolds were washed two times with PBS and placed in new wells. Cells were detached with trypsin-EDTA (HyClone) at 37 °C and 5% CO₂ atmosphere. Detached cells were centrifuged 5 min at 1000 rpm. Cell pellets were resuspended in DMEM/F12 medium (HyClone) supplemented with 0.2% B27 (Gibco, Waltham, MA, USA), epidermal growth factor (EGF) and fibroblast growth factor (FGF) (final concentration of 20 ng/mL; Milteny Biotec, Bergisch Gladbach, Germany), 1% L-glutamine, and 1% sodium pyruvate. A suspension of 2000 cells/well was seeded onto non-adherent 6-well cell culture microplates (Sarstedt) and incubated for 7 days at 37 °C and 5% CO₂. Afterward, mammospheres bigger than 50 µm were counted. The mammosphere-forming Index (MFI) was calculated for each culture condition following the next equation, as described in previous works [26,29].

2.11. Statistical Analysis

All data results are expressed as mean ± standard error of the mean (SEM) and were analyzed by Student's t test. The P value is shown in results when significance was reached (*: $p < 0.05$; **: $p < 0.01$; ***: $p < 0.001$). The results obtained were confirmed by at least three independent experiments.

3. Results

3.1. Thermal Characterization of PLA

The PLA filament's thermal properties were studied through TGA and DSC. The DSC curve shows a T_g of 61.55 °C, crystallization at 119.26 °C, and a T_m of 149.57 °C (Figure 1). Furthermore, the TGA curve shows a complete degradation in one step between 310 and 380 °C (Figure 2).

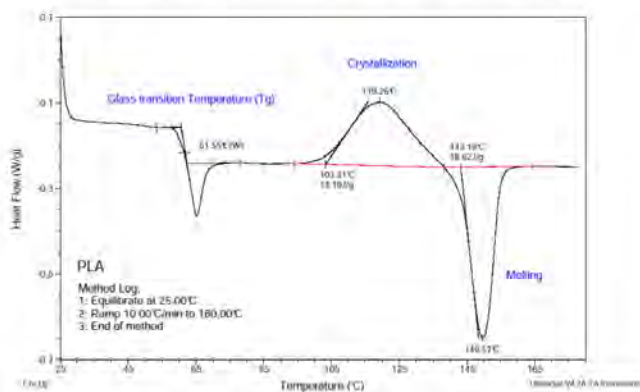


Figure 1. DSC curve of poly(lactic acid) (PLA).

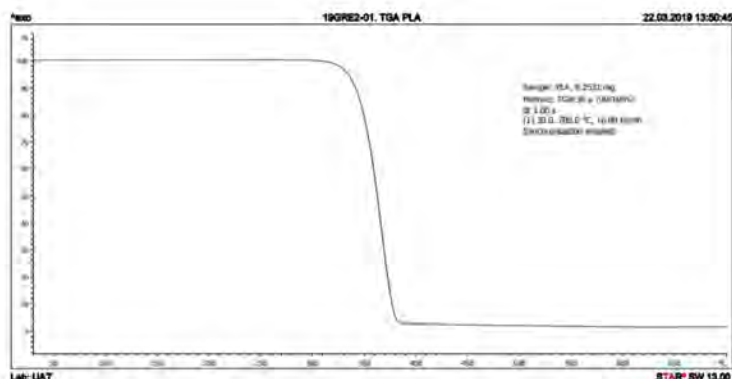


Figure 2. TGA curve of PLA.

3.2. Physical Characterization of ES-PLA Scaffolds

In an initial attempt to seek the proper scaffold to be used in 3D cell culture, different PLA-concentrations were used. Lower polymer concentrations than 12% led to electrospay instead of electrospinning. On the other hand, concentrations higher than 15% PLA resulted in electrospinning emitter obstruction (data not shown). Therefore, we decided to test the two possible extremes, i.e., 12% and 15% PLA. Once manufactured, the two different PLA-concentration scaffolds were cut into squares of 1.6 cm² and then they were characterized by different approaches. Due to the similar quantity of polymer dissolved in the solutions to manufacture 12% and 15% ES-PLA scaffolds, no significant differences for weight or thickness values were found in any of the resulting scaffolds (Table 3).

Table 3. Weight and thickness of 12% and 15% PLA scaffolds.

Scaffold trait	12%	15%
Weight (mg)	5.83 ± 0.63	6.23 ± 0.44
Thickness (µm)	68.33 ± 6.89	68.00 ± 3.51

Afterward, both structures were visualized by SEM to study the microscopic structure (Table 4). The uniformity of the fibers was confirmed through the visualization of the bottom and top sides. Scaffolds from 12% PLA showed two different types of filaments. One of them showed a diameter of roughly 7 µm, whereas the second type exhibited fibers nearly 20 times thinner. In contrast, 15% PLA scaffolds presented one filament population, lacking the slight ones (Figure 3). Both sides' images from the lower PLA-concentration meshes revealed the possible presence of beads; this was not found in the higher PLA percentage on any side. Non-significant differences regarding the pore area or surface porosity were found between the two polymer concentrations, although it was observed that 15% PLA scaffolds had a non-significant higher surface porosity compared to 12% PLA scaffolds (Figure 3).

Table 4. Microscopic characterization of 12% and 15% electrospun (ES)-PLA scaffolds (7 kV, 5 mL/h). Micrographs from the top and bottom sides at different magnifications were visualized using SEM.

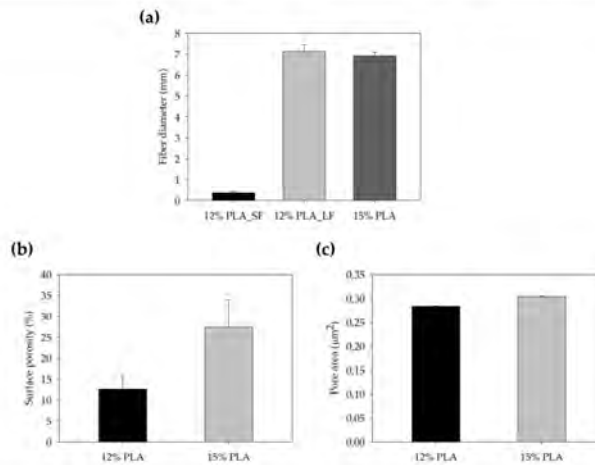
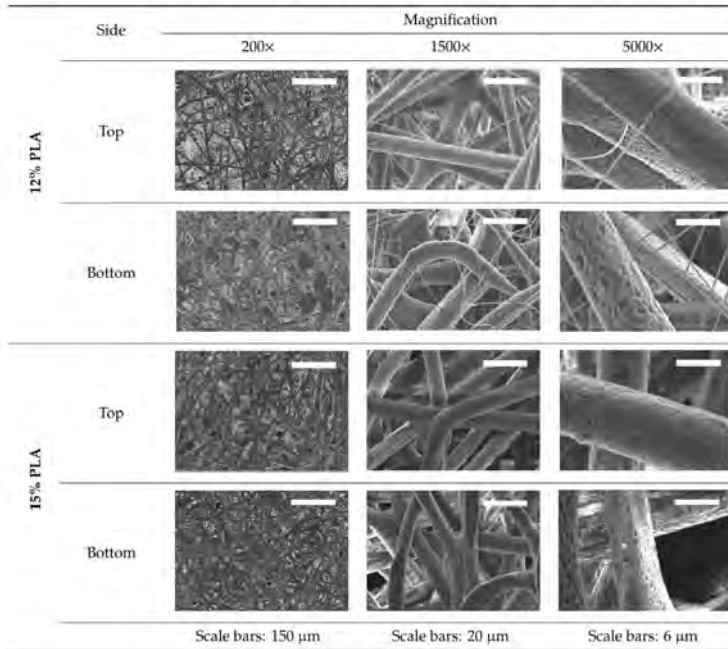


Figure 3. Features of 12% and 15% ES-PLA scaffolds. Images taken from the top and bottom sides were used to calculate (a) fiber diameter, (b) surface porosity, and (c) pore diameter. Results are shown as average \pm SE. SF: small fibers; LF: large fibers.

3.3. High Proliferation Rates are Obtained in Both 12% and 15% ES-PLA Scaffolds

Differences among microscopic features due to the percentage of PLA used may influence cell adhesion and growth. Therefore, cell viability assays were performed to ascertain whether MDA-MB-231 cells can be cultured using ES-PLA scaffolds and determine the optimal PLA concentration (Figure 4). Two culture periods were chosen, i.e., three and six days. As expected, cells cultured in 3D presented a lower proliferation rate than cells growing in a monolayer. Accordingly, these differences were more noticeable after six days. Nonetheless, cell growth was surprisingly high in both 12% and 15% PLA scaffolds, with no significant differences in any of the times assayed. Henceforth, the experiments were carried out using the non-beading 15% concentration PLA meshes.

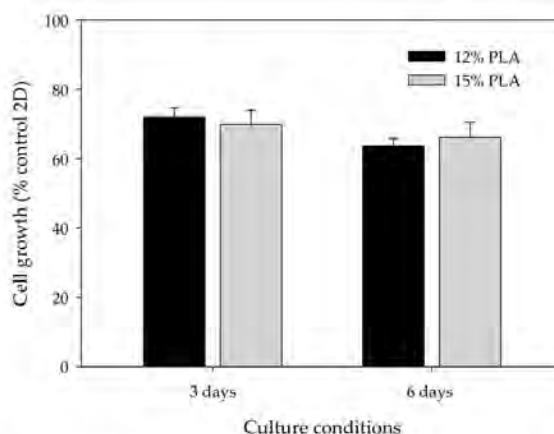


Figure 4. Cell proliferation analysis for MDA-MB-231 cells cultured in 3D using 12% PLA scaffolds (black bars) or 15% PLA scaffolds (grey bars) over three days (left) or six days (right). MDA-MB-231 cells cultured in 2D were used as a control. Experiments were performed at least three times.

3.4. EGFR and STAT3 are Altered in 3D-Cultured Cells

Previous investigations have demonstrated that EGFR gene expression, as well as STAT3 and EGFR protein activation, was altered in 3D-cultured cells [30,31]. For this reason, EGFR and STAT3 gene and protein levels were assessed by quantitative real time PCR and Western blotting (Figure 5). As expected, EGFR gene expression levels were significantly lower in 3D-cultured cells compared to cells cultured in monolayer. However, no changes in STAT3 gene expression were visualized in the three or six day cultures when comparing 2D and 3D cultures (Figure 5a). Furthermore, EGFR protein phosphorylation levels were decreased, whereas phosphorylation levels of STAT3 increased in 3D culture conditions, both in three and six day cultures (Figure 5b).

Moreover, it has been demonstrated that the STAT3 pathway is involved in cancer stem cell (CSC) self-renewal and cancer chemoresistance [29,30]. Hence, ES-PLA scaffolds' capacity to enrich the breast CSC (BCSC) population was evaluated.

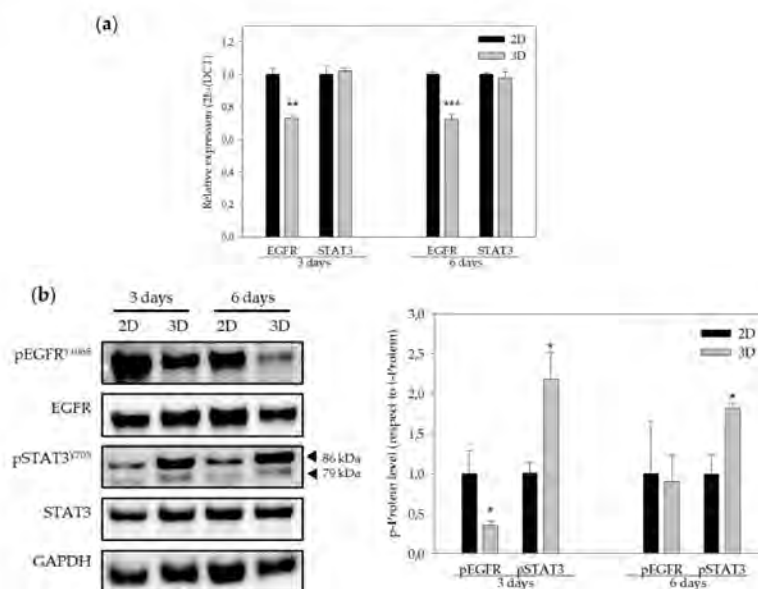


Figure 5. EGFR and STAT3 genes expression and protein levels. (a) EGFR and STAT3 gene expression of MDA-MB-231 cells cultured in 2D (black bars) and in 3D (grey bars) using 15% PLA scaffolds over three days (left) or six days (right). (b) Quantification of protein levels (EGFR and STAT3) obtained by Western blot analyses (right panel) of MDA-MB-231 cells cultured in 2D (black bars) and in 3D (grey bars) using 15% PLA scaffolds over three days (left) or six days (right). Results are expressed as the ratio of activated protein (p-Protein) vs. total levels of protein (t-Protein). Experiments were performed at least three times. * ($p < 0.05$) indicates levels of statistical significance. For an easier interpretation, the value obtained for cells cultured in 2D was adjusted to 1 and that of the 3D-cultured cells was calculated based on this.

3.5. ES-PLA Scaffolds Do Not Increase BCSC Population

Previously, our research group set up the conditions of the ES-scaffolds using polycaprolactone (PCL) to enrich the BCSC population in MDA-MB-231 cells [26,32]. BCSCs are a small subpopulation of cells capable of self-renewal, giving rise to the bulk of the tumour and responsible for relapse due to their chemoresistance [33–35]. We aimed then to discern the impact of ES-PLA scaffold culture on BCSC niche.

The BCSC population also exhibits the capability to grow in non-adherent surfaces, proliferating into suspension spheres called mammospheres [36]. Taking advantage of this capability, the mammosphere-forming (MF) assay was performed in cells previously cultured in monolayer and 15% ES-PLA meshes. Different cell culture periods, three and six days, were also assessed. As exhibited in Figure 6 monolayer-cultured cells displayed MFI values close to 2% in both culture periods. In contrast, cells from 3D cultures showed a slightly higher MF capacity compared with its correspondent 2D control, although no significant differences were found. This trend was found in both culture days tested.

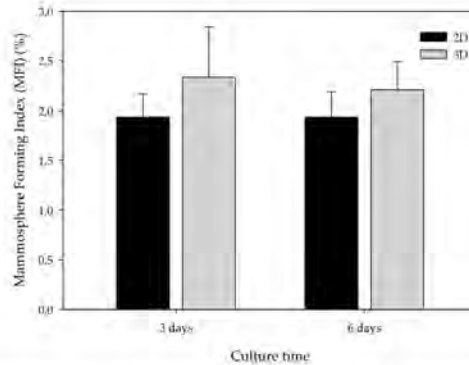


Figure 6. Mammosphere-forming Index (MFI) of MDA-MB-231 TNBC cells after monolayer (2D) or 15% PLA scaffolds (3D) culture. Experiments were performed at least three times.

CSCs showed higher expression of some stem cell markers, including Sox2 [37]. The role of epithelial-to-mesenchymal transition (EMT) has been related to the stem features acquisition [38–40]. EMT comprises different molecular alterations, including transcription factors such as Snail (zinc-finger protein SNAIL), among others, which modulate mesenchymal proteins like Vimentin (Vim) and downregulate epithelial proteins such as E-cadherin (E-cadh) [41]. EMT confers stem traits in non-stem cancer cells, possibly leading to BCSC enrichment during 3D culturing. For this reason, we evaluated the RNA expression of Snail, E-cadh, Vim, and Sox2 on 2D- and 3D-cultured cells (Figure 7).

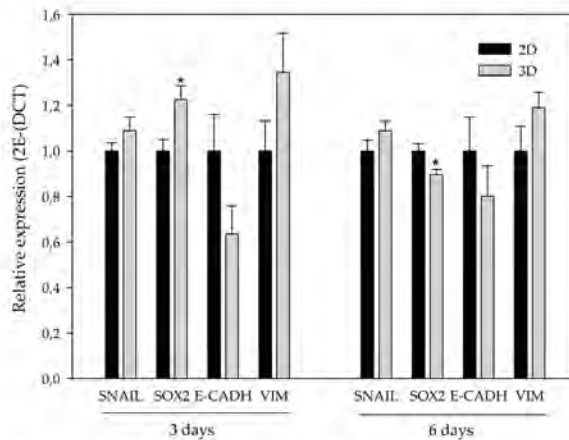


Figure 7. Epithelial-to-mesenchymal transition (EMT)-related and stemness gene expression. Stemness (Sox2) and EMT-related (Snail, E-cadherin, and Vimentin) gene expression of MDA-MB-231 culture in 2D (black bars) and in 3D (grey bars) using 15% PLA ES scaffolds over three days (left) and six days (right). Experiments were performed at least three times. For an easier interpretation, the value obtained for cells cultured in 2D was adjusted to 1 and that of the 3D-cultured cells was calculated based on this. * ($p < 0.05$) indicates levels of statistical significance.

Regarding EMT-related genes, the transcription factor Snail and the mesenchymal protein Vim presented a subtle trend to be upregulated in 3D-cultured cells with no significance. In addition, the observed tendency of Vim was higher after three days. In contrast, the expression of the epithelial protein E-cadh presented a non-significant decrease when comparing 3D-cultured cells with the monolayer culture. Again, the aforementioned decrease also exhibited a stronger trend after three days of culturing. Sox2 was significantly upregulated on cells cultured in scaffolds over three days, whereas it presented a downregulation at six days of culture.

4. Discussion

Despite the numerous advantages of traditional cell cultures in the field of cancer research, the monolayer growth of cells lacks a large number of tumor characteristics, including interactions with the ECM. This interactivity with non-cellular elements not only affects the morphological organization but also the activation of signaling pathways or the expression of proteins which may be biologically relevant [42]. In order to better understand the tumor behavior and improve the development of new therapeutic drugs, *in vitro* cells cultured in 3D systems will undoubtedly be of help. In this sense, ES-polymeric scaffolds have emerged as a cost-effective alternative to grow *in vitro* cells in 3D [43,44]. In this work, we studied for the first time the polymer PLA to manufacture scaffolds through ES for 3D culturing of breast cancer cells. The chosen PLA was first characterized in order to confirm its purity. Obtained DSC values, including glass transition, crystallization and melting temperature, were in concordance with those presented by Zou et al. [45]. Regarding the values showed in Table 1, the experimental PLA T_g was in agreement with the data provided by the manufacturer, whereas the obtained T_m was slightly lower. Moreover, the TGA curve acquired showed the same distribution in one step and temperatures than the TGA described in Zou et al. [45]. Consequently, the PLA used to electrospin scaffolds showed an optimal purity.

Both scaffolds from 12% and 15% PLA solution displayed similar weight and thickness values, due to the little difference of material amount of each solution. Moreover, they exhibited comparable filament diameter and porosity. Interestingly, 12% PLA meshes also possessed a secondary filament population, with a lower average diameter of 385 nm, as well as the presence of a non-filamented material known as beads. Previous works also observed the aforementioned phenomenon. For instance, Damanik et al. electrospun a 15% PLA solution at 12 kV and 7.5 mL/h, resulting in PLA meshes with a filament diameter close to 4.5 μm as well as the presence of a minor, thinner filament population [46]. The presence of beads was widely related to the use of a low polymer concentration [26,47,48].

3D-cultured cells are known to proliferate more slowly and survive for a longer period of time than 2D-cultured cells [49]. These microarchitecture differences in the PLA scaffolds did not directly affect MDA-MB-231 proliferation rate, with values around 70% compared to monolayer culture. The same cell line was previously cultured on PLA scaffolds made by FFF technology, resulting in larger pores and filament diameters. In this case, MDA-MB-231 cell proliferation was much lower, ranging from 5% to 25% compared to 2D-cultured cells, with significant differences between scaffold designs [32]. The improvement of cell proliferation into ES-PLA scaffolds makes them an optimal device for *in vitro* 3D cell culture, reproducing the spatial architecture of tumors.

EGFR signaling transduction pathways are related to cell proliferation, metabolism, migration, and survival [50]. Approximately 45% of TNBC patients show a higher expression of EGFR [51]. The results obtained showed a significant decrease in EGFR gene expression. Moreover, phosphorylation levels were significantly reduced after three days, whereas no change in total protein levels was noticed in the 3D cultures. Howes et al. observed that EGFR protein phosphorylation decreased whereas EGFR total protein levels increased in BT-474 Luminal B breast carcinoma cells co-cultured with human fibroblast and endothelial cells in 3D cultures compared to monolayer cultures [30]. Ekert et al. demonstrated that different lung adenocarcinoma cell lines showed a reduction of EGFR total protein levels in 3D cultures compared to monolayer cultures. In addition, EGFR phosphorylation levels decreased when cells were stimulated with growth factors in 3D cultures [52]. Unlike cells cultured using 3D systems,

monolayer-cultured cells are directly exposed to a medium rich in growth factors that might stimulate EGFR expression.

STAT3 is a transcription factor which controls the expression of different genes involved in tumor progression [53]. Despite STAT3 gene expression being similar in both cultures' systems, MDA-MB-231 cells exhibited an increase in STAT3 phosphorylation levels when cultured in ES-PLA scaffolds. This result is in agreement with that of Leslie et al., who demonstrated that mammary epithelial cells transformed with H-rasV12 and, when grown in mouse tissues, resulted in higher STAT3 phosphorylation levels compared to monolayer cultures [31], suggesting that STAT3 has a role in a 3D environment. Furthermore, it has been demonstrated that the STAT3 pathway is involved in CSCs self-renewal. Kroon et al. observed that STAT3 signaling was related to clonogenic and tumorigenic potential of CSCs in prostate cancer [54]. Also, Lin et al. showed that STAT3 was related to tumor growth and tumor-initiating potential in colon cancer [55].

According to these results, we wanted to discern whether ES-PLA scaffolds at the conditions assayed favored the maintenance of the BCSC population. CSCs have the capability to grow in suspension, forming mammospheres and showing greater expression of some stem cell markers, including Sox2 and OCT3/4 [36,37]. CSCs are related to the EMT process, a well-regulated cell program in embryogenesis which is responsible for much of tissue development [36]. Cancer epithelial cells can lose epithelial cell polarity and acquire mesenchymal abilities, such as invasion and migration, through EMT [56]. Hence, EMT confers stem traits, possibly leading to BCSC-enrichment in 3D cultures. Consequently, the capacity to form mammospheres, as well as the expression of genes related to EMT and stemness, was assessed. Cells previously cultured in scaffolds exhibited a subtle, non-significant, higher MF Index value, with a maximum at day three of culturing. Interestingly, it was also at this incubation period when significant overexpression of the Sox2 stemness marker was found on 3D-cultured cells. Likewise, expression of mesenchymal markers Snail and Vim on cells cultured in scaffolds exhibited uniformity or a non-significant upregulation, respectively, when compared with the monolayer control. Therefore, cells cultured into ES-PLA scaffolds seem to maintain a more epithelial phenotype rather than acquiring mesenchymal and more invasive features of CSCs. It is noteworthy that expression of the epithelial protein E-cadherin, which can be repressed by some transcription factors, including Snail, to induce EMT [41,56], seems to be downregulated on cells cultured in scaffolds at three days.

5. Conclusions

The high cell proliferation rates obtained using ES-PLA scaffolds make them a useful tool for 3D TNBC cell culture, taking the *in vitro* culture a step closer to physiological conditions and facilitating the study within a 3D environment of this aggressive cancer subtype devoid of a validated targeted therapy. In this sense, scaffolds may fill in the large gap between *in vitro* cell culture and *in vivo* experimentation, which could be useful for applications such as drug screening. Despite the fact that some stem features tend to be empowered on 3D-cultured cells, ES-PLA scaffolds do not show an important CSC-enrichment at the conditions assayed. However, taken altogether, these results set up the basis for future studies using ES-PLA scaffolds for oncology research purposes.

Author Contributions: Conceptualization, T.P., J.C. and S.R.-M.; methodology, E.P.-A., M.R.; validation, E.P.-A., M.R. and S.R.-M.; resources, T.P., J.C.; writing—original draft preparation, E.P.-A., M.R., D.A., X.G.; writing—review and editing E.P., M.R., J.C., S.R.-M., and T.P.; supervision, T.P. and S.R.-M.; funding acquisition, J.C. and T.P.

Funding: The authors acknowledge the financial support from the Ministry of Economy and Competitiveness (MINECO), Spain grants from DPI2016-77156-R, the financial support from the University of Girona (Spain) MPCUdG2016/036 and the pre-doctoral grant (IFUdG2017/62), and the support of the Catalan Government (2017SGR00385). This work was also partially supported by the grants from the Fundació Ramón Areces (Spain), the Instituto de Salud Carlos III (Spain) (PI1400329), and Fundació Oncolliga and RadikalSwim (OncoSwim).

Conflicts of Interest: The authors declare no conflict of interest. The funders had no role in the design of the study; in the collection, analyses, or interpretation of data; in the writing of the manuscript, or in the decision to publish the results.

References

- Frantz, C.; Stewart, K.M.; Weaver, V.M. The extracellular matrix at a glance. *J. Cell Sci.* **2010**, *123*, 4195–4200. [[CrossRef](#)] [[PubMed](#)]
- Theocharis, A.D.; Skandalis, S.S.; Gialeli, C.; Karamanos, N.K. Extracellular matrix structure. *Adv. Drug Deliv. Rev.* **2016**, *97*, 4–27. [[CrossRef](#)] [[PubMed](#)]
- Abbott, A. Cell culture: Biology's new dimension. *Nature* **2003**, *424*, 870–872. [[CrossRef](#)] [[PubMed](#)]
- Weigelt, B.; Ghajar, C.M.; Bissell, M.J. The need for complex 3D culture models to unravel novel pathways and identify accurate biomarkers in breast cancer. *Adv. Drug Deliv. Rev.* **2014**, *69–70*, 42–51. [[CrossRef](#)] [[PubMed](#)]
- DesRochers, T.M.; Palma, E.; Kaplan, D.L. Tissue-engineered kidney disease models. *Adv. Drug Deliv. Rev.* **2014**, *69–70*, 67–80. [[CrossRef](#)] [[PubMed](#)]
- Pampaloni, F.; Stelzer, E.H.K.; Leicht, S.; Marcelllo, M. Madin-Darby canine kidney cells are increased in aerobic glycolysis when cultured on flat and stiff collagen-coated surfaces rather than in physiological 3-D cultures. *Proteomics* **2010**, *10*, 3394–3413. [[CrossRef](#)]
- Loessner, D.; Stok, K.S.; Lutolf, M.P.; Huttmacher, D.W.; Clements, J.A.; Rizzi, S.C. Bioengineered 3D platform to explore cell-ECM interactions and drug resistance of epithelial ovarian cancer cells. *Biomaterials* **2010**, *31*, 8494–8506. [[CrossRef](#)]
- Ridky, T.W.; Chow, J.M.; Wong, D.J.; Khavari, P.A. Invasive three-dimensional organotypic neoplasia from multiple normal human epithelia. *Nat. Med.* **2010**, *16*, 1450–1455. [[CrossRef](#)]
- Li, C.-L.; Tian, T.; Nan, K.-J.; Zhao, N.; Guo, Y.-H.; Cui, J.; Wang, J.; Zhang, W.-G. Survival advantages of multicellular spheroids vs. monolayers of HepG2 cells in vitro. *Oncol. Rep.* **2008**, *20*, 1465–1471. [[CrossRef](#)]
- Chopra, V.; Dinh, T.V.; Hannigan, E.V. Three-dimensional endothelial-tumor epithelial cell interactions in human cervical cancers. *In Vitro Cell. Dev. Biol. Anim.* **1997**, *33*, 432–442. [[CrossRef](#)]
- Polonio-Alcalá, E.; Rabionet, M.; Ruiz-Martínez, S.; Ciurana, J.; Puig, T. Three-Dimensional Manufactured Supports for Breast Cancer Stem Cell Population Characterization. *Curr. Drug Targets* **2018**, *20*. [[CrossRef](#)]
- Sill, T.J.; von Recum, H.A. Electrospinning: Applications in drug delivery and tissue engineering. *Biomaterials* **2008**, *29*, 1989–2006. [[CrossRef](#)]
- Knight, E.; Przyborski, S. Advances in 3D cell culture technologies enabling tissue-like structures to be created in vitro. *J. Anat.* **2014**, *1–11*. [[CrossRef](#)]
- Sun, Y.; Shan, H.; Wang, J.; Wang, X.; Yang, X.; Ding, J. Laden Nanofiber Capsules for Local Malignancy Chemotherapy. *J. Biomed. Nanotechnol.* **2019**, *15*, 939–950. [[CrossRef](#)]
- Zhang, J.; Liu, H.; Xu, H.; Ding, J.-X.; Zhuang, X.-L.; Chen, X.-S.; Chang, F.; Xu, J.-Z.; Li, Z.-M. Molecular weight-modulated electrospun poly(ϵ -caprolactone) membranes for postoperative adhesion prevention. *RSC Adv.* **2014**, *4*, 41696–41704. [[CrossRef](#)]
- Liu, X.; Holzwarth, J.M.; Ma, P.X. Functionalized Synthetic Biodegradable Polymer Scaffolds for Tissue Engineering. *Macromol. Biosci.* **2012**, *12*, 911–919. [[CrossRef](#)]
- Gregor, A.; Filová, E.; Novák, M.; Kronek, J.; Chlup, H.; Buzgo, M.; Blahnová, V.; Lukášová, V.; Bartoš, M.; Nečas, A.; Hošek, J. Designing of PLA scaffolds for bone tissue replacement fabricated by ordinary commercial 3D printer. *J. Biol. Eng.* **2017**, *11*, 31. [[CrossRef](#)]
- Tamai, H.; Igaki, K.; Kyo, E.; Kosuga, K.; Kawashima, A.; Matsui, S.; Komori, H.; Tsuji, T.; Motohara, S.; Uehata, H. Initial and 6-month results of biodegradable poly-l-lactic acid coronary stents in humans. *Circulation* **2000**, *102*, 399–404. [[CrossRef](#)]
- Ferlay, J.; Steliarova-Foucher, E.; Lortet-Tieulent, J.; Rosso, S.; Coebergh, J.W.W.; Comber, H.; Forman, D.; Bray, F. Cancer incidence and mortality patterns in Europe: Estimates for 40 countries in 2012. *Eur. J. Cancer* **2013**, *49*, 1374–1403. [[CrossRef](#)]
- Siegel, R.L.; Miller, K.D.; Jemal, A. Cancer statistics, 2018. *CA. Cancer J. Clin.* **2018**, *68*, 7–30. [[CrossRef](#)]
- Dent, R.; Trudeau, M.; Pritchard, K.I.; Hanna, W.M.; Kahn, H.K.; Sawka, C.A.; Lickley, L.A.; Rawlinson, E.; Sun, P.; Narod, S.A. Triple-negative breast cancer: Clinical features and patterns of recurrence. *Clin. Cancer Res.* **2007**, *13*, 4429–4434. [[CrossRef](#)]
- Anders, C.K.; Carey, L.A. Biology, Metastatic Patterns, and Treatment of Patients with Triple-Negative Breast Cancer. *Clin. Breast Cancer* **2009**, *9*, S73–S81. [[CrossRef](#)] [[PubMed](#)]

23. Liedtke, C.; Rody, A.; Gluz, O.; Baumann, K.; Beyer, D.; Kohls, E.-B.; Lausen, K.; Hankaer, L.; Holtrich, U.; Becker, S.; et al. The prognostic impact of age in different molecular subtypes of breast cancer. *Breast Cancer Res. Treat.* **2015**, *152*, 667–673. [[CrossRef](#)] [[PubMed](#)]
24. Cinkaya, A.; Akin, M.; Sengul, A. Evaluation of treatment outcomes of triple-negative breast cancer. *J. Cancer Res. Ther.* **2016**, *12*, 150. [[CrossRef](#)] [[PubMed](#)]
25. Guerra, A.J.; Cano, P.; Rabionet, M.; Puig, T.; Ciurana, J. Effects of different sterilization processes on the properties of a novel 3D-printed polycaprolactone stent. *Polym. Adv. Technol.* **2018**, *29*, 2327–2335. [[CrossRef](#)]
26. Rabionet, M.; Yeste, M.; Puig, T.; Ciurana, J. Electrospinning PCL scaffolds manufacture for three-dimensional breast cancer cell culture. *Polymers (Basel)*. **2017**, *9*, 328. [[CrossRef](#)] [[PubMed](#)]
27. Giró-Perafita, A.; Palomerias, S.; Lum, D.H.; Blancafort, A.; Viñas, G.; Oliveras, G.; Pérez-Bueno, F.; Sarrats, A.; Welm, A.L.; Puig, T. Preclinical Evaluation of Fatty Acid Synthase and EGFR Inhibition in Triple Negative Breast Cancer. *Clin. Cancer Res.* **2016**, *22*, 4687–4697. [[CrossRef](#)]
28. Livak, K.J.; Schmittgen, T.D. Analysis of Relative Gene Expression Data Using Real-Time Quantitative PCR and the 2^{-Delta Delta} C(T) Method. *METHODS* **2001**, *25*, 402–408. [[CrossRef](#)]
29. Giró-Perafita, A.; Rabionet, M.; Puig, T.; Ciurana, J. Optimization of Poly(ϵ -caprolactone) scaffolds suitable for 3D cancer cell culture. *Procedia CIRP* **2016**, *49*, 61–66.
30. Howes, A.L.; Richardson, R.D.; Finlay, D.; Vuori, K. 3-Dimensional culture systems for anti-cancer compound profiling and high-throughput screening reveal increases in EGFR inhibitor-mediated cytotoxicity compared to monolayer culture systems. *PLoS ONE* **2014**, *9*, e108283. [[CrossRef](#)]
31. Leslie, K.; Gao, S.P.; Berishaj, M.; Podyspanina, K.; Ho, H.; Ivashkiv, L.; Bromberg, J. Differential interleukin-6/Stat3 signaling as a function of cellular context mediates Ras-induced transformation. *Breast Cancer Res.* **2010**, *12*, R80. [[CrossRef](#)]
32. Polonio-Alcalá, E.; Rabionet, M.; Guerra, A.; Yeste, M.; Ciurana, J.; Puig, T.; Polonio-Alcalá, E.; Rabionet, M.; Guerra, A.J.; Yeste, M.; et al. Screening of Additive Manufactured Scaffolds Designs for Triple Negative Breast Cancer 3D Cell Culture and Stem-Like Expansion. *Int. J. Mol. Sci.* **2018**, *19*, 3148. [[CrossRef](#)] [[PubMed](#)]
33. Palomerias, S.; Ruiz-Martínez, S.; Puig, T. Targeting Breast Cancer Stem Cells to Overcome Treatment Resistance. *Molecules* **2018**, *23*, 2193. [[CrossRef](#)] [[PubMed](#)]
34. Diehn, M.; Cho, R.W.; Lobo, N.A.; Kalisky, T.; Dorie, M.J.; Kulp, A.N.; Qian, D.; Lam, J.S.; Ailles, L.E.; Wong, M.; et al. Association of reactive oxygen species levels and radioresistance in cancer stem cells. *Nature* **2009**, *458*, 780–783. [[CrossRef](#)] [[PubMed](#)]
35. Nakamura, K.; Iinuma, H.; Aoyagi, Y.; Shibuya, H.; Watanabe, T. Predictive value of cancer stem-like cells and cancer-associated genetic markers for peritoneal recurrence of colorectal cancer in patients after curative surgery. *Oncology* **2010**, *78*, 309–315. [[CrossRef](#)]
36. Dontu, G.; Abdallah, W.M.; Foley, J.M.; Jackson, K.W.; Clarke, M.F.; Kawamura, M.J.; Wicha, M.S. In vitro propagation and transcriptional profiling of human mammary stem / progenitor cells. *Genes Dev.* **2003**, *17*, 1253–1270. [[CrossRef](#)]
37. Okumura-Nakanishi, S.; Saito, M.; Niwa, H.; Ishikawa, F. Oct-3/4 and Sox2 Regulate Oct-3/4 Gene in Embryonic Stem Cells. *J. Biol. Chem.* **2005**, *280*, 5307–5317. [[CrossRef](#)]
38. Kotiyal, S.; Bhattacharya, S. Breast cancer stem cells, EMT and therapeutic targets. *Biochem. Biophys. Res. Commun.* **2014**, *453*, 112–116. [[CrossRef](#)]
39. Luo, M.; Brooks, M.; Wicha, M.S. Epithelial-mesenchymal plasticity of breast cancer stem cells: Implications for metastasis and therapeutic resistance. *Curr. Pharm. Des.* **2015**, *21*, 1301–1310. [[CrossRef](#)]
40. Mani, S.A.; Guo, W.; Liao, M.-J.; Eaton, E.N.; Ayyanan, A.; Zhou, A.Y.; Brooks, M.; Reinhard, F.; Zhang, C.C.; Shipitsin, M.; et al. The Epithelial-Mesenchymal Transition Generates Cells with Properties of Stem Cells. *Cell* **2008**, *133*, 704–715. [[CrossRef](#)]
41. Moreno-Bueno, G.; Portillo, F.; Cano, A. Transcriptional regulation of cell polarity in EMT and cancer. *Oncogene* **2008**, *27*, 6958–6969. [[CrossRef](#)]
42. Xu, X.; Farach-Carson, M.C.; Jia, X. Three-dimensional in vitro tumor models for cancer research and drug evaluation. *Biotechnol. Adv.* **2014**, *32*, 1256–1268. [[CrossRef](#)]
43. Palomerias, S.; Rabionet, M.; Ferrer, I.; Sarrats, A.; Garcia-Romeu, M.L.; Puig, T.; Ciurana, J. Breast Cancer Stem Cell Culture and Enrichment Using Poly(ϵ -Caprolactone) Scaffolds. *Molecules* **2016**, *21*, 537. [[CrossRef](#)]
44. Feng, S.; Duan, X.; Lo, P.-K.; Liu, S.; Liu, X.; Chen, H.; Wang, Q. Expansion of breast cancer stem cells with fibrous scaffolds. *Integr. Biol. (Camb)*. **2013**, *5*, 768–777. [[CrossRef](#)]

45. Zou, W.; Chen, R.; Zhang, H.; Qu, J. Preparation, melting behavior and thermal stability of poly(lactic acid)/poly(propylene carbonate) blends processed by vane extruder. In *AIP Conference Proceedings*; AIP Publishing LLC: Melville, NY, USA, 2016; Volume 1713, p. 050003.
46. Damanik, F.F.R.; Spadolini, G.; Rotmans, J.; Farè, S.; Moroni, L. Biological activity of human mesenchymal stromal cells on polymeric electrospun scaffolds. *Biomater. Sci.* **2019**. [[CrossRef](#)]
47. Fong, H.; Chun, L.; Reneker, D. Beaded nanofibers formed during electrospinning. *Polymer (Guildf)*. **1999**, *40*, 4585–4592. [[CrossRef](#)]
48. Chen, M.; Patra, P.K.; Warner, S.B.; Bhowmick, S. Optimization of electrospinning process parameters for tissue engineering scaffolds. *Biophys. Rev. Lett.* **2006**, *01*, 153–178. [[CrossRef](#)]
49. Li, S.; Lao, J.; Chen, B.P.; Li, Y.S.; Zhao, Y.; Chu, J.; Chen, K.D.; Tsou, T.C.; Peck, K.; Chien, S. Genomic analysis of smooth muscle cells in 3-dimensional collagen matrix. *FASEB J.* **2003**, *17*, 97–99. [[CrossRef](#)]
50. Citri, A.; Yarden, Y. EGF–ERBB signalling: Towards the systems level. *Nat. Rev. Mol. Cell Biol.* **2006**, *7*, 505–516. [[CrossRef](#)]
51. Nielsen, T.O.; Hsu, F.D.; Jensen, K.; Cheang, M.; Karaca, G.; Hu, Z.; Hernandez-Boussard, T.; Livasy, C.; Cowan, D.; Dressler, L.; et al. Immunohistochemical and Clinical Characterization of the Basal-Like Subtype of Invasive Breast Carcinoma. *Clin. Cancer Res.* **2004**, *10*, 5367–5374. [[CrossRef](#)]
52. Ekert, J.E.; Johnson, K.; Strake, B.; Pardin, J.; Jarantow, S.; Perkinson, R.; Colter, D.C. Three-dimensional lung tumor microenvironment modulates therapeutic compound responsiveness in vitro—implication for drug development. *PLoS ONE* **2014**, *9*, e92248. [[CrossRef](#)]
53. Yu, H.; Lee, H.; Herrmann, A.; Buettner, R.; Jove, R. Revisiting STAT3 signalling in cancer: New and unexpected biological functions. *Nat. Rev. Cancer* **2014**, *14*, 736–746. [[CrossRef](#)] [[PubMed](#)]
54. Kroon, P.; Berry, P.A.; Stower, M.J.; Rodrigues, G.; Mann, V.M.; Simms, M.; Bhasin, D.; Chettiar, S.; Li, C.; Li, P.-K.; et al. JAK-STAT Blockade Inhibits Tumor Initiation and Clonogenic Recovery of Prostate Cancer Stem-like Cells. *Cancer Res.* **2013**, *73*, 5288–5298. [[CrossRef](#)] [[PubMed](#)]
55. Lin, L.; Liu, A.; Peng, Z.; Lin, H.J.; Li, P.K.; Li, C.; Lin, J. STAT3 Is Necessary for Proliferation and Survival in Colon Cancer-Initiating Cells. *Cancer Res.* **2011**, *71*, 7226–7237. [[CrossRef](#)] [[PubMed](#)]
56. Tomaskovic-Crook, E.; Thompson, E.W.; Thiery, J.P. Epithelial to mesenchymal transition and breast cancer. *Breast Cancer Res.* **2009**, *11*, 213. [[CrossRef](#)]



© 2019 by the authors. Licensee MDPI, Basel, Switzerland. This article is an open access article distributed under the terms and conditions of the Creative Commons Attribution (CC BY) license (<http://creativecommons.org/licenses/by/4.0/>).

Results II. Evaluation of PCL scaffolds manufactured by ES
technology for 3D cell culture of LCSCs

This section is based on the following publication:

Title	Polycaprolactone Electrospun Scaffolds Produce an Enrichment of Lung Cancer Stem Cells in Sensitive and Resistant EGFRm Lung Adenocarcinoma
Authors	Emma Polonio-Alcalá, Marc Rabionet, Santiago Ruiz-Martínez, Sònia Palomeras, Rut Porta, Carmen Vásquez-Dongo, Joaquim Bosch-Barrera, Teresa Puig*, and Joaquim Ciurana*
Journal	Cancers
Publication Year	2021
Impact Factor <small>2020</small>	6.575 (Q1 in Oncology; Position 60 of 245)
DOI	10.3390/cancers13215320

Abstract

Although PLA scaffolds were useful for 3D cell culture, these structures did not show a significant BCSC expansion. Moreover, previous studies demonstrated that the use of PCL-ES scaffolds to culture TNBC cell models provided an enrichment of the BCSC niche.

This chapter aims to evaluate PCL-ES scaffolds for culturing LCSCs in sensitive and resistant EGFRm NSCLC cell models. First, thermal characterization of these 3D structures was performed by TGA, DSC, and DMA. The microstructure was also described through the analysis of SEM images. Then, the effect of the sterilization process and medium soaking on PCL-ES scaffolds was tested through the weight degradation assay and the adsorption protein capacity. Second, cell morphology and viability of sensitive and resistant EGFRm NSCLC cell models, PC9 and PC9-GR3 cells, cultured on PCL-ES matrices were examined through confocal laser scanning microscope (CLSM) and the MTT assay, respectively. Additionally, EGFR status was determined in cell models seeded on 3D scaffolds. Third, several LCSC features were investigated to assess a potential LCSC enrichment of PC9 and PC9-GR3 cells grown on PCL-ES structures, such as resistance to the treatment, or gene and protein expression of multi-drug efflux pumps, EMT and stemness markers, membrane receptors, and Hedgehog and Canonical pathways. Finally, Vimentin and CD133 tumor expression of samples from patients with EGFRm NSCLC was analyzed to corroborate *in vitro* results.

The results obtained revealed that PCL-ES scaffolds were stiffer than healthy lung tissue but softer than 2D cell culture plates. Furthermore, only the sterilization process caused changes in the weight of 3D structures. The microarchitecture of PCL-ES scaffolds supported cell attachment, growth, and morphology changes. It was also observed that the protein adsorbed for these 3D matrices was correlated to cell viability. Furthermore, PC9 and PC9-GR3 cells cultured on PCL-ES scaffolds enriched several LCSC features. Concretely, 3D-cultured cells exhibited higher resistance to osimertinib treatment, enhanced levels of the multi-drug efflux pump *ABCB1*, upregulation of Vimentin, *SNAIL*, *TWIST*, *Sox2*, *Oct-4*, and *CD166*, downregulation of E-cadherin and *CD133*, and the activation of Hedgehog pathway.

Results II

No differences were observed in phosphorylated EGFR levels in cells seeded on PCL-ES scaffolds, probably as a consequence of the maintenance of LCSC properties. Moreover, the non-expression of CD133 from tumor samples from patients with EGFRm NSCLC was significantly associated with a low degree of histological differentiation, disease progression, and distant metastasis, features directly connected to the LCSC population. Therefore, PCL-ES scaffolds provide a reliable 3D cell culture strategy to mimic a physiological environment allowing the investigation of EGFRm NSCLC to explore new biomarkers or test new drugs.



Article

Polycaprolactone Electrospun Scaffolds Produce an Enrichment of Lung Cancer Stem Cells in Sensitive and Resistant EGFRm Lung Adenocarcinoma

Emma Polonio-Alcalá ^{1,2}, Marc Rabionet ^{1,2}, Santiago Ruiz-Martínez ², Sònia Palomeras ², Rui Porta ^{2,3}, Carmen Vázquez-Dongo ^{2,4}, Joaquim Bosch-Barrera ³, Teresa Puig ^{2,4} and Joaquim Ciurana ^{1,4}

¹ Product, Process and Production Engineering Research Group (GREP), Department of Mechanical Engineering and Industrial Construction, University of Girona, 17003 Girona, Spain; emma.polonio@udg.edu (E.P.-A.); m.rabionet@udg.edu (M.R.)

² New Therapeutic Targets Laboratory (TargetsLab)-Oncology Unit, Department of Medical Sciences, Faculty of Medicine, University of Girona, 17003 Girona, Spain; santiago.ruiz@udg.edu (S.R.-M.); sonia.palomeras@udg.edu (S.P.); rporta@iconcologia.net (R.P.); cavasquez.girona.ics@genecat.cat (C.V.-D.)

³ Medical Oncology Department, Catalan Institute of Oncology, 17007 Girona, Spain; jbosch@iconcologia.net

⁴ Department of Pathology, Dr. Josep Trueta University Hospital, 17007 Girona, Spain

* Correspondence: teresa.puig@udg.edu (T.P.); quim.ciurana@udg.edu (J.C.);

Tel.: +34-972-419-628 (T.P.); +34-972-418-384 (J.C.)



Citation: Polonio-Alcalá, E.; Rabionet, M.; Ruiz-Martínez, S.; Palomeras, S.; Porta, R.; Vázquez-Dongo, C.; Bosch-Barrera, J.; Puig, T.; Ciurana, J. Polycaprolactone Electrospun Scaffolds Produce an Enrichment of Lung Cancer Stem Cells in Sensitive and Resistant EGFRm Lung Adenocarcinoma. *Cancers* **2021**, *13*, 5320. <https://doi.org/10.3390/cancers13215320>

Academic Editor: Marielena Loizidou

Received: 8 September 2021

Accepted: 21 October 2021

Published: 22 October 2021

Publisher's Note: MDPI stays neutral with regard to jurisdictional claims in published maps and institutional affiliations.



Copyright: © 2021 by the authors. Licensee MDPI, Basel, Switzerland. This article is an open access article distributed under the terms and conditions of the Creative Commons Attribution (CC BY) license (<https://creativecommons.org/licenses/by/4.0/>).

Simple Summary: The culture of lung cancer stem cells (LCSCs) is not possible using traditional flat polystyrene surfaces. The study of these tumor-initiating cells is fundamental due to their key role in the resistance to anticancer therapies, tumor recurrence, and metastasis. Hence, we evaluated the use of polycaprolactone electrospun (PCL-ES) scaffolds for culturing LCSC population in sensitive and resistant EGFR-mutated lung adenocarcinoma models. Our findings revealed that both cell models seeded on PCL-ES structures showed a higher drug resistance, enhanced levels of several genes and proteins related to epithelial-to-mesenchymal process, stemness, and surface markers, and the activation of the Hedgehog pathway. We also determined that the non-expression of CD133 was associated with a low degree of histological differentiation, disease progression, distant metastasis, and worse overall survival in EGFR-mutated non-small cell lung cancer patients. Therefore, we confirmed PCL-ES scaffolds as a suitable three-dimensional cell culture model for the study of LCSC niche.

Abstract: The establishment of a three-dimensional (3D) cell culture model for lung cancer stem cells (LCSCs) is needed because the study of these stem cells is unable to be done using flat surfaces. The study of LCSCs is fundamental due to their key role in drug resistance, tumor recurrence, and metastasis. Hence, the purpose of this work is the evaluation of polycaprolactone electrospun (PCL-ES) scaffolds for culturing LCSCs in sensitive and resistant EGFR-mutated (EGFRm) lung adenocarcinoma cell models. We performed a thermal, physical, and biological characterization of 10% and 15% PCL-ES structures. Several genes and proteins associated with LCSC features were analyzed by RT-qPCR and Western blot. Vimentin and CD133 tumor expression were evaluated in samples from 36 patients with EGFRm non-small cell lung cancer through immunohistochemistry. Our findings revealed that PC9 and PC9-GR3 models cultured on PCL-ES scaffolds showed higher resistance to osimertinib, upregulation of ABCB1, Vimentin, Snail, Twist, Sox2, Oct-4, and CD166, downregulation of E-cadherin and CD133, and the activation of Hedgehog pathway. Additionally, we determined that the non-expression of CD133 was significantly associated with a low degree of histological differentiation, disease progression, and distant metastasis. To sum up, we confirmed PCL-ES scaffolds as a suitable 3D cell culture model for the study of the LCSC niche.

Keywords: NSCLC; cancer stem cells; 3D cell culture; electrospinning; CD133; Vimentin

1. Introduction

Lung cancer is the leading cause of cancer-related mortality worldwide among men and women [1]. The 5-year survival rate is 19.4%, and about 57% of lung cancer cases are diagnosed at advanced stages of the disease when surgical resection is not possible and radio- and chemotherapy show a response rate of roughly 25% [2,3]. Non-small cell lung cancer (NSCLC) is the most common subtype, and approximately 40% of cases are diagnosed as adenocarcinoma [4]. The discovery of activating mutations in the tyrosine kinase domain of the epidermal growth factor receptor (EGFR) led to the development of different targeted therapies, such as gefitinib or osimertinib. Despite the good initial response to these therapies, most patients develop progressive disease, acquiring resistance through different mechanisms [5,6]. Therefore, there is an indubitable need to better understand the disease in order to identify new biomarkers.

Cancer stem cells (CSCs) are a small subpopulation within the tumor responsible for cancer recurrence, metastasis, and resistance to current therapies. These tumor-initiating cells have self-renewal and pluripotency capacities [7–9]. The stemness potential is closely regulated by several transcription factors, such as Sox2, Oct-4, and Nanog [10–12]. Consequently, lung cancer stem cells (LCSCs) play a key role in the occurrence and development of lung cancer by driving intratumor heterogeneity [13]. Different surface markers have been linked to this malignant subpopulation, such as CD133, CD166, CD24, or CD90 [14–17]. Cancer cells are also capable of removing cell–cell and cell–matrix interactions to migrate from the primary tumor to other organs through the epithelial-to-mesenchymal transition (EMT) process [18]. EMT is also related to cancer stemness and resistance to anticancer therapies [19]. Furthermore, researchers have reported that the canonical Wnt/ β -catenin and the Hedgehog signaling pathways are crucial for the LCSC population [20,21].

Lung cancer is traditionally studied using two-dimensional (2D) cell culture and animal models. Nonetheless, these methodologies have some limitations. Monolayer culture does not fully mimic the tumor microenvironment where the extracellular matrix (ECM) has an essential role in some processes, for example gene expression and drug response. At the same time, cancer cells affect ECM deposition, degradation, and remodeling, influencing tumor progression and invasiveness [22]. Although 2D cell culture is a well-established, simple, and economical method, flat surfaces alter apical-basal polarity, nutrient and oxygen distribution, soluble gradients, and cell proliferation, morphology, and interactions [23]. Additionally, monolayer culture causes the differentiation of CSCs, which lose their stemness behavior [24]. Animal models offer a natural *in vivo* environment, but they are expensive and their use is discouraged due to the 3R (Replacement, Reduction, and Refinement) principle. Only 8% of drugs tested in animal systems remain in clinical trials; hence, they do not predict human responses properly [25]. Thus, more reliable and suitable *in vitro* culture systems are required to reduce the number of animals for scientific research.

In the past few years, researchers have studied several three-dimensional (3D) strategies to simulate physiological lung tissue conditions, such as decellularized lung scaffolds [26], hydrogel matrices [27], tumors-on-chip [28], patient-derived organoids [29], cell-line spheroids [30], or biopolymeric structures [31,32], among others. Chen et al. highlighted that not only oncogenic changes but also the surrounding microenvironment are crucial for the definitive cell phenotype in lung adenocarcinoma [33]. Cell proliferation, genetic and protein expression, and response to drugs are modified in cells cultured on 3D models compared to monolayer culture [22]. Besides this, researchers have pointed out that mechanical signals induced by cell-generated physical force cause changes in cell morphology, adhesion, alignment, differentiation, and migration [34]. Electrospinning is a cost-effective and simple technique that produces nanofibers similar to the ECM structure [35]. Moreover, electrospun (ES) scaffolds provide a 3D configuration that possesses a high surface area-to-volume ratio, allowing cell attachment. Polycaprolactone (PCL) is a synthetic polymer frequently selected for scaffold manufacturing. It is commonly used with electrospinning technology because of its low melting temperature (around 60 °C)

and easy adjustability. This low-cost material is suitable for biomedical and cell culture applications due to its biocompatibility, bioresorbability, and long-term biodegradability [36]. Previously, our research group reported that PCL-ES platforms increase the CSC population in breast cancer [37].

The main aim of this study was to evaluate the effectiveness of PCL-ES scaffolds for culturing the LCSC niche. Sensitive and resistant EGFR-mutated (EGFRm) lung adenocarcinoma cell models were seeded on the resulting meshes from two different PCL concentrations (10 and 15% *w/v*), and then several LCSC features were analyzed. Moreover, Vimentin and CD133 tumor expression were also evaluated in 36 samples from patients with EGFRm NSCLC in order to validate *in vitro* results.

2. Materials and Methods

2.1. Chemicals & Reagents

Polycaprolactone (PCL, Mn 80,000 g/mol), paraformaldehyde, Triton™ X-100, 3-(4,5-dimethyl-2-thiazolyl)-2,5-diphenyl-2H-tetrazolium bromide (MTT), bovine serum albumin (BSA) (≥98.0%), phenylmethylsulfonylfluoride (PMSF), TWEEN® 20, and primers (Table S1) were purchased from Sigma-Aldrich (St. Louis, MO, USA). BSA Fraction V pH for Western blotting (min. 96%), acetone (min. ≥99.8%), and tris-buffered saline (TBS) were provided from PanReac AppliChem (Gatersleben, Germany). Ethanol absolute was obtained from Labkem-Labbox Labware S.L. (Barcelona, Spain) and Qiazol was acquired by Qiagen (Hilden, Germany). Roswell Park Memorial Institute (RPMI-1640) medium, penicillin/streptomycin 10,000 U/mL, phosphate-buffered saline (PBS), and trypsin 10× were supplied from Lonza (Basilea, Switzerland) and fetal bovine serum (FBS) was purchased from HyClone (Logan, UT, USA). DC Protein Assay, 40% acrylamide solution, and Clarity™ Western ECL Substrate were obtained from Bio-Rad (Hercules, CA, USA). Rhodamine-phalloidin was acquired from Cytoskeleton Inc. (Denver, CO, USA) and 4,6-diamidino-2-phenylindole (DAPI) was provided from BD Pharmingen (Franklin Lakes, NJ, USA). GeneJET RNA Purification Kit, nitrocellulose membranes, and West Femto Maximum Sensitivity Substrate were supplied by Thermo Fisher Scientific Inc. (Waltham, MA, USA). High Capacity cDNA Archive Kit was purchased from Applied Biosystems (Foster City, CA, USA) and qPCRBIO SyGreen Mix Lo-Rox was obtained from PCR Biosystems Inc. (Wayne, PA, USA). Lithium dodecyl sulfate (LDS) sample buffer and sample reducing agent were acquired from Invitrogen (Carlsbad, CA, USA). Lysis buffer was purchased from Cell Signaling Technology (CST) Inc. (Danvers, MA, USA). Antibodies (Table S2) were provided from CST, Abcam (Cambridge, UK), ProteinTech® (Manchester, UK), and Roche Diagnostics (Basilea, Switzerland). Osimertinib was kindly supplied by AstraZeneca (Cambridge, UK). UltraView Universal DAB Detection Kit and Amplification Kit were purchased from Roche Diagnostics.

2.2. Electrospun Scaffolds Manufacturing

PCL was dissolved in acetone at 10% and 15% (*w/v*) under agitation at 60 °C for 24 h. Scaffolds were manufactured by an electrospinning machine (Spraybase, Dublin, Ireland). The solution was moved to a 20 mL syringe connected to a stainless steel 18G needle (inner diameter of 0.8 mm) through a polytetrafluoroethylene tube (inner diameter of 1 mm). The distance between the emitter and collector was 10 cm. The electrospinning process was established by Syringe Pump Pro software (New Era Pump Systems; Farmingdale, NY, USA). For the 10% PCL concentration, 8.5 mL of solution was ejected at a voltage of 9 kV and a flow rate of 6 mL/h. For the 15% PCL concentration, 5 mL was ejected at a voltage of 7 kV and a flow rate of 6 mL/h. The resulting meshes were cut and sterilized as described elsewhere [38].

2.3. Thermal Analysis

2.3.1. Thermogravimetric Analysis

The thermal stability of PCL-ES scaffolds was determined by thermogravimetric analysis (TGA) using Mettler-Toledo TGA/DSC 1 (Mettler-Toledo; Columbus, OH, USA). Samples (11.45 mg for 10% PCL; 10.03 mg for 15% PCL) were performed at a heating rate of 10 °C/min at a temperature range from 30 to 700 °C under a nitrogen atmosphere.

2.3.2. Differential Scanning Calorimetry

The calorimetric behavior of PCL-ES structures was measured by differential scanning calorimetry (DSC) using TA Instruments Q2000 (TA Instruments; New Castle, DE, USA). Samples (4.71 mg for 10% PCL; 5.42 mg for 15% PCL) were contained in an aluminum pan under a dynamic nitrogen atmosphere (50 mL/min) at a heating rate of 10 °C/min from 30 to 100 °C.

2.3.3. Dynamic Mechanical Analysis

The viscoelastic property of PCL-ES scaffolds was measured by dynamic mechanical analysis (DMA) using Mettler-Toledo DMA/SDTA861e (Mettler-Toledo). The size samples were 5.50 mm of length, 7.00 mm of width, and 0.65 mm of thickness. DMA was performed in tensile test mode, at a heating rate of 5 °C from −85 °C to 45 °C with 1 Hz of frequency and 50 µm of amplitude.

2.4. PCL Electrospun Scaffolds Observation through Scanning Electron Microscopy

The weight and thickness of PCL-ES scaffolds were measured by the Sartorius ED224S analytical balance (Sartorius; Göttingen, Germany) and the Mahr Micromar 40 EWV digital micrometer (Mahr; Göttingen, Germany), respectively. Samples were cut and stuck with a carbon bioadhesive. To provide conductivity, a layer of colloidal silver surrounded the sample and afterwards, the carbon was eliminated by the Quorum Emitech K950 Turbo Evaporator (Emitech, Kent, UK). The microarchitecture was examined by the Hitachi S4100 field emission scanning electron microscope (FESEM) (Hitachi; Tokyo, Japan) and images were captured by Quartz PCI software (Quartz; Vancouver, Canada). The average values of fiber diameter, surface porosity, and pore area were determined from top and bottom sides via ImageJ software (National Institutes of Health; Bethesda, MD, USA).

2.5. Weight Degradation Assay

PCL-ES structures were firstly weighed using the analytical balance (Sartorius). Afterward, they were sterilized, relocated to non-adherent cell culture 12-well plates (Sarstedt, Nümbrecht, Germany), and 2 mL of supplemented medium was added into the wells. Scaffolds were maintained in the incubator for 3, 6, 14, or 28 days, and then they were washed twice with PBS, air-dried, and weighed again. Control samples were directly air-dried and weighed after their sterilization.

2.6. Protein Adsorption Assay

Sterilized scaffolds were soaked in 2 mL of supplemented medium and blank samples in PBS. Structures were placed in the incubator at 37 °C and 5% CO₂ for 3 and 6 days. In order to guarantee that only proteins attached to meshes were analyzed, PCL-ES scaffolds were put into new wells after their PBS rinsing. The protein amount from each sample was calculated through a BSA standard curve by DC Protein Assay. Absorbance was measured at 700 nm in a microplate reader (Bio-Rad).

2.7. Cell Models

Human EGFRm lung adenocarcinoma PC9 and its gefitinib and osimertinib resistant derivative PC9-GR3 models were kindly provided by Dr. R. Rosell and Dr. M. A. Molina (Barcelona, Spain). Cells were routinely grown in RPMI-1640 medium supplemented with

10% FBS, and 50 U/mL penicillin/streptomycin. Cells were maintained at 37 °C and 5% CO₂ atmosphere, regularly monitored, and remained mycoplasma-free.

2.8. Three-Dimensional Cell Culture

Sterilized scaffolds were put in non-adherent cell culture plates (Sarstedt) and immersed in supplemented medium for 30 min at 37 °C and in a 5% CO₂ atmosphere to ensure cell attachment. The appropriate cell density was prepared in 50 µL of medium for 12-well scaffolds and 75 µL for 6-well ones. PC9 and PC9-GR3 models were seeded in scaffolds as previously described [39].

2.9. Nucleus and Cytoplasm Elongation

Cells were seeded on adherent coverslips (Sarstedt) and sterilized scaffolds for 3 and 6 days. After the PBS rinsing, cells were fixed with 4% (*w/v*) paraformaldehyde, permeated using 0.2% (*v/v*) Triton X-100, blocked using 3% (*w/v*) BSA, and dyed the actin cytoskeleton by rhodamine-phalloidin (1:250) and the nucleus by DAPI (1:1000). Fluorescence was examined through a Nikon A1R confocal laser scanning microscope (CLSM) (Nikon, Tokyo, Japan) and all images were taken by Nikon NIS-Elements AR v4.10 software (Nikon). Image J (National Institutes of Health, Bethesda, MD, USA) software was used to determine nuclear and cytoplasmic elongation. As described elsewhere [40], five cells from each image were randomly chosen to measure the length and width of the nucleus and cytoplasm.

2.10. Cell Viability Assays

To compare cell viability rate in 2D and 3D cell cultures, sensitive and resistant models were cultured on adherent cell culture 12-well plates and 10–15% PCL-ES scaffolds for 3 and 6 days. Afterward, PCL-ES structures were rinsed twice with PBS and placed in new wells. Finally, the MTT assay was performed as previously described [38].

To investigate osimertinib resistance of cells cultured on 2D and 3D culture, PC9 and PC9-GR3 models were seeded as previously mentioned. After 3 or 6 days, cells were treated with different concentrations of osimertinib for 48 h. Thereafter, the MTT assay was performed.

2.11. Quantitative Real-Time PCR Analysis

Cells cultured on 2D and PCL-ES scaffolds for 3 and 6 days were trypsinized, recollected, and resuspended in 700 µL of Qiazol. In order to obtain RNA from samples, the GeneJET RNA Purification Kit was performed following the manufacturer's protocol and the RNA isolated was quantified by a NanoDrop 2000 Spectrophotometer (ThermoFisher Scientific). RNA was reverse-transcribed into complementary DNA (cDNA) using the High Capacity cDNA Archive Kit. Gene expression levels were detected using primers (Table S1) and qPCR BIO SyGreen Mix Lo-Rox through the QuantStudio3 Real-Time PCR System (ThermoFisher Scientific Inc., Waltham, MA, USA). Results obtained were transformed using the standard formula $2^{-\Delta\Delta CT}$ and normalized to the housekeeping GAPDH.

2.12. Immunoblotting Analysis

Cells cultured on 2D and PCL-ES scaffolds for 3 and 6 days were trypsinized, recollected and lysed by vortexing every 5 min for 30 min in ice-cold lysis buffer with 100 µg/mL PMSE. Protein concentration was calculated through a BSA standard curve by DC Protein Assay. Equal amounts of protein were heated in LDS and reducing agent for 10 min at 70 °C. Thereafter, total protein was separated by SDS-polyacrylamide gel (SDS-PAGE) and moved to nitrocellulose membranes. Membranes were incubated for 3 h at room temperature in blocking buffer (5% BSA in TBS 0.05% Tween (TBS-T)) and overnight at 4 °C with the corresponding primary antibody (Table S2) diluted in blocking buffer. Specific horseradish peroxidase (HRP)-conjugated secondary antibodies were incubated for 90 min at room temperature before being detected in the Bio-Rad ChemiDoc™ MP Imaging System (Bio-Rad

Laboratories, Inc., Hercules, CA, USA) using a chemiluminescent HRP substrate Clarity™ Western ECL Substrate or West Femto Maximum Sensitivity Substrate.

2.13. Selection of Patients

Between 2006 and 2019, at the Dr. Josep Trueta University Hospital (Girona, Spain), 45 patients met inclusion criteria. Clinical characteristics of the patients and pathological features of the tumors were analyzed retrospectively and obtained from the medical records. However, only 36 patients had sufficient tumor sample for immunohistochemical analysis. The samples were from biopsy, but all patients had received EGFR-tyrosine kinase inhibitors (TKIs) at some point.

2.14. Immunohistochemistry Assay of Tissue Samples

CD133 and Vimentin tumor expression were determined by immunohistochemistry (IHC) in 3 µm thick slides from formalin-fixed paraffin-embedded tissue blocks of the primary tumor using a BenchMark ULTRA-Ventana instrument (Roche Diagnostics). The UltraView Universal DAB Detection Kit and the Amplification Kit were used for the detection of CD133 and Vimentin antibodies. A negative control was included by using mouse IgG at a comparable concentration instead of the primary antibody. Kidney and colon tissue were also examined as a control expression of CD133 and Vimentin, respectively. CD133 expression was considered as positive when at least 1% of the cells showed cytoplasmic and/or membrane staining. Vimentin expression was classified as positive when 10% or more of the cells were stained.

2.15. Data Analysis

The statistical analysis was performed through the IBM SPSS software (Version 25.0; SPSS Inc., Chicago, IL, USA) and R software (Version 4.0.4; The R Foundation, Vienna, Austria). For in vitro experiments, they were performed at least three times and the results obtained are expressed as mean ± standard error of the mean (SEM). For samples from patients, categorical variables are summarized as counts and percentages, and continuous variables as the number of non-missing observations, the mean ± standard deviation (SD), or the median and interquartile range [IQR], depending on the distribution of the variable. Categorical variables were compared by Fisher's exact tests. Overall Survival (OS) and Progression Free Survival (PFS) probabilities were estimated according to the method of Kaplan–Meier. Statistical differences between curves were calculated using the log-rank test. For two-group comparisons, parametric data were analyzed by Student's *t* test and non-parametric data by Mann–Whitney U test. For more than two groups' comparisons, parametric data were analyzed by one-way analysis of variance (ANOVA) using Bonferroni or Tamhane's T2 post hoc test and non-parametric data were analyzed by Kruskal–Wallis test. Levels of significance were established at $p < 0.050$ and are represented by asterisks, as follows: $p < 0.050$ (*), $p < 0.010$ (**), and $p < 0.001$ (***)

3. Results

3.1. Characterization of PCL-ES Scaffolds

3.1.1. Thermal Characterization of PCL-ES Scaffolds

The thermal stability of structures was tested by TGA (Figure S1a,b). The first stage of the curve, from 30 °C to 380 °C with a slight weight loss of about 10%, corresponded to water vaporization and the elimination of unstable fragments. The weight degradation occurred from 387 °C to 430 °C for 10%-PCL-ES meshes and from 388 °C to 429 °C for 15%-PCL ones. After their decomposition, 10% and 15%-PCL-ES supports showed a residual weight of 9.88% and 9.66%, respectively.

The thermal properties of scaffolds were revealed by DSC (Figure S1c,d). A single peak was observed in both 3D platforms corresponding to melting temperature (T_m) which was 59.66 °C for 10%-PCL-ES matrices and 59.52 °C for 15%-PCL ones. Regard-

ing the enthalpy of fusion (ΔH_f), 10% and 15%-PCL-ES meshes absorbed 74.90 J/g and 73.69 J/g, respectively.

The structural and viscoelastic behavior of 3D supports were examined by DMA (Figure 1e,f). We determined a storage modulus (E') value of 6.25 MPa and 7.22 MPa at 25 °C (room temperature), and 4.52 MPa and 5.40 MPa at 37 °C (physiological conditions) for 10% and 15%-PCL-ES platforms, respectively. In terms of the Tan Delta curve, the glass transition temperature (T_g) was -42.56 °C and -49.65 °C for 10% and 15%-PCL-ES structures, respectively.

3.1.2. Microarchitecture of PCL-ES Scaffolds

The top (TS) and bottom (BS) sides of 3D meshes were displayed using SEM (Table 1) to expose their microarchitecture and measure their filament diameter, porosity, and pore area.

One filament population was confirmed in 10%-PCL-ES matrices, whereas 15%-PCL ones exhibited two subpopulations of filaments (Figure S2). Additionally, beads (non-filamentous polymer) were observed in 10%-PCL-ES platforms. On the other hand, 15%-PCL-ES scaffolds showed higher fiber diameter, lower surface porosity, and larger pore area compared to 10%-PCL ones, in a significant way (Table 2). Significant differences were also found between top and bottom sides in the fiber diameter (329.69 ± 33.97 nm for TS, 297.94 ± 24.89 nm for BS; $p = 0.007$) and the surface porosity ($66.13 \pm 1.29\%$ for TS, $70.34 \pm 1.20\%$ for BS; $p = 0.036$) of 10%-PCL-ES structures and the fiber diameter (1501.42 ± 570.10 nm for TS, 1979.60 ± 376.64 nm for BS; $p = 1.000 \times 10^{-4}$) and pore area ($0.70 \pm 0.35 \mu\text{m}^2$ for TS, $0.76 \pm 0.36 \mu\text{m}^2$ for BS; $p = 0.019$) of 15%-PCL ones.

A weight degradation assay was performed to discern whether the sterilization procedure and medium soaking altered PCL-ES matrices (Figure 1a). The process of sterilization resulted in an increase of approximately 5–7% of their weight. Significant differences were found between the weight before and after sterilization in 3D supports. However, no significant variations were found between their weight after sterilization and medium immersion for 3, 6, 14, or 28 days. The medium soaking neither changed the weight of PCL-ES platforms throughout the 28-day period.

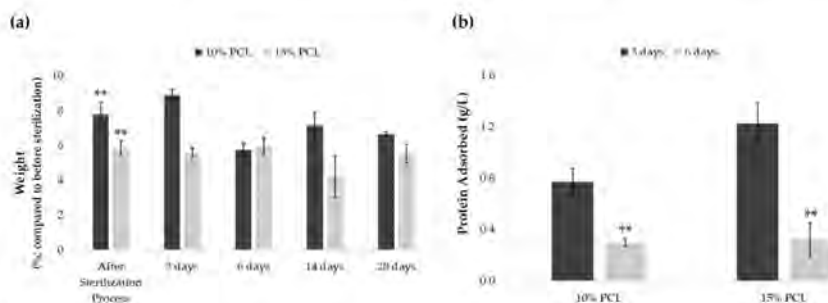


Figure 1. (a) Effect of sterilization process and medium soaking on the weight of PCL-ES scaffolds for 3, 6, 14, and 28 days. Results are shown as mean \pm SEM from at least three independent experiments. Levels of statistical significance are indicated as ** ($p > 0.010$) compared to the weight before the sterilization process. (b) Capacity to adsorb protein from medium of PCL-ES scaffolds after 3 and 6 days of incubation. The results are shown as mean \pm SEM from at least three independent experiments. Levels of statistical significance are indicated as ** ($p > 0.010$) compared to 3 days of incubation.

Table 1. Pictures from the top and bottom sides of 10% and 15%-PCL-ES scaffolds at different magnifications displayed by scanning electronic microscopy (SEM).

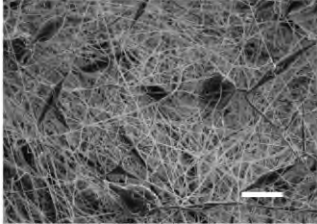
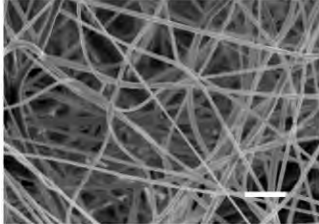
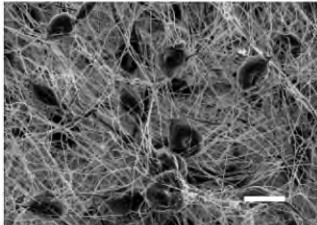
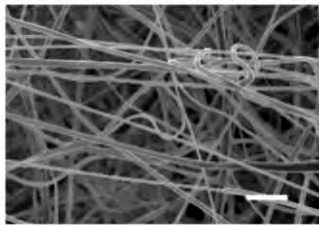
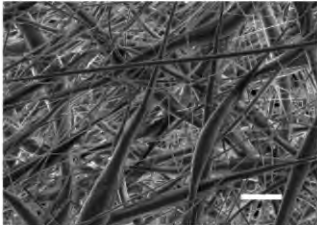
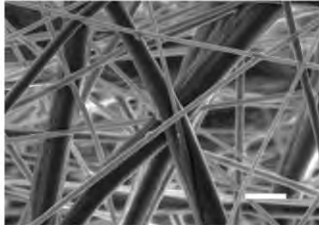
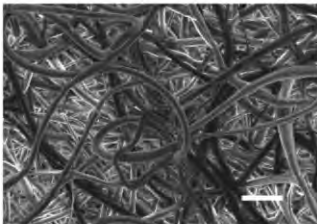
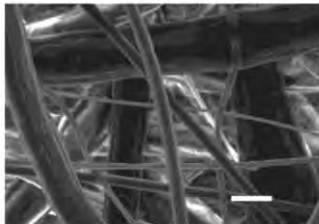
	Side	Magnification	
		×1000	×5000
10% PCL	Top		
	Bottom		
15% PCL	Top		
	Bottom		
		Scale bars: 15 μm	Scale bars: 3 μm

Table 2. Filament diameter, surface porosity, and pore area of 10% and 15%-PCL-ES scaffolds. Images from the top and bottom sides were used to calculate the parameters. The results are shown as mean \pm SEM. Levels of statistical significance are indicated as *** ($p > 0.001$).

Parameter	10% PCL	15% PCL
Filament diameter (nm)	315.67 \pm 21.84	1764.42 \pm 333.43 (***)
Surface Porosity (%)	68.26 \pm 1.06	82.29 \pm 3.68 (**)
Pore Area (μm^2)	0.36 \pm 0.13	0.73 \pm 0.25 (***)

3.1.3. Effect of the Sterilization Process and Medium Immersion on PCL-ES Scaffolds

We also investigated the scaffold capacity to adsorb protein from the medium on their surface after 3 and 6 days of incubation (Figure 1b). Both 3D structures were able to adsorb protein, which was significantly greater after 3 days than 6 days. Moreover, 15%-PCL-ES meshes exhibited a higher capacity to adsorb protein than 10%-PCL ones after 3 days.

3.2. Morphology of Sensitive and Resistant EGFR^m Lung Adenocarcinoma Cell Models Cultured on PCL-ES Scaffolds

To examine possible changes in cell morphology, PC9 and PC9-GR3 models were cultured on 2D and 3D (10% and 15%-PCL-ES) matrices for 3 and 6 days. The stained nucleus and actin cytoskeleton were displayed using CLSM (Figure 2a,b).

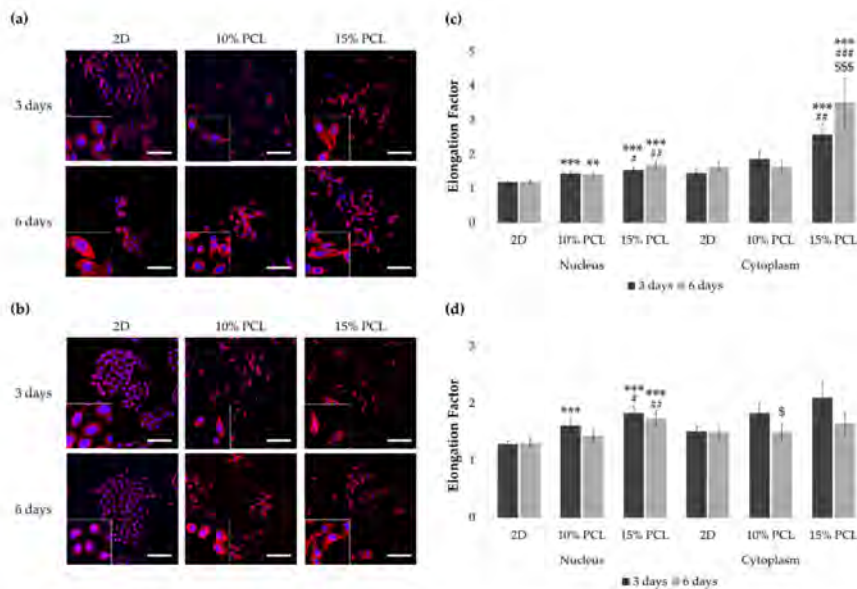


Figure 2. Images of (a) PC9 and (b) PC9-GR3 cell models cultured on monolayer, 10% and 15%-PCL-ES scaffolds for 3 and 6 days displayed by a confocal laser scanning microscope (CLSM) at a magnification of $\times 200$ (scale bars: 100 μm) and partial pictures enlarged ($\times 3$). The actin cytoskeleton was stained with rhodamine-phalloidin (red) and the nucleus with DAPI (blue). Nuclear and cytoplasmic elongation factors from (c) PC9 and (d) PC9-GR3 cell models cultured on monolayer, 10% and 15%-PCL-ES scaffolds. Levels of statistical significance are indicated as *, #, \$ ($p < 0.050$), **, ## ($p < 0.010$), and ***, ###, \$\$\$ ($p < 0.001$). The symbol * indicates the comparison with monolayer, \$ indicates the comparison with 3 days of culture, and # indicates the comparison with 10%-PCL-ES scaffolds.

PC9 cells seeded on 3D platforms showed a significantly higher nucleus elongation compared to the monolayer and 10%-PCL ones (Figure 2c). Additionally, a significantly larger cytoplasmic lengthening was observed on cells grown on 15%-PCL-ES scaffolds for 3 and 6 days. Regarding culture time, PC9 cultured on 15%-PCL-ES structures also exhibited a more extended cytoplasm for 6 days than 3 days.

PC9-GR3 seeded on 15%-PCL-ES meshes for 3 and 6 days showed a significantly larger nucleus extension in comparison with 2D and 10%-PCL ones (Figure 2d). After 3 days, cells grown on 10%-PCL-ES supports also demonstrated a significantly higher elongated nucleus in contrast to the monolayer. It was observed a tendency to elongate the cytoplasm in cells seeded on 3D culture for 3 days in contrast to 2D. Nonetheless, PC9-GR3 grown on 10%-PCL-ES scaffolds for 6 days exhibited a shrunken cytoplasm compared to those grown for 3 days. The largest elongation of nucleus and cytoplasm were determined in cells seeded on 15%-PCL-ES meshes compared to the monolayer, for 6 days in PC9 and 3 days in PC9-GR3.

Actin and tubulin were analyzed by RT-qPCR and Western blot (Figure 3) in order to clarify whether cells changed their expression as a consequence of 3D culture. The uncropped immunoblottings can be found in Figure S3.

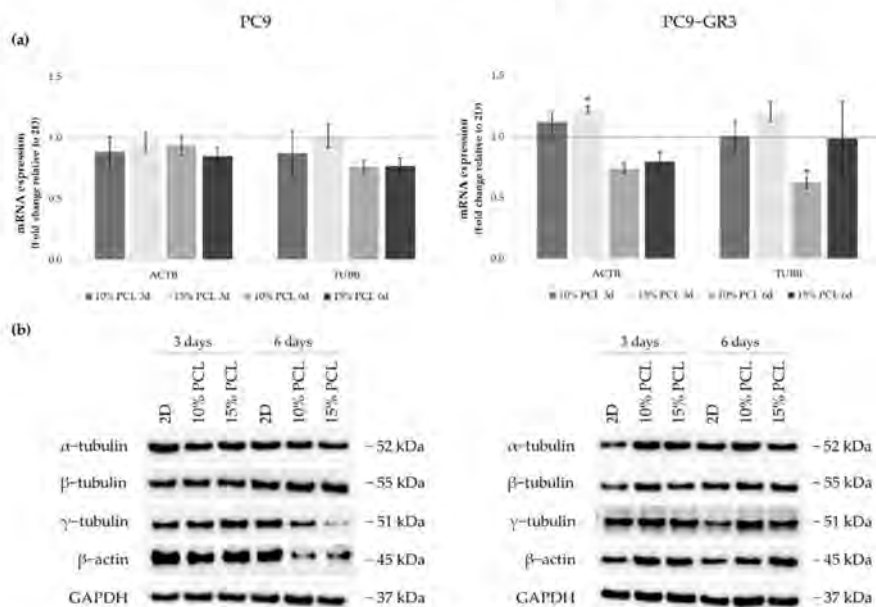


Figure 3. (a) *ACTB* and *TUBB* mRNA levels of PC9 and PC9-GR3 cell models cultured on monolayer, 10% and 15%-PCL-ES scaffolds for 3 and 6 days. mRNA expression was normalized against the GAPDH gene. All cell culture conditions were compared to 2D, which was normalized to 1 (marked by the dotted line) and shown as fold change. The results are shown as mean \pm SEM from at least three independent experiments. Levels of statistical significance are indicated as * ($p < 0.050$) compared to 2D. (b) α -tubulin, β -tubulin, γ -tubulin, and β -actin protein expression of PC9 and PC9-GR3 models cultured on monolayer, 10% and 15%-PCL-ES scaffolds for 3 and 6 days. The 2D culture was used as an internal control and GAPDH as a loading control. The results shown are representative from at least three independent experiments.

Although no changes were observed in *ACTB* expression in PC9, β -actin protein levels were decreased in cells cultured on 3D supports for 6 days. *TUBB* mRNA expression and γ -tubulin protein levels were also diminished in the same culture conditions. No alterations were detected in α - and β -tubulin protein levels.

Regarding the PC9-GR3 cell model, *ACTB* mRNA levels were upregulated in cells cultured on 3D platforms for 3 days compared to 2D, being statistically significant in 15%-PCL ones. β -actin protein expression was also increased in cells seeded on 3D culture for 3 and 6 days, despite the *ACTB* reduction in scaffolds for 6 days. Cells grown on 3D structures exhibited an increase of α - and β -tubulin proteins expression for 3 days and an increase of γ -tubulin for 6 days. No changes were exhibited in *TUBB* mRNA levels, except for the significant reduction shown in 10%-PCL-ES meshes compared to the monolayer for 6 days.

3.3. Viability of Sensitive and Resistant EGFR^m Lung Adenocarcinoma Cell Models Cultured on PCL-ES Scaffolds

Differences in the viability of PC9 and PC9-GR3 cell models cultured on PCL-ES matrices or monolayer were studied through the MTT assay for 3 and 6 days (Figure 4). In both models, cells grown on 3D culture exhibited a lower rate compared to 2D. Cells seeded on 15%-PCL-ES meshes showed a higher viability than on 10%-PCL ones. Furthermore, it was observed that there was a tendency to decrease cell viability in cells cultured on 3D supports after 6 days in contrast to 3 days.

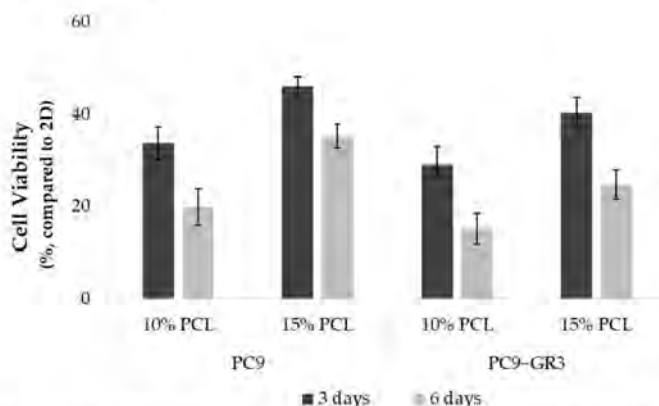


Figure 4. Cell viability of PC9 and PC9-GR3 cell models cultured on monolayer, 10% and 15%-PCL-ES scaffolds for 3 and 6 days. The results are shown as mean \pm SEM from at least three independent experiments. All cell culture conditions were compared to 2D, which was normalized to 100%.

3.4. Evaluation of EGFR Status in Sensitive and Resistant EGFR^m Lung Adenocarcinoma Cell Models Cultured on PCL-ES Scaffolds

The status of EGFR in PC9 and PC9-GR3 cell models cultured on PCL-ES scaffolds was evaluated after 3 and 6 days of culture (Figure 5). The uncropped immunoblottings can be found in Figure S3.

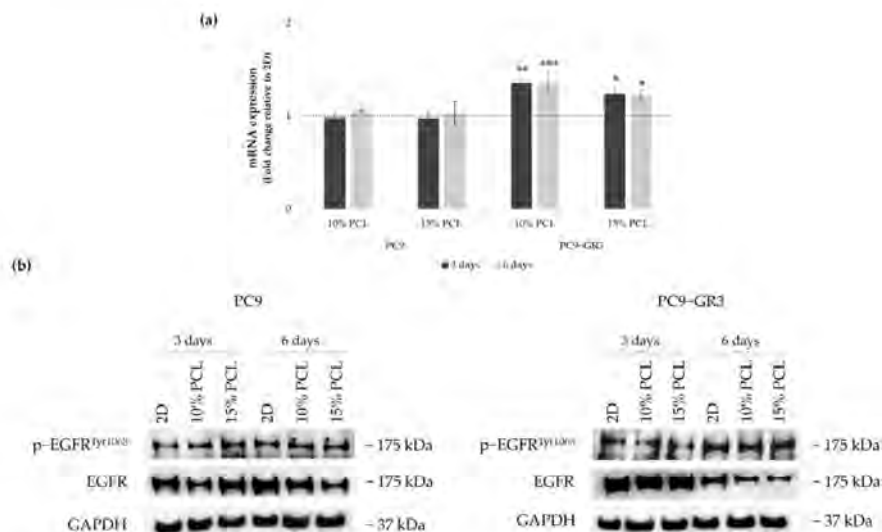


Figure 5. (a) *EGFR* mRNA levels of PC9 and PC9-GR3 cell models cultured on monolayer, 10% and 15%-PCL-ES scaffolds for 3 and 6 days. mRNA expression was normalized against GAPDH gene. All cell culture conditions were compared to 2D, which was normalized to 1 (marked by the dotted line) and shown as fold change. Results are shown as mean \pm SEM from at least three independent experiments. Levels of statistical significance are indicated as * ($p < 0.050$), ** ($p < 0.010$), and *** ($p < 0.001$) compared to 2D. (b) *EGFR* protein expression of PC9 and PC9-GR3 models cultured on monolayer, 10% and 15%-PCL-ES scaffolds for 3 and 6 days. The 2D culture was used as an internal control and GAPDH as a loading control. The results shown are representative from at least three independent experiments.

Although no changes were observed in *EGFR* mRNA expression and phosphorylated *EGFR* protein levels in PC9 seeded on 3D matrices, a slight reduction in total *EGFR* protein expression was observed in 10%-PCL-ES meshes after 3 days of culture and in both 3D platforms after 6 days.

EGFR mRNA levels were significantly higher in PC9-GR3 grown on PCL-ES structures. However, total *EGFR* protein expression was reduced in 3D supports after 6 days of culture. No changes were exhibited in phosphorylated *EGFR* expression.

3.5. Study of LCSC population in Sensitive and Resistant *EGFR*m Lung Adenocarcinoma Cell Models Cultured on PCL-ES Scaffolds

3.5.1. Resistance to Osimertinib of Sensitive and Resistant *EGFR*m Lung Adenocarcinoma Cell Models Cultured on PCL-ES Scaffolds

To evaluate the capacity of PCL-ES matrices to culture the LCSC population, the resistance to osimertinib was investigated in PC9 and PC9-GR3 cell models seeded on 2D or 3D culture for 3 or 6 days, and then treated with the *EGFR*-TKI for an extra 48 h.

As shown in Figure 6a, no differences were found between PC9 seeded on PCL-ES structures and 2D after the treatment with 0.001 and 1 μ M of osimertinib. Moreover, cells grown on 10%-PCL-ES meshes for 6 days exhibited significantly lower cell viability in comparison with control. Nevertheless, at the highest concentrations of osimertinib, PC9 cultured on 3D supports was significantly more resistant than on 2D culture.

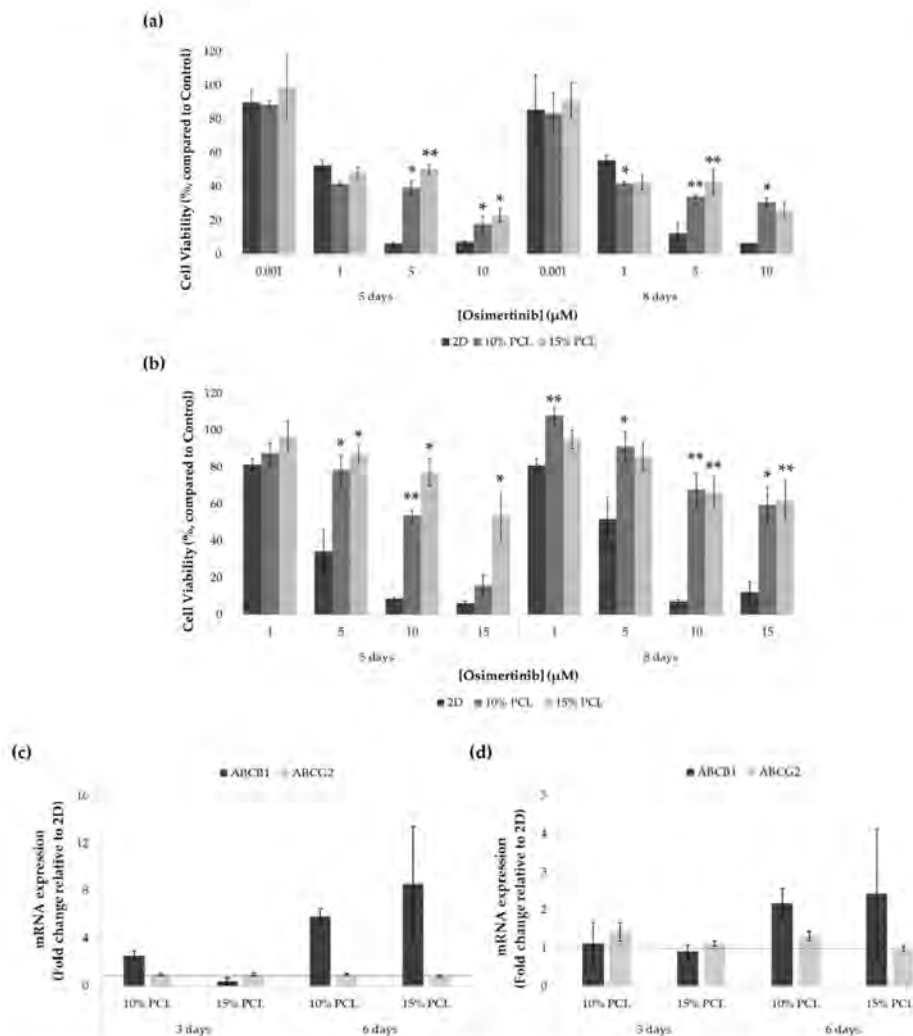


Figure 6. Cell viability of (a) PC9 and (b) PC9-GR3 cell models cultured on monolayer, 10% and 15%-PCL-ES scaffolds for 3 and 6 days and then treated with osimertinib for 48 h. Results are expressed as the percentage of surviving cells (mean \pm SEM) compared to control (untreated cells) from at least three independent experiments. Levels of statistical significance are indicated as * ($p < 0.050$) and ** ($p < 0.010$) compared to 2D. *ABCB1* and *ABCG2* mRNA levels of (c) PC9 and (d) PC9-GR3 models cultured on monolayer, 10% and 15%-PCL-ES scaffolds for 3 and 6 days. mRNA expression was normalized against the GAPDH gene. All cell culture conditions were compared to 2D, which was normalized to 1 (marked by the dotted line) and shown as fold change. The results are shown as mean \pm SEM from at least three independent experiments.

Regarding the PC9-GR3 model, cells seeded on 3D culture were more resistant to osimertinib compared to the monolayer in all treatments assayed, as displayed in Figure 6b. As the EGFR-TKI concentration increased, the differences exhibited between 2D and 3D culture became more evident.

ABCB1 and *ABCG2* mRNA expression was also determined through RT-qPCR in both cell models cultured on PCL-ES platforms for 3 and 6 days (Figure 6c,d).

ABCB1 levels were increased in cells cultured on 10%-PCL-ES structures for 3 days in PC9 and both 3D meshes after 6 days in PC9 and PC9-GR3 models. No changes were found in *ABCG2* expression in PC9 in any cell culture condition. However, *ABCG2* was slightly higher in PC9-GR3 seeded on 10%-PCL-ES meshes for 3 and 6 days.

3.5.2. Epithelial-to-Mesenchymal Transition (EMT) of Sensitive and Resistant EGFRm Lung Adenocarcinoma Cell Models Cultured on PCL-ES Scaffolds

We examined different transcription factors that trigger EMT, such as Snail, Slug, Twist, and Zeb1, by RT-qPCR, and E-cadherin and Vimentin by RT-qPCR and immunoblotting to determine the capacity of PCL-ES scaffolds to induce this process (Figure 7). The uncropped Western blots can be found in Figure S4 and Figure S5.

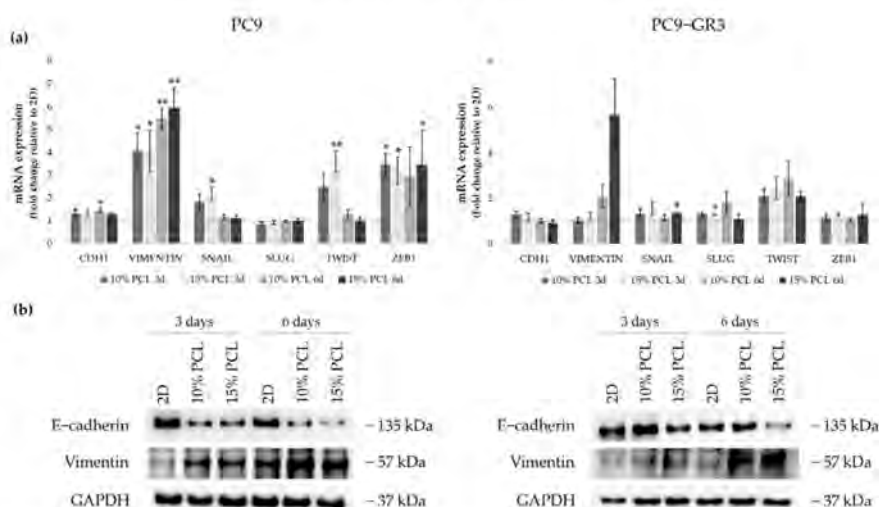


Figure 7. (a) *CDH1*, *VIMENTIN*, *SNAIL*, *SLUG*, *TWIST*, and *ZEB1* mRNA levels of PC9 and PC9-GR3 cell models cultured on monolayer, 10% and 15%-PCL-ES scaffolds for 3 and 6 days. mRNA expression was normalized against the GAPDH gene. All cell culture conditions were compared to 2D, which was normalized to 1 (marked by the dotted line) and shown as fold change. The results are shown as mean \pm SEM from at least three independent experiments. Levels of statistical significance are indicated as * ($p < 0.050$) and ** ($p < 0.010$) compared to 2D. (b) E-cadherin and Vimentin protein expression of PC9 and PC9-GR3 models cultured on monolayer, 10% and 15%-PCL-ES scaffolds for 3 and 6 days. The 2D culture was used as an internal control and GAPDH as a loading control. The results shown are representative from at least three independent experiments.

CDH1 mRNA expression was slightly increased in PC9 grown on PCL-ES supports, being statistically significant in 10%-PCL ones compared to 2D after 6 days of culture. Nonetheless, E-cadherin protein levels were clearly diminished in cells on 3D culture after 3 and 6 days. *VIMENTIN* mRNA expression was significantly higher in PC9 cultured on 3D for 3 and 6 days in comparison with the monolayer, which is in agreement with its

protein levels. Regarding the transcriptional factors, a significant enhancement of *SNAIL* and *TWIST* was shown in PC9 cultured on 15%-PCL-ES scaffolds for 3 days. No changes were found in *SLUG*. *ZEB1* mRNA levels were approximately three times greater in cells seeded on 3D in contrast to 2D, being statistically significant for both PCL-ES matrices after 3 days and only 15%-PCL ones after 6 days of culture.

Although no changes in *CDH1* were observed in PC9-GR3, a reduction in E-cadherin protein levels was determined in cells grown on 15%-PCL-ES meshes for 6 days. mRNA and protein expression of Vimentin were higher in 3D supports after 6 days of culture. *SNAIL* and *SLUG* expression were significantly increased in PC9-GR3 cultured on 15%-PCL-ES platforms compared to the monolayer after 6 days and 3 days of culture, respectively. *TWIST* mRNA levels were approximately two times larger in cells seeded on 3D in comparison with 2D, but no changes were found for *ZEB1*.

3.5.3. Self-Renewal, Stemness and Pluripotency Markers of Sensitive and Resistant EGFR Lung Adenocarcinoma Cell Models Cultured on PCL-ES Scaffolds

Sox2, Oct-4, and Nanog expression were determined in 3D culture by RT-qPCR and Western blot to examine the capacity of PCL-ES scaffolds to culture this malignant subpopulation (Figure 8). The uncropped immunoblottings can be found in Figures S4 and S5.

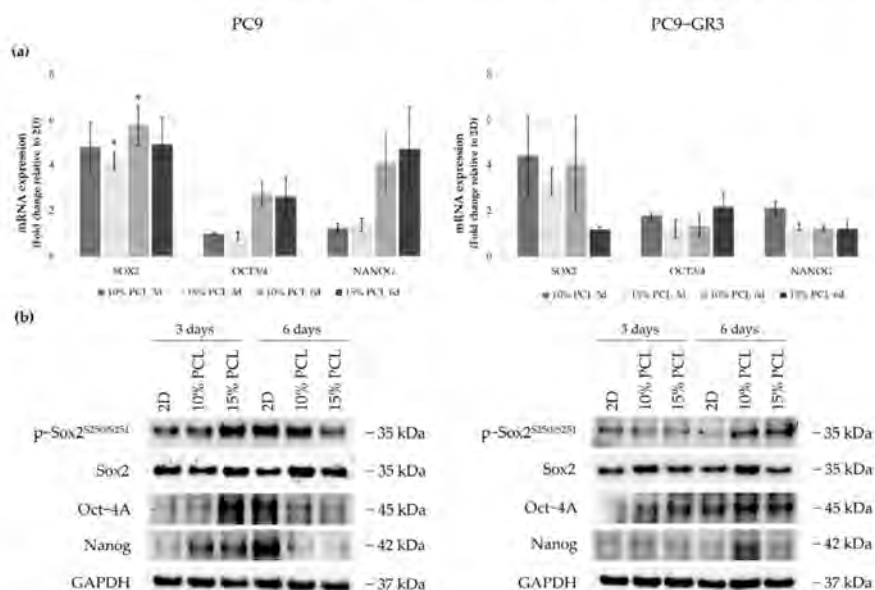


Figure 8. (a) *SOX2*, *OCT3/4*, and *NANOG* mRNA levels of PC9 and PC9-GR3 cell models cultured on monolayer, 10% and 15%-PCL-ES scaffolds for 3 and 6 days. mRNA expression was normalized against the GAPDH gene. All cell culture conditions were compared to 2D, which was normalized to 1 (marked by the dotted line) and shown as fold change. The results are shown as mean \pm SEM from at least three independent experiments. Levels of statistical significance are indicated as * ($p < 0.050$) compared to 2D. (b) Sox2, Oct-4A, and Nanog protein expression of PC9 and PC9-GR3 models cultured on monolayer, 10% and 15%-PCL-ES scaffolds for 3 and 6 days. The 2D culture was used as an internal control and GAPDH as a loading control. The results shown are representative from at least three independent experiments.

SOX2 mRNA levels increased about five times in PC9 grown on PCL-ES matrices, being statistically significant in 15%-PCL ones after 3 days and 10%-PCL ones after 6 days of culture in contrast to the monolayer. Sox2 total protein levels were slightly greater in 3D after 6 days of culture. *OCT3/4* and *NANOG* expression were also larger in cells cultured on 3D for 6 days compared to 2D. Nevertheless, phosphorylated Sox2 and total Oct-4A protein were enhanced on cells seeded on 15%-PCL-ES structures for 3 days, and Nanog in both 3D meshes in comparison with the monolayer, but then their levels were diminished after 6 days of culture.

PC9-GR3 cultured on 10%-PCL-ES supports for 3 days caused a slight enhancement of *SOX2*, *OCT3/4*, and *NANOG* mRNA expression in contrast to 2D. An important increase of *SOX2* was also shown in cells grown on 10%-PCL-ES platforms for 6 days and on 15%-PCL ones after 3 days of culture. Phosphorylated levels of Sox2 were higher in 3D culture after 6 days of culture, but Oct-4A protein levels were larger after 3 days compared to the monolayer. Although no changes were observed in mRNA expression, PC9-GR3 seeded on 10%-PCL-ES structures for 6 days produced a slight increase in Oct-4A and Nanog protein levels.

3.5.4. Membrane Receptors of Sensitive and Resistant EGFRm Lung Adenocarcinoma Cell Models Cultured on PCL-ES Scaffolds

The expression of CD133, CD166, CD24, and CD90 were evaluated in 3D culture by RT-qPCR and immunoblotting to determine the capacity of ES-PCL scaffolds to culture LCSC population (Figure 9). The uncropped Western blots can be found in Figures S4 and S5.

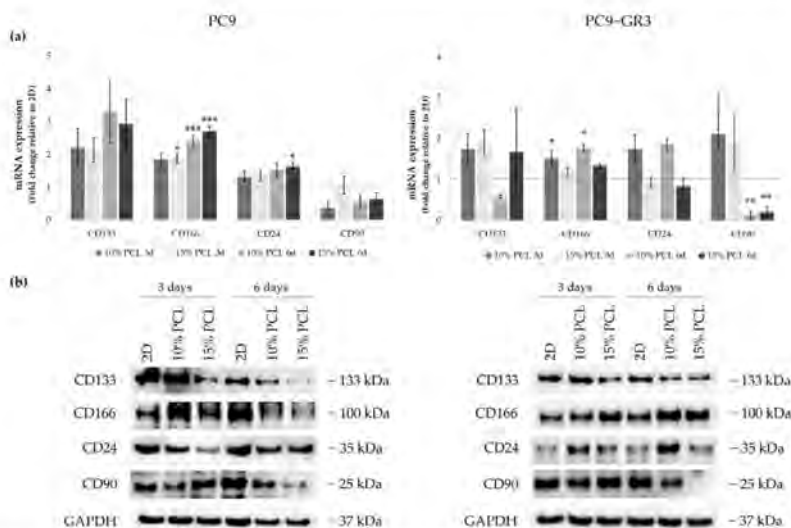


Figure 9. (a) CD133, CD166, CD24, and CD90 mRNA levels of PC9 and PC9-GR3 cell models cultured on monolayer, 10% and 15%-PCL-ES scaffolds for 3 and 6 days. mRNA expression was normalized against the GAPDH gene. All cell culture conditions were compared to 2D, which was normalized to 1 (marked by the dotted line) and shown as fold change. The results are shown as mean \pm SEM from at least three independent experiments. Levels of statistical significance are indicated as * ($p < 0.050$), ** ($p < 0.010$) and *** ($p < 0.001$) compared to 2D. (b) CD133, CD166, CD24, and CD90 protein expression of PC9 and PC9-GR3 models cultured on monolayer, 10% and 15%-PCL-ES scaffolds for 3 and 6 days. The 2D culture was used as an internal control and GAPDH as a loading control. The results shown are representative from at least three independent experiments.

Although *CD133* mRNA expression slightly increased in PC9 cultured on 3D matrices, a reduction was determined in its protein levels. The same results were found in CD24 mRNA and protein expression. *CD166* mRNA levels were greater in 3D in comparison with 2D, being statistically significant in 15%-PCL-ES supports after 3 days of culture and 10% and 15%-PCL ones after 6 days. *CD166* protein levels were larger in PC9 cultured on 3D for 3 days, however they were reduced after 6 days of culture in contrast to the monolayer. *CD90* mRNA and protein expression trended to decrease in cells seeded on PCL-ES scaffolds, except for 15%-PCL ones after 3 days of culture, which did not change their expression.

CD133 mRNA expression was slightly higher in PC9-GR3 grown on PCL-ES scaffolds compared to 2D after 3 days of culture. Nevertheless, a decrease in its protein levels was exhibited in cells cultured on 15%-PCL-ES meshes after 3 days and on both PCL-ES supports after 6 days. *CD166* mRNA and protein expression were increased in 3D culture in comparison with the monolayer, being statistically significant in 10%-PCL-ES platforms. In contrast, *CD24* mRNA and protein levels were larger in PC9-GR3 seeded on 10%-PCL-ES matrices, but did not change on 15%-PCL ones. No changes were observed in *CD90* in 3D after 3 days of culture, but a significant reduction was demonstrated after 6 days. These results are in agreement with *CD90* protein levels.

3.5.5. Hedgehog and Canonical Pathway of Sensitive and Resistant EGFRm Lung Adenocarcinoma Cell Models Cultured on PCL-ES Scaffolds

We analyzed the role of the canonical (Wnt/ β -catenin) and the Hedgehog signaling pathways in PC9 and PC9-GR3 cell models cultured on PCL-ES scaffolds for 3 and 6 days (Figure 10). The uncropped immunoblottings can be found in Figures S4 and S5.

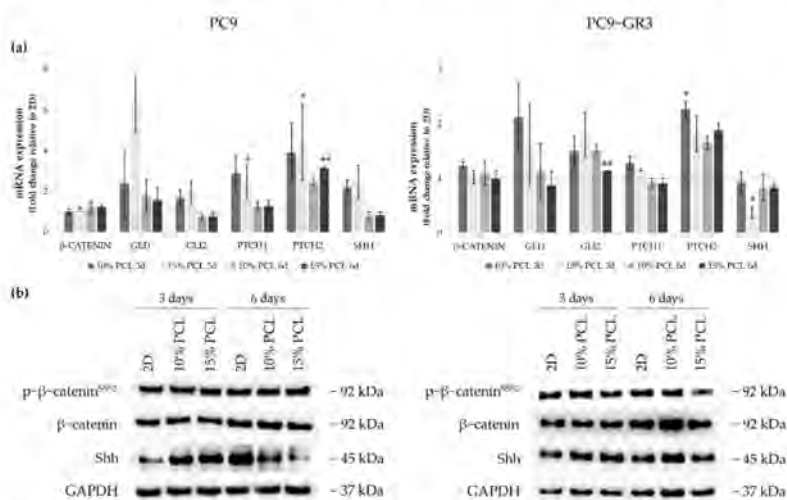


Figure 10. (a) β -CATENIN, *GLI1*, *GLI2*, *PTCH1*, *PTCH2*, and *SHH* mRNA levels of PC9 and PC9-GR3 cell models cultured on monolayer, 10% and 15%-PCL-ES scaffolds for 3 and 6 days. mRNA expression was normalized against the GAPDH gene. All cell culture conditions were compared to 2D, which was normalized to 1 (marked by the dotted line) and shown as fold change. The results are shown as mean \pm SEM from at least three independent experiments. Levels of statistical significance are indicated as * ($p < 0.050$) and ** ($p < 0.010$) compared to 2D. (b) β -catenin and Shh protein expression of PC9 and PC9-GR3 models cultured on monolayer, 10% and 15%-PCL-ES scaffolds for 3 and 6 days. The 2D culture was used as an internal control and GAPDH as a loading control. The results shown are representative from at least three independent experiments.

Regarding β -catenin mRNA and protein expression, no changes were exhibited in neither the cell model nor the cell culture condition. The mRNA expression of the transcriptional regulators *GLI1/2*, *PTCH1/2* receptors, and Sonic ligand (*SHH*) were increased in PC9 grown on PCL-ES meshes, being statistically significant in 15%-PCL ones for *PTCH1/2* compared to 2D after 3 days of culture. Nonetheless, no changes were found in *GLI1/2*, *PTCH1*, and *SHH* in 3D after 6 days of culture. *PTCH2* expression was larger in PC9 cultured on 3D for 6 days. Significant differences were observed in 15%-PCL ones in comparison with the monolayer. Shh protein levels were enhanced on cells seeded on PCL-ES supports, but then their levels were decreased after 6 days of culture.

Regarding changes in PC9-GR3, *GLI1* and *PTCH1* mRNA expression were greater in cells grown on 3D for 3 days in contrast to 2D. PCL-ES platforms caused an enhancement of *GLI2* and *PTCH2*. Significant differences were found in 15%-PCL-ES scaffolds after 6 days of culture for *GLI2* and in 10%-PCL ones after 3 days for *PTCH2* compared to the monolayer. No changes in *SHH* mRNA and its protein levels were exhibited, except for a significant reduction in 15%-PCL-ES structures after 3 days of culture.

3.6. CD133 and Vimentin Expression in EGFRm NSCLC Patient-Derived Tumors

3.6.1. Patient and Tumor Characteristics

We analyzed data from 45 patients, who met inclusion criteria, with EGFRm NSCLC harboring exon 19 deletion and exon 21 L858R activating mutations (Table S3).

Regarding patients and tumor features, more than 75% were women with a median age of 68 years. Approximately 73% of patients were never smokers and most of them showed an ECOG of 0–1. The histology mainly identified was adenocarcinoma exhibiting a poor grade of differentiation. Almost 60% of the tumors harbored the exon 19 deletion and brain metastasis was observed in 20% of the patients before starting the treatment with the EGFR-TKI. Approximately 70% of the patients achieved a partial or a complete response to first or second generation EGFR-TKI.

3.6.2. CD133 and Vimentin Tumor Expression in EGFRm NSCLC Patients

CD133 and Vimentin tumor expression were evaluated in 36 biopsies which had sufficient tumor sample for immunohistochemical analysis. The expression of CD133 and Vimentin were detected in 50% and 58% of tumor samples, respectively.

The non-expression of the CD133 surface marker was significantly associated with a low degree of histological differentiation ($p = 0.018$) (Figure 11a). From all patients, 14 cases showed CD133 negative expression and poor tumor differentiation. In contrast, 11 CD133 positive patients exhibited well and moderate tumor differentiation. Furthermore, CD133 negative tumor expression significantly correlated with higher disease progression ($p = 0.019$) (Figure 11b) and a higher number of distant metastasis ($p = 0.040$) (Figure 11c).

We also observed that the non-expression of CD133 showed a trend to worse OS ($p = 0.064$) (Figure 12a). On the other hand, high Vimentin tumor expression has a trend to a poor PFS ($p = 0.056$) (Figure 12b).

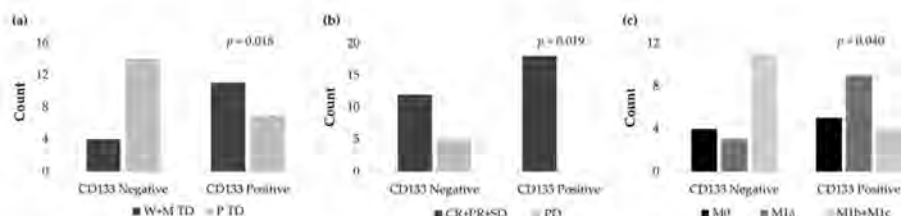


Figure 11. (a) Count of well and moderately tumor differentiation (W+M TD) and poorly tumor differentiation (P TD) cases according to the IHC expression levels of CD133. (b) Count of complete response, partial response, and stable disease (CR+PR+SD) and progression disease (PD) cases according to the IHC expression levels of CD133. (c) Count of non-metastasis (M0), local metastasis (M1a), and distant metastasis (M1b+M1c) cases according to the IHC expression levels of CD133.

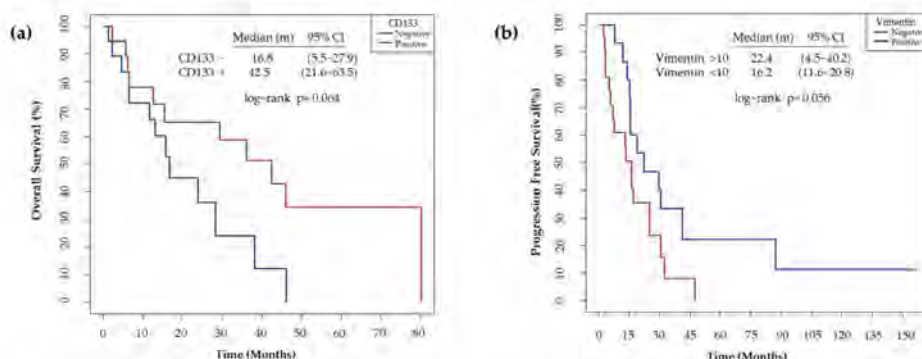


Figure 12. (a) Median overall survival according to the IHC expression levels of CD133. The non-expression of CD133 was considered as negative and the expression of > 1 %, as positive. (b) Median progression free survival according to the IHC expression levels of Vimentin. The expression of Vimentin <10% was considered as negative and >10%, as positive.

4. Discussion

Although researchers have developed several EGFR-TKIs for the treatment of EGFRm NSCLC, the majority of patients are diagnosed at advanced stages of the disease and eventually acquire resistance to the therapy through different mechanisms [2,6]. LCSCs have been identified as responsible for resistance to anticancer drugs, tumor relapse, and metastasis [7–9], but the research of this malignant subpopulation is not possible using monolayer cell culture [24,37]. Hence, different 3D culture strategies have been described to provide a more physiological environment for cells [26,28,32]. In this study, we evaluated the capacity of PCL-ES scaffolds to culture the LCSC niche in sensitive and resistant EGFRm lung adenocarcinoma cell models.

The use of PCL for biomedical applications has been increased over the years. Biocompatibility, bioresorbability, and low cost are very attractive features of this Food and Drug Administration (FDA) approved polymer [36]. Regarding the thermal characterization of PCL-ES matrices (Figure S1), the values obtained by TGA and DSC for weight degradation, T_m , and ΔH_f of 3D structures coincide with the literature about PCL [41,42], and no differences were found between 10% and 15%-PCL-ES meshes. Stiffness and viscoelastic properties were also analyzed by DMA. An optimal stiffness of 3D structures is fundamental for cell adhesion, morphology, growth, and differentiation [43]. The E'

value for a healthy lung tissue is approximately 1.4 kPa, whereas that for polystyrene, the main component of 2D cell culture plates, is around 2100 MPa [44,45]. Thus, PCL-ES meshes are softer than 2D cell culture surfaces but stiffer than lung tissue, ranging from 4.52 to 5.40 MPa at 37 °C. According to the literature, the T_g for PCL is -60 °C, which is very similar to the values obtained for PCL-ES supports [41].

The spatial architecture is an important characteristic of 3D cell culture matrices. Through the analysis of SEM images, we calculated fiber diameter, porosity, and pore area of PCL-ES scaffolds (Table 2). The average filament diameter was 316 and 1764 nm for 10% and 15%-PCL-ES structures, respectively, which are in agreement with the literature [36,46–50]. A large porosity (approximately 90%) is recommended to provide a suitable space for cell attachment and a high-quality exchange of nutrients and metabolic waste [51,52]. On account of this, the porosity of 15%-PCL-ES meshes was 82%, which was significantly higher than 10%-PCL ones. Rabionet et al. demonstrated comparable findings with 7.5% and 15%-PCL-ES scaffolds [37]. Additionally, only 10%-PCL-ES supports showed beads. According to Nottelet and coworkers, beads were found in 7.5% and 9%-PCL-ES platforms, but not in 12% and 15%-PCL ones [49].

PCL-ES matrices increased their weight approximately 5% due to the sterilization process. In our study, we used overnight ethanol and 30 min of UV light. Guerra et al. concluded that the use of ethanol 70% for sterilization did not produce any significant effect on surface roughness, structure, distribution, and crystallinity of PCL structures, but it was observed a reduction of 11.9% in the Mw [53]. The soaking of PCL-ES meshes on RPMI-1640 for 28 days did not cause any change in their weight. Bölgen and colleagues described that PCL nanofibers with an average diameter of 196 nm reduced their elongation at break from 82 to 5.7% after 6 months in Ringer solution at 37 °C and pH 7.4 [54].

The protein adsorption on the surface of a scaffold strongly influences cell-scaffold interactions, determining cell attachment and proliferation [55]. Our findings showed that PCL-ES structures adsorb a great protein concentration (~ 0.8 and 1.2 g/L for 10% and 15%-PCL-ES meshes, respectively) after 3 days of incubation. Kumar et al. pointed out that the hydrophobic surfaces, i.e., PCL, were more covered by proteins than hydrophilic surfaces [56]. Besides this, no significant differences were found between both PCL-ES supports, which have similar surface roughness and chemistry, essential features for protein adsorption [57,58]. Nevertheless, a significant reduction in protein adsorption was also shown after 6 days of incubation due to the protein desorption rate and the exceeding of adsorption after a certain time [59].

Thereafter, PC9 and PC9-GR3 cell models were cultured on PCL-ES scaffolds for 3 and 6 days. Cell attachment to the 3D matrices was confirmed and the elongation of the nucleus in PC9-GR3 and the nucleus and cytoplasm in PC9 were determined in cells seeded on 15%-PCL-ES structures (Figure 2). Other researchers also found cell elongation on nanofibers in breast cancer cells [37] or fibroblasts [60]. In contrast, Moghadas et al. stated the formation of spheroids using highly hydrophobic ES meshes [32]. We also evaluated the expression of actin and tubulin (Figure 3). β -actin and γ -tubulin protein expression were reduced in PC9 cultured on 3D supports for 6 days, resulting in a more motile cell phenotype, oncogenic potential, and lower survival of NSCLC patients [61,62]. In PC9-GR3, α - and β -tubulin protein expression after 3 days and γ -tubulin after 6 days were upregulated on cells grown on PCL-ES scaffolds. High levels of β III-tubulin have been associated with tumorigenic activity, chemoresistance, and poor survival of NSCLC patients [63,64].

The cell viability of PC9 and PC9-GR3 models cultured on PCL-ES structures were lower compared to monolayer (Figure 4). The same results were reported for different lung cancer cell lines seeded on decellularized lung scaffolds [26], chitosan-hyaluronic acid membranes [65], and gelatin meshes [66]. On the contrary, researchers proved that lung adenocarcinoma cell lines grown on silk/fibroin supports or AlgiMatrix™ scaffolds showed higher viability compared to 2D [27,67]. Furthermore, cell models exhibited a significantly greater viability rate when cultured on 15%-PCL-ES platforms after 3 days. Pore size, surface availability, and porosity of 3D platforms as well as initial seeding cell

density or time of culture, influence cell colonization [22,51]. The cell viability was also correlated to the protein adsorbed, which directly affected cell division [55,68].

Total EGFR protein levels were decreased in both cell models seeded on PCL-ES scaffolds (Figure 5), which are in agreement with the literature [69]. These results suggest a mechanism by which EGFR^m lung adenocarcinoma cells acquire resistance to the EGFR-TKIs (Figure 6). Moreover, no changes were observed in phosphorylated EGFR expression in cells grown on PCL-ES platforms, probably as a consequence of the maintenance of LCSC features, for instance, self-renewal and pluripotency capacities [70,71]. The enrichment of the LCSC population was confirmed in sensitive and resistant lung adenocarcinoma models cultured on both PCL-ES scaffolds. According to Wang and coworkers, the identification of LCSCs can be carried out by three or more specific stem cell markers [72], which was fully accomplished in our study.

PC9 and PC9-GR3 cell models seeded on PCL-ES structures showed higher resistance to osimertinib (Figure 6), an irreversible small-molecule that binds covalently to the ATP-binding site of the tyrosine kinase domain of the EGFR and it is effective in the presence of activating mutations and T790M resistance mutation in the EGFR [6]. Additionally, a recent report proved that the LCSC niche was responsible for therapeutic resistance in NSCLC patients [73]. Previous studies demonstrated that lung cancer cells grown on AlgimatrixTM scaffolds [27], chitosan-hyaluronic acid membranes [65], or silk/fibroin structures [67] were less responsive to anticancer drugs in contrast to monolayer culture. PC9 cells cultured on PCL-ES supports also displayed upregulation of Nanog, which is also related to resistance to the treatment and tumor relapse and progression [74]. The multi-drug efflux pumps ABCB1 and ABCG2 are members of the ATP-binding cassette (ABC) family of transmembrane proteins [75]. Although ABCG2 has been commonly reported as a LCSC marker [71,76], our findings revealed enhanced levels of *ABCB1*. The expression of *ABCB1* in patient samples has been linked to a poor response to chemotherapy [77,78]. In addition, several studies have associated the modulation of *ABCB1* activity with the EGFR-TKIs [79,80]. Thus, the lower *ABCB1* enhancement found in PC9-GR3 compared to PC9 could be another intrinsic mechanism of resistance of PC9-GR3 [81].

Regarding the EMT process, both cell models cultured on PCL-ES meshes exhibited upregulation of Vimentin, *SNAIL*, and *TWIST* and downregulation of E-cadherin (Figure 7). The EMT process provides the capacity to metastasize by migrating from the primary tumor to another organ, and then, LCSCs can initiate another tumor [82,83]. Several researchers have observed that 3D culture using chitosan-hyaluronic acid matrices, spheroids, or hydrogel induced EMT through the modulation of different transcription factors and related proteins, such as Snail, Slug, Twist, Zeb1, E-cadherin, N-cadherin, or Fibronectin [84–87], which is consistent with our work. The EMT process has also been involved in the resistance to chemotherapy and EGFR-TKIs. PC9 cells seeded on decellularized lung scaffolds showed EMT induction and resistance to erlotinib and cisplatin [26]. PC9 grown on PCL-ES supports displayed a significantly greater *ZEB1* mRNA expression in comparison with the monolayer, which may lead to the resistance to osimertinib in the sensitive cell model (Figure 6) [88]. According to Tiran and colleagues, the activity of EMT transcription factors triggers LCSC genes, leading to cancer cell plasticity [89]. For instance, the induction of EMT results in decreased levels of CD24 [86,90], as shown in PC9 cultured on scaffolds (Figure 9). In addition, the softness of PCL-ES structures (Figure S1) influences EMT induction in sensitive and resistant lung adenocarcinoma models [91].

LCSCs possess self-renewal and pluripotency capacities that are usually controlled by Sox2, Oct-4, and Nanog [7–12]. However, Singh and Chellappan pointed out that Sox2 may regulate these capacities independently of Oct-4 and Nanog [8]. Sox2 is also related to high tumorigenic potential [92,93]. We observed increased levels of *SOX2*, Oct-4A, and p-Sox2 in PC9 and PC9-GR3 cell models grown on 3D meshes in comparison with 2D (Figure 8). An upregulation of Sox2 has also been found in lung cancer cells cultured on 3D cultures, such as chitosan-hyaluronan matrices [65,84] and spheroids [85]. The genomic amplification of Sox2 was detected in about 20% of lung adenocarcinoma patients

and its high expression was significantly associated with a lower overall survival [93,94]. Furthermore, Sox2 overexpression has been linked to resistance to chemotherapy [73,85] and EGFR-TKIs [92]. Li and coworkers demonstrated that treatment with gefitinib causes the overexpression of Sox2 [95]. Furthermore, the continuous activation of EGFR leads to an increase in Sox2 expression, resulting in the maintenance of LCSC features in EGFRm lung adenocarcinoma [70,71].

Several surface markers have been described to identify LCSCs, such as CD133 and CD166 [14,15]. We observed upregulation of CD166 and reduced CD133 protein expression in both cell models cultured on PCL-ES supports (Figure 9). Different researchers found that CD166+ cells displayed self-renewal capacity and high tumorigenic activity [15,96,97]. Additionally, this cell population showed molecular signatures related to stem cells and biological functions related to angiogenesis, migration, or anti-apoptosis [15]. Zakaria et al. described that CD166+ cells overexpressed Sox2 and Oct-4A and interacted with the Hedgehog pathway [15]. Conversely, another study revealed that CD166 expression was associated with smaller tumors without lymph node metastasis [98]. Regarding CD133, the role of this marker remains unclear [72,99]. Different researchers demonstrated that CD133+ cells derived from NSCLC patients expressed high tumorigenic activity, enhanced levels of different stemness genes, high resistance to cisplatin, and self-renewal capacity [100,101]. Nevertheless, Zhang et al. pointed out that no differences in the tumorigenic activity were found between CD133- and CD133+ populations from NSCLC patient samples using a more sensitive mouse xenotransplantation assay [97]. Other studies discovered that CD133- and CD133+ populations had the same self-renewal and tumorigenic capacities [102,103]. Additionally, the CD133+ population was sensitive to the EGFR-TKI afatinib in EGFRm lung adenocarcinoma H1650 and H1975 cell lines [104]. The variability of the CD133 marker in the aforementioned studies may be a consequence of the heterogeneity of NSCLC. Although the samples were classified by histologic subtypes, mutations in oncogenes were not taken into account, which may influence the results.

The Hedgehog signaling pathway plays an important role in the development and repair of normal lung tissue [105]. Researchers have related its inhibition to the loss of LCSC properties [21]. We also found the activation of the Hedgehog pathway in PC9 and PC9-GR3 cell models cultured on PCL-ES scaffolds (Figure 10). A recent study reported that 76% of lung adenocarcinoma patients express GLI1, the amplifier of the pathway [106]. Besides this, GLI1 also supports the EMT process leading to resistance to EGFR-TKIs in EGFRm lung adenocarcinoma [107–109]. Schnidar et al. demonstrated that an oncogenic transformation could be induced by the synergic activation of EGFR/MAPK and Hedgehog/GLI1 pathways [110]. The Hedgehog pathway and EGFR co-stimulate LCSC markers, e.g., Sox2 [109]. While PC9 seeded on 3D structures exhibited an upregulation of Shh after 3 days of culture, no changes were observed in PC9-GR3. According to Lauth et al., other pathways such as RAS, TGF β , and PI3K can activate the non-canonical Hedgehog pathway, inducing GLI expression [111].

Taking all this into account, 15%-PCL-ES scaffolds may be a better 3D strategy than 10%-PCL ones. Cells cultured on 15%-PCL-ES structures exhibited a higher cell elongation and cell viability (Figure 2; Figure 3). Some LCSC properties were also significantly upregulated only in 15%-PCL-ES supports compared to monolayer, such as *SNAIL* in PC9 and PC9-GR3 models, *TWIST* in PC9, and *SLUG* in PC9-GR3 (Figure 7a). Another example is the CD133 reduction in PC9 and PC9-GR3, which was more notable in cells grown on 15%-PCL-ES platforms for 3 days (Figure 9b). Although the behavior of PC9 and PC9-GR3 cultured on PCL-ES matrices were similar, some variations were found in the EMT process and stemness and pluripotency capacities (Figure 7; Figure 8). Differences between cells seeded on 2D and PCL-ES meshes were already observed after 3 days of culture in PC9. However, PC9-GR3 grown on 3D matrices required 6 days to express these changes. Resistance to EGFR-TKIs has been linked to EMT and stemness and pluripotency capacities [88,92]. PC9-GR3 may already have a baseline upregulation of these properties and more days were needed to show differences between monolayer and 3D culture.

Patients' data analysis agrees with the literature about NSCLC patients harboring EGFR sensitive mutations in the European population [112]. Hence, our sample is representative of the patient profile and tumor type. High levels of Vimentin were associated with lower PFS in our cohort of patients (Figure 12b). Previous studies observed that high expression of Vimentin was associated with a poor outcome to first generation EGFR-TKI and the development of brain metastasis in EGFRm NSCLC patients [113,114]. Our findings also revealed that non-expression of CD133 was associated with a poor degree of histological differentiation, progression to the disease, distant metastasis (Figure 11), and a low OS (Figure 12a). Wen and coworkers determined that high CD133 mRNA levels were related to a better survival rate in lung cancer [115]. Different studies concluded that there was no relationship between CD133 expression and prognosis in NSCLC patients [116,117]. Conversely, other studies established CD133 as an independent prognostic marker for NSCLC [118,119]. Nevertheless, to the best of our knowledge, basal CD133 expression levels in NSCLC patients harboring EGFR sensitivity mutations have not been previously investigated. CD133+ expression was associated with a better prognosis in EGFRm NSCLC patients. Our study has demonstrated that the use of PCL-ES scaffolds allows the enrichment of LCSCs, which are associated with cancer recurrence, resistance to therapies, and metastasis [7–9]. Cells cultured on these 3D supports exhibited higher levels of Vimentin (Figure 7) and lower expression of CD133 (Figure 9) compared to 2D. Taking into account *in vitro* results, the behavior of cells seeded on PCL-ES scaffolds is more similar to the results found in patients (Figure 11; Figure 12). The following limitations in our study may have influenced the results. First, it was a retrospective study with the biases that this entails. Second, the number of samples with enough tissue available to perform IHC was less than expected, and third, some tumor samples were quite old, which could modify the IHC results. However, in relation to this issue, the percentage of Vimentin expression observed in our samples is consistent with that reported in previous studies [113].

5. Conclusions

PCL-ES scaffolds are useful for the 3D cell culture of EGFRm lung adenocarcinoma cell models. The 3D structures displayed different properties that support cell attachment, proliferation, and morphology changes. Consequently, cell models grown on PCL-ES matrices amplified several LCSC characteristics. We showed higher resistance to osimertinib, upregulation of drug efflux pumps, EMT process, stemness, and surface markers, and the activation of the Hedgehog pathway. Additionally, our study demonstrated that the lack of CD133 expression is related to the LCSC population. *In vitro*, we observed a downregulation of CD133 protein expression when the LCSC niche was enriched. Moreover, in tumor tissue samples of EGFRm NSCLC patients, the non-expression of CD133 was significantly associated with a low degree of histological differentiation, progression of the disease, and distant metastasis, features directly connected to LCSCs. Regarding the results of Vimentin, the same correlation was revealed between *in vitro* and IHC patient results. Therefore, we conclude that the use of PCL-ES scaffolds for culturing EGFRm lung adenocarcinoma cell models is a trustworthy 3D strategy to simulate physiological conditions allowing the study of this lung cancer subtype in order to find new biomarkers or test new drugs.

Supplementary Materials: The following are available online at <https://www.mdpi.com/article/10.3390/cancers13215320/s1>. Figure S1: Thermogravimetric analysis of (a) 10%-PCL-ES scaffolds and (b) 15%-PCL-ES scaffolds. Differential scanning calorimetry of (c) 10%-PCL-ES scaffolds and (d) 15%-PCL-ES scaffolds. Dynamic mechanical analysis of (e) 10%-PCL-ES scaffolds and (f) 15%-PCL-ES scaffolds; Figure S2: Filament diameter histogram of (a) 10%-PCL-ES scaffolds and (b) 15%-PCL-ES scaffolds; Figure S3: Whole Western blot figures from Figure 7b and 5 showing α -tubulin, β -tubulin, γ -tubulin, β -actin, p-EGFR, EGFR, and GAPDH protein bands with molecular weight markers (merge of colorimetric and chemiluminescence) of PC9 and PC9-GR3; Figure S4: Whole Western blot figures protein bands of (a) Figure 7b, (b) Figure 8b, (c) Figure 9b, and (d) Figure 10b with molecular weight markers (merge of colorimetric and chemiluminescence) of PC9; Figure S5: Whole Western blot figures protein bands of (a) Figure 7b, (b) Figure 8b, (c) Figure 9b, and (d) Figure 10b with molecular

weight markers (merge of colorimetric and chemiluminescence) of PC9-GR3; Table S1: Primer design; Table S2: List of antibodies; Table S3: Patient and tumor characteristics at baseline.

Author Contributions: Conceptualization, E.P.-A., J.C., and T.P.; methodology, E.P.-A. and C.V.-D.; validation, E.P.-A., S.R.-M., M.R., S.P., C.V.-D., R.P. and J.B.-B.; formal analysis, E.P.-A., S.R.-M., S.P., R.P. and J.B.-B.; investigation, E.P.-A., R.P. and C.V.-D.; resources, J.C., T.P., R.P. and J.B.-B.; data curation, E.P.-A., S.R.-M., S.P., R.P. and J.B.-B.; writing—original draft preparation, E.P.-A. and R.P.; writing—review and editing, E.P.-A.; visualization, E.P.-A.; supervision, J.C., T.P.; project administration, J.C., T.P., R.P. and J.B.-B.; funding acquisition, J.C. and T.P. All authors have read and agreed to the published version of the manuscript.

Funding: This research was funded by Fundación Ramón Areces, Instituto de Salud Carlos III (PI1900372), Ministerio de Economía y Competitividad (DPI2016-77156-R), and AstraZeneca.

Institutional Review Board Statement: Samples from patients included in this study were processed following standard operating procedures with the appropriate approval of the Ethics and Scientific Committees. Approval of the study protocol was obtained from the Dr. Josep Trueta University Hospital Clinical Research Ethics Committee (CP_FASN_T790M_2017; approved 1 June 2017). We only use publicly available data provided through the Hartwig Medical Foundation (controlled access). Samples from the HMF cohort were from patients included in two clinical studies: CPCT-02 (NCT01855477) and DRUP (NCT0295234), which were approved by the medical ethical committees (METC) of the University Medical Center Utrecht and the Netherlands Cancer Institute, respectively.

Informed Consent Statement: Samples from patients included in this study were provided by the Girona Biomedical Research Institute (IDIBGI) Biobank (Biobanc IDIBGI, B.0000872), integrated into the Spanish National Biobanks Network and in the Xarxa de Bancs de Tumors de Catalunya (XBTC) financed by the Pla Director d'Oncologia de Catalunya. All patients consented to the storage of the samples in the biobank and for their use in research projects. The blank copy of informed consent is waived and we do have a license agreement with the HMF and obtained the explicit permission of the HMF to send out our paper for publication.

Data Availability Statement: The data presented in this study are available in this article (and Supplementary Materials).

Acknowledgments: The authors thank the E.P.-A. pre-doctoral grant (2019FI_B01011), the S.R.-M. post-doctoral grant (POSTDOCUDG-2020-0002), the M.R. pre-doctoral grant (IFUDG2017/62), the S.P. post-doctoral grant (POSTDOCUDG-2020), the support of Catalan Government (2017SGR00385) and Oncolliga Foundation and RadikalSwim (OncoSwim). The authors are grateful to R. Rosell and M. A. Molina from the laboratory of Oncology Pangaea (Barcelona, Spain) for kindly providing PC9 models. The authors thank Research Technical Services from the University of Girona. The authors want to particularly acknowledge the patients and the IDIBGI Biobank for their collaboration. The authors are grateful to the pharmacist Maria López and the Clinical Trial Unit of Catalan Institute of Oncology for the help provided in the identification of patients treated with EGFR-TKI. The authors thank Maria Buxó for their statistical analysis support of patients' samples. The authors also acknowledge Glòria Oliveres for the help provided in samples identification and management.

Conflicts of Interest: The authors declare no conflict of interest. The funders had no role in the design of the study; in the collection, analyses, or interpretation of data; in the writing of the manuscript, or in the decision to publish the results.

References

1. Bray, F.; Ferlay, J.; Soerjomataram, I.; Siegel, R.L.; Torre, L.A.; Jemal, A. Global Cancer Statistics 2018: GLOBOCAN Estimates of Incidence and Mortality Worldwide for 36 Cancers in 185 Countries. *CA Cancer J. Clin.* **2018**, *68*, 394–424. [[CrossRef](#)] [[PubMed](#)]
2. Bade, B.C.; Dela Cruz, C.S. Lung Cancer 2020: Epidemiology, Etiology, and Prevention. *Clin. Chest Med.* **2020**, *41*, 1–24. [[CrossRef](#)]
3. Travis, W.D.; Brambilla, E.; Nicholson, A.G.; Yatabe, Y.; Austin, J.H.M.; Beth Beasley, M.; Chirieac, L.R.; Dacic, S.; Duhig, E.; Flieder, D.B.; et al. The 2015 World Health Organization Classification of Lung Tumors. *J. Thorac. Oncol.* **2015**, *10*, 1243–1260. [[CrossRef](#)] [[PubMed](#)]
4. Forsythe, M.L.; Alwithehani, A.; Bethune, D.; Castonguay, M.; Drucker, A.; Flowerdew, G.; French, D.; Fris, J.; Greer, W.; Henteleff, H.; et al. Molecular profiling of non-small cell lung cancer. *PLoS ONE* **2020**, *15*, e0236580. [[CrossRef](#)] [[PubMed](#)]
5. Lynch, T.J.; Bell, D.W.; Sordella, R.; Gurubhagavatula, S.; Okimoto, R.A.; Brannigan, B.W.; Harris, P.L.; Haserlat, S.M.; Supko, J.G.; Haluska, F.G.; et al. Activating Mutations in the Epidermal Growth Factor Receptor Underlying Responsiveness of Non-Small-Cell Lung Cancer to Gefitinib. *N. Engl. J. Med.* **2004**, *350*, 2129–2139. [[CrossRef](#)]

6. Wu, S.G.; Shih, J.Y. Management of acquired resistance to EGFR TKI-targeted therapy in advanced non-small cell lung cancer. *Mol. Cancer* **2018**, *17*, 38. [CrossRef]
7. Yu, Y.; Ramena, G.; Elble, R.C. The role of cancer stem cells in relapse of solid tumors. *Front. Biosci.* **2012**, *1*, 1528. [CrossRef]
8. Singh, S.; Chellappan, S. Lung cancer stem cells: Molecular features and therapeutic targets. *Mol. Aspects Med.* **2014**, *39*, 50–60. [CrossRef]
9. Medema, J.P. Cancer stem cells: The challenges ahead. *Nat. Cell Biol.* **2013**, *15*, 338–344. [CrossRef]
10. Hyslop, L.; Stojkovic, M.; Armstrong, L.; Walter, T.; Stojkovic, P.; Przyborski, S.; Herbert, M.; Murdoch, A.; Strachan, T.; Lakó, M. Downregulation of NANOG Induces Differentiation of Human Embryonic Stem Cells to Extraembryonic Lineages. *Stem Cells* **2005**, *23*, 1035–1043. [CrossRef]
11. Sarkar, A.; Hochedlinger, K. The Sox family of transcription factors: Versatile regulators of stem and progenitor cell fate. *Cell Stem Cell* **2013**, *12*, 15–30. [CrossRef]
12. Kumar, S.M.; Liu, S.; Lu, H.; Zhang, H.; Zhang, P.J.; Gimotty, P.A.; Guerra, M.; Guo, W.; Xu, X. Acquired cancer stem cell phenotypes through Oct4-mediated dedifferentiation. *Oncogene* **2012**, *31*, 4898–4911. [CrossRef]
13. Nassar, D.; Blanpain, C. Cancer Stem Cells: Basic Concepts and Therapeutic Implications. *Annu. Rev. Pathol. Mech. Dis.* **2016**, *11*, 47–76. [CrossRef]
14. Zhang, D.G.; Jiang, A.G.; Lu, H.Y.; Zhang, L.X.; Gao, X.Y. Isolation, cultivation and identification of human lung adenocarcinoma stem cells. *Oncol. Lett.* **2015**, *9*, 47–54. [CrossRef] [PubMed]
15. Zakaria, N.; Yusoff, N.M.; Zakaria, Z.; Lim, M.N.; Baharuddin, P.J.N.; Fakiruddin, K.S.; Yahaya, B. Human non-small cell lung cancer expresses putative cancer stem cell markers and exhibits the transcriptomic profile of multipotent cells. *BMC Cancer* **2015**, *15*, 84. [CrossRef]
16. Akunuru, S.; Zhai, Q.J.; Zheng, Y. Non-small cell lung cancer stem/progenitor cells are enriched in multiple distinct phenotypic subpopulations and exhibit plasticity. *Cell Death Dis.* **2012**, *3*, e352. [CrossRef] [PubMed]
17. Yan, X.; Luo, H.; Zhou, X.; Zhu, B.; Wang, Y.; Bian, X. Identification of CD90 as a marker for lung cancer stem cells in A549 and H446 cell lines. *Oncol. Rep.* **2013**, *30*, 2733–2740. [CrossRef] [PubMed]
18. Zhang, Y.; Weinberg, R.A. Epithelial-to-mesenchymal transition in cancer: Complexity and opportunities. *Front. Med.* **2018**, *12*, 361–373. [CrossRef]
19. Pastushenko, I.; Brisebarre, A.; Sifrim, A.; Fioramonti, M.; Revenco, T.; Boumahdi, S.; Van Keymeulen, A.; Brown, D.; Moers, V.; Lemaire, S.; et al. Identification of the tumour transition states occurring during EMT. *Nature* **2018**, *556*, 463–468. [CrossRef]
20. Teng, Y.; Wang, X.; Wang, Y.; Ma, D. Wnt/ β -catenin signaling regulates cancer stem cells in lung cancer A549 cells. *Biochem. Biophys. Res. Commun.* **2010**, *392*, 373–379. [CrossRef]
21. Park, K.S.; Martelotto, L.G.; Peifer, M.; Sos, M.L.; Karnezis, A.N.; Mahjoub, M.R.; Bernard, K.; Conklin, J.F.; Szczepny, A.; Yuan, J.; et al. A crucial requirement for Hedgehog signaling in small cell lung cancer. *Nat. Med.* **2011**, *17*, 1504–1508. [CrossRef] [PubMed]
22. Costard, L.S.; Hosn, R.R.; Ramanayake, H.; O'Brien, F.J.; Curtin, C.M. Influences of the 3D microenvironment on cancer cell behaviour and treatment responsiveness: A recent update on lung, breast and prostate cancer models. *Acta Biomater.* **2021**, *132*, 360–378. [CrossRef]
23. Boucherit, N.; Gorvel, L.; Olive, D. 3D Tumor Models and Their Use for the Testing of Immunotherapies. *Front. Immunol.* **2020**, *11*, 3220. [CrossRef] [PubMed]
24. Chitcholtan, K.; Asselin, E.; Parent, S.; Sykes, P.H.; Evans, J.J. Differences in growth properties of endometrial cancer in three dimensional (3D) culture and 2D cell monolayer. *Exp. Cell Res.* **2013**, *319*, 75–87. [CrossRef] [PubMed]
25. Mak, I.W.; Evaniew, N.; Ghert, M. Lost in translation: Animal models and clinical trials in cancer treatment. *Am. J. Transl. Res.* **2014**, *6*, 114–118.
26. Tapias, L.F.; Gilpin, S.E.; Ren, X.; Wei, L.; Fuchs, B.C.; Tanabe, K.K.; Lanuti, M.; Ott, H.C. Assessment of Proliferation and Cytotoxicity in a Biomimetic Three-Dimensional Model of Lung Cancer. *Ann. Thorac. Surg.* **2015**, *100*, 414–421. [CrossRef] [PubMed]
27. Godugu, C.; Patel, A.R.; Desai, U.; Andey, T.; Sams, A.; Singh, M. Alginate-Chitosan Based 3D Cell Culture System as an In-Vitro Tumor Model for Anticancer Studies. *PLoS ONE* **2013**, *8*, e53708. [CrossRef]
28. Yao, K.; Li, W.; Li, K.; Wu, Q.; Gu, Y.; Zhao, L.; Zhang, Y.; Gao, X. Simple Fabrication of Multicomponent Heterogeneous Fibers for Cell Co-Culture via Microfluidic Spinning. *Macromol. Biosci.* **2020**, *20*, 1900395. [CrossRef]
29. Sachs, N.; Papaspyropoulos, A.; Zomer-van Ommen, D.D.; Heo, I.; Böttinger, L.; Klay, D.; Weeber, F.; Huelsz-Prince, G.; Jakobachvili, N.; Amatngalin, G.D.; et al. Long-term expanding human airway organoids for disease modeling. *EMBO J.* **2019**, *38*, e100300. [CrossRef] [PubMed]
30. Nakamura, H.; Sugano, M.; Miyashita, T.; Hashimoto, H.; Ochiai, A.; Suzuki, K.; Tsuboi, M.; Ishii, G. Organoid culture containing cancer cells and stromal cells reveals that podoplanin-positive cancer-associated fibroblasts enhance proliferation of lung cancer cells. *Lung Cancer* **2019**, *134*, 100–107. [CrossRef]
31. Herreros-Pomares, A.; Zhou, X.; Calabuig-Fariñas, S.; Lee, S.-J.; Torres, S.; Esworthy, T.; Hann, S.Y.; Jantus-Lewintre, E.; Camps, C.; Zhang, L.G. 3D printing novel in vitro cancer cell culture model systems for lung cancer stem cell study. *Mater. Sci. Eng. C* **2021**, *122*, 111914. [CrossRef] [PubMed]

32. Moghadas, H.; Saidi, M.S.; Kashaninejad, N.; Kiyomarsioskouei, A.; Nguyen, N.T. Fabrication and characterization of low-cost, bead-free, durable and hydrophobic electrospun membrane for 3D cell culture. *Biomed. Microdevices* **2017**, *19*, 74. [CrossRef]
33. Chen, S.; Giannakou, A.; Wyman, S.; Gruzas, J.; Golas, J.; Zhong, W.; Loreth, C.; Sridharan, L.; Yamin, T.-T.; Damelin, M.; et al. Cancer-associated fibroblasts suppress SOX2-induced dysplasia in a lung squamous cancer coculture. *Proc. Natl. Acad. Sci. USA* **2018**, *115*, E11671–E11680. [CrossRef]
34. Hu, S.; Dasbiswas, K.; Guo, Z.; Tee, Y.H.; Thiagarajan, V.; Hersen, P.; Chew, T.L.; Safran, S.A.; Zaidel-Bar, R.; Bershadsky, A.D. Long-range self-organization of cytoskeletal myosin II filament stacks. *Nat. Cell Biol.* **2017**, *19*, 133–141. [CrossRef]
35. Reneker, D.H.; Chun, I. Nanometre diameter fibres of polymer, produced by electrospinning. *Nanotechnology* **1996**, *7*, 216–223. [CrossRef]
36. Cipitria, A.; Skelton, A.; Dargaville, T.R.; Dalton, P.D.; Hutmacher, D.W. Design, fabrication and characterization of PCL electrospun scaffolds—A review. *J. Mater. Chem.* **2011**, *21*, 9419–9453. [CrossRef]
37. Rabionet, M.; Yeste, M.; Puig, T.; Ciurana, J. Electrospinning PCL Scaffolds Manufacture for Three-Dimensional Breast Cancer Cell Culture. *Polymers* **2017**, *9*, 328. [CrossRef] [PubMed]
38. Polonio-Alcalá, E.; Rabionet, M.; Guerra, A.; Yeste, M.; Ciurana, J.; Puig, T.; Polonio-Alcalá, E.; Rabionet, M.; Guerra, A.; Yeste, M.; et al. Screening of Additive Manufactured Scaffolds Designs for Triple Negative Breast Cancer 3D Cell Culture and Stem-Like Expansion. *Int. J. Mol. Sci.* **2018**, *19*, 3148. [CrossRef]
39. Polonio-Alcalá, E.; Rabionet, M.; Gallardo, X.; Angelats, D.; Ciurana, J.; Ruiz-Martinez, S.; Puig, T. PLA Electrospun Scaffolds for Three-Dimensional Triple-Negative Breast Cancer Cell Culture. *Polymers* **2019**, *11*, 916. [CrossRef] [PubMed]
40. Saha, S.; Duan, X.; Wu, L.; Lo, P.-K.; Chen, H.; Wang, Q. Electrospun fibrous scaffolds promote breast cancer cell alignment and epithelial-mesenchymal transition. *Langmuir* **2012**, *28*, 2028–2034. [CrossRef]
41. Mohamed, A.; Gordon, S.H.; Biresaw, G. Polyacrylate/polystyrene bioblends characterized by thermogravimetry, modulated differential scanning calorimetry and infrared photoacoustic spectroscopy. *Polym. Degrad. Stab.* **2007**, *92*, 1177–1185. [CrossRef]
42. Wang, Y.; Rodriguez-Perez, M.A.; Reis, R.L.; Mano, J.F. Thermal and thermomechanical behaviour of polycaprolactone and starch/polycaprolactone blends for biomedical applications. *Macromol. Mater. Eng.* **2005**, *290*, 792–801. [CrossRef]
43. Balgude, A.P.; Yu, X.; Szymanski, A.; Bellamkonda, R.V. Agarose gel stiffness determines rate of DRG neurite extension in 3D cultures. *Biomaterials* **2001**, *22*, 1077–1084. [CrossRef]
44. Singh, D.; Zo, S.M.; Kumar, A.; Han, S.S. Engineering three-dimensional macroporous hydroxyethyl methacrylate–alginate–gelatin cryogel for growth and proliferation of lung epithelial cells. *J. Biomater. Sci. Polym. Ed.* **2013**, *24*, 1343–1359. [CrossRef] [PubMed]
45. Russo, P.; Aciermo, D.; Corradi, A.; Leonelli, C. Dynamic-mechanical behavior and morphology of polystyrene/perovskite composites: Effects of filler size. *Procedia Eng.* **2011**, *10*, 1017–1022. [CrossRef]
46. Wu, H.; Fan, J.; Chu, C.C.; Wu, J. Electrospinning of small diameter 3-D nanofibrous tubular scaffolds with controllable nanofiber orientations for vascular grafts. *J. Mater. Sci. Mater. Med.* **2010**, *21*, 3207–3215. [CrossRef] [PubMed]
47. Shin, M.; Ishii, O.; Sueda, T.; Vacanti, J.P. Contractile cardiac grafts using a novel nanofibrous mesh. *Biomaterials* **2004**, *25*, 3717–3723. [CrossRef]
48. Ishii, O.; Shin, M.; Sueda, T.; Vacanti, J.P. In vitro tissue engineering of a cardiac graft using a degradable scaffold with an extracellular matrix-like topography. *J. Thorac. Cardiovasc. Surg.* **2005**, *130*, 1358–1363. [CrossRef]
49. Nottelet, B.; Pektok, E.; Mandracchia, D.; Tille, J.C.; Walpoth, B.; Gurny, R.; Möller, M. Factorial design optimization and in vivo feasibility of poly(ϵ -caprolactone)-micro- and nanofiber-based small diameter vascular grafts. *J. Biomed. Mater. Res. Part A* **2009**, *89*, 865–875. [CrossRef]
50. Pektok, E.; Nottelet, B.; Tille, J.C.; Gurny, R.; Kalangos, A.; Moeller, M.; Walpoth, B.H. Degradation and healing characteristics of small-diameter poly(ϵ -caprolactone) vascular grafts in the rat systemic arterial circulation. *Circulation* **2008**, *118*, 2563–2570. [CrossRef]
51. Lawrence, B.J.; Madhally, S.V. Cell colonization in degradable 3D porous matrices. *Cell Adhes. Migr.* **2008**, *2*, 9–16. [CrossRef]
52. Li, W.J.; Laurencin, C.T.; Caferson, E.J.; Tuan, R.S.; Ko, F.K. Electrospun nanofibrous structure: A novel scaffold for tissue engineering. *J. Biomed. Mater. Res.* **2002**, *60*, 613–621. [CrossRef]
53. Guerra, A.J.; Cano, P.; Rabionet, M.; Puig, T.; Ciurana, J. Effects of different sterilization processes on the properties of a novel 3D-printed polycaprolactone stent. *Polym. Adv. Technol.* **2018**, *29*, 2327–2335. [CrossRef]
54. Bölgen, N.; Menciloğlu, Y.Z.; Acatay, K.; Vargel, I.; Pişkin, E. In vitro and in vivo degradation of non-woven materials made of poly(ϵ -caprolactone) nanofibers prepared by electrospinning under different conditions. *J. Biomater. Sci. Polym. Ed.* **2005**, *16*, 1537–1555. [CrossRef]
55. Firkowska-Boden, I.; Zhang, X.; Jandt, K.D. Controlling Protein Adsorption through Nanostructured Polymeric Surfaces. *Adv. Healthc. Mater.* **2018**, *7*, 1700995. [CrossRef] [PubMed]
56. Kumar, N.; Parajuli, O.; Gupta, A.; Hahm, J.I. Elucidation of protein adsorption behavior on polymeric surfaces: Toward high-density, high-payload protein templates. *Langmuir* **2008**, *24*, 2688–2694. [CrossRef] [PubMed]
57. Nandakumar, A.; Tahmasebi Birgani, Z.; Santos, D.; Mentink, A.; Auffermann, N.; Van Der Werf, K.; Bennink, M.; Moroni, L.; Van Blitterswijk, C.; Habibovic, P. Surface modification of electrospun fibre meshes by oxygen plasma for bone regeneration. *Biofabrication* **2013**, *5*, 015006. [CrossRef]
58. Santos, M.L.; Pashkuleva, I.; Alves, C.M.; Gomes, M.E.; Fuchs, S.; Unget, R.E.; Reis, R.L.; Kirkpatrick, C.J. Surface-modified 3D starch-based scaffold for improved endothelialization for bone tissue engineering. *J. Mater. Chem.* **2009**, *19*, 4091–4101. [CrossRef]

59. Smith, J. *Chemical Engineering Kinetics*; McGraw Hill: New York, NY, USA, 1981.
60. Li, D.; Wu, T.; He, N.; Wang, J.; Chen, W.; He, L.; Huang, C.; El-Hamshary, H.A.; Al-Deyab, S.S.; Ke, Q.; et al. Three-dimensional polycaprolactone scaffold via needleless electrospinning promotes cell proliferation and infiltration. *Colloids Surfaces B Biointerfaces* **2014**, *121*, 432–443. [CrossRef]
61. Dugina, V.; Khromova, N.; Rybko, V.; Blizniukov, O.; Shagieva, G.; Chaponnier, C.; Kopnin, B.; Kopnin, P. Tumor promotion by γ and suppression by β non-muscle actin isoforms. *Oncotarget* **2015**, *6*, 14556–14571. [CrossRef]
62. Maounis, N.E.; Dráberová, E.; Trakas, N.; Chortfi, M.; Riga, D.; Tzannis, K.; Kanakis, M.; Vóralu, K.; Ellina, E.; Mahera, E.; et al. Expression of γ -tubulin in non-small cell lung cancer and effect on patient survival. *Histol. Histopathol.* **2018**, *34*, 81–90. [PubMed]
63. Levallet, G.; Bergot, E.; Antoine, M.; Creveuil, C.; Santos, A.O.; Beau-Faller, M.; De Fraipont, F.; Brambilla, E.; Levallet, J.; Morin, F.; et al. High TUBB3 expression, an independent prognostic marker in patients with early non-small cell lung cancer treated by preoperative chemotherapy, is regulated by K-ras signaling pathway. *Mol. Cancer Ther.* **2012**, *11*, 1203–1213. [CrossRef] [PubMed]
64. McCarroll, J.A.; Gan, P.P.; Liu, M.; Kavallaris, M. β III-tubulin is a multifunctional protein involved in drug sensitivity and tumorigenesis in non-small cell lung cancer. *Cancer Res.* **2010**, *70*, 4995–5003. [CrossRef]
65. Huang, Y.J.; Hsu, S. Acquisition of epithelial-mesenchymal transition and cancer stem-like phenotypes within chitosan-hyaluronan membrane-derived 3D tumor spheroids. *Biomaterials* **2014**, *35*, 10070–10079. [CrossRef] [PubMed]
66. Yan, X.; Zhou, L.; Wu, Z.; Wang, X.; Chen, X.; Yang, F.; Guo, Y.; Wu, M.; Chen, Y.; Li, W.; et al. High throughput scaffold-based 3D micro-tumor array for efficient drug screening and chemosensitivity testing. *Biomaterials* **2019**, *198*, 167–179. [CrossRef]
67. Li, J.; Zhou, Y.; Chen, W.; Yuan, Z.; You, B.; Liu, Y.; Yang, S.; Li, F.; Qu, C.; Zhang, X. A Novel 3D in Vitro Tumor Model Based on Silk Fibroin/Chitosan Scaffolds to Mimic the Tumor Microenvironment. *ACS Appl. Mater. Interfaces* **2018**, *10*, 36641–36651. [CrossRef]
68. Baxter, G.C.; Stanners, C.P. The effect of protein degradation on cellular growth characteristics. *J. Cell. Physiol.* **1978**, *96*, 139–145. [CrossRef]
69. Ekert, J.E.; Johnson, K.; Strake, B.; Pardinas, J.; Jarantow, S.; Perkinson, R.; Colter, D.C. Three-dimensional lung tumor microenvironment modulates therapeutic compound responsiveness in vitro—implication for drug development. *PLoS ONE* **2014**, *9*, e92248. [CrossRef] [PubMed]
70. Du, W.; Ni, L.; Liu, B.; Wei, Y.; Lv, Y.; Qiang, S.; Dong, J.; Liu, X. Upregulation of SALL4 by EGFR activation regulates the stemness of CD44-positive lung cancer. *Oncogenesis* **2018**, *7*, 36. [CrossRef] [PubMed]
71. Singh, S.; Trevino, J.; Bora-Singhal, N.; Coppola, D.; Haura, E.; Altioik, S.; Chellappan, S.P. EGFR/Src/Akt signaling modulates Sox2 expression and self-renewal of stem-like side-population cells in non-small cell lung cancer. *Mol. Cancer* **2012**, *11*, 73. [CrossRef]
72. Wang, Y.; Jiang, M.; Du, C.; Yu, Y.; Liu, Y.; Li, M.; Luo, F. Utilization of lung cancer cell lines for the study of lung cancer stem cells. *Oncol. Lett.* **2018**, *15*, 6791–6798. [CrossRef] [PubMed]
73. Wang, L.; Liu, X.; Ren, Y.; Zhang, J.; Chen, J.; Zhou, W.; Guo, W.; Wang, X.; Chen, H.; Li, M.; et al. Cisplatin-enriching cancer stem cells confer multidrug resistance in non-small cell lung cancer via enhancing TRIB1/HDAC activity. *Cell Death Dis.* **2017**, *8*, e2746. [CrossRef] [PubMed]
74. Gong, S.; Li, Q.; Jeter, C.R.; Fan, Q.; Tang, D.G.; Liu, B. Regulation of NANOG in cancer cells. *Mol. Carcinog.* **2015**, *54*, 679–687. [CrossRef] [PubMed]
75. Robey, R.W.; Pluchino, K.M.; Hall, M.D.; Fojo, A.T.; Bates, S.E.; Gottesman, M.M. Revisiting the role of ABC transporters in multidrug-resistant cancer. *Nat. Rev. Cancer* **2018**, *18*, 452–464. [CrossRef]
76. Liu, Y.P.; Yang, C.J.; Huang, M.S.; Yeh, C.T.; Wu, A.T.H.; Lee, Y.C.; Lai, T.C.; Lee, C.H.; Hsiao, Y.W.; Lu, J.; et al. Cisplatin selects for multidrug-resistant CD133+ cells in lung adenocarcinoma by activating notch signaling. *Cancer Res.* **2013**, *73*, 406–416. [CrossRef]
77. Amiri-Kordestani, L.; Basseville, A.; Kurdziel, K.; Fojo, A.T.; Bates, S.E. Targeting MDR in breast and lung cancer: Discriminating its potential importance from the failure of drug resistance reversal studies. *Drug Resist. Updat.* **2012**, *15*, 50–61. [CrossRef]
78. Goldstein, L.J.; Galski, H.; Fojo, A.; Willingham, M.; Lai, S.L.; Gazdar, A.; Pirker, R.; Green, A.; Crist, W.; Brodeur, G.M.; et al. Expression of multidrug resistance gene in human cancers. *J. Natl. Cancer Inst.* **1989**, *81*, 116–124. [CrossRef]
79. Liu, B.; Guo, Z.; Dong, H.; Daofeng, T.; Cai, Q.; Ji, B.; Zhang, S.; Wu, L.; Wang, J.; Wang, L.; et al. LRG1, human EGFR inhibitor, reverses multidrug resistance through modulation of ABCB1 and ABCG2. *Brain Res.* **2015**, *1611*, 93–100. [CrossRef]
80. Shi, Z.; Tiwari, A.K.; Shukla, S.; Robey, R.W.; Kim, I.W.; Parmar, S.; Bates, S.E.; Si, Q.S.; Goldblatt, C.S.; Abraham, I.; et al. Inhibiting the function of ABCB1 and ABCG2 by the EGFR tyrosine kinase inhibitor AG1478. *Biochem. Pharmacol.* **2009**, *77*, 781–793. [CrossRef]
81. Jacobsen, K.; Bertran-Alamillo, J.; Molina, M.A.; Teixidó, C.; Karachaliou, N.; Pedersen, M.H.; Castellví, J.; Garzón, M.; Codony-Servat, C.; Codony-Servat, J.; et al. Convergent Akt activation drives acquired EGFR inhibitor resistance in lung cancer. *Nat. Commun.* **2017**, *8*, 410. [CrossRef]
82. Nieto, M.A. Epithelial-Mesenchymal Transitions in development and disease: Old views and new perspectives. *Int. J. Dev. Biol.* **2009**, *53*, 1541–1547. [CrossRef] [PubMed]
83. Li, S.; Li, Q. Cancer stem cells and tumor metastasis (review). *Int. J. Oncol.* **2014**, *44*, 1806–1812. [CrossRef]
84. Han, H.-W.; Hsu, S. Chitosan-hyaluronan based 3D co-culture platform for studying the crosstalk of lung cancer cells and mesenchymal stem cells. *Acta Biomater.* **2016**, *42*, 157–167. [CrossRef]

85. Choe, C.; Kim, H.; Min, S.; Park, S.; Seo, J.; Roh, S. SOX2, a stemness gene, induces progression of NSCLC A549 cells toward anchorage-independent growth and chemoresistance to vinblastine. *Oncol. Targets Ther.* **2018**, *11*, 6197–6207. [CrossRef] [PubMed]
86. Liu, P.; Zhang, R.; Yu, W.; Ye, Y.; Cheng, Y.; Han, L.; Dong, L.; Chen, Y.; Wei, X.; Yu, J. FGF1 and IGF1-conditioned 3D culture system promoted the amplification and cancer stemness of lung cancer cells. *Biomaterials* **2017**, *149*, 63–76. [CrossRef] [PubMed]
87. Kumar, M.; Allison, D.F.; Baranova, N.N.; Wamsley, J.J.; Katz, A.J.; Bekiranov, S.; Jones, D.R.; Mayo, M.W. NF- κ B Regulates Mesenchymal Transition for the Induction of Non-Small Cell Lung Cancer Initiating Cells. *PLoS ONE* **2013**, *8*, e68597.
88. Song, K.A.; Niederst, M.J.; Lochmann, T.L.; Hata, A.N.; Kitai, H.; Ham, J.; Floros, K.V.; Hicks, M.A.; Hu, H.; Mulvey, H.E.; et al. Epithelial-to-mesenchymal transition antagonizes response to targeted therapies in lung cancer by suppressing BIM. *Clin. Cancer Res.* **2018**, *24*, 197–208. [CrossRef]
89. Tiran, V.; Lindenmann, J.; Brcic, L.; Heitzer, E.; Stanzer, S.; Tabrizi-Wizsy, N.G.; Stacher, E.; Stoeger, H.; Popper, H.H.; Balic, M.; et al. Primary patient-derived lung adenocarcinoma cell culture challenges the association of cancer stem cells with epithelial-to-mesenchymal transition. *Sci. Rep.* **2017**, *7*, 10040. [CrossRef] [PubMed]
90. Mani, S.A.; Guo, W.; Liao, M.J.; Eaton, E.N.; Ayyanan, A.; Zhou, A.Y.; Brooks, M.; Reinhard, F.; Zhang, C.C.; Shiptsin, M.; et al. The Epithelial-Mesenchymal Transition Generates Cells with Properties of Stem Cells. *Cell* **2008**, *133*, 704–715. [CrossRef]
91. Mihalko, E.P.; Brown, A.C. Material Strategies for Modulating Epithelial to Mesenchymal Transitions. *ACS Biomater. Sci. Eng.* **2018**, *4*, 1149–1161. [CrossRef] [PubMed]
92. Murakami, A.; Takahashi, F.; Nurwidya, F.; Kobayashi, I.; Minakata, K.; Hashimoto, M.; Nara, T.; Kato, M.; Tajima, K.; Shimada, N.; et al. Hypoxia increases gefitinib-resistant lung cancer stem cells through the activation of insulin-like growth factor I receptor. *PLoS ONE* **2014**, *9*, e86459. [CrossRef]
93. Nakatsugawa, M.; Takahashi, A.; Hirohashi, Y.; Torigoe, T.; Inoda, S.; Murase, M.; Asanuma, H.; Tamura, Y.; Morita, R.; Michifuri, Y.; et al. SOX2 is overexpressed in stem-like cells of human lung adenocarcinoma and augments the tumorigenicity. *Lab. Investig.* **2011**, *91*, 1796–1804. [CrossRef]
94. Sholl, L.M.; Barletta, J.A.; Yeap, B.Y.; Chirieac, L.R.; Hornick, J.L. Sox2 protein expression is an independent poor prognostic indicator in stage I lung adenocarcinoma. *Am. J. Surg. Pathol.* **2010**, *34*, 1193–1198. [CrossRef]
95. Li, M.; Yang, J.; Zhou, W.; Ren, Y.; Wang, X.; Chen, H.; Zhang, J.; Chen, J.; Sun, Y.; Cui, L.; et al. Activation of an AKT/FOXM1/STMN1 pathway drives resistance to tyrosine kinase inhibitors in lung cancer. *Br. J. Cancer* **2017**, *117*, 974–983. [CrossRef]
96. Jiang, Z.; Hao, Y.; Ding, X.; Zhang, Z.; Liu, P.; Wei, X.; Xi, J. The effects and mechanisms of SLC34A2 on tumorigenicity in human non-small cell lung cancer stem cells. *Tumor Biol.* **2016**, *37*, 10383–10392. [CrossRef]
97. Zhang, W.C.; Ng, S.C.; Yang, H.; Rai, A.; Umashankar, S.; Ma, S.; Soh, B.S.; Sun, L.L.; Tai, B.C.; Nga, M.E.; et al. Glycine decarboxylase activity drives non-small cell lung cancer tumor-initiating cells and tumorigenesis. *Cell* **2012**, *148*, 259–272. [CrossRef]
98. Tachezy, M.; Zander, H.; Wolters-Eisfeld, G.; Müller, J.; Wicklein, D.; Gebauer, F.; Izbicki, J.R.; Bockhorn, M. Activated leukocyte cell adhesion molecule (CD166): An “inert” cancer stem cell marker for non-small cell lung cancer? *Stem Cells* **2014**, *32*, 1429–1436. [CrossRef]
99. Wang, J.; Li, Z.; White, J.; Zhang, L. Lung Cancer Stem Cells and Implications for Future Therapeutics. *Cell Biochem. Biophys.* **2014**, *69*, 389–398. [CrossRef]
100. Bertolini, G.; Roz, L.; Perego, P.; Tortoreto, M.; Fontanella, E.; Gatti, L.; Pratesi, G.; Fabbri, A.; Andriani, F.; Tinelli, S.; et al. Highly tumorigenic lung cancer CD133+ cells display stem-like features and are spared by cisplatin treatment. *Proc. Natl. Acad. Sci. USA* **2009**, *106*, 16281–16286. [CrossRef]
101. Eramo, A.; Lotti, F.; Sette, G.; Pilozzi, E.; Biffoni, M.; Di Virgilio, A.; Conticello, C.; Ruco, L.; Peschle, C.; De Maria, R. Identification and expansion of the tumorigenic lung cancer stem cell population. *Cell Death Differ.* **2008**, *15*, 504–514. [CrossRef]
102. Zhang, Y.; Xu, W.; Guo, H.; Zhang, Y.; He, Y.; Lee, S.H.; Song, X.; Li, X.; Guo, Y.; Zhao, Y.; et al. NOTCH1 signaling regulates self-renewal and platinum chemoresistance of cancer stem-like cells in human non-small cell lung cancer. *Cancer Res.* **2017**, *77*, 3082–3091. [CrossRef]
103. Meng, X.; Wang, X.; Wang, Y. More than 45% of A549 and H446 cells are cancer initiating cells: Evidence from cloning and tumorigenic analyses. *Oncol. Rep.* **2009**, *21*, 995–1000. [PubMed]
104. Alama, A.; Gangemi, R.; Ferrini, S.; Barisione, G.; Orengo, A.M.; Truini, M.; Bello, M.G.D.; Grossi, F. CD133-Positive Cells from Non-Small Cell Lung Cancer Show Distinct Sensitivity to Cisplatin and Afatinib. *Arch. Immunol. Ther. Exp.* **2015**, *63*, 207–214. [CrossRef]
105. Watkins, D.N.; Berman, D.M.; Burkholder, S.G.; Wang, B.; Beachy, P.A.; Baylin, S.B. Hedgehog signalling within airway epithelial progenitors and in small-cell lung cancer. *Nature* **2003**, *422*, 313–317. [CrossRef]
106. Po, A.; Silvano, M.; Miele, E.; Capalbo, C.; Eramo, A.; Salvati, V.; Todaro, M.; Besharat, Z.M.; Catanzaro, G.; Cucchi, D.; et al. Noncanonical GLI1 signaling promotes stemness features and in vivo growth in lung adenocarcinoma. *Oncogene* **2017**, *36*, 4641–4652. [CrossRef]
107. Li, H.; Yue, D.; Jin, J.Q.; Woodard, G.A.; Tolani, B.; Luh, T.M.; Giroux-Leprieur, E.; Mo, M.; Chen, Z.; Che, J.; et al. Gli promotes epithelial-mesenchymal transition in human lung adenocarcinomas. *Oncotarget* **2016**, *7*, 80415–80425. [CrossRef]

108. Della Corte, C.M.; Malapelle, U.; Vigliar, E.; Pepe, F.; Troncione, G.; Ciaramella, V.; Troiani, T.; Martinelli, E.; Belli, V.; Ciardiello, F.; et al. Efficacy of continuous EGFR-inhibition and role of Hedgehog in EGFR acquired resistance in human lung cancer cells with activating mutation of EGFR. *Oncotarget* **2017**, *8*, 23020–23032. [CrossRef]
109. Bora-Singhal, N.; Perumal, D.; Nguyen, J.; Chellappan, S. Gli1-Mediated Regulation of Sox2 Facilitates Self-Renewal of Stem-Like Cells and Confers Resistance to EGFR Inhibitors in Non-Small Cell Lung Cancer. *Neoplasia* **2015**, *17*, 538–551. [CrossRef]
110. Schnidar, H.; Eberl, M.; Klingler, S.; Mangelberger, D.; Kasper, M.; Hauser-Kronberger, C.; Regl, G.; Kroismayr, R.; Moriggl, R.; Sibilä, M.; et al. Epidermal Growth Factor Receptor Signaling Synergizes with Hedgehog/GLI in Oncogenic Transformation via Activation of the MEK/ERK/JUN Pathway. *Cancer Res.* **2009**, *69*, 1284–1292. [CrossRef]
111. Lauth, M.; Toftgård, R. Non-canonical activation of GLI transcription factors: Implications for targeted anti-cancer therapy. *Cell Cycle* **2007**, *6*, 2458–2463. [CrossRef]
112. Rosell, R.; Moran, T.; Queralt, C.; Porta, R.; Cardenal, F.; Camps, C.; Majem, M.; Lopez-Vivanco, G.; Isla, D.; Provencio, M.; et al. Screening of epidermal growth factor receptor mutation in lung cancer. *N. Engl. J. Med.* **2009**, *361*, 958–967. [CrossRef]
113. Teocharoen, R.; Ruangritchankul, K.; Vinayanuwattikun, C.; Sriuranpong, V.; Sitthideatphaiboon, P. Vimentin expression status is a potential biomarker for brain metastasis development in EGFR-mutant NSCLC patients. *Transl. Lung Cancer Res.* **2021**, *10*, 790–801. [CrossRef]
114. Richardson, F.; Young, G.D.; Sennello, R.; Wolf, J.; Argast, G.M.; Mercado, P.; Davies, A.; Epstein, D.M.; Wacker, B. The Evaluation of E-Cadherin and Vimentin as Biomarkers of Clinical Outcomes Among Patients with Non-small Cell Lung Cancer Treated with Erlotinib as Second- or Third-line Therapy. *Anticancer Res.* **2012**, *32*, 537–552.
115. Wen, G.-M.; Mou, F.-F.; Hou, W.; Wang, D.; Xia, P. Integrative Analysis of CD133 mRNA in Human Cancers Based on Data Mining. *Stem Cell Rev. Rep.* **2019**, *15*, 23–34. [CrossRef]
116. Janikova, M.; Skarda, J.; Dziechciarkova, M.; Radova, L.; Chmelova, J.; Krejci, V.; Sedlakova, E.; Zapletalova, J.; Langova, K.; Klein, J.; et al. Identification of CD133+/Nestin+ Putative Cancer Stem Cells in Non-Small Cell Lung Cancer. *Biomed. Pap. Med. Fac. Univ. Palacky Olomouc Czech Repub.* **2010**, *154*, 321–326. [CrossRef]
117. Herpel, E.; Jensen, K.; Muley, T.; Warth, A.; Schnabel, P.A.; Meister, M.; Herth, F.J.F.; Dienemann, H.; Thomas, M.; Gottschling, S. The cancer stem cell antigens CD133, BCRP1/ABCG2 and CD117/c-KIT are not associated with prognosis in resected early-stage non-small cell lung cancer. *Anticancer Res.* **2011**, *31*, 4491–4500.
118. Okudela, K.; Woo, T.; Mitsui, H.; Tajiri, M.; Masuda, M.; Ohashi, K. Expression of the potential cancer stem cell markers, CD133, CD44, ALDH1, and β -catenin, in primary lung adenocarcinoma—their prognostic significance. *Pathol. Int.* **2012**, *62*, 792–801. [CrossRef]
119. Mizugaki, H.; Sakakibara-Komishi, J.; Kikuchi, J.; Moriya, J.; Hatanaka, K.C.; Kikuchi, E.; Kinoshita, I.; Oizumi, S.; Dosaka-Akita, H.; Matsuno, Y.; et al. CD133 expression: A potential prognostic marker for non-small cell lung cancers. *Int. J. Clin. Oncol.* **2014**, *19*, 254–259. [CrossRef]

Results III. Inhibition of FASN as a new therapeutic strategy for
the treatment of EGFRm NSCLC

This section is based on the following publications:

Title Fatty Acid Synthase Inhibitor G28 Shows Anticancer Activity in EGFR Tyrosine Kinase Inhibitor Resistant Lung Adenocarcinoma Models

Authors Emma Polonio-Alcalá[†], Sònia Palomerast[†], Daniel Torres-Oteros, Joana Relat, Marta Planas, Lidia Feliu, Joaquim Ciurana, Santiago Ruiz-Martínez*, and Teresa Puig*

Journal Cancers

Publication Year 2020

Impact Factor ₂₀₂₀ 6.639 (Q1 in Oncology; Position 51 of 242)

DOI 10.3390/cancers12051283

Title AZ12756122, a Novel Fatty Acid Synthase Inhibitor, Decreases Resistance Features in EGFR-TKI Resistant EGFR mutated NSCLC Cell Models

Authors Emma Polonio-Alcalá, Rut Porta, Santiago Ruiz-Martínez, Carmen Vázquez-Dongo, Joana Relat, Joaquim Bosch-Barrera, Joaquim Ciurana*, and Teresa Puig*

Journal Biomedicine & Pharmacotherapy

Publication Year 2022

Impact Factor ₂₀₂₁ 7.419 (Q1 in Pharmacology & Pharmacy; Position 26 of 279)

DOI 10.1016/j.biopha.2022.113942

Abstract

This chapter aims to evaluate the inhibition of FASN as a new therapeutic strategy for EGFRm NSCLC cell models. Overexpression and/or hyperactivation of this enzyme has been described as a resistance mechanism of cancer cells, thereby FASN is an interesting target for cancer treatment.

First, gene and protein expression of FASN was determined in sensitive and resistant EGFRm NSCLC cell models. Second, the cytotoxic effect and the capacity to inhibit the FASN activity of three compounds were investigated in sensitive and resistant EGFRm NSCLC cell models. The compounds studied were (1) EGCG; (2) a synthetic derivative of EGCG, G28; and (3) a novel synthetic compound, AZ12756122. Then, the molecular effect caused by the compounds on FASN, EGFR, STAT3, AKT/PRAS40, and MAPK pathways was studied in sensitive and resistant EGFRm NSCLC cell models, alone and in combination with EGFR-TKIs. Third, FASN inhibition was assessed as a therapeutic strategy against LCSCs in sensitive and resistant EGFRm NSCLC cell models. Finally, FASN tumor expression of samples from patients with EGFRm NSCLC was evaluated to validate *in vitro* results.

EGFRm NSCLC cell models resistant to EGFR-TKIs overexpressed FASN. Furthermore, treatment with the compounds showed a similar cytotoxic effect, which was independent of EGFR-TKI's resistance mechanisms. Synergistic effects were observed when the synthetic compounds, G28 or AZ12756122, were combined with EGFR-TKIs. Additionally, the combinatorial treatment reduced of phosphorylated levels of EGFR, AKT/PRAS40, and MAPK. FASN inhibition also decreased cancer stem-like cells. Moreover, the expression of FASN in tumor samples obtained from the biopsy of EGFRm NSCLC patients was associated with a longer PFS in patients who responded to EGFR-TKI treatment.



Article

Fatty Acid Synthase Inhibitor G28 Shows Anticancer Activity in EGFR Tyrosine Kinase Inhibitor Resistant Lung Adenocarcinoma Models

Emma Polonio-Alcalá ^{1,2,†}, Sònia Palomeras ^{1,†}, Daniel Torres-Oteros ³, Joana Relat ^{3,4,5}, Marta Planas ⁶, Lidia Feliu ⁶, Joaquim Ciurana ², Santiago Ruiz-Martínez ^{1,*} and Teresa Puig ^{1,*}

¹ New Therapeutic Targets Laboratory (TargetsLab)-Oncology Unit, Department of Medical Sciences, Faculty of Medicine, University of Girona, 17003 Girona, Spain; emma.polonio@udg.edu (E.P.-A.); sonia.palomeras@udg.edu (S.P.)

² Product, Process and Production Engineering Research Group (GREP), Department of Mechanical Engineering and Industrial Construction, University of Girona, 17003 Girona, Spain; quim.ciurana@udg.edu

³ Department of Nutrition, Food Sciences and Gastronomy, School of Pharmacy and Food Sciences, Food Torribera Campus, University of Barcelona, E-08921 Santa Coloma de Gramanet, Spain; danytoot@hotmail.com (D.T.-O.); jrelat@ub.edu (J.R.)

⁴ Institute of Nutrition and Food Safety of the University of Barcelona (INSA-UB), E-08921 Santa Coloma de Gramanet, Spain

⁵ CIBER Physiopathology of Obesity and Nutrition (CIBER-OBN), Instituto de Salud Carlos III, E-28029 Madrid, Spain

⁶ LIPPSO, Department of Chemistry, University of Girona, 17003 Girona, Spain; marta.planas@udg.edu (M.P.); lidia.feliu@udg.edu (L.F.)

* Correspondence: santiago.ruiz@udg.edu (S.R.-M.); teresa.puig@udg.edu (T.P.); Tel.: +34-972-419-548 (S.R.-M.); +34-972-419-628 (T.P.)

† These authors contributed equally to this work.

Received: 26 March 2020; Accepted: 16 May 2020; Published: 19 May 2020



Abstract: Epidermal growth factor receptor (EGFR) tyrosine kinases inhibitors (TKIs) are effective therapies for non-small cell lung cancer (NSCLC) patients whose tumors harbor an EGFR activating mutation. However, this treatment is not curative due to primary and secondary resistance such as T790M mutation in exon 20. Recently, activation of transducer and activator of transcription 3 (STAT3) in NSCLC appeared as an alternative resistance mechanism allowing cancer cells to elude the EGFR signaling. Overexpression of fatty acid synthase (FASN), a multifunctional enzyme essential for endogenous lipogenesis, has been related to resistance and the regulation of the EGFR/Jak2/STAT signaling pathways. Using EGFR mutated (EGFR^m) NSCLC sensitive and EGFR TKIs' resistant models (Gefitinib Resistant, GR) we studied the role of the natural polyphenolic anti-FASN compound (–)-epigallocatechin-3-gallate (EGCG), and its derivative G28 to overcome EGFR TKIs' resistance. We show that G28's cytotoxicity is independent of TKIs' resistance mechanisms displaying synergistic effects in combination with gefitinib and osimertinib in the resistant T790M negative (T790M–) model and showing a reduction of activated EGFR and STAT3 in T790M positive (T790M+) models. Our results provide the bases for further investigation of G28 in combination with TKIs to overcome the EGFR TKI resistance in NSCLC.

Keywords: NSCLC; EGFR TKI; FASN inhibitors; resistance; STAT3; EGCG

1. Introduction

Lung cancer is the most incident and the leading cause of cancer death worldwide. Non-small cell lung cancer (NSCLC) subtype is the most common and it represents 80–85% of lung cancers diagnosed. Early-stage NSCLC patients have long-term survival after surgery. However, approximately 75% of patients are diagnosed in advanced stages [1,2].

Gefitinib is a first generation epidermal growth factor receptor (EGFR) tyrosine kinase inhibitor (TKI). It was approved in 2003 by the Food and Drug Administration (FDA) for the treatment of patients whose tumors harbor an EGFR sensitizing/activating mutation (EGFRm) i.e., exon 19 deletion ($\Delta E746-A750$) or the point mutation in exon 21 that leads to the amino acid substitution L858R [3–5]. Despite this therapy represents a breakthrough in the treatment of EGFRm NSCLC patients, in a median time of 9–16 months nearly all patients do not achieve a complete response. One of the most common resistance mechanisms described is the EGFR point mutation in exon 20 that leads to the replacement of threonine 790 by methionine (T790M), which normally derives to lethal disease progression [6]. Osimertinib is an irreversible third generation TKI effective in EGFRm T790M positive (T790M+) patients. However, the point mutation C797S in exon 20 has appeared as the main resistance mechanism to the latest FDA-approved TKI [6]. Other mechanisms for EGFR TKI resistance include Met amplification, phosphatidylinositol-4,5-bisphosphate 3-kinase catalytic subunit alpha (PI3KCA) mutations, appearance of stem-like properties as evidenced by increase in epithelial–mesenchymal transition (EMT) and histological transformation, epidermal growth factor receptor type 2 (ErbB2) gene amplification, increase of insulin-like growth factor 1 receptor (IGF-1R) signaling pathway through the loss of inhibitory insulin-like growth factor-binding protein (IGF-BP) and loss or reduction of phosphatase and tensin homolog (PTEN), activation of AXL tyrosine kinase receptor or B-Raf proto-oncogene, and serine/threonine kinase (BRAF) mutations [6–12].

Recently, the activation of a signal transducer and activator of transcription 3 (STAT3) has been described as an alternative resistance mechanism allowing cancer cells to escape the EGFR signaling or the TKI suppression [13]. STAT3 is involved in the transcription of many genes related to cell differentiation, proliferation, resistance to apoptosis, angiogenesis, metastasis, and immune response [14–16]. Besides being phosphorylated by EGFR [17], STAT3 can also be activated in response to different cytokines and growth factors such as interleukin 6 (IL-6), interferon-alpha (IFN- α) or epidermal growth factor (EGF), among others [18]. Approximately 60% of patients show STAT3 activation, which correlates with poorly differentiated tumors, the presence of metastasis, and the late clinical stage [19,20]. STAT3 phosphorylation has been related to disease progression in a small cohort of patients after EGFR TKI treatment [21]. Additionally, neither gefitinib nor osimertinib are able to inhibit STAT3 activation [22,23].

Energy metabolism deregulation has been described as a hallmark of cancer, allowing cell growth and proliferation [24]. Fatty acid synthase (FASN) is an essential enzyme for the de novo synthesis of long-chain fatty acids from acetyl-CoA, malonyl-CoA, and NADPH [25]. Unlike most normal cells, highly-proliferative cancer cells overexpress this lipogenic enzyme, being an interesting target in cancer therapy [26,27]. FASN is strongly associated to poor prognosis and resistance to treatment in different human tumors such as breast [28], bladder [29], pancreatic [30], or lung cancer [31]. Moreover, FASN overexpression has also been proposed as a multidrug resistance mechanism, protecting cells from drug-induced apoptosis through the overproduction of palmitic acid [32]. The natural compound (–)-epigallocatechin-3-gallate (EGCG) is a polyphenolic flavonoid from green tea that has been broadly studied for its cardiovascular, neuroprotective, anticancer, and antimicrobial properties [33,34]. EGCG has been reported to compete with NADPH to bind the β -ketoacyl reductase domain of FASN [35]. The ability of several FASN inhibitors to regulate the canonical EGFR/Jak2/STAT pathway has also been stated in the literature [36,37]. We and others have shown that FASN inhibition is mainly related to EGFR/HER2 signaling pathways, leading to cytotoxic effects in vitro and in vivo in a wide range of carcinomas, including breast and lung [38–42]. To date, many EGCG derivatives have been developed to improve efficacy and increase stability in physiological conditions. Among them, the naphthalene

derivative G28 has shown interesting antiproliferative features against sensitive and resistant breast cancer cells [38,43,44].

The purpose of this work was to study the role of FASN inhibitors (EGCG and G28) to overcome TKI resistance in NSCLC. FASN inhibitors were tested alone and in combination with EGFR TKIs (gefitinib and osimertinib) in EGFRm NSCLC models resistant to EGFR TKIs (Gefitinib Resistant, GR). In addition, we also evaluated gene and protein expression changes of FASN, EGFR, and STAT3 resulting from treatments with FASN inhibitors and EGFR TKIs alone or in combination. We show that FASN inhibitor G28 cytotoxicity is independent of EGFR TKI resistance mechanisms. Interestingly, G28 compound exhibited a cytotoxic effect in combination with gefitinib showing changes in EGFR/STAT3 pathway in T790M positive (T790M+) GR models and strong synergism in combination with gefitinib or osimertinib in T790M negative (T790M-) GR model.

2. Results

2.1. EGFRm GR NSCLC Models Are Sensitive to FASN Inhibition

In order to study the role of FASN in the acquisition of EGFR TKI resistance in NSCLC, we used the sensitive PC9 cell line carrying the EGFR exon 19 deletion (ELREA) and three GR models, two T790M+ models (PC9-GR1 and PC9-GR4), and one T790M- model (PC9-GR3) [45].

2.1.1. EGFRm NSCLC Models Overexpress FASN

Firstly, we determined whether EGFRm NSCLC models express FASN enzyme. Hence, FASN protein (Figure 1a) and mRNA expression levels (Figure 1b) were analyzed by immunoblotting and quantitative real time PCR (qRT-PCR), respectively.

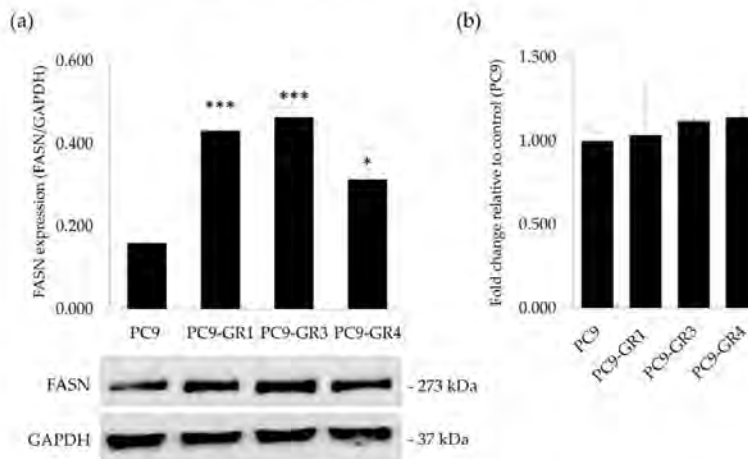


Figure 1. FASN protein and mRNA expression levels in sensitive (PC9) and Gefitinib Resistant (GR) models (PC9-GR1, PC9-GR3, and PC9-GR4). (a) Western blot analysis (quantification in upper panel and bands in lower panel) of FASN protein expression. GAPDH was used as a loading control. Results shown are representative from at least three independent experiments. (b) FASN endogenous mRNA levels were obtained by qRT-PCR and normalized against the GAPDH gene. FASN expression in the sensitive cells was normalized to 1 and expressed as a fold change, to which all other conditions were compared. Results shown are mean \pm SE from three independent experiments. * $p < 0.050$, *** $p < 0.001$ indicate levels of statistical significance.

All models showed FASN protein and mRNA expression. Despite no differences in mRNA, GR models presented significantly higher protein expression levels (PC9-GR1 $p = 8.710 \times 10^{-4}$; PC9-GR3 $p = 3.160 \times 10^{-4}$, and PC9-GR4 $p = 0.049$) in comparison to PC9.

2.1.2. PC9-GR3 Model Is Resistant to Gefitinib and Osimertinib

We confirmed the resistance to EGFR TKIs in PC9 and GR models. For that, we measured the cytotoxic effect of gefitinib and osimertinib on all models by determining the half-maximal inhibitory concentration (IC_{50}) using the MTT assay (Figure 2).

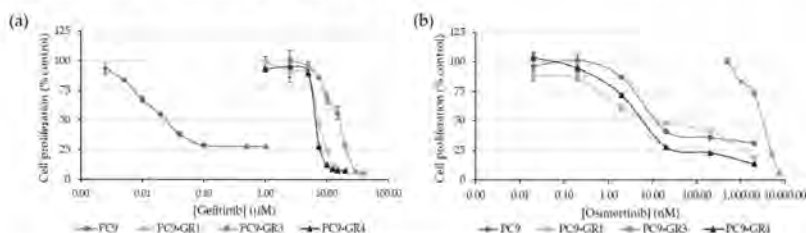


Figure 2. Cell proliferation inhibition of EGFR TKIs (gefitinib and osimertinib) in parental and Gefitinib Resistant (GR) models. Sensitive (PC9) and GR models (PC9-GR1, PC9-GR3, and PC9-GR4) were treated with increasing concentrations of (a) gefitinib (from 2.5×10^{-3} to $1 \mu\text{M}$ for PC9 and $1\text{--}40 \mu\text{M}$ for GR models) and (b) osimertinib ($0.02\text{--}2000 \text{ nM}$ for PC9, PC9-GR1, and PC9-GR4 and $500\text{--}7500 \text{ nM}$ for PC9-GR3) for 72 h. Results shown are expressed as percentage of surviving cells after drug treatment (mean \pm SE) and are representative from at least three independent experiments.

As expected, GR models were significantly more resistant to gefitinib with IC_{50} values in the micromolar range compared to the nanomolar IC_{50} found in the PC9 cell line (PC9-GR1 $p = 2.793 \times 10^{-7}$; PC9-GR3 $p = 1.631 \times 10^{-10}$, and PC9-GR4 $p = 1.000 \times 10^{-6}$). Although no significant differences were found in the IC_{50} value for gefitinib between the two T790M+ GR models, the IC_{50} value of the PC9-GR3 model for gefitinib was significantly greater than PC9-GR1 ($p = 7.953 \times 10^{-7}$) and PC9-GR4 ($p = 1.659 \times 10^{-7}$). PC9-GR3 model was also resistant to osimertinib compared to other models (PC9 $p = 2.799 \times 10^{-9}$; PC9-GR1 $p = 3.749 \times 10^{-8}$, and PC9-GR4 $p = 5.200 \times 10^{-9}$).

2.1.3. FASN Inhibitors Present Cytotoxic Effects in NSCLC Models

Cancer cells have been described to increase the de novo lipogenesis through the activation of FASN and its inhibition has proven to cause cell death. Therefore, this enzyme has become a promising candidate for the development of new anticancer therapies. Here we tested the cytotoxic activity of the two FASN inhibitors, EGCG and its derivative G28. MTT cell viability assays showed that the natural polyphenolic compound EGCG was cytotoxic for PC9 ($IC_{50} = 77.9 \pm 1.9 \mu\text{M}$), PC9-GR1 ($IC_{50} = 74.3 \pm 4.3 \mu\text{M}$), PC9-GR3 ($IC_{50} = 91.0 \pm 5.5 \mu\text{M}$), and PC9-GR4 ($IC_{50} = 75.6 \pm 2.4 \mu\text{M}$) NSCLC models with no significant differences ($p = 0.358$; Figure 3a).

The synthetic EGCG derivative G28 showed higher cytotoxicity in all tested models with IC_{50} of $12.8 \pm 1.3 \mu\text{M}$ for PC9, $12.0 \pm 0.8 \mu\text{M}$ for PC9-GR1, $17.8 \pm 1.3 \mu\text{M}$ for PC9-GR3, and $11.2 \pm 1.2 \mu\text{M}$ for PC9-GR4 (Figure 3b). Besides, only PC9-GR3 showed a significantly higher IC_{50} value compared to PC9 ($p = 0.030$), PC9-GR1 ($p = 0.005$), and PC9-GR4 ($p = 0.002$).

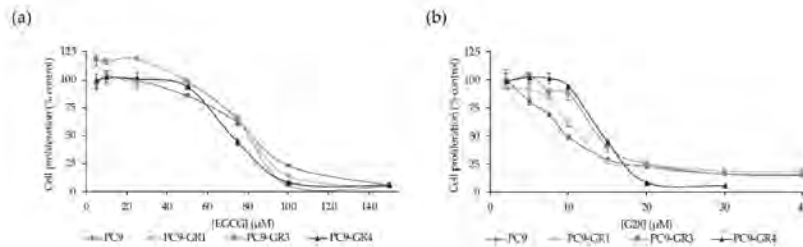


Figure 3. Cell proliferation inhibition of FASN inhibitors in parental and Gefitinib Resistant (GR) models. Sensitive (PC9) and GR models (PC9-GR1, PC9-GR3, and PC9-GR4) were treated with increasing concentrations of (a) EGCG (5–150 μM) and (b) G28 (2–40 μM) for 72 h. Results shown are expressed as the percentage of surviving cells after drug treatment (mean \pm SE) and are representative from at least three independent experiments.

2.1.4. G28 Inhibits FASN in EGFRm NSCLC Models

The ability to internalize and inhibit FASN activity of EGCG and G28 after being exogenously added to the media was tested in sensitive and GR models (Figure 4). EGCG and G28 inhibited FASN in PC9 cells, resulting in a similar FASN activity reduction of roughly 80% ($p = 0.265$). Moreover, G28 significantly reduced FASN activity in all GR models in comparison with EGCG (PC9-GR1 $p = 3.000 \times 10^{-5}$; PC9-GR3 $p = 0.001$; PC9-GR4 $p = 0.008$) while the EGCG compound was not able to diminish FASN activity.

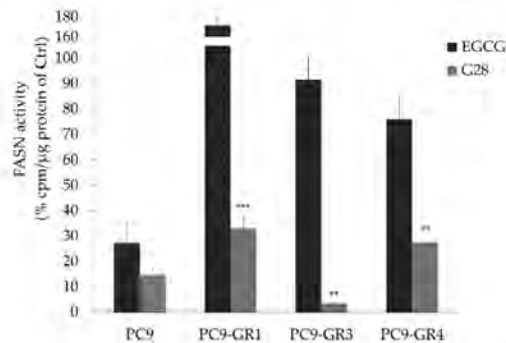


Figure 4. G28 compound inhibits FASN activity in Gefitinib Resistant (GR) models. Cells were treated for 72 h with EGCG or G28 at a concentration equal to their IC_{50} and with DMSO as control. FASN activity was assayed by counting radiolabeled fatty acids synthesized *de novo*. Bars represent the remaining activity as a percentage in treated versus untreated cells (control, Ctrl). Data are mean \pm SE from at least three independent experiments. ** $p < 0.010$, *** $p < 0.001$ indicate levels of statistical significance.

2.1.5. Apoptosis Induction of FASN Inhibitors and EGFR TKIs Treatments

We also investigated whether the cell death caused by treatment with EGFR TKIs or FASN inhibitors was the result of apoptosis induction in both sensitive and GR models. Poly(ADP-ribose) polymerase (PARP) terminal proapoptotic protein activated after cleavage was used as an apoptosis

marker. The effects of all compounds on PARP was determined by Western blot analysis in all models (Figure 5). The uncropped Western blots can be found in Figure S2a.

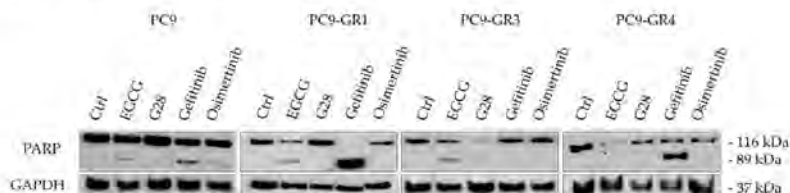


Figure 5. Effects of FASN inhibitors and EGFR TKIs on apoptosis determined by PARP cleavage. Sensitive (PC9) and Gefitinib Resistant (GR) models (PC9-GR1, PC9-GR3, and PC9-GR4) were treated for 72 h with a concentration equivalent to IC_{50} of each drug. Untreated cells were used as an internal control (Ctrl) and GAPDH as a loading control. Results shown are representative from at least three independent experiments.

The cleaved form of PARP (89 kDa) appeared in either sensitive or resistant T790M⁻ models after treatment with the IC_{50} concentration of both EGFR TKIs (gefitinib and osimertinib) and FASN inhibitors (EGCG and G28), indicating the induction of apoptosis. Gefitinib treatment led to PARP cleavage in T790M⁺ GR models. Additionally, EGCG and osimertinib led to the formation of cleaved PARP in PC9-GR1 model.

2.2. G28 Increases EGFR Activation in EGFR^m NSCLC Models

FASN has been previously related to AKT/ERK/EGFR signaling pathways [46] and the inhibition of the transcription factor STAT3 [36] in lung adenocarcinomas. Thus, differences in FASN, EGFR, and STAT3 protein and mRNA expression levels after FASN inhibitors or EGFR TKIs treatment were analyzed through immunoblotting (Figure 6a) and qRT-PCR (Figure 6b) in PC9 and GR models. The uncropped Western blots can be found in Figure S2b.

A reduction of FASN mRNA expression levels was observed in sensitive and GR models treated with FASN inhibitors, being statistically significant in the PC9-GR4 treated with G28 ($p = 0.004$) and PC9 cells treated with G28 ($p = 7.370 \times 10^{-4}$) and gefitinib ($p = 3.210 \times 10^{-4}$). T790M⁺ GR models presented a basal hyperactivation of EGFR that was inhibited after treatment with EGFR TKIs. Regarding FASN inhibitors, EGCG and G28 increased its activation in PC9 cells contrary to the PC9-GR1 model, while no changes were observed in PC9-GR3 and PC9-GR4 models.

EGCG reduced EGFR protein levels in sensitive and T790M⁺ GR models that did not correlate with mRNA expression levels. Contrary, G28 significantly increased EGFR mRNA expression in all models, without protein level modification. No changes in EGFR mRNA levels were observed after gefitinib treatment, however higher protein levels were detected in T790M⁻ GR models. Osimertinib treatment did not lead to EGFR protein nor mRNA expression alteration. EGFR TKIs treatment increased STAT3 activation in all GR models. Gefitinib increased p-STAT3 levels in sensitive cells, while the highest STAT3 activation in GR models was found with osimertinib treatment. No STAT3 protein or mRNA expression differences were found in any of the models and treatments assayed.

Lung carcinomas are highly proliferative and resistance acquisition after EGFR TKI-based therapy is a major problem. Overproduction of palmitic acid by FASN emerges as a resistance mechanism, protecting cells from drug-induced apoptosis [47]. The combination of these drugs with a different mechanism of action may decrease resistance development and improve treatment response.

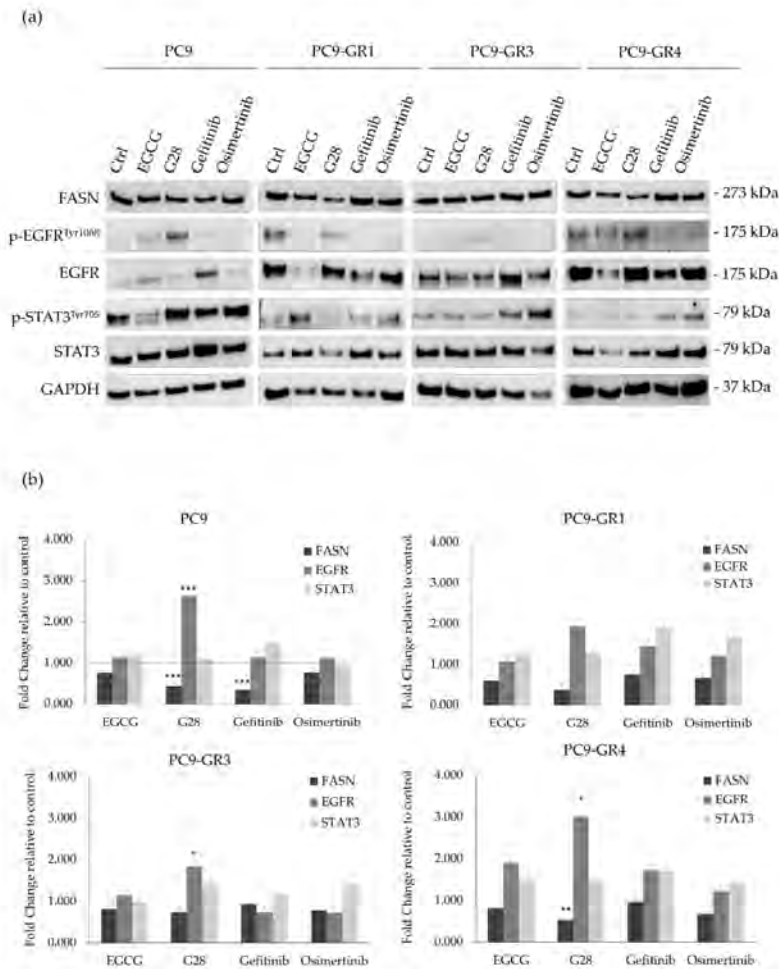


Figure 6. FASN, EGFR, and STAT3 protein and mRNA expression levels after FASN inhibitors (EGCG and G28) and EGFR TKIs (gefitinib and osimertinib) treatment in sensitive (PC9) and Gefitinib Resistant (GR) models (PC9-GR1, PC9-GR3, and PC9-GR4). (a) Western blot analysis of FASN, EGFR, and STAT3 protein expression after 72 h of FASN inhibitors (IC_{50}) and EGFR TKIs (IC_{50}) treatment in EGFR TKI sensitive and GR models. Untreated cells were used as an internal control (Ctrl) and GAPDH as a loading control. Results shown are representative from at least three independent experiments. (b) FASN, EGFR, and STAT3 mRNA levels after treatment with FASN inhibitors and EGFR TKIs in sensitive and GR models. mRNA levels were obtained by qRT-PCR and normalized against the GAPDH gene. All conditions were compared to control (untreated cells), which was normalized to 1 (indicated by the dotted line) and expressed as a fold change. Experiments were performed at least three times. * $p < 0.050$, ** $p < 0.010$, *** $p < 0.001$, indicate levels of statistical significance. 2.3. G28 Combined with EGFR TKIs Outcomes in Synergistic Effects.

Once the effects of FASN inhibitors and EGFR TKIs alone were analyzed in all models, the combinatorial treatment between FASN inhibitors and EGFR TKIs was also studied in order to evaluate the possible synergistic interactions (Figure 7 and Figure S1). Despite the fact that EGCG did not reduce FASN activity in GR models, no IC_{50} differences were found in comparison with sensitive cells. Therefore, GR models were treated with EGCG or G28 in combination with the EGFR TKI to which they were resistant. Three EGFR TKIs concentrations were chosen based on MTT assays (vide supra). The combination of EGCG with either gefitinib or osimertinib resulted in mostly additive effect as shown by the combination index (CI; Figure 7a). The combination of G28 with gefitinib generally led to additivism in T790M+ GR models, with some synergism found in G28 concentrations ranging from 10 to 20 μ M. Remarkably, T790M– GR model treated with G28 combined with gefitinib or osimertinib showed greater synergistic effects (Figure 7b).

2.3. G28 Reduces STAT3 Activation in T790M+ GR Models Alone or in Combination with Gefitinib

In order to discern whether G28 is able to reduce the STAT3 activation produced by EGFR TKIs, a combinatorial analysis was performed (Figure 8). As before, FASN, EGFR, and STAT3 protein and mRNA levels were analyzed using Western blot (Figure 8a) and qRT-PCR (Figure 8b) in GR models treated with synergistic drug concentrations (all of them under the IC_{50} value). The uncropped Western blots can be found in Figure S2c. Therefore, GR models were treated with G28 at 15 μ M in combination with 1 μ M gefitinib, which is the highest clinically achievable plasma concentration [5]. Osimertinib-resistant PC9-GR3 model was co-treated with 15 μ M G28 and 0.5 μ M osimertinib. All concentrations were also used in single-treatment to elucidate the effects produced by the combination.

T790M+ GR models treated with G28 alone and in combination with gefitinib showed both FASN protein and mRNA expression decrease. In the PC9-GR3 model, the FASN protein was slightly diminished in mono- and co-treatments. This decrease is in accordance to FASN mRNA expression, which was significantly reduced in combination with osimertinib. Although G28 alone showed more activated EGFR compared to control in all GR models, the combination of G28 with both EGFR TKIs decreased p-EGFR levels. Regarding the total EGFR, co-treatment resulted in higher protein levels compared to monotreatment in all GR models. However, only T790M+ GR models treated with G28 in combination with gefitinib presented significantly higher EGFR mRNA expression (PC9-GR1 $p = 0.036$ and PC9-GR4 $p = 0.040$). Moreover, G28 both alone and in combination with gefitinib reduced STAT3 activation in T790M+ GR models. No changes in STAT3 activation were seen in PC9-GR3 in any treatment. None of the models analyzed showed alterations in the STAT3 protein or mRNA expression levels.

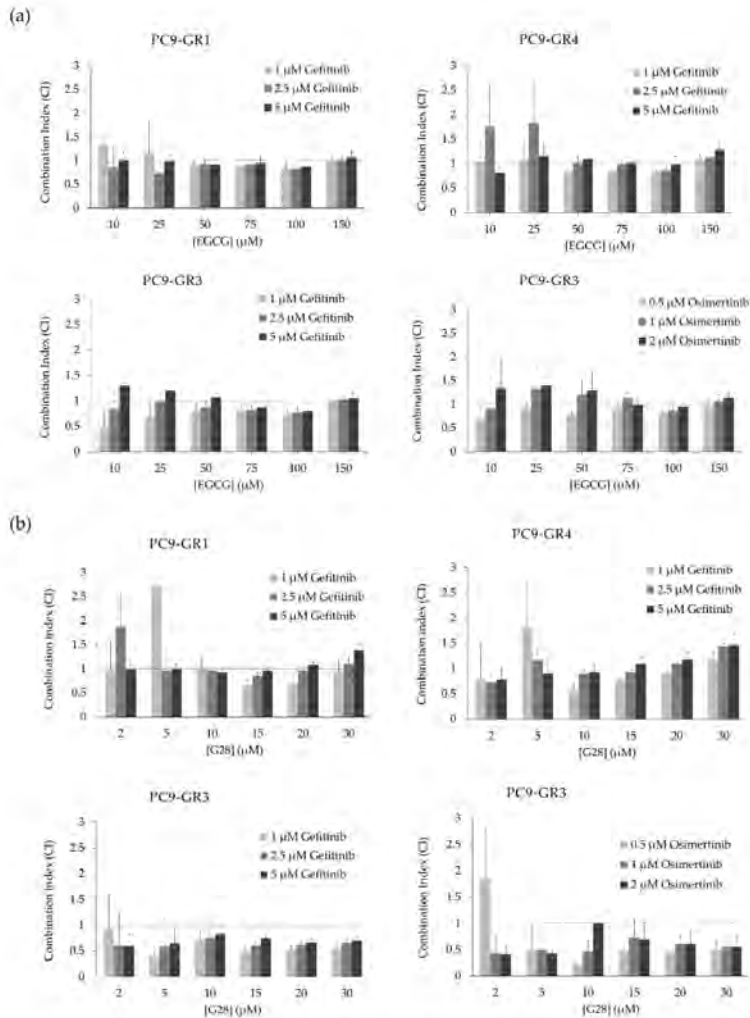


Figure 7. Combination index (CI) of FASN inhibitors (EGCG and G28) and EGFR TKIs (gefitinib and osimertinib) treatment in Gefitinib Resistant (GR) models (PC9-GR1, PC9-GR3, and PC9-GR4). (a) CI of EGCG and gefitinib in PC9-GR1, PC9-GR3, and PC9-GR4 models or osimertinib in PC9-GR3. (b) CI of G28 and gefitinib in PC9-GR1, PC9-GR3, and PC9-GR4 models or osimertinib in PC9-GR3. PC9-GR1, PC9-GR3, and PC9-GR4 models were treated with EGCG (10–150 μM) or G28 (2–30 μM) in combination with gefitinib (1, 2.5, and 5 μM) for 72 h. PC9-GR3 cells were also treated with EGCG (10–150 μM) or G28 (2–30 μM) in combination with osimertinib (0.5, 1, and 2 μM) for 72 h. Results were determined using the MTT assay and are expressed as the CI based on the Chou and Talalay method [48]. The dotted line indicates additivity (CI approximately equal to 1). CI > 1 designates antagonistic effects and CI < 1 synergistic effects. Experiments were performed at least three times. Results shown are mean \pm SE.

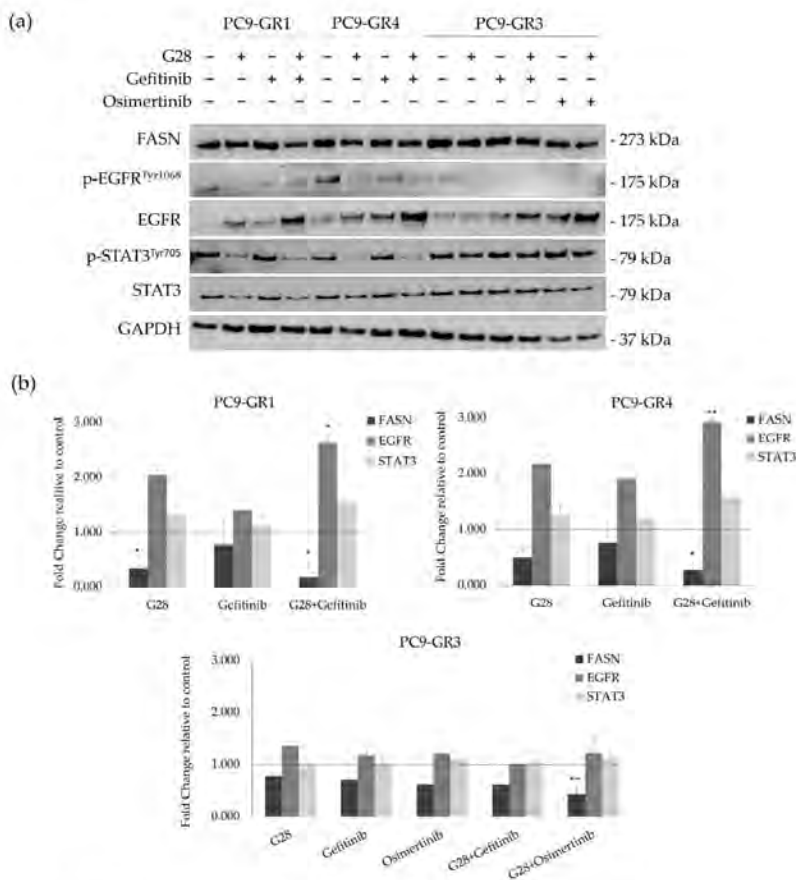


Figure 8. FASN, EGFR, and STAT3 protein and mRNA expression in sensitive (PC9) and Gefitinib Resistant (GR) models (PC9-GR1, PC9-GR3, and PC9-GR4) treated with FASN inhibitors (EGCG and G28) in combination with EGFR TKIs (gefitinib and osimertinib). (a) Western blot analysis of FASN, EGFR, and STAT3 in PC9-GR1, PC9-GR3, and PC9-GR4 models treated with G28 alone and in combination with gefitinib, and PC9-GR3 treated with G28 and osimertinib for 72 h. Results shown are representative from three independent experiments. Untreated cells are used as internal control (Ctrl) and GAPDH as a loading control. (b) FASN, EGFR, and STAT3 mRNA levels analysis in PC9-GR1, PC9-GR3, and PC9-GR4 models treated with G28 in combination with gefitinib, PC9-GR3 model treated with the combination G28 and osimertinib for 72 h. mRNA levels were obtained by qRT-PCR and normalized against the GAPDH gene. All conditions were compared to the control (untreated cells), which was normalized to 1 (indicated by the dotted line) and expressed as a fold change. Experiments were performed at least three times. * $p < 0.050$, ** $p < 0.010$, *** $p < 0.001$ indicate levels of statistical significance.

3. Discussion

Despite significant advances in EGFRm NSCLC treatment, current therapy is still ineffective to many patients due to the late stage of diagnosis and acquisition of resistance to EGFR TKIs [2,6]. Hence, several efforts have been made on the identification of EGFR TKIs resistance mechanisms to develop an effective treatment for these patients. Some authors pointed out the important role of FASN in drug resistance due to its capacity to allow fast synthesis of new phospholipids for membrane remodeling and plasticity [49,50]. Although the relationship between EGFR and FASN remains unclear, it has recently been described that EGFR upregulates FASN in TKI-resistant EGFRm NSCLC [41]. In addition, FASN inhibition showed cytotoxic effects in lung cancer [40] and resensitized cells to chemotherapy, anti-EGFR and anti-HER2 therapies in breast cancer [38,51]. Therefore, the FASN enzyme may become a promising target for anticancer therapy in EGFRm NSCLC.

Here we studied the effects of natural polyphenolic compound EGCG and its derivative G28 to overcome EGFR TKI resistance in sensitive and GR models. The higher FASN protein levels observed in EGFR TKI resistant models (Figure 1) demonstrated its potential involvement in EGFR TKI resistance acquisition. FASN inhibitors showed similar cytotoxic effects between sensitive and resistant models with IC_{50} values ranging from 75 to 90 μ M for EGCG and from 12 to 18 μ M for G28 (Figure 3). As determined by K. Jacobsen and coworkers, PC9-GR1 is a T790M+ GR model that also presents MET and EphA2 activation, the PC9-GR3 model exhibits AXL overexpression, and the T790M+ PC9-GR4 model shows EphA2 activation and AXL overexpression [45]. In correlation with this, the higher G28 IC_{50} found in PC9-GR3 model and the significantly similar IC_{50} values in the two T790M+ GR models indicate that none of the known resistance mechanisms described are related to FASN inhibition.

Both compounds have the ability to internalize and inhibit FASN activity as observed in parental PC9 cells (Figure 4), however G28 was of average 5.5 times more effective than EGCG. We have previously shown the ability of the natural compound EGCG to inhibit FASN activity in wild type EGFR NSCLC cells and different breast cancer subtypes [40,43]. Despite their cytotoxicity, only the synthetic compound significantly reduced FASN activity in GR models (Figure 4). Other studies proved the ability of G28 to inhibit FASN activity in triple-negative breast cancer (TNBC) cells [43]. Nevertheless, our study demonstrated that EGCG anticancer activity was independent of FASN inhibition in GR models. It has been extensively described that EGCG has multiple targets and it is involved in multiple signaling pathways and transcription factors, membrane-associated receptors tyrosine kinase (RTKs), or DNA methylation [33]. Some authors exposed that the mechanism underlying EGCG antitumor potency is due to the suppression of the EGFR signaling pathway in NSCLC [52]. Others observed a very stable complex between EGCG and EGFRm (exon 19 ELREA deletion) that was lost with the T790M substitution [53]. Kozue and coworkers showed that EGCG reduced stemness and immunogenicity in EGFR wild type NSCLC cells in vitro and in vivo through the inhibition of AXL [54]. AXL is a tyrosine kinase receptor that has been related to drug resistance and the induction of malignant properties [55] and is overexpressed in GR models [45].

The apoptosis induction was verified by PARP cleavage for all treatments in sensitive and T790M- GR models (Figure 5). However, no PARP cleavage was observed through Western blot analysis in T790M+ GR models after G28 treatment. These results suggest that G28 might cause an apoptosis-independent proliferation reduction in T790M+ GR models as found by others in NSCLC wild-type EGFR models treated with the natural plant polyphenol resveratrol (3,5,40-trihydroxystilben) [56]. The anticancer activity of polyphenols has been shown to be mediated by numerous mechanisms including cell cycle arrest. EGCG, among other natural compounds, showed down-regulation of cyclin-dependent kinases (CDK) and modulation in CDK inhibitors in different human carcinomas [33,57]. The lack of PARP cleavage in some of the treatments and models could be due to the activation of other programmed cell death mechanisms such as autophagy [58].

Alteration in EGFR expression was observed after treatment with FASN inhibitors. EGCG produced a decrease in EGFR protein levels in T790M+ GR models, which is in agreement with Ali et al., who observed an EGFR decrease in sensitive and resistant PC9 cells treated with Orlistat,

a FDA-approved FASN inhibitor for obesity management [41]. The synthetic G28 compound increased EGFR mRNA levels in all models, indicating that EGFR overexpression could be an alternative pathway to FASN inhibition. The EGFR activation after FASN gene overexpression in epithelial breast cells has been previously shown [42]. Furthermore, our results suggest that the EGFR pathway could be implicated in FASN regulation at a transcriptional or translational level as exposed before [40]. Despite all models increased EGFR mRNA expression after G28 treatment, only PC9 cells seemed to compensate the effect of G28 by increasing EGFR activation. Therefore, cell proliferation reduction found in all models after FASN inhibition (Figure 3) could be due to the lack of post-translational palmitoylation substrate [41].

It seems increasingly clear that persistent STAT3 activation is related to EGFR-based therapies resistance [13]. STAT3 is under the control of different cytokines and growth factors playing an important role in metastasis, proliferation, survival, invasion, migration, and angiogenesis [14–16]. Natural polyphenols, normally multitarget inhibitors, are now emerging as promising STAT3 inhibitors or its upstream signaling molecules Src, gp130, or NF κ B [18]. Among them, EGCG has been reported to reduce STAT3 phosphorylation in head and neck carcinomas [59] and pancreatic cancer [60]. Based on the above, we hypothesized that EGCG and its derivative G28 would diminish the STAT3 activation produced by EGFR TKIs in NSCLC cells. Both compounds reduced p-STAT3 levels in a dose-dependent manner when used alone in comparison to control samples. In agreement with previous studies, STAT3 was activated by EGFR TKIs (Figure 6) [22].

Combinatorial treatments of EGCG and G28 with EGFR TKIs were performed in order to study their effects on GR models (Figure S1). The combination of gefitinib and osimertinib with EGCG showed additivity whereas synergistic effects were identified in combination with G28 (Figure 7). Other authors have previously reported synergistic outcomes after co-treatment with a STAT3 inhibitor (TPCA-1) and EGFR TKI in EGFRm NSCLC models [61]. Previous results from our group demonstrated that G28 compound had a synergistic interaction with pertuzumab and tamsirolium in HER2+ breast cancer cells [38] and EGCG with cetuximab in TNBC [51]. Interestingly, G28 in combination with gefitinib decreased the activation of STAT3 to the same extent as when used alone in T790M+ GR models. Thus, other mechanisms must be involved in the synergistic effects found. On the other hand, no differences in p-STAT3 were observed in PC9-GR3. This could be, in part, due to the multiple pathways that can be altered in the acquisition of gefitinib and osimertinib double-resistance in PC9-GR3 model such as mutations in EGFR/STAT3 or other related up- or downstream signaling molecules, leading to the constitutive activation of STAT3. The analysis of the main genes regulated by the STAT3 transcription factor could provide relevant information to identify some pathways alterations after FASN inhibitors treatment. The synergistic effects found in GR models co-treated with FASN inhibitor G28 and EGFR TKIs supports the idea that EGFR palmitoylation mediated by FASN leads to TKI resistance acquisition in EGFRm NSCLC [41]. However, the specific G28 mechanism of action and possible targets are still unknown and further studies are needed. Wu et al. suggested that FASN inhibition may cause an imbalance in the membrane lipids levels, which may produce a membrane localization decrease of IGF-1R, and the inactivation of the downstream STAT3 signaling pathway [36]. Furthermore, the IGF-1R is a transmembrane tyrosine kinase linked to MAPK and PI3K/AKT pathways, shared with EGFR, which could explain the effects found only in T790M+ GR models [62].

Taken together, our observations suggest that FASN has a key role in acquired TKI-resistant EGFRm NSCLC. The inhibition of this enzyme resensitizes cells to EGFR TKIs treatments. These results encourage for further studies to analyze the combinatorial treatment of FASN inhibitors and EGFR TKIs to overcome the EGFR TKI resistance in NSCLC.

4. Materials and Methods

4.1. Cell Lines and Culture Conditions

Human adenocarcinoma PC9 cells and its gefitinib resistant derivatives PC9-GR1, PC9-GR3, and PC9-GR4 models [45] were kindly provided by Dr. R. Rosell and Dr. M. A. Molina (Barcelona, Spain). All cells were routinely grown in RPMI-1640 medium (Lonza, Basel, Switzerland), supplemented with 10% fetal bovine serum (FBS; HyClone Laboratories, GE Healthcare, Chicago, IL, USA), 50 U/mL penicillin, and 50 µg/mL streptomycin (Lonza). In all cases, the cells were used immediately after resuscitation and were maintained at 37 °C in a humidified atmosphere with 5% CO₂, propagated following established protocols, remaining free of mycoplasma throughout the experiments.

4.2. Cell Proliferation Assays

To investigate the effect of EGFR TKIs or FASN inhibitors cells were seeded into 96-well plates at the appropriate density in their growth medium. Gefitinib and osimertinib were kindly provided by AstraZeneca. EGCG was purchased from Sigma (USA) and G28 was synthesized as described elsewhere [43]. For monotreatment assays, after 24 h cells were treated with different concentrations of each drug for 72 h. Cell viability was determined by the 3-(4,5-dimethyl-2-thiazolyl)-2,5-diphenyl-tetrazolium bromide (MTT) assay (Sigma) as described elsewhere [43]. For drug combination experiments, cells were treated with three fixed concentrations of gefitinib (1, 2.5, and 5 µM) or osimertinib (0.5, 1, and 2 µM) in combination of a series of increasing concentrations of EGCG or G28 for 72 h. Following treatment, cell proliferation was measured using the standard colorimetric MTT assay. Using the multi-well plate reader Benchmark Plus (Bio-Rad Laboratories, Inc., CA, USA), absorbance was determined at 570 nm. Combinatorial effects were evaluated using the combination index (CI) based on the Chou and Talalay method [48] using the CompuSyn™ software (Biosoft, MO, USA). CompuSyn™ calculates the CI values; if the value equals 1 the effect is considered additive, if above 1 antagonistic and below 1 synergistic. Data presented are from three separate wells per assay, and the assay was performed at least three times.

4.3. Western Blot Analysis of Cell Lysates

Gefitinib-sensitive and -resistant models were treated with EGFR TKI, FASN inhibitor, or the combination of both drugs for 72 h. Afterwards, attached and floating cells were harvested and lysed in ice-cold lysis buffer (Cell Signaling Technology Inc., MA, USA) containing 100 µg/mL phenylmethylsulfonyl fluoride (PMSF; Sigma) by vortexing every 5 min for 30 min. Protein concentration was determined by the Lowry method (DC Protein Assay, Bio-Rad Laboratories, Inc.). Equal amounts of protein were heated in lithium dodecyl sulfate (LDS) sample buffer with a sample reducing agent (Invitrogen, CA, USA) for 10 min at 70 °C, separated by SDS-PAGE and transferred to nitrocellulose membranes (ThermoFisher Scientific Inc., MA, USA). Membranes were incubated for 1 h at room temperature in blocking buffer (5% skim milk powder in Tris-buffered saline (TBS)) 0.05% Tween (TBS-T) and overnight at 4 °C with the following primary antibodies diluted in blocking buffer: FASN (Cell Signaling Technology Inc.; #3180), p-STAT3^{Tyr705} (Cell Signaling Technology Inc.; #9131), p-EGFR^{Tyr1068} (Cell Signaling Technology Inc.; #2234), PARP (Cell Signaling Technology Inc.; #9542), EGFR (Cell Signaling Technology Inc.; #2232), STAT3 (Cell Signaling Technology Inc.; #4904), and GAPDH (Proteintech, Manchester, UK; #60004-1-IG). Specific horseradish peroxidase (HRP)-conjugated secondary antibodies were incubated for 1 h at room temperature. The immune complexes were detected using chemiluminescent HRP substrate Clarity™ Western ECL Substrate (Bio-Rad Laboratories, Inc.) or West Femto Maximum Sensitivity Substrate (ThermoFisher Scientific Inc.) in a Bio-Rad ChemiDoc™ MP Imaging System (Bio-Rad Laboratories, Inc.). Western blot analyses were repeated at least three times and representative results are shown.

4.4. Quantitative Real-Time PCR (qRT-PCR) Analysis

Cells were treated with EGFR TKIs or FASN inhibitors as a single agent or in combination for 72 h. Then, cells were PBS washed and resuspended in 1 mL of Qiazol (Qiagen, Hilden, Germany). GeneJET RNA Purification Kit (ThermoFisher Scientific Inc.) was used to isolate total RNA following the manufacturer's instructions. RNA samples were quantified using a Nano-Drop 2000 Spectrophotometer (ThermoFisher Scientific). Total RNA was reverse-transcribed into complementary DNA (cDNA) using a High Capacity cDNA Archive Kit (Applied Biosystems, CA, USA). Different gene expression levels were determined using QuantStudio3 Real-time PCR System (ThermoFisher Scientific Inc.) with qPCR BIO SyGreen Mix Lo-Rox real-time PCR (PCR Biosystems Inc., PA, USA), following manufacture instructions. Primers used are shown in Table 1. qRT-PCR analyses were performed at least four times and each gene was run in triplicate. Gene expression levels were quantified using the standard formula $2^{-\Delta\Delta CT}$ and normalized to the housekeeping GAPDH ($2^{-\Delta CT}$).

Table 1. Primer design.

FASN	Forward	CAGGCACACACCGATGGAC
	Reverse	CGGAGTGAATCTGGGTTGAT
STAT3	Forward	CACCTTCAGGATGTCCGGAA
	Reverse	ATCCTGGAGATTCTCTACCACCTTCA
EGFR7	Forward	CATGTCCGATGGACTTCCAGA
	Reverse	GGGACAGCTTGGATCACACT
GAPDH	Forward	TCTTCCAGGAGCGAGATC
	Reverse	CAGAGATGATGACCCITTTG

4.5. Inhibition of Fatty Acid Synthase Activity

Cells were seeded in 24-well plates at a density of 3×10^4 cells/well in RPMI supplemented with 10% fetal bovine serum (FBS). 24 h later, the maintenance medium was replaced by the treatment medium (RPMI-1640 supplemented with 1% lipoprotein-deficient FBS (Sigma-Aldrich)) along with the assayed compounds or vehicle (dimethyl sulfoxide, DMSO, Sigma-Aldrich). Cells were treated with a concentration corresponding to the previously determined IC_{50} for 72 h. For the last 6 h (1,2-14C) acetic acid sodium salt (53.9 mCi/mmol, Perkin Elmer Biosciences, Waltham, MA, USA) was added to the medium (0.5 μ Ci/mL). The lipid extraction was performed as previously described [43]. Cells were washed twice with phosphate-buffered saline (PBS, HyClone Laboratories, Logan, UT, USA) and once with MeOH/PBS (2:3). Cell pellets were resuspended in 0.2 M NaCl and lysed with freeze (liquid N_2)—thaw (37 °C) cycles. Then, lipids were extracted with $CHCl_3$ /MeOH (2:1) and 0.1 M KOH. The organic phase was washed with $CHCl_3$ /MeOH/ H_2O (3:48:47) and the solvents were evaporated under vacuum conditions. Finally, pellets were resuspended in EtOH and counted by scintillation. The total protein content was quantified by the Bradford assay (Sigma-Aldrich).

4.6. Statistical Analysis

Parametric data were analyzed by the Student's *t* test when comparing two groups or the one-way analysis of variance (ANOVA) followed by Bonferroni or Tamhane's T2 post hoc test for multiple comparisons. The non-parametric data were analyzed with the Mann–Whitney U tests for non-normally independent variables; otherwise, the Kruskal–Wallis test was used for more than two groups. All data are expressed as mean \pm SE. Levels of significance were set at $p < 0.050$ and are represented by asterisks, as follows: $p < 0.050$ (denoted as *), $p < 0.010$ (denoted as **), and $p < 0.001$ (denoted as ***). The statistical analysis was performed using the IBM SPSS software (Version 21.0; SPSS Inc., IL, USA).

5. Conclusions

The need to find more effective and less toxic therapeutic treatments for EGFRm NSCLC patients is one of the major challenges in lung cancer research. Natural compounds are emerging as potential anticancer candidates for their safety and multitarget intrinsic features. Improvement of the properties of natural compounds through the design of synthetic derivatives is aimed at maintaining these features while increasing, efficacy, bioavailability, and stability in physiological conditions.

Here we show additive and synergistic effects of the polyphenolic plant-derived EGCG compound and its derivative G28, respectively, in combination with EGFR TKIs in GR models. Despite the exact mechanism by which these compounds are cytotoxic is still unknown, our results shed light on their ability to modulate FASN/EGFR/STAT3 pathways. The capacity to affect multiple pathways might prove useful in overcoming other drug resistances. Further analyses are required to completely understand the mechanism of action.

Taken together, this paper supports the inhibition of the metabolic enzyme FASN by G28 compound in combination with EGFR TKIs as a new potential strategy for resistant EGFRm NSCLC.

Supplementary Materials: The following are available online at <http://www.mdpi.com/2072-6694/12/5/1283/s1>, Figure S1: Proliferative curves of FASN inhibitors (EGCG and G28) alone and in combination with EGFR TKIs (gefitinib and osimertinib) in EGFR TKIs resistant models, Figure S2. Whole Western blot figures showing PARP, FASN, EGFR, STAT3 and GAPDH protein bands with molecular weight markers (merge of colorimetric and chemiluminescence). (a) Western blot images from Figure 5. (b) Western blot images from Figure 6. (c) Western blot images from Figure 8.

Author Contributions: Conceptualization, T.P. and S.R.-M.; methodology, E.P.-A., S.P., S.R.-M., J.R., D.T.-O., M.P., L.F.; validation, E.P.-A., S.P., S.R.-M.; resources, T.P., and J.C.; writing—original draft preparation, E.P.-A., S.P., S.R.-M.; writing—review and editing, E.P.-A., S.P., S.R.-M., T.P. and J.C.; supervision, T.P. and S.R.-M.; funding acquisition, T.P. and J.C. All authors have read and agreed to the published version of the manuscript.

Funding: The authors acknowledge the financial support from AstraZeneca, the E. P.-A pre-doctoral grant (2019FL_B01011), and the support of the Catalan Government (2017SGR00385).

Acknowledgments: Authors thank R. Rosell and M. A. Molina from laboratory of Oncology Pangea (Barcelona, Spain) for kindly provided PC9 models and AstraZeneca (London, UK) for supplying gefitinib and osimertinib.

Conflicts of Interest: The authors declare no conflict of interest. The funders had no role in the design of the study; in the collection, analyses, or interpretation of data; in the writing of the manuscript, or in the decision to publish the results.

References

1. Testa, U.; Castelli, G.; Pelosi, E. Lung Cancers: Molecular Characterization, Clonal Heterogeneity and Evolution, and Cancer Stem Cells. *Cancers* **2018**, *10*. [[CrossRef](#)] [[PubMed](#)]
2. Sun, W.; Song, L.; Ai, T.; Zhang, Y.; Gao, Y.; Cui, J. Prognostic value of MET, cyclin D1 and MET gene copy number in non-small cell lung cancer. *J. Biomed. Res.* **2013**, *27*, 220. [[CrossRef](#)] [[PubMed](#)]
3. Choo, J.R.E.; Tan, C.S.; Soo, R.A. Treatment of EGFR T790M-Positive Non-Small Cell Lung Cancer. *Target. Oncol.* **2018**, *13*, 141–156. [[CrossRef](#)] [[PubMed](#)]
4. Lynch, T.J.; Bell, D.W.; Sordella, R.; Gurubhagavatula, S.; Okimoto, R.A.; Brannigan, B.W.; Harris, P.L.; Haserlat, S.M.; Supko, J.G.; Haluska, R.G.; et al. Activating Mutations in the Epidermal Growth Factor Receptor Underlying Responsiveness of Non-Small-Cell Lung Cancer to Gefitinib. *N. Engl. J. Med.* **2004**, *350*, 2129–2139. [[CrossRef](#)] [[PubMed](#)]
5. Cohen, M.H.; Williams, G.A.; Sridhara, R.; Chen, G.; McGuinn, W.D.; Morse, D.; Abraham, S.; Rahman, A.; Liang, C.; Lostritto, R.; et al. United States Food and Drug Administration Drug Approval summary: Gefitinib (ZD1839; Iressa) tablets. *Clin. Cancer Res.* **2004**, *10*, 1212–1218. [[CrossRef](#)]
6. Barnes, T.A.; O’Kane, G.M.; Vincent, M.D.; Leigh, N.B. Third-Generation Tyrosine Kinase Inhibitors Targeting Epidermal Growth Factor Receptor Mutations in Non-Small Cell Lung Cancer. *Front. Oncol.* **2017**, *7*, 113. [[CrossRef](#)]
7. Bean, J.; Brennan, C.; Shih, J.-Y.; Riely, G.; Viale, A.; Wang, L.; Chitale, D.; Motoi, N.; Szoke, J.; Broderick, S.; et al. MET amplification occurs with or without T790M mutations in EGFR mutant lung tumors with acquired resistance to gefitinib or erlotinib. *Proc. Natl. Acad. Sci. USA* **2007**, *104*, 20932–20937. [[CrossRef](#)]

8. Marks, J.L.; Gong, Y.; Chitale, D.; Golas, B.; McLellan, M.D.; Kasai, Y.; Ding, L.; Mardis, E.R.; Wilson, R.K.; Solit, D.; et al. Novel MEK1 mutation identified by mutational analysis of epidermal growth factor receptor signaling pathway genes in lung adenocarcinoma. *Cancer Res.* **2008**, *68*, 5524–5528. [[CrossRef](#)]
9. Shien, K.; Toyooka, S.; Yamamoto, H.; Soh, J.; Jida, M.; Thu, K.L.; Hashida, S.; Maki, Y.; Ichihara, E.; Asano, H.; et al. Acquired Resistance to EGFR Inhibitors Is Associated with a Manifestation of Stem cell-like Properties in Cancer Cells. *Cancer Res.* **2013**, *73*, 3051. [[CrossRef](#)]
10. Byers, L.A.; Diao, L.; Wang, J.; Saintigny, P.; Girard, L.; Peyton, M.; Shen, L.; Fan, Y.; Giri, U.; Tumula, P.K.; et al. An Epithelial-Mesenchymal Transition Gene Signature Predicts Resistance to EGFR and PI3K Inhibitors and Identifies Axl as a Therapeutic Target for Overcoming EGFR Inhibitor Resistance. *Clin. Cancer Res.* **2013**, *19*, 279–290. [[CrossRef](#)]
11. Takezawa, K.; Pirazzoli, V.; Arcila, M.E.; Nebhan, C.A.; Song, X.; de Stanchina, E.; Ohashi, K.; Janjigian, Y.Y.; Spitzler, P.J.; Melnick, M.A.; et al. HER2 amplification: A potential mechanism of acquired resistance to EGFR inhibition in EGFR-mutant lung cancers that lack the second-site EGFR T790M mutation. *Cancer Discov.* **2012**, *2*, 922–933. [[CrossRef](#)] [[PubMed](#)]
12. Ohashi, K.; Sequist, L.V.; Arcila, M.E.; Moran, T.; Chmielecki, J.; Lin, Y.-L.; Pan, Y.; Wang, L.; de Stanchina, E.; Shien, K.; et al. Lung cancers with acquired resistance to EGFR inhibitors occasionally harbor BRAF gene mutations but lack mutations in KRAS, NRAS, or MEK1. *Proc. Natl. Acad. Sci. USA* **2012**, *109*, E2127–E2133. [[CrossRef](#)] [[PubMed](#)]
13. Zulkifli, A.A.; Tan, F.H.; Putoczki, T.L.; Stylli, S.S.; Luwor, R.B. STAT3 signaling mediates tumour resistance to EGFR targeted therapeutics. *Mol. Cell. Endocrinol.* **2017**, *451*, 15–23. [[CrossRef](#)] [[PubMed](#)]
14. Germain, D.; Frank, D.A. Targeting the Cytoplasmic and Nuclear Functions of Signal Transducers and Activators of Transcription 3 for Cancer Therapy. *Clin. Cancer Res.* **2007**, *13*, 5665–5669. [[CrossRef](#)]
15. Frank, D.A. STAT3 as a central mediator of neoplastic cellular transformation. *Cancer Lett.* **2007**, *251*, 199–210. [[CrossRef](#)]
16. Aggarwal, B.B.; Kunnumakkara, A.B.; Harikumar, K.B.; Gupta, S.R.; Tharakan, S.T.; Koca, C.; Dey, S.; Sung, B. Signal transducer and activator of transcription-3, inflammation, and cancer: How intimate is the relationship? *Am. N. Y. Acad. Sci.* **2009**, *1171*, 59–76. [[CrossRef](#)]
17. Rosell, R.; Karachaliou, N. Large-scale screening for somatic mutations in lung cancer. *Lancet* **2016**, *387*, 1354–1356. [[CrossRef](#)]
18. Levy, D.E.; Darnell, J.E. Stats: Transcriptional control and biological impact. *Nat. Rev. Mol. Cell Biol.* **2002**, *3*, 651–662. [[CrossRef](#)]
19. Yu, Y.; Zhao, Q.; Wang, Z.; Liu, X.Y. Activated STAT3 correlates with prognosis of non-small cell lung cancer and indicates new anticancer strategies. *Cancer Chemother. Pharmacol.* **2015**, *75*, 917–922. [[CrossRef](#)]
20. Xu, Y.H.; Lu, S. A meta-analysis of STAT3 and phospho-STAT3 expression and survival of patients with non-small-cell lung cancer. *Eur. J. Surg. Oncol.* **2014**, *40*, 311–317. [[CrossRef](#)]
21. Lee, H.J.; Zhuang, G.; Cao, Y.; Du, P.; Kim, H.J.; Settleman, J. Drug resistance via feedback activation of stat3 in oncogene-addicted cancer cells. *Cancer Cell* **2014**, *26*, 207–221. [[CrossRef](#)]
22. Ninomiya, T.; Takigawa, N.; Ichihara, E.; Ochi, N.; Murakami, T.; Honda, Y.; Kubo, T.; Minami, D.; Kudo, K.; Tanimoto, M.; et al. Afatinib Prolongs Survival Compared with Gefitinib in an Epidermal Growth Factor Receptor-Driven Lung Cancer Model. *Mol. Cancer Ther.* **2013**, *12*, 589–597. [[CrossRef](#)] [[PubMed](#)]
23. Chaib, I.; Karachaliou, N.; Pilotto, S.; Servat, J.C.; Cai, X.; Li, X.; Drozdowskyj, A.; Servat, C.C.; Yang, J.; Hu, C.; et al. Co-activation of STAT3 and YES-Associated Protein 1 (YAP1) Pathway in EGFR-Mutant NSCLC. *J. Natl. Cancer Inst.* **2017**, *109*, 1–12. [[CrossRef](#)] [[PubMed](#)]
24. Hanahan, D.; Weinberg, R.A. Hallmarks of cancer: The next generation. *Cell* **2011**, *144*, 646–674. [[CrossRef](#)] [[PubMed](#)]
25. Jayakumar, A.; Tai, M.H.; Huang, W.Y.; al-Feel, W.; Hsu, M.; Abu-Elheiga, L.; Chirala, S.S.; Wakil, S.J. Human fatty acid synthase: Properties and molecular cloning. *Proc. Natl. Acad. Sci. USA* **1995**, *92*, 8695–8699. [[CrossRef](#)] [[PubMed](#)]
26. Kuhajda, F.P. Fatty acid synthase and cancer: New application of an old pathway. *Cancer Res.* **2006**, *66*, 5977–5980. [[CrossRef](#)] [[PubMed](#)]
27. Liu, H.; Liu, J.-Y.; Wu, X.; Zhang, J.-T. Biochemistry, molecular biology, and pharmacology of fatty acid synthase, an emerging therapeutic target and diagnosis/prognosis marker. *Int. J. Biochem. Mol. Biol.* **2010**, *1*, 69–89.

28. Puig, T.; Vázquez-Martin, A.; Relat, J.; Pétriz, J.; Menéndez, J.A.; Porta, R.; Casals, G.; Marrero, P.F.; Haro, D.; Brunet, J.; et al. Fatty acid metabolism in breast cancer cells: Differential inhibitory effects of epigallocatechin gallate (EGCG) and C75. *Breast Cancer Res. Treat.* **2008**, *109*, 471–479. [CrossRef]
29. Jiang, B.; Li, E.-H.; Lu, Y.-Y.; Jiang, Q.; Cui, D.; Jing, Y.-F.; Xia, S.-J. Inhibition of Fatty-acid Synthase Suppresses P-AKT and Induces Apoptosis in Bladder Cancer. *Urology* **2012**, *80*, 484.e9–484.e15. [CrossRef]
30. Yang, Y.; Liu, H.; Li, Z.; Zhao, Z.; Yip-Schneider, M.; Fan, Q.; Schmidt, C.M.; Chiorean, E.G.; Xie, J.; Cheng, L.; et al. Role of fatty acid synthase in gemcitabine and radiation resistance of pancreatic cancers. *Int. J. Biochem. Mol. Biol.* **2011**, *2*, 89–98.
31. Zhan, N.; Li, B.; Xu, X.; Xu, J.; Hu, S. Inhibition of FASN expression enhances radiosensitivity in human non-small cell lung cancer. *Oncol. Lett.* **2018**, *15*, 4578–4584. [CrossRef] [PubMed]
32. Flavin, R.; Peluso, S.; Nguyen, P.L.; Loda, M. Fatty acid synthase as a potential therapeutic target in cancer. *Futur. Oncol.* **2010**, *6*, 551–562. [CrossRef] [PubMed]
33. Colomer, R.; Sarrats, A.; Lupu, R.; Puig, T. Natural Polyphenols and their Synthetic Analogs as Emerging Anticancer Agents. *Curr. Drug Targets* **2016**, *18*, 147–159. [CrossRef] [PubMed]
34. Chakrawarti, L.; Agrawal, R.; Dang, S.; Gupta, S.; Gabrani, R. Therapeutic effects of EGCG: A patent review. *Expert Opin. Ther. Pat.* **2016**, *26*, 907–916. [CrossRef]
35. Wang, X.; Tian, W. Green Tea Epigallocatechin Gallate: A Natural Inhibitor of Fatty-Acid Synthase. *Biochem. Biophys. Res. Commun.* **2001**, *288*, 1200–1206. [CrossRef]
36. Wu, J.; Du, J.; Fu, X.; Liu, B.; Cao, H.; Li, T.; Su, T.; Xu, J.; Tse, A.K.-W.; Yu, Z.-L. Icaritin, a novel FASN inhibitor, exerts anti-melanoma activities through IGF-1R/STAT3 signaling. *Oncotarget* **2016**, *7*, 51251–51269. [CrossRef]
37. Ou, Y.-C.; Li, J.-R.; Kuan, Y.-H.; Raung, S.-L.; Wang, C.-C.; Hung, Y.-Y.; Pan, P.-H.; Lu, H.-C.; Chen, C.-J. Luteolin sensitizes human 786-O renal cell carcinoma cells to TRAIL-induced apoptosis. *Life Sci.* **2014**, *100*, 110–117. [CrossRef]
38. Blancafort, A.; Giró-Perafita, A.; Oliveras, G.; Palomeras, S.; Turrado, C.; Campuzano, Ó.; Carrión-Salip, D.; Massagué, A.; Brugada, R.; Palafox, M.; et al. Dual fatty acid synthase and HER2 signaling blockade shows marked antitumor activity against breast cancer models resistant to anti-HER2 drugs. *PLoS ONE* **2015**, *10*, e0131241. [CrossRef]
39. Giró-Perafita, A.; Rabionet, M.; Puig, T.; Ciurana, J. Optimization of Poly(ϵ -caprolactone) Scaffolds Suitable for 3D Cancer Cell Culture. *Procedia CIRP* **2016**, *49*, 61–66. [CrossRef]
40. Relat, J.; Blancafort, A.; Oliveras, G.; Cufi, S.; Haro, D.; Marrero, P.F.; Puig, T. Different fatty acid metabolism effects of (-)-epigallocatechin-3-gallate and C75 in adenocarcinoma lung cancer. *BMC Cancer* **2012**, *12*, 280. [CrossRef]
41. Ali, A.; Levantini, E.; Teo, J.T.; Goggi, J.; Clohessy, J.G.; Wu, C.S.; Chen, L.; Yang, H.; Krishnan, I.; Kocher, O.; et al. Fatty acid synthase mediates EGFR palmitoylation in EGFR mutated non-small cell lung cancer. *EMBO Mol. Med.* **2018**, *10*. [CrossRef] [PubMed]
42. Vázquez-Martin, A.; Colomer, R.; Brunet, J.; Lupu, R.; Menéndez, J.A. Overexpression of fatty acid synthase gene activates HER1/HER2 tyrosine kinase receptors in human breast epithelial cells. *Cell Prolif.* **2008**, *41*, 59–85. [CrossRef] [PubMed]
43. Crous-Masó, J.; Palomeras, S.; Relat, J.; Camó, C.; Martínez-Garza, Ú.; Planas, M.; Feliu, L.; Puig, T. (-)-Epigallocatechin 3-gallate synthetic analogues inhibit fatty acid synthase and show anticancer activity in triple negative breast cancer. *Molecules* **2018**, *23*. [CrossRef]
44. Giró-Perafita, A.; Rabionet, M.; Planas, M.; Feliu, L.; Ciurana, J.; Ruiz-Martínez, S.; Puig, T. EGCG-Derivative G28 Shows High Efficacy Inhibiting the Mammosphere-Forming Capacity of Sensitive and Resistant TNBC Models. *Molecules* **2019**, *24*, 1027. [CrossRef]
45. Jacobsen, K.; Bertran-Alamillo, J.; Molina, M.A.; Teixidó, C.; Karachaliou, N.; Pedersen, M.H.; Castellví, J.; Garzón, M.; Codony-Servat, C.; Codony-Servat, J.; et al. Convergent Akt activation drives acquired EGFR inhibitor resistance in lung cancer. *Nat. Commun.* **2017**, *8*. [CrossRef] [PubMed]
46. Chang, L.; Fang, S.; Chen, Y.; Yang, Z.; Yuan, Y.; Zhang, J.; Ye, L.; Gu, W. Inhibition of FASN suppresses the malignant biological behavior of non-small cell lung cancer cells via deregulating glucose metabolism and AKT/ERK pathway. *Lipids Health Dis.* **2019**, *18*, 118. [CrossRef]
47. Liu, H.; Liu, Y.; Zhang, J.-T. A new mechanism of drug resistance in breast cancer cells: Fatty acid synthase overexpression-mediated palmitate overproduction. *Mol. Cancer Ther.* **2008**, *7*, 263–270. [CrossRef]

48. Chou, T.C.; Talalay, P. Quantitative analysis of dose-effect relationships: The combined effects of multiple drugs or enzyme inhibitors. *Adv. Enzym. Regul.* **1984**, *22*, 27–55. [CrossRef]
49. Wu, X.; Qin, L.; Fako, V.; Zhang, J.-T. Molecular mechanisms of fatty acid synthase (FASN)-mediated resistance to anti-cancer treatments. *Adv. Biol. Regul.* **2014**, *54*, 214–221. [CrossRef]
50. Liu, H.; Wu, X.; Dong, Z.; Luo, Z.; Zhao, Z.; Xu, Y.; Zhang, J.-T. Fatty acid synthase causes drug resistance by inhibiting TNF- α and ceramide production. *J. Lipid Res.* **2013**, *54*, 776–785. [CrossRef]
51. Giró-Perafita, A.; Palomeras, S.; Lum, D.H.; Blancafort, A.; Viñas, G.; Oliveras, G.; Pérez-Bueno, F.; Sarrats, A.; Welm, A.L.; Puig, T. Preclinical Evaluation of Fatty Acid Synthase and EGFR Inhibition in Triple Negative Breast Cancer. *Clin. Cancer Res.* **2016**, *22*, 4687–4697. [CrossRef] [PubMed]
52. Ma, Y.C.; Li, C.; Gao, F.; Xu, Y.; Jiang, Z.B.; Liu, J.X.; Jin, L.Y. Epigallocatechin gallate inhibits the growth of human lung cancer by directly targeting the EGFR signaling pathway. *Oncol. Rep.* **2014**, *31*, 1343–1349. [CrossRef] [PubMed]
53. Minnelli, C.; Laudadio, E.; Mobbili, G.; Galeazzi, R. Conformational Insight on WT- and Mutated-EGFR Receptor Activation and Inhibition by Epigallocatechin-3-Gallate: Over a Rational Basis for the Design of Selective Non-Small-Cell Lung Anticancer Agents. *Int. J. Mol. Sci.* **2020**, *21*, 1721. [CrossRef] [PubMed]
54. Namiki, K.; Wongsirisin, P.; Yokoyama, S.; Sato, M.; Rawangkan, A.; Sakai, R.; Iida, K.; Suganuma, M. (–)-Epigallocatechin gallate inhibits stemness and tumorigenicity stimulated by AXL receptor tyrosine kinase in human lung cancer cells. *Sci. Rep.* **2020**, *10*, 1–11. [CrossRef] [PubMed]
55. Zhu, C.; Wei, Y.; Wei, X. AXL receptor tyrosine kinase as a promising anti-cancer approach: Functions, molecular mechanisms and clinical applications. *Mol. Cancer* **2019**, *18*. [CrossRef] [PubMed]
56. Yousef, M.; Vlachogiannis, I.; Tsiani, E. Effects of Resveratrol against Lung Cancer: In Vitro and In Vivo Studies. *Nutrients* **2017**, *9*, 1231. [CrossRef]
57. Bailon-Moscoso, N.; Cevallos-Solorzano, G.; Romero-Benavides, J.C.; Orellana, M.I.R. Natural Compounds as Modulators of Cell Cycle Arrest: Application for Anticancer Chemotherapies. *Curr. Genom.* **2017**, *18*, 106–131. [CrossRef]
58. Hasima, N.; Ozpolat, B. Regulation of autophagy by polyphenolic compounds as a potential therapeutic strategy for cancer. *Cell Death Dis.* **2014**, *5*, e1509. [CrossRef]
59. Lin, H.-Y.; Hou, S.-C.; Chen, S.-C.; Kao, M.-C.; Yu, C.-C.; Funayama, S.; Ho, C.-T.; Way, T.-D. (–)-Epigallocatechin Gallate Induces Fas/CD95-Mediated Apoptosis through Inhibiting Constitutive and IL-6-Induced JAK/STAT3 Signaling in Head and Neck Squamous Cell Carcinoma Cells. *J. Agric. Food Chem.* **2012**, *60*, 2480–2489. [CrossRef]
60. Tang, S.-N.; Fu, J.; Shankar, S.; Srivastava, R.K. EGCG Enhances the Therapeutic Potential of Gemcitabine and CP690550 by Inhibiting STAT3 Signaling Pathway in Human Pancreatic Cancer. *PLoS ONE* **2012**, *7*, e31067. [CrossRef]
61. Codony-servat, C.; Codony-servat, J.; Karachaliou, N.; Angel, M.; Chaib, I.; Ramirez, J.L.; Gil, M.D.L.L.; Solca, F. Activation of signal transducer and activator of transcription 3 (STAT3) signaling in EGFR mutant non-small-cell lung cancer (NSCLC). *Oncotarget* **2017**, *8*, 47305–47316. [CrossRef] [PubMed]
62. Steelman, L.S.; Chappell, W.H.; Abrams, S.L.; Kempf, C.R.; Long, J.; Laidler, P.; Mijatovic, S.; Maksimovic-Ivanic, D.; Stivala, F.; Mazzarino, M.C.; et al. Roles of the Raf/MEK/ERK and PI3K/PTEN/Akt/mTOR pathways in controlling growth and sensitivity to therapy-implications for cancer and aging. *Aging (Albany, N.Y.)* **2011**, *3*, 192–222. [CrossRef] [PubMed]



© 2020 by the authors. Licensee MDPI, Basel, Switzerland. This article is an open access article distributed under the terms and conditions of the Creative Commons Attribution (CC BY) license (<http://creativecommons.org/licenses/by/4.0/>).



Contents lists available at ScienceDirect

Biomedicine & Pharmacotherapy

Journal homepage: www.elsevier.com/locate/bioph

AZ12756122, a novel fatty acid synthase inhibitor, decreases resistance features in EGFR-TKI resistant EGFR-mutated NSCLC cell models

Emma Polonio-Alcalá^{a,b}, Rut Porta^{a,c}, Santiago Ruiz-Martínez^a, Carmen Vázquez-Dongo^{b,d}, Joana Relat^{e,f,g}, Joaquim Bosch-Barrera^e, Joaquim Ciurana^{h,i}, Teresa Puig^{a,i}^a New Therapeutic Targets Laboratory (TargetsLab)-Oncology Unit, Department of Medical Sciences, University of Girona, Spain^b Product, Process and Production Engineering Research Group (GREP), Department of Mechanical Engineering and Industrial Construction, University of Girona, Spain^c Medical Oncology Department, Catalan Institute of Oncology, Spain^d Department of Pathology, Dr. Josep Trueta University Hospital, Spain^e Department of Nutrition, Food Sciences and Gastronomy, School of Pharmacy and Food Sciences, Food Tarrübera Campus, University of Barcelona, Spain^f Institute of Nutrition and Food Safety of the University of Barcelona (INSA-UB), Spain^g CIBER Physiopathology of Obesity and Nutrition (CIBER-OBN), Instituto de Salud Carlos III, Spain

ARTICLE INFO

Keywords:

NSCLC

FASN

EGFR

Osimertinib

Drug combination

ABSTRACT

Different EGFR tyrosine kinase inhibitors (TKIs) have been developed for the treatment of non-small cell lung cancer (NSCLC) patients harboring sensitizing mutations in the EGFR gene. Apart from acquired secondary mutations, multiple resistance mechanisms have been reported, such as the overexpression of fatty acid synthase (FASN), a multi-functional enzyme essential for the *de novo* lipogenesis, or the increase of cancer stem cells, a small subpopulation within the tumor responsible for relapse, metastasis, and resistance to therapies. Hence, the purpose of this work is to evaluate the novel FASN inhibitor AZ12756122, both alone and in combination with gefitinib and osimertinib, in EGFR-mutated (EGFRm) lung adenocarcinoma cell models sensitive and resistant to EGFR-TKIs. The molecular effect of AZ12756122 (alone and in combination with EGFR-TKI) on FASN, EGFR/STAT3, Akt/mTOR, and MAPK signaling pathways was analyzed using RT-qPCR and Western blot. FASN expression was also evaluated in samples from patients with EGFRm NSCLC through immunohistochemistry. Our findings revealed that AZ12756122 caused cytotoxic effects inducing apoptosis, downregulated FASN expression and activity, decreased the activation of EGFR and Akt/mTOR pathway, and reduced cancer stem-like cells. Furthermore, the combination of AZ12756122 and osimertinib sensitized cells to EGFR-TKI, showing a synergistic effect that resulted in a reduction in the activation of EGFR, Akt/mTOR, and MAPK signaling pathways. Our study also showed that FASN+ EGFRm NSCLC patients exhibited a longer mPFS in patients who responded to EGFR-TKI treatment. In conclusion, FASN inhibition should be further studied for the treatment, alone or in combination with EGFR-TKIs, for EGFRm NSCLC patients.

1. Introduction

Lung cancer is the second most common cancer diagnosed and the

first leading cause of cancer-related death. In 2020, more than 2.2 million new cases were reported and approximately 1.8 million deaths were recorded worldwide in both sexes, according to the World Health

Abbreviations: CSCs, Cancer Stem Cells; CI, Combination Index; EGFR, Epidermal Growth Factor Receptor; FASN, Fatty Acid Synthase; IC₅₀, Half-maximal Inhibitory Concentration; IHC, Immunohistochemistry; GR, Gefitinib-Resistant; LC3, Light Chain 3; mPFS, Median Progression-Free Survival; NSCLC, Non-Small Cell Lung Cancer; PARP, Poly (ADP-Ribose) Polymerase; STAT3, Signal Transducer and Activator of Transcription 3; TKI, Tyrosine Kinase Inhibitor.

* Correspondence to: Product, Process and Production Engineering Research Group (GREP), Department of Mechanical Engineering and Industrial Construction, University of Girona, 17003 Girona, Spain.

** Correspondence to: New Therapeutic Targets Laboratory (TargetsLab)-Oncology Unit, Department of Medical Sciences, University of Girona, Girona 17003, Spain.

E-mail addresses: emma.polonio@udg.edu (E. Polonio-Alcalá), rpporta@iccom001.qui.ub.edu (R. Porta), santiago.ruiz@udg.edu (S. Ruiz-Martínez), carmen.vazquez@iccom001.qui.ub.edu (C. Vázquez-Dongo), jrelat@ub.edu (J. Relat), jbosch@iccom001.qui.ub.edu (J. Bosch-Barrera), jciurana@iccom001.qui.ub.edu (J. Ciurana), teresa.puig@udg.edu (T. Puig).

<https://doi.org/10.1016/j.bioph.2022.11.1917>

Received 6 September 2022; Received in revised form 25 October 2022; Accepted 26 October 2022

Available online 29 October 2022

0753-3322/Published by Elsevier Masson SAS. This is an open access article under the CC BY-NC-ND license (<http://creativecommons.org/licenses/by-nc-nd/4.0/>).

Organization [1]. The most frequent subtype is non-small cell lung cancer (NSCLC), and around 40% of all lung cancer cases are classified as adenocarcinoma.

Sensitizing mutations in the tyrosine kinase domain of the epidermal growth factor receptor (EGFR) gene are frequently found in adenocarcinoma and most patients with these mutations are female and non-smokers [2–4]. The most common mutations are the exon 19-deletion (delE746_A750) and the L858R exon 21-point mutation, which together account for 90% of all EGFR mutations [4]. EGFR tyrosine kinase inhibitors (EGFR-TKIs) were designed as targeted therapy against these tumors [2]. In 2003, the Food and Drug Administration (FDA) approved the first EGFR-TKI, gefitinib, to treat patients with locally advanced or metastatic EGFR-mutated (EGFRm) NSCLC for whom chemotherapy has failed [5,6]. Despite the good response to the treatment using first- and second-generation EGFR-TKIs compared to chemotherapy, 60% of patients developed resistance after the therapy due to the acquisition of the secondary point mutation T790M in exon 20 of the receptor [7]. Hence, a third-generation EGFR-TKI, osimertinib, was approved by the FDA in 2015 to treat patients whose tumors harbored a sensitizing mutation and/or T790M point mutation [8,9]. However, the acquisition of the secondary point mutation C797 in exon 20 led to patients developing resistance to osimertinib [10].

Apart from acquired secondary mutations in the EGFR gene, other resistance mechanisms have been described such as the activation of a signal transducer and activator of transcription 3 (STAT3) [11], c-Met amplification [12], IGF-1R activation [13], HER2 amplification [14], AXL activation [15], loss of PTEN expression, PIK3CA and BRAF mutations [16,17], and SCLC transformation [17]. Cancer stem cells (CSCs) are tumor-initiating cells resistant to radio- and chemotherapy that exhibit self-renewal and pluripotency capacities. This small proportion of tumor cells is responsible for relapse and metastasis [18,19]. Furthermore, CSCs have demonstrated clonogenic capacity and are able to grow in anchorage-independent *in vitro* conditions forming spheres [20].

Deregulation of cellular energy metabolism has been identified as a hallmark of cancer, and is fundamental for cell growth and division of cancer cells [21]. Fatty acid synthase (FASN) is a homodimeric and multi-functional enzyme responsible for *de novo* lipogenesis by catalyzing palmitate from acetyl CoA and malonyl CoA in a NADPH-dependent reaction [22]. It has been demonstrated that EGFRm mediates the resistance to EGFR-TKIs through the upregulation of the FASN expression [23], and consequently the inhibition of FASN resulted in cytotoxic effects on sensitive and EGFR-TKI-resistant EGFRm NSCLC cells [23,24]. Additionally, FASN inhibition caused the increase of radiosensitivity [25] and the reduction of cancer stem-like cells in NSCLC [26,27].

Therefore, the main objective of this study was to evaluate the novel FASN inhibitor, AZ12756122, both alone and in combination with gefitinib and osimertinib, in EGFRm lung adenocarcinoma cell models sensitive and resistant to EGFR-TKIs. Moreover, the molecular effect of AZ12756122 (again both alone and in combination with EGFR-TKI) was also analyzed on FASN, EGFR/STAT3, Akt/mTOR, and MAPK signaling pathways. The effect of the AZ12756122 compound against cancer stem-like cells was also explored. Furthermore, the FASN expression was evaluated in 36 tumor samples from patients with EGFRm NSCLC in order to validate *in vitro* results.

2. Material & methods

2.1. Chemicals & reagents

Roswell Park Memorial Institute (RPMI-1640) medium, L-glutamine 200 nM, phosphate-buffered saline (PBS), penicillin/streptomycin 10,000 U/mL, sodium pyruvate 100 nM, and trypsin 10⁻⁶ were provided by Lonza (Basilea, Switzerland). Fetal bovine serum (FBS) and Dulbecco's Modified Eagle Medium (DMEM)/F12 (1:1) were obtained from

HyClone (Logan, UT, USA). The bovine serum albumin (BSA) ($\geq 98.0\%$), Bradford assay, crystal violet, lipoprotein-deficient FBS, paraformaldehyde, phenylmethylsulfonyl fluoride (PMSF), TWEEN® 20, 3-(4,5-dimethyl-2-thiazolyl)-2,5-diphenyl-2 H-tetrazolium bromide (MTT), and primers (Supplementary Table 1) were acquired from Sigma-Aldrich (St. Louis, MO, USA). The BSA Fraction V pH for Western blotting (min. 96%) and tris-buffered saline (TBS) were purchased from PanReac AppliChem (Gatersleben, Germany). Ethanol absolute, dimethyl sulfoxide (DMSO), methanol, chloroform, sodium chloride, and potassium hydroxide were supplied by Labkem-Labbox Labware S. L. (Barcelona, Spain). Qiazol was provided from Qiagen (Hilden, Germany). The GeneJET RNA Purification Kit, West Femto Maximum Sensitivity Substrate, nitrocellulose membranes, and B-27™ supplement (50X) were obtained from Thermo Fisher Scientific Inc. (Waltham, MA, USA). The High-Capacity cDNA Archive Kit was acquired from Applied Biosystems (Foster City, CA, USA). The qPCR BIO SyGreen Mix Lo-Rox was purchased from PCR Biosystems Inc. (Wayne, PA, USA). DC Protein Assay, Clarity™ Western ECL Substrate, and 40% acrylamide solution were supplied by Bio-Rad (Hercules, CA, USA). The sample reducing agent and lithium dodecyl sulfate (LDS) sample buffer were provided by Invitrogen (Carlsbad, CA, USA) and the lysis buffer was obtained from Cell Signaling Technology (CST) Inc. (Danvers, MA, USA). Antibodies (Supplementary Table 1) were provided by CST, Abcam (Cambridge, UK), ProteinTech® (Manchester, UK), and Roche Diagnostics (Basilea, Switzerland). (1,2–14 C) acetic acid sodium salt was acquired from Perkin Elmer Biosciences (Waltham, MA, USA). Human epidermal growth factor (hEGF) 100 µg and human fibroblast growth factor (hFGF) 50 µg were purchased from Miltenyi Biotec (Bergisch Gladbach, Germany). The UltraView Universal DAB Detection Kit and Amplification Kit were supplied by Roche Diagnostics. The AZ12756122 compound, gefitinib, and osimertinib were kindly provided by AstraZeneca (London, UK).

2.2. Cell models

Human lung adenocarcinoma PC9 and its gefitinib-resistant (GR) derivative cell models PC9-GR1, PC9-GR3, and PC9-GR4 were kindly provided by Dr. R. Rosell and Dr. M.A. Molina (Barcelona, Spain). Mechanisms of resistance in GR models are indicated in Table 1. Cells were cultured in RPMI-1640 medium supplemented with 10% FBS and 50 U/mL penicillin/streptomycin and incubated at 37 °C in 5% CO₂ humidified environment and maintained mycoplasma-free.

2.3. Cell viability assay

Cells were seeded in adherent cell culture 96-well plates at the proper cell density. After 24 h, the cells were treated with a range of increasing concentrations of gefitinib, osimertinib, or AZ12756122 for 72 h for the monotherapy experiments. For the drug combination assay, cells were treated with three fixed concentrations of gefitinib (1, 2.5, and 5 µmol/L) or osimertinib (0.5, 1, and 2 µmol/L) in combination of different concentrations of AZ12756122 for 72 h. The MTT assay was employed to evaluate cell viability, as reported elsewhere [24]. Combinatorial effects were examined using the CompuSyn™ software (BioSoft, MO, USA) based on the Chou and Talalay approach [28]. The combination index (CI) value determines the effect of the drug combinations: CI < 1 designates a synergistic effect, CI = 1 designates an additive effect, and CI > 1 designates an antagonistic effect.

2.4. Fatty acid synthase activity assay

Cells were seeded in adherent cell culture 24-well plates at the appropriate cell density. After 24 h, the cells were treated with AZ12756122 at a concentration equivalent to their IC₅₀ or with the vehicle (DMSO) for 72 h and the medium was replaced by RPMI-1640 supplemented with 1% lipoprotein-deficient FBS. (1,2–¹⁴C) acetic acid

Table 1
Mechanisms of resistance in gefitinib-resistant (GR) derivative PC9 cell models.

Cell Model	T790M mutation	AXL overexpression	MET activation	EphA2 activation	Bcl-2 expression	FASN overexpression
PC9-GR1	+	-	+	+	-	-
PC9-GR3	-	+	-	-	+	-
PC9-GR4	-	+	-	+	-	-

Source: Modified from [29].

sodium salt (0.5 $\mu\text{Ci}/\text{mL}$) was added to the medium for the last 6 h. The cell lysis and lipid extraction was accomplished as previously described [30]. Afterwards, cell pellets were radioactive-counted, and the Bradford assay was employed to quantify the total protein content.

2.5. Quantitative real-time PCR analysis

Cells were seeded in adherent cell culture plates at the proper cell density. After 24 h, the cells were treated with gefitinib, osimertinib or AZ12756122 at a concentration equivalent to their IC_{50} as monotherapy or 25 $\mu\text{mol}/\text{L}$ of AZ12756122 in combination with 1 $\mu\text{mol}/\text{L}$ osimertinib for 72 h. Thereafter, the cells were rinsed with PBS and resuspended in 700 μL of Qiazol. RNA was isolated using a GeneJET RNA Purification Kit, quantified by a NanoDrop™ One Micro-volume UV-Vis spectrophotometer (Thermo Fisher Scientific, Waltham, MA, USA), and reverse-transcribed into complementary DNA (cDNA) employing a HighCapacity cDNA Archive Kit. Through the QuantStudio3 Real-Time PCR System (Thermo Fisher Scientific Inc., Waltham, MA, USA), different gene expression levels were determined using qPCR BIO SyGreen Mix Lo-Rox and primers (Table S1). The results were calculated using the standard formula $2^{-\Delta\Delta\text{CT}}$ and normalized to the housekeeping GAPDH.

2.6. Western blotting analysis

Cells were seeded in adherent cell culture plates at the appropriate cell density. After 24 h, the cells were treated with gefitinib, osimertinib or AZ12756122 at a concentration equivalent to their IC_{50} as monotherapy or 25 $\mu\text{mol}/\text{L}$ AZ12756122 in combination with 1 $\mu\text{mol}/\text{L}$ osimertinib for 72 h. Then, attached and floating cells were collected and lysed by vortexing every 5 min for 30 min in an ice-cold lysis buffer with 100 $\mu\text{g}/\text{mL}$ PMFS. A DC Protein Assay was performed to obtain the protein concentration of each sample using a BSA standard curve. The same amounts of protein were heated in LDS and reducing agent buffers for 10 min at 70 °C, separated using SDS-polyacrylamide gel (SDS-PAGE) and moved to nitrocellulose membranes. Membranes were incubated for 1 h at room temperature in blocking buffer (5% skim milk powder in TBS 0.05% Tween (TBS-T)) and overnight at 4 °C with the corresponding primary antibody (Table S1) diluted in blocking buffer. Specific horseradish peroxidase (HRP)-conjugated secondary antibodies were incubated for 1 h at room temperature before being detected in the Bio-Rad ChemiDoc™ MP Imaging System (Bio-Rad Laboratories, Inc., Hercules, CA, USA) using an HRP substrate Clarity™ Western ECL Substrate or a West Femto Maximum Sensitivity Substrate.

2.7. Sphere formation assay

Cells were seeded in non-adherent cell culture 6-well plates at a low cell density for 7 days using DMEM/F12 medium supplemented with 20 ng/mL B27, hEGF, and hFGF, 1% L-glutamine, and 1% sodium pyruvate. The treatment with AZ12756122 at a concentration equivalent to their IC_{10} and IC_{30} was added at the moment of seeding. Thereafter, spheres bigger than 50 μm were counted using an inverted optical microscope. The Sphere Formation Index (SFI) was calculated using the following formula:

$$\text{SFI} = \frac{\text{num. spheres}}{\text{num. cells seeded}}$$

2.8. Colony formation assay

Cells were seeded in adherent cell culture 6-well plates at a low cell density for 7 days. The treatment with AZ12756122 at a concentration equivalent to their IC_{10} and IC_{30} was added at the moment of seeding. Afterwards, cells were rinsed with PBS and 2 mL of 6% paraformaldehyde + 0.5% of crystal violet was added to each well. After 30 min, the mixture was removed, the plates were washed by immersing them in tap water, and air-dried at room temperature. The Colony Formation Index (CFI) was calculated using the following formula:

$$\text{CFI} = \frac{\text{num. colonies}_{\text{treated}}}{\text{num. colonies}_{\text{control}}}$$

2.9. Selection of patients

Between 2006 and 2019, forty-five patients from the Dr. Josep Trueta University Hospital (Girona, Spain) with NSCLC harboring exon 19 deletion and exon 21 L858R activating mutations in EGFR met the inclusion criteria. Tumor samples were obtained at the time of diagnostic biopsy prior to any treatment. The patients' clinical characteristics and pathological features of their tumors were examined retrospectively and obtained from their medical records. The Response Evaluation Criteria in Solid Tumors (RECIST) (version 1.1) was used to establish the response to the treatment (complete response, partial response, stable disease, and progression disease). All patients had received EGFR-TKI, gefitinib or erlotinib, at some point. It should be noted that some of patients in our study received other lines of treatment after receiving the EGFR-TKI. Thirty-six patients had sufficient tumor sample from their biopsies for immunohistochemical analysis.

2.10. Immunohistochemistry assay of tissue samples

BenchMark ULTRA-Ventana equipment (Roche Diagnostics) was employed to evaluate FASN (tumor expression by immunohistochemistry (IHC) in 3 μm thick slides from formalin-fixed paraffin-embedded tissue blocks of the tumor. The FASN rabbit monoclonal antibody was detected using an UltraView Universal DAB Detection Kit and an Amplification Kit. Instead of the primary antibody, a similar concentration of mouse IgG was used as a negative control. Adipose tissue next to a FASN-overexpressing ductal-type breast carcinoma were also analyzed as a positive control for FASN expression. Negative FASN expression was deemed when none of the cells showed cytoplasmic staining. In contrast, any expression of FASN at the cytoplasmic level was classified as positive.

2.11. Data analysis

The statistical analysis was conducted using the IBM SPSS software (Version 25.0; SPSS Inc., Chicago, IL, USA) and R software (Version 4.0.4; The R Foundation, Vienna, Austria). The in vitro assays were replicated at least three times and the results expressed as mean \pm standard error of the mean (SE). For two-group comparisons, non-parametric data were analyzed with the Mann-Whitney U test and

parametric data with the Student's t test. For the comparisons of more than two groups, non-parametric data were examined with the Kruskal-Wallis test and parametric data by one-way analysis of variance (ANOVA) using Bonferroni or Tamhane's T2 post hoc test. Data from patients were summarized as counts and percentages for categorical variables, and the number of non-missing observations, the mean \pm standard deviation (SD), the median, or interquartile range [IQR] for continuous variables. Progression-free survival (PFS) probability was estimated according to the method of Kaplan-Meier and statistical differences were calculated using the log-rank test. Fisher's exact tests were employed to compare categorical variables. Levels of significance were determined at $p < 0.050$ (*), $p < 0.010$ (**), and $p < 0.001$ (***)

3. Results

3.1. Characterization of AZ12756122 compound

The cytotoxic effect of AZ12756122 was investigated through dose-response curves in lung adenocarcinoma cell models sensitive and resistant to EGFR-TKIs (Fig. 1A). The PC9-GR1 and PC9-GR4 cell models (T790M-) exhibit resistance exclusively to gefitinib, while the PC9-GR3 cell model (T790M-) is resistant to both gefitinib and osimertinib [28]. The half-maximal inhibitory concentration (IC₅₀) value of the compound was $64.3 \pm 1.3 \mu\text{M}$ for PC9, $75.2 \pm 6.4 \mu\text{M}$ for PC9-GR1, $45.7 \pm 5.2 \mu\text{M}$ for PC9-GR3, and $76.8 \pm 4.1 \mu\text{M}$ for PC9-GR4. Although no significant differences were found between the IC₅₀ value of PC9 and the GR models (PC9-GR1 $p = 1.000$; PC9-GR3 $p = 0.115$; PC9-GR4 $p = 0.756$), the IC₅₀ concentration of PC9-GR3 was significantly lower compared to the T790M+ models (PC9-GR1 $p = 9.960 \times 10^{-4}$; PC9-GR4 $p = 3.220 \times 10^{-4}$).

The ability of AZ12756122 to inhibit FASN activity was analyzed in sensitive and resistant models (Fig. 1B). The compound equally inhibited the enzyme activity in all cell models ($p = 0.566$), ranging from 38% to 54%, regardless of their sensitivity or resistance to EGFR-TKIs.

AZ12756122 treatment was also evaluated by Western blot to determine whether cell death was caused through the induction of apoptosis and/or autophagy in sensitive and GR models (Fig. 1C). The cleavage of poly (ADP-ribose) polymerase (PARP) and the conversion of the Light Chain 3 (LC3) into LC3-II were used as apoptosis and autophagy markers, respectively. The cleaved form of PARP (89 kDa) was observed in PC9, PC9-GR1, and PC9-GR3 following treatment with the compound, thus showing the induction of apoptosis. However, the LC3-II form did not appear, therefore the AZ12756122 treatment did not trigger autophagy.

3.2. Molecular effects caused by AZ12756122 and EGFR-TKIs treatments as single agents in EGFR lung adenocarcinoma cell models

FASN, EGFR, and STAT3 mRNA expression were analyzed after AZ12756122 or EGFR-TKIs treatment by means of RT-qPCR in cell models sensitive and resistant to EGFR-TKIs (Fig. 2). The mRNA expression of these genes was compared among cell lines and no significant differences were found. However, the EGFR levels tended to increase in the two T790M+ cell models, whereas the STAT3 expression tended to decrease, especially in PC9-GR3 and PC9-GR4 cells (Supplementary Fig. 1).

While the AZ12756122 treatment reduced FASN mRNA levels in all models, it was statistically significant in PC9 ($p = 5.5 \times 10^{-4}$), PC9-GR1 ($p = 0.009$), and PC9-GR4 ($p = 0.049$) compared to the control. Furthermore, gefitinib and osimertinib treatments also diminished the FASN mRNA expression in the T790M- models (PC9 $p = 4.5 \times 10^{-4}$)

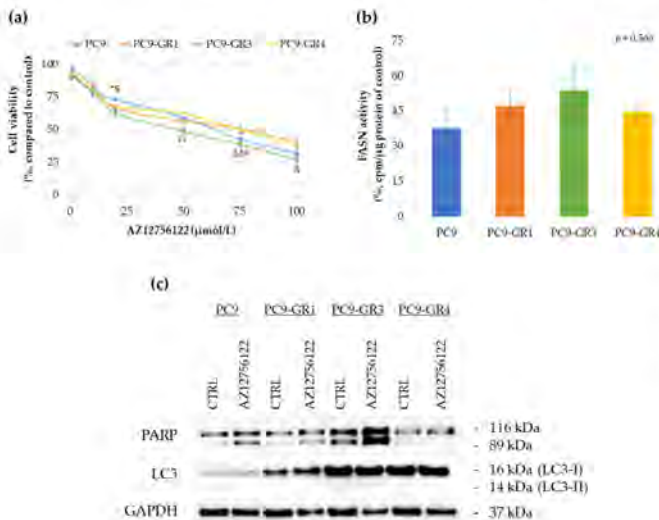


Fig. 1. (a) Dose-response curves of AZ12756122 compound in sensitive (PC9) and gefitinib-resistant (GR) models. Sensitive (PC9) and GR models (PC9-GR1, PC9-GR3, and PC9-GR4) were treated with increasing concentrations of AZ12756122 (from 1 to 100 μmol/L) for 72 h. Results shown are expressed as percentage of surviving cells after drug treatment (mean \pm SE) from at least three independent experiments. * $p < 0.050$, ** $p < 0.010$, and *** $p < 0.001$ indicate levels of statistical significance. The symbol * indicates differences between PC9 and PC9-GR1, \$ indicates differences between PC9 and PC9-GR3, # indicates differences between PC9-GR3 and PC9-GR4, and Δ indicates differences between PC9-GR1 and PC9-GR3. (b) AZ12756122 compound inhibits FASN activity in sensitive and GR models. PC9 and GR models were treated with AZ12756122 at a concentration equivalent to their IC₅₀ and with DMSO as the control for 72 h. FASN activity was assayed by counting radiolabeled fatty acids synthesized *de novo*. Results shown are the percentage of remaining activity (mean \pm SE) in treated versus untreated cells (control) from at least three independent experiments. (c) Effect of AZ12756122 on apoptosis and autophagy determined by PARP cleavage and LC3 conversion in sensitive and GR models. PC9 and GR models were treated with the AZ12756122 compound at a concentration equal to their IC₅₀ for 72 h. Untreated cells were used as an internal control (CTRL), and GAPDH as a loading control. Results shown are representative from at least

three independent experiments.

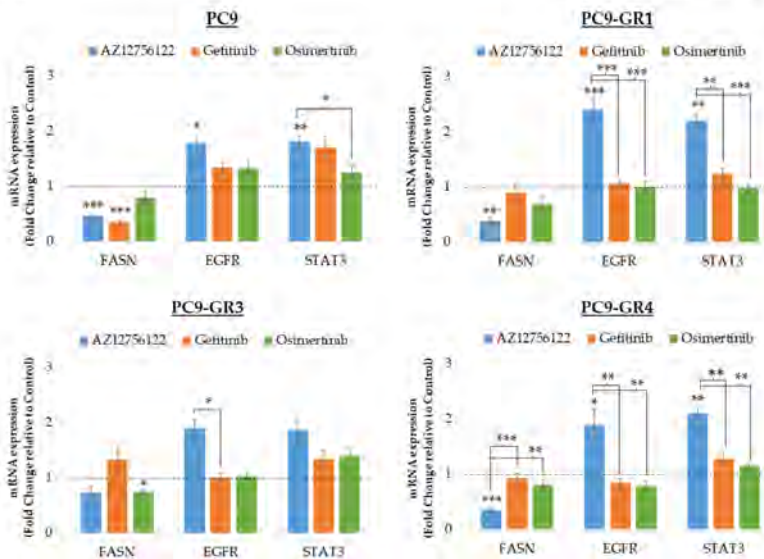


Fig. 2. *FASN*, *EGFR*, and *STAT3* mRNA expression after AZ12756122 and EGFR-TKIs (gefitinib and osimertinib) treatments in sensitive and gefitinib-resistant (GR) models. Sensitive (PC9) and GR models (PC9-GR1, PC9-GR3, and PC9-GR4) were treated with AZ12756122, gefitinib or osimertinib at a concentration equivalent to their IC_{50} for 72 h. mRNA levels were obtained by RT-qPCR and normalized against the GAPDH gene. All conditions were compared to the control (untreated cells), which was normalized to 1 (indicated by the dotted line) and expressed as a fold change. Experiments were performed at least three times. * $p < 0.050$, ** $p < 0.010$, and *** $p < 0.001$ indicate levels of statistically significance.

and PC9-GR3 ($p = 0.046$), respectively), compared to control. An increase in *EGFR* mRNA levels was observed in the AZ12756122 treatment, which was statistically significant in PC9 ($p = 0.021$), PC9-GR1 ($p = 6.0 \times 10^{-6}$), and PC9-GR4 ($p = 0.014$) compared to control and also in comparison with the gefitinib treatment in the GR models (PC9-GR1 $p = 1.0 \times 10^{-5}$; PC9-GR3 $p = 0.036$; PC9-GR4 $p = 0.004$) and with the osimertinib treatment in the T790M+ cell models (PC9-GR1 $p = 6.0 \times 10^{-6}$; PC9-GR4 $p = 0.003$). The AZ12756122 treatment also upregulated the *STAT3* mRNA expression in all models, and was statistically significant in PC9 ($p = 0.006$), PC9-GR1 ($p = 0.003$), and PC9-GR4 ($p = 0.009$) compared to control and also in comparison with the gefitinib treatment in the T790M+ cell models (PC9-GR1 $p = 0.003$; PC9-GR4 $p = 0.009$) and with the osimertinib treatment (PC9 $p = 0.049$; PC9-GR1 $p = 3.5 \times 10^{-3}$; PC9-GR4 $p = 0.002$). Additionally, an increase of *STAT3* was also shown in the gefitinib treatment in the sensitive model.

Alterations in protein expression caused by AZ12756122, gefitinib and osimertinib were also evaluated in both sensitive and GR models (Fig. 3).

The FASN protein expression was decreased by the AZ12756122 treatment in all cell models. Moreover, the treatment using the compound or EGFR-TKIs reduced phosphorylated levels of EGFR in both the sensitive and GR models. The osimertinib treatment activated *STAT3* levels, whereas AZ12756122 did not cause variations in the GR cell models. The gefitinib treatment also increased the phosphorylated levels of *STAT3* in all models. No alterations were showed in the *STAT3* total protein expression. Moreover, no changes were found in MAPK signaling pathway activation or expression. Focusing on the Akt/PRAS40 signaling pathway, the treatment using the compound reduced the activation of Akt in the GR models and PRAS40 in all cell models.

Furthermore, the AZ12756122 treatment slightly decreased PRAS40 total protein expression. Although the gefitinib treatment reduced Akt and PRAS40 total protein levels in PC9, their phosphorylated levels were higher than untreated cells. The osimertinib treatment diminished the activation of Akt in all cell models and PRAS40 in PC9 and PC9-GR1.

3.3. Pharmacological interaction between AZ12756122 and EGFR-TKIs

The combinatorial treatment using AZ12756122 and EGFR-TKIs was studied to find synergistic interactions and overcome the acquired resistance to gefitinib in the T790M+ models, PC9-GR1 and PC9-GR4, and to gefitinib and osimertinib in the T790M- model, and PC9-GR3 (Fig. 4). Furthermore, IC_{50} values of all combinatorial treatments were calculated (Supplementary Table 2).

None of the combinations tested showed synergism in PC9-GR1. The different combinatorial treatments resulted in an antagonism or additive effect. The AZ12756122 IC_{50} value significantly decreased in combination with 2.5 μ M gefitinib ($p = 0.037$) and 5 μ M gefitinib ($p = 1.0 \times 10^{-9}$) in comparison with the AZ12756122 monotherapy and other combinations (AZ12756122 + 1 μ M gefitinib $p = 2.2 \times 10^{-4}$; AZ12756122 + 2.5 μ M gefitinib $p = 0.019$).

In the PC9-GR4 cell model, some combinations exhibited synergistic effects. It should be highlighted that the highest concentration of gefitinib (5 μ M) was required with lower concentrations of AZ12756122 to obtain a synergistic effect, and vice versa. The combination of AZ12756122 + 5 μ M gefitinib was the only one that showed a significantly lower IC_{50} value compared to monotherapy ($p = 5.7 \times 10^{-9}$) and to the other combinations (AZ12756122 + 1 μ M gefitinib $p = 4.8 \times 10^{-7}$; AZ12756122 + 2.5 μ M gefitinib $p = 3.0 \times 10^{-6}$).

Regarding the T790M- GR model, the combination using gefitinib

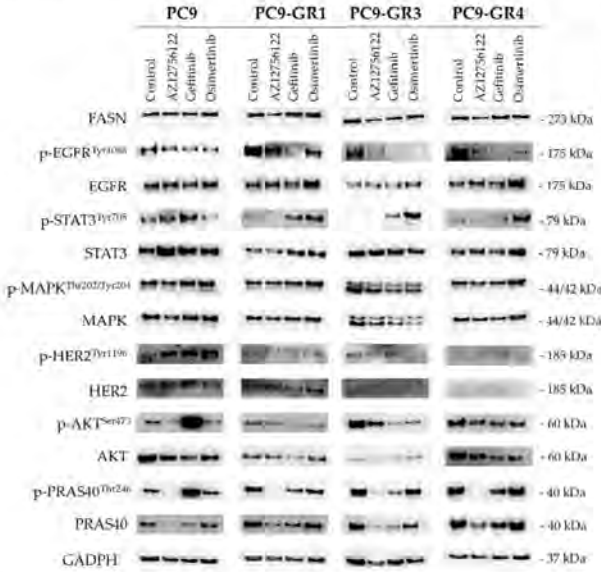


Fig. 3. Analysis of protein expression after treatment using AZ12756122 and EGFR-TKIs (gefitinib and osimertinib) in sensitive and gefitinib-resistant (GR) models. Sensitive (PC9) and GR models (PC9-GR1, PC9-GR3, and PC9-GR4) were treated with AZ12756122, gefitinib or osimertinib at a concentration equal to their IC₅₀ for 72 h. Untreated cells were used as an internal control (CTRL) and GAPDH as a loading control. Results shown are representative of at least three independent experiments.

demonstrated mostly additive and synergistic effects. Nevertheless, combinations with synergistic effects were obtained at higher concentrations. No significant differences were found between the IC₅₀ value of AZ12756122 monotherapy and combinatorial treatments or among combination curves. The combination of AZ12756122 and osimertinib exhibited only additive or synergistic effects. Unlike the combinatorial treatments using gefitinib, the combination with the lowest concentrations showing synergistic effects (25 μM AZ12756122 + 1 μM osimertinib) also demonstrated a cell viability above 50%. Additionally, the IC₅₀ value diminished with increasing osimertinib concentrations, and was significantly lower in the combination of AZ12756122 + 1 μM osimertinib in comparison with monotherapy ($p = 0.003$),

and the combination AZ12756122 + 2 μM osimertinib, in contrast to monotherapy ($p = 3.9 \times 10^{-5}$) and other combinations (AZ12756122 + 0.5 μM osimertinib $p = 0.002$; AZ12756122 + 1 μM osimertinib $p = 0.016$).

Therefore, the effects of the combinatorial treatment of 25 μM AZ12756122 and 1 μM osimertinib on mRNA and protein expression were studied in the PC9-GR3 cell model (Fig. 5).

In terms of mRNA expression, no changes were observed in the FASN expression for monotherapies or combinatorial treatment. The EGFR expression was significantly enhanced by AZ12756122 monotherapy compared to untreated cells ($p = 0.022$). Moreover, AZ12756122 monotherapy and its combination with osimertinib demonstrated increased EGFR expression in comparison with osimertinib monotherapy (AZ12756122 $p = 0.004$; AZ12756122 + osimertinib $p = 0.041$). Although the STAT3 expression did not show significant variations as a result of the monotherapies, the combinatorial therapy upregulated its expression compared to untreated cells and osimertinib monotherapy (control $p = 0.012$; osimertinib $p = 0.014$).

The FASN protein expression was only slightly decreased in the AZ12756122 monotherapy. All treatments caused a reduction in EGFR activation, and furthermore AZ12756122 monotherapy slightly diminished total EGFR expression. Although no changes in total STAT3

levels were observed, both osimertinib monotherapy and combinatorial treatment showed high levels of phosphorylated-STAT3 compared to untreated cells. Both AZ12756122 monotherapy and combinatorial treatment decreased MAPK activation and total expression, whereas osimertinib monotherapy increased its phosphorylated levels. Regarding Akt/mTOR signaling pathways, although AZ12756122 monotherapy reduced total Akt expression, osimertinib monotherapy and combinatorial treatment decreased its activation. The activation of PRAS40 was diminished in both monotherapies and combinatorial therapy, but total PRAS40 protein levels were only reduced in AZ12756122 monotherapy and combinatorial therapy.

3.4. AZ12756122 activity against cancer stem-like population

AZ12756122 activity against cancer stem-like cells was evaluated using sphere and colony formation assays in sensitive and gefitinib- and osimertinib-resistant cell models (Fig. 6).

AZ12756122 treatment, using its IC₁₀ concentration, resulted in a significant reduction of spheres ($p = 0.023$) and colonies ($p = 9.7 \times 10^{-5}$) in PC9 cells and of spheres in PC9-GR3 cells ($p = 0.009$). No changes in colony formation were found in PC9-GR3 cells. Furthermore, the IC₃₀ concentration treatment exhibited a significant decrease in spheres (PC9-GR3, $p = 0.008$) and colonies (PC9, $p = 2.0 \times 10^{-6}$; PC9-GR3, $p = 2.5 \times 10^{-5}$) in contrast to untreated cells and the treatment using IC₁₀ concentration (colonies PC9, $p = 1.3 \times 10^{-4}$; spheres PC9-GR3, $p = 0.009$; colonies PC9-GR3, $p = 9.0 \times 10^{-5}$). Total inhibition of sphere formation was observed in PC9 cells.

3.5. FASN expression in EGFRm NSCLC patients

Data were collected from forty-five NSCLC patients harboring exon 19 deletion or exon 21 L858R sensitizing mutations (Table 2). Data for FASN expression levels were also collected (Supplementary Table 3).

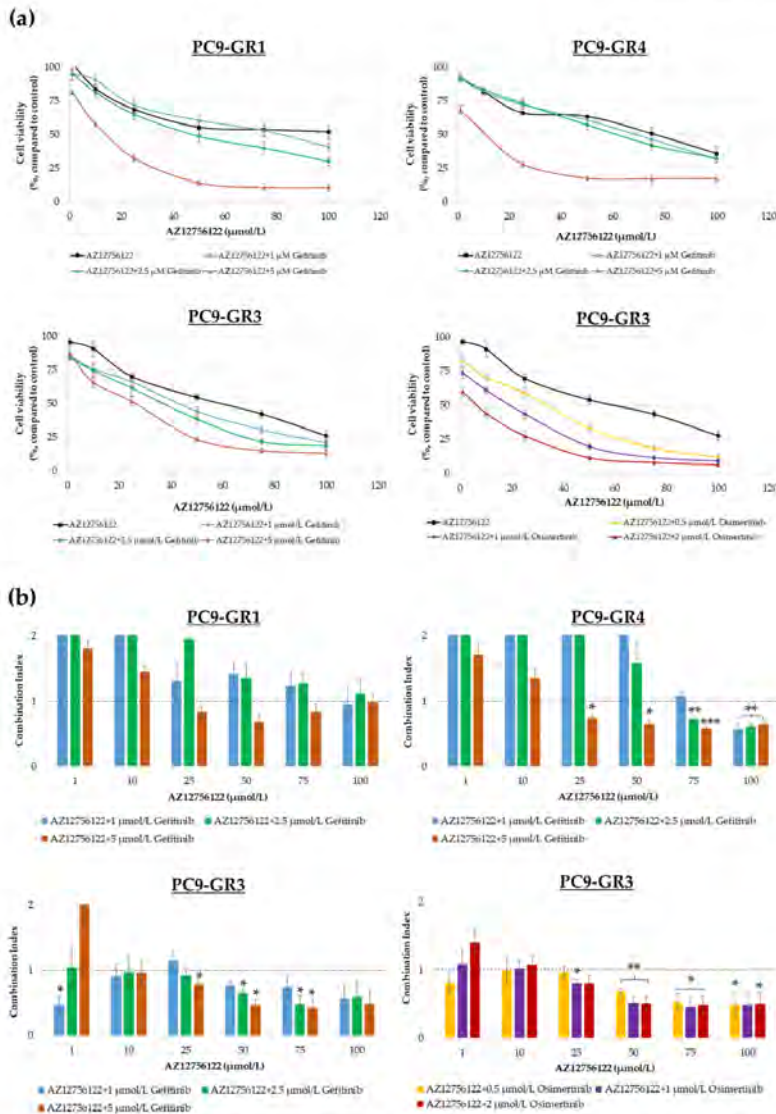


Fig. 4. Combinatorial treatment between AZ12756122 and EGFR-TKIs (gefitinib and osimertinib) in gefitinib-resistant (GR) models. (a) Dose-response curves of AZ12756122 (from 1 to 100 μM) alone and in combination with gefitinib (1, 2.5 and 5 μM) in PC9-GR1, PC9-GR3, and PC9-GR4 models and osimertinib (0.5, 1 and 2 μM) in PC9-GR3 for 72 h. Results shown are expressed as percentage of surviving cells after drug treatment (mean ± SE) from at least three independent experiments. (b) Combination Index (CI) from treatments with AZ12756122 (from 1 to 100 μM) and gefitinib (1, 2.5 and 5 μM) in PC9-GR1, PC9-GR3, and PC9-GR4 models or osimertinib (0.5, 1 and 2 μM) in PC9-GR3 for 72 h. Results shown are mean ± SE from at least three independent experiments and are based on the Chou and Talalay method. The dotted line indicates additive (CI approximately equal to 1). CI > 1 designates antagonistic effect and CI < 1 synergistic effect * p < 0.050, ** p < 0.01, *** p < 0.001 indicate levels of statistical significance.

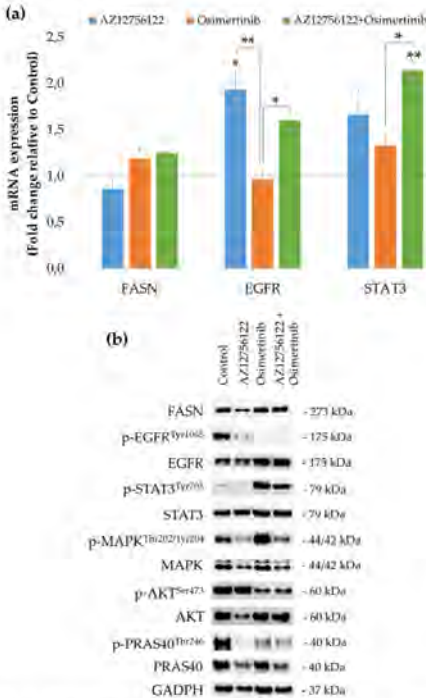


Fig. 5. Effects on mRNA levels and protein expression caused by the combination treatment in the PC9-GR3 cell model. (a) FASN, EGFR, and STAT3 mRNA expression levels after the combination treatment. PC9-GR3 models were treated with 25 μ M AZ12756122, 1 μ M osimertinib or both treatments for 72 h. mRNA levels were obtained by RT-qPCR and normalized against the GAPDH gene. All conditions were compared to the control (untreated cells), which was normalized to 1 (indicated by the dotted line) and expressed as a fold change. Experiments were performed at least three times. * $p < 0.050$, ** $p < 0.010$, and *** $p < 0.001$ indicate levels of statistical significance. The symbol * indicates in comparison with control, \$ indicates in comparison with AZ12756122 treatment, and # indicates in comparison with osimertinib treatment. (b) Protein expression after the combination treatment. PC9-GR3 models were treated with 25 μ M of AZ12756122, 1 μ M of osimertinib or both treatments for 72 h. Untreated cells were used as an internal control (CTRL) and GAPDH as a loading control. Results shown are representative of at least three independent experiments.

FASN tumor expression was analyzed in thirty-six biopsies with sufficient tumor sample for immunohistochemical (IHC) evaluation (Fig. 7). A positive expression of FASN was observed in seventeen (47.2%) of the tumor samples. Median progression-free survival (mPFS) was significantly longer in patients whose tumors expressed some levels of FASN at baseline ($p = 0.039$) (Fig. 7A). PFS refers to the time from the onset of treatment to the occurrence of disease progression or death. The expression of FASN also tend to a better response rate to the EGFR-TKI ($p = 0.060$) (Supplementary Fig. 2B). Furthermore, mPFS was analyzed according to the response to the EGFR-TKI treatment and FASN expression. Patients who responded to EGFR-TKI treatment and who expressed FASN showed significantly longer mPFS than those who did not express FASN ($p = 0.015$) (Fig. 7B). However, no relationship

between FASN tumor expression and overall survival (OS) was detected ($p = 0.490$) (Supplementary Fig. 2A). OS refers to the time elapsing from the beginning of treatment to death for any reason.

4. Discussion

Although different EGFR-TKIs have been approved for the treatment of EGFRm NSCLC patients [5,9], several mechanisms have been described by which cells acquire resistance, such as FASN overexpression [23,24] or the increase of CSCs [18,19]. Previous studies have showed that FASN inhibition caused cytotoxic effects in EGFRm lung adenocarcinoma [23,24] and reduced cancer stem-like cells in NSCLC [26,27]. Therefore, this study evaluated the effect of a novel FASN inhibitor, AZ12756122, both alone and in combination with EGFR-TKIs, in cell models sensitive and resistant to EGFR-TKIs, and in their cancer stem-like cell populations. Furthermore, the FASN expression was analyzed in EGFRm NSCLC patients to validate the in vitro results.

The AZ12756122 compound inhibited FASN activity in both sensitive and resistant to EGFR-TKIs cell models (Fig. 1B). Other compounds inhibited FASN activity [24,31], such as Orlistat, an FDA-approved anti-obesity drug, which reduced FASN activity in H1975 cells, but not in PC14 and H3255 cells [31]. Additionally, it was previously observed that FASN knockdown inhibited cell proliferation [32] inducing apoptosis through the increase of the autophagosomal marker LC3-II [33]. However, only apoptosis induction was observed in PC9, PC9-GR1, and PC9-GR3 (Fig. 1C). Despite that, AZ12756122 exhibited cytotoxic effects in all cell models tested (Fig. 1A), suggesting that AZ12756122 treatment only affected cell growth in PC9-GR4. AZ12756122 IC₅₀ values oscillated from 45 to 77 μ M, lower concentrations than those used with (-)-epigallocatechin-3-gallate (EGCG) or Orlistat [23,24]. PC9-GR3 cells were significantly more sensitive to the AZ12756122 treatment than the T790M+ cell models were. These results may be due to the activation of EphA2 exhibited by the T790M+ models [28]. Youngblood et al., demonstrated that EphA2 overexpression led to increased lipogenesis and tumor growth in breast cancer cells [34]. Other FASN inhibitors also reduce the cell viability of cisplatin-resistant cells [27] and induced apoptosis in NSCLC cells [26].

GR EGFRm NSCLC cells exhibited overexpression of FASN [24,24]. Despite this, the AZ12756122 treatment decreased FASN mRNA and protein expression in all cell models (Figs. 2 and 3). This may influence the lipid content of cell membranes, since the main product of FASN is palmitate, from which different fatty acids can be formed. Moreover, the sterol regulatory element binding protein (SREBP)-1 is a master regulator of FASN and its ablation induces the apoptosis of cancer cells [35,36]. Phosphorylated EGFR levels were also diminished in all cell models (Figs. 2 and 3). Previous findings revealed that FASN inhibition also reduced FASN and EGFR protein expression in GR EGFRm NSCLC [23] and EGFRwt NSCLC [37]. Nonetheless, our research group and other researchers proved that the inhibition of FASN activity did not affect EGFR activation or its expression [24], nor did it affect FASN protein levels [24,38]. All together this suggests that although EGFR is involved in FASN regulation [23,39], the inhibition of FASN activity may not directly affect EGFR. Regarding Akt/mTOR signaling pathway, AZ12756122 reduced phosphorylated levels of Akt and PRAS40 in all cell models (Fig. 3), irrespective of their resistance to EGFR-TKIs. These results are in line with previous research [26,32,39,40]. Hence, EGFR may be another AZ12756122-direct target. The compound inhibited the Akt/PRAS40 pathway resulting in lower levels of sterol response element-binding proteins 1c (SREBP-1c) [35] and/or downstream effectors such as S6K [41] and, consequently, in FASN downregulation.

The sustained STAT3 activation found after the EGFR-TKI treatment is consistent with the literature [42]. STAT3 remained inactive after the AZ12756122 treatment in the GR models (Fig. 3). Similar results have been observed with other FASN inhibitors in EGFRm NSCLC [24], head and neck carcinomas [43], and pancreatic cancer [44]. Previously,

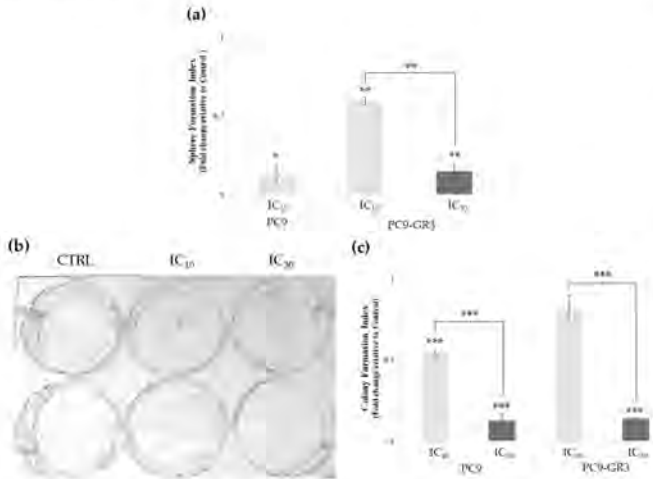


Fig. 6. AZI2756122 activity against cancer stem-like cells in sensitive and gefitinib-resistant (GR) models. (a) Sphere formation after AZI2756122 treatment. Cells were treated at concentrations equivalent to their IC₁₀ and IC₃₀ for 7 days. All conditions were compared to the control (untreated cells), which was normalized to 1 and expressed as a fold change. (b) Colony formation assay (c) Colony formation after AZI2756122 treatment. Cells were treated at concentrations equivalent to their IC₁₀ and IC₃₀ for 7 days. All conditions were compared to the control (untreated cells), which was normalized to 1 and expressed as a fold change. Experiments were performed at least three times. Statistical differences are indicated as * p < 0.05, ** p < 0.01 and *** p < 0.001.

Table 2
Patient and tumor characteristics at baseline.

	Number	Percentage
Gender		
Female	34	75.6
Male	11	24.4
Age (Years)		
Median (Q1:Q3)	68	58:74
Min: Max	46:88	
Smoking Habit		
Never	33	73.3
Former	8	17.8
Current	4	8.9
ECOG		
0	15	33.3
1	26	57.8
2	4	8.9
Histology		
Adenocarcinoma	41	91.2
Adenosquamous	2	4.4
Squamous	2	4.4
EGFR Mutation		
Exon 19	26	57.8
Exon 21	19	42.2
Response Rate to TKI		
Complete Response	1	2.2
Partial Response	30	66.7
Stable Disease	7	15.6
Progression Disease	6	13.3
Missing	1	2.2
FASN Expression		
Negative	19	42.2
Positive	17	37.8
Missing	9	20.0
EGFR-TKI Treatment Line		
First Line	37	82.2
Second Line	8	17.8

inhibition of the MAPK pathway was exhibited after treatments using FASN inhibitors or EGFR-TKIs in lung cancer [28,32,39]; which disagrees with our findings from the sensitive and T790M+ cell models. However, Geng et al. proved that the constant activation of MAPK pathway caused by a FASN inhibitor resulted in the induction of

apoptosis by upregulating apoptosis-related proteins and down-regulating pro-survival ones [45].

A combination of therapies is a widely-studied strategy to overcome EGFR-TKI resistance [32]. Palmitate overproduction has been linked to alterations in cellular response to anticancer drugs [46] and the survival of EGFR-TKI resistant EGFRm NSCLC cells [25]. Our findings show that the combinatorial treatment of AZI2756122 and gefitinib had mostly additive effects (Fig. 4). Only PC9-GR3 and PC9-GR4 cell models exhibited synergistic effects in some combinations. These results could be related to the inability of gefitinib to inhibit the Akt/mTOR signaling pathway in PC9-GR1 cells (Fig. 3), most likely due to the MET activation observed in this cell model [28]. Moreover, the Akt/mTOR signaling pathway has been proven to play an essential role in the survival of GR EGFRm NSCLC cells [23]. In PC9-GR3, the combination of AZI2756122 and osimertinib demonstrated synergistic effects and inhibition EGFR, Akt, PRAS40, and MAPK activation compared to untreated cells (Figs. 4 and 5). However, the combinatorial treatment did not prevent the STAT3 activation caused by osimertinib, which is consistent with the literature [24]. Previous studies have also found synergistic effects using the combinatorial treatment of EGFR-TKIs and Akt [26] and MAPK [47] inhibitors in EGFR-TKI-resistant NSCLC cells. Jacobsen et al., proved that Akt and MAPK activation persisted in resistant cells treated using EGFR-TKI and Akt inhibitors [28]. Akt/mTOR and MAPK signaling pathway activation is directly related to the activation and over-expression of FASN [48]. All together this suggests that FASN inhibition may be a better strategy to reduce the activation of these signaling pathways which play a key role in EGFR-TKI resistance.

The treatment using the AZI2756122 compound showed a reduction of CSC population PC9 and PC9-GR3 (Fig. 6). This subpopulation is related to resistance, relapse, and metastasis [18,19]. Similar findings were exhibited in breast cancer [49–51] and colorectal cancer [52,53]. In NSCLC, FASN inhibition has been demonstrated to cause a decrease of clonogenicity [26], migration and invasion capacities [32]. As shown in Fig. 3, AZI2756122 also caused the inhibition of Akt and PRAS40. Different studies have demonstrated that the Akt/mTOR signaling pathway is directly related to the CSC niche [50,54]. All together this suggests that FASN inhibition may reduce the CSC population by inhibiting the Akt/mTOR signaling pathway.

The demographic characteristics of our population with NSCLC

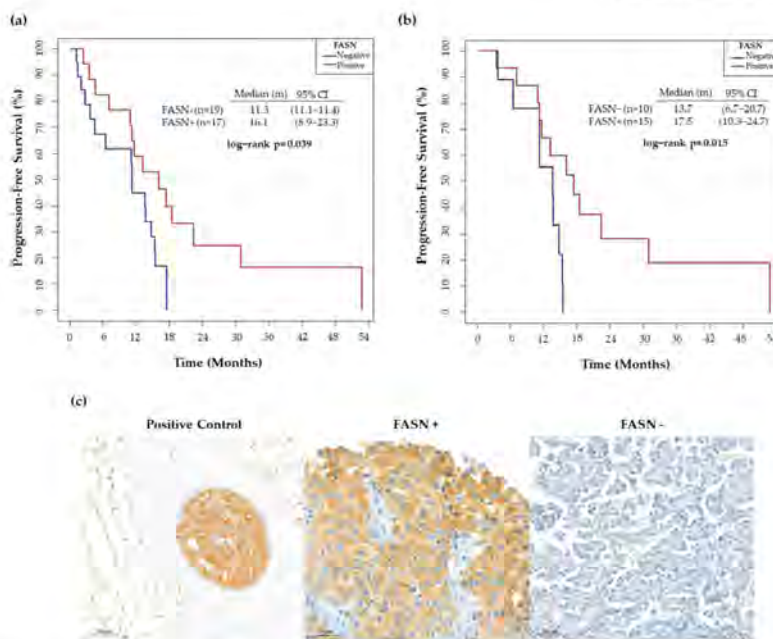


Fig. 7. (a) Median progression-free survival according to the immunohistochemistry (IHC) expression levels of FASN. The non-expression of FASN was considered as negative and any expression of FASN as positive. (b) Median progression-free survival in EGFR-TKI responders (complete response + partial response) according to the IHC expression levels of FASN. The non-expression of FASN was considered as negative and any expression of FASN as positive. (c) IHC staining of FASN in paraffin-embedded core biopsies from NSCLC patients harboring sensitizing mutations in the EGFR gene.

harboring EGFR sensitive mutations are consistent with those published in large European studies [55]. To the best of our knowledge, this is the first study to report standard levels of FASN expression in EGFRm NSCLC patients. Previous studies observed that FASN expression was higher in tumor tissues than normal and adjacent tissues [33,38,56]. FASN expression was found in 47.2% of tumor samples. Other researchers have observed FASN expression in lung adenocarcinoma samples ranging from 22% to 81% [38,57,58]. However, mutations in the EGFR gene or in other oncogenes were not considered in these investigations. No relationship was found between FASN expression and overall survival in our population, which is in agreement with the literature [38,57,59]. Additionally, FASN expression was significantly associated with longer mPFS, longer mPFS in patients who responded to EGFR-TKI treatment, and trends to a better response to the EGFR-TKI [Fig. 7], suggesting that FASN expression at baseline may have a role in a better outcome in patients with NSCLC harboring EGFR sensitizing mutations. In fact, our study (Fig. 3) and other authors [23] have demonstrated that the gefitinib treatment diminished mRNA and protein expression of FASN only in PC9 cells, i.e., the sensitive cell model. Researchers have also reported that: [1] EGFRm regulates the expression of FASN to palmitoylate EGFR and localizes it into the cell membrane of PC9 cells [23,60], and [2] FASN inhibition results in EGFR ubiquitination [23]. Taken all together, our hypothesis is that the mPFS, the response to EGFR-TKI treatment, and the mPFS according to the response to the EGFR-TKI treatment, were better in tumor samples from biopsies of FASN+ EGFRm NSCLC patients because the EGFR-TKI therapy had a dual effect: downregulating the FASN expression and inhibiting EGFR

activation. Nevertheless, our study had some methodological limitations that may have influenced the results. First, it was retrospective research, with the biases that involves. Second, the number of samples with sufficient tissue to perform IHC was lower than expected. Third, some tumor samples were relatively old, which may have influenced the IHC results. Nonetheless, in this regard, the percentage of FASN expression detected in our samples is comparable to that observed in previous studies.

5. Conclusions

Inhibition of FASN activity is a promising strategy for treating EGFRm NSCLC. The novel FASN inhibitor AZ12756122 downregulated FASN expression and activity, caused cytotoxic effects, and induced apoptosis in sensitive and EGFR-TKI-resistant EGFRm NSCLC cells. The compound also reduced phosphorylated levels of EGFR and Akt/PRAS40. Furthermore, the combinatorial treatment of AZ12756122 and osimertinib overcame resistance to EGFR-TKI, exhibiting a synergistic effect which resulted in a decrease of EGFR, Akt/PRAS40, and MAPK activation. AZ12756122 also showed activity against cancer stem-like cells in both sensitive and gefitinib- and osimertinib-resistant cell models. Finally, our study revealed that FASN+ EGFRm NSCLC patients who responded to EGFR-TKI treatment exhibited a significantly longer mPFS than those who did not express FASN. Therefore, these findings suggest that FASN inhibition should be studied further in the treatment, alone or in combination with EGFR-TKIs, of EGFRm NSCLC patients.

Funding

This research was funded by AstraZeneca (NCR-18-13804). The funders had no role in the design of the study, in the collection, analyses, or interpretation of data, in the writing of the manuscript, or in the decision to publish the results.

CRedit authorship contribution statement

EPA, RP, SRM, JC, and TP: Conceptualization. **EPA, JR, and CVD:** Methodology. **EPA, SRM, CVD, JR, RP, and JBB:** Validation. **EPA, RP and JBB:** Formal analysis. **EPA, JR, RP, and CVD:** Investigation. **JC, TP, RP, and JBB:** Resources. **EPA, RP and JBB:** Data curation. **EPA and RP:** Writing – original draft. **EPA, RP, SRM, and JBB:** Writing – review & editing. **EPA:** Visualization. **JC, TP:** Supervision. **JC, TP, RP, and JBB:** Project administration. **JC and TP:** Funding acquisition. All authors have read and agreed to the published version of the manuscript.

Conflict of interest statement

The authors declare the following financial interests/personal relationships which may be considered as potential competing interests: Teresa Puig reports financial support was provided by AstraZeneca. Joaquim Bosch-Barrera reports a relationship with Roche-Genentech that includes: funding grants. Joaquim Bosch-Barrera reports a relationship with Pfizer that includes: funding grants. Joaquim Bosch-Barrera reports a relationship with MSD Spain that includes: funding grants. Joaquim Bosch-Barrera reports a relationship with BMS that includes: funding grants. Joaquim Bosch-Barrera reports a relationship with AstraZeneca that includes: funding grants. Joaquim Bosch-Barrera reports a relationship with Novartis that includes: funding grants. Joaquim Bosch-Barrera reports a relationship with Boehringer-Ingelheim that includes: funding grants and travel reimbursement. Joaquim Bosch-Barrera reports a relationship with Vifor that includes: funding grants. Joaquim Bosch-Barrera reports a relationship with Sanofi that includes: funding grants. Joaquim Bosch-Barrera reports a relationship with LEO Pharma that includes: funding grants. Rut Porta reports a relationship with Pfizer that includes: funding grants. Rut Porta reports a relationship with Rovi that includes: funding grants. Rut Porta reports a relationship with Sanofi that includes: funding grants. Dra. Porta reports personal fees from Pfizer, Rovi, and Sanofi, outside the submitted work. Dr. Bosch-Barrera reports grants and personal fees from Roche-Genentech and Pfizer, and personal fees from MSD, BMS, AstraZeneca, Novartis, Boehringer-Ingelheim, Vifor, Sanofi, and LEO Pharma, outside the submitted work. The other authors declare that they have no competing interests.

Acknowledgments

The authors acknowledge the pre-doctoral grant of E.P.A. (2019FLB01011), and the post-doctoral grant of S.R.M. (POST-DOCUDG-2020-0002), as well as the support of the Catalan Government (2017SGR00385), the Oncolliga Foundation and RadikalSwim (OncoSwim). The authors are grateful to R. Rosell and M. A. Molina from the laboratory of Oncology Pangaea (Barcelona, Spain) for kindly providing PC9 models. The authors would particularly like to acknowledge the patients and the IDIBGI Biobank for their collaboration. The authors are also grateful to the pharmacist Maria López and the Clinical Trial Unit of Catalan Institute of Oncology for the help provided in identifying the patients treated with EGFR-TKI. The authors also thank Maria Buxó for her statistical analysis support of patients' samples. The authors also acknowledge Glòria Oliveres for the help provided in sample identification and management.

Institutional Review Board Statement

Samples from patients included in this study were processed following standard operating procedures with the appropriate approval from the Ethics and Scientific Committees. Approval of the study protocol was obtained from the Dr. Josep Trueta University Hospital Clinical Research Ethics Committee (CP_FASN_T790M_2017; approved 1 June 2017).

Informed Consent Statement

Samples from patients included in this study were provided by the Girona Biomedical Research Institute (IDIBGI) Biobank (Biobanc IDIBGI, B.0000872), integrated into the Spanish National Biobanks Network and in the Xarxa de Bancs de Tumors de Catalunya (XBTC) financed by the Pla Director d'Oncologia de Catalunya. All patients consented to the storage of the samples in the biobank and for their use in research projects.

Data availability

All data generated or analyzed during this study are included in this published article [and its supplementary information files].

Appendix A. Supporting information

Supplementary data associated with this article can be found in the online version at doi:10.1016/j.biopha.2022.113942.

References

- [1] H. Sung, J. Ferlay, R.L. Siegel, M. Laversanne, I. Soerjomataram, A. Jemal, et al., Global Cancer Statistics 2020: GLOBOCAN estimates of incidence and mortality worldwide for 36 cancers in 185 countries, *CA Cancer J. Clin.* (3) (2021) 209–249.
- [2] M.L. Foraythe, A. Al-Wethanani, O. Berthune, M. Cartonguay, A. Drucker, G. Flavosedeo, et al., Molecular profiling of non-small cell lung cancer, *PLoS One* 15 (8) (2020), e02306580.
- [3] J.L. Lynch, D.W. Bell, R. Sordella, S. Gurubhagavatula, R.A. Okimoto, B. W. Brannigan, et al., Activating mutations in the epidermal growth factor receptor underlying responsiveness of non-small-cell lung cancer to gefitinib, *N. Engl. J. Med.* 350 (21) (2004) 2129–2139.
- [4] A.R. Li, D. Chitale, G.J. Riely, W. Pao, V.A. Miller, M.F. Zakowski, et al., EGFR Mutations in Lung Adenocarcinoma: clinical testing experience and relationship to EGFR gene copy number and immunohistochemical expression, *J. Mol. Diagn.* 10 (3) (2008) 242–248.
- [5] M.H. Cohen, G.A. Williams, R. Sridhara, G. Chen, R. Pazdur, FDA drug approval summary: Gefitinib (ZD1875) (Iressa®) tablet, *Oncologist* 8 (4) (2003) 303–306.
- [6] J.E. Pezet, P.A. Janne, J.C. Lee, S. Tracy, H. Greulich, S. Gabriel, et al., EGFR mutations in lung cancer: correlation with clinical response to gefitinib therapy, *Science* 304 (5676) (2004) 1497–1500.
- [7] S. Kobayashi, T.J. Boggon, T. Dayaram, P.A. Janne, O. Kocher, M. Meyerson, et al., EGFR mutation and resistance of non-small-cell lung cancer to Gefitinib, *N. Engl. J. Med.* 352 (8) (2009) 786–792.
- [8] M.R.V. Finlay, M. Anderson, S. Ashton, P. Ballard, P.A. Bethel, M.R. Box, et al., Discovery of a potent and selective EGFR inhibitor (AZD9291) of both sensitizing and T790M resistance mutations that spares the wild type form of the receptor, *J. Med. Chem.* 57 (20) (2014) 8249–8267.
- [9] S.L. Greig, Osimertinib: first global approval, *Drugs* 76 (2) (2016) 263–273.
- [10] R.S. Thress, C.F. Pawelczak, E. Felip, B.C. Chu, D. Steirson, B. Dougherty, et al., Acquired EGFR C797S mutation mediates resistance to AZD9291 in non-small cell lung cancer harboring EGFR T790M, *Nat. Med.* 21 (6) (2015) 560–562.
- [11] A.R. Zukirli, F.H. Tan, T.L. Pnosccki, S.S. Seylli, B.B. Jusow, STAT3 signaling mediates tumor resistance in EGFR targeted therapeutics, *Mol. Cell Endocrinol.* 451 (2019) 15–24.
- [12] Q. Wang, S. Yang, K. Wang, S.Y. Sun, MET inhibitors for targeted therapy of EGFR TKI-resistant lung cancer, *J. Hematol. Oncol.* 12 (1) (2019) 63.
- [13] A.R. Corcos, C.E. Repellin, T. Shimamura, M. Capriles, K. Zeynalova, D. Jysan, et al., Resistance to irreversible EGFR receptor tyrosine kinase inhibitors through a multistep mechanism involving the EGFR pathway, *Cancer Res.* 73 (2) (2013) 834–843.
- [14] Q. Lai, S. Yu, W. Zhao, S. Qin, Q. Chu, K. Wu, EGFR-TKI resistance via EGFR-independent signaling pathways, *Mol. Cancer* 17 (1) (2018) 53.
- [15] H. Tamaguchi, T. Yamada, R. Wang, R. Tamamura, Y. Adachi, A. Nishiyama, et al., ALI confers intrinsic resistance to osimertinib and advances the emergence of tolerant cells, *Nat. Commun.* 10 (1) (2019) 259.
- [16] R. Ohashi, L.V. Sequist, M.E. Arcella, T. Moran, J. Chmielecki, V.L. Lin, et al., Lung cancers with acquired resistance to EGFR inhibitors occasionally harbor BRAF gene

- mutations but lack mutations in KRAS, NRAS, or MER1. Proc. Natl. Acad. Sci. USA 109 (31) (2012) E2127–E2133.
- [17] L.V. Sequist, B.A. Waltman, D. Dias-Santagata, S. Digumarthy, A.B. Turke, P. Fidias, et al., Genotypic and histological evolution of lung cancers acquiring resistance to EGFR inhibitors, *Sci. Transl. Med.* 3 (75) (2011) 75ra26.
- [18] S. Singh, S. Chellappan, Lung cancer stem cells: molecular features and therapeutic targets, *Mol. Asp. Med.* 39 (2014) 50–60.
- [19] Y. Yu, G. Ramena, R.C. Eblbe, The role of cancer stem cells in relapse of solid tumors, *Front. Biosci.* 1 (4) (2012) 1528.
- [20] J. Wang, Z. hong Li, J. White, L. bo Zhang, Lung cancer stem cells and implications for future therapeutics, *Cell Biochem. Biophys.* 69 (3) (2014) 389–398.
- [21] D. Hanahan, R.A. Weinberg, Hallmarks of cancer: the next generation, *Cell* 144 (5) (2011) 646–674.
- [22] L.S.S. Pulla, S. Begum Ahil, Review on target domains and natural compound-based inhibitors of fatty acid synthase for anticancer drug discovery, *Chem. Biol. Drug Des.* 98 (5) (2021) 869–884.
- [23] A. Ali, E. Levantini, J.T. Teo, J. Goggi, J.G. Clohessy, C.S. Wu, et al., Fatty acid synthase mediates EGFR palmitoylation in EGFR mutated non-small cell lung cancer, *EMBO Mol. Med.* 10 (2018) 1–19.
- [24] E. Polonio-Alcalá, S. Palomerias, D. Torres-Otero, J. Relat, M. Planas, L. Feliu, et al., Fatty acid synthase inhibitor G28 shows anticancer activity in EGFR tyrosine kinase inhibitor resistant lung adenocarcinoma models, *Cancers* 12 (5) (2020) 1–18.
- [25] N. Zhao, B. Li, X. Xu, J. Xu, S. Hu, Inhibition of FASN expression enhances radiosensitivity in human non-small cell lung cancer, *Oncol. Lett.* 15 (4) (2018) 4578.
- [26] R. Ventura, K. Mordec, J. Waszczuk, Z. Wang, J. Lai, M. Fridlib, et al., Inhibition of de novo palmitate synthesis by fatty acid synthase induces apoptosis in tumor cells by remodeling cell membranes, inhibiting signaling pathways, and reprogramming gene expression, *EBioMedicine* 2 (8) (2015) 808.
- [27] L. Yang, F. Zhang, X. Wang, Y. Tsai, K.H. Chuang, P.C. Keng, et al., A FASN-TGF- β 1-FASN regulatory loop contributes to high EMT/ metastatic potential of cisplatin-resistant non-small cell lung cancer, *Oncotarget* 7 (34) (2016) 55543–55554.
- [28] K. Jacobsen, J. Berran-Alamillo, M.A. Molina, C. Teixidó, N. Karachaliou, M. H. Pedersen, et al., Convergent Akt activation drives acquired EGFR inhibitor resistance in lung cancer, *Nat. Commun.* 8 (1) (2017) 410.
- [29] T.G. Chou, P. Talalay, Quantitative analysis of dose-effect relationships: the combined effects of multiple drugs or enzyme inhibitors, *Adv. Enzym. Regul.* 22 (C) (1984) 27–55.
- [30] J. Crous-Masó, S. Palomerias, J. Relat, C. Camó, Ú. Martínez-Garza, M. Planas, et al., (–)-Epigallocatechin 3-gallate synthetic analogues inhibit fatty acid synthase and show anticancer activity in triple negative breast cancer, *Molecules* 23 (5) (2018) 1160.
- [31] M. Sankaranarayananpillai, N. Zhang, K.A. Baggerly, J.G. Gelovani, Metabolic shifts induced by fatty acid synthase inhibitor orlistat in non-small cell lung carcinoma cells provide novel pharmacodynamic biomarkers for positron emission tomography and magnetic resonance spectroscopy, *Mol. Imaging Biol.* 15 (2) (2013) 136–147.
- [32] L. Chang, S. Pang, Y. Chen, Z. Yang, Y. Yuan, J. Zhang, et al., Inhibition of FASN suppresses the malignant biological behavior of non-small cell lung cancer cells via deregulating glucose metabolism and AKT/ERK pathway, *Lipids Health Dis.* 18 (1) (2019) 118.
- [33] Y. Yan, Y. Zhou, J. Li, Z. Zheng, Y. Hu, L. Li, et al., Sulforaphane downregulated fatty acid synthase and inhibited microtubule-mediated mitophagy leading to apoptosis, *Cell Death Dis.* 12 (10) (2021) 917.
- [34] V.M. Youngblood, L.C. Kim, D.N. Edwards, Y. Hwang, P.R. Santapuram, S. M. Stridivan, et al., The ephrin-A1/EPHA2 signaling axis regulates glutamine metabolism in HER2-positive breast cancer, *Cancer Res.* 76 (7) (2016) 1825.
- [35] J.A. Menendez, R. Lupu, Fatty acid synthase: a druggable driver of breast cancer brain metastasis, *Expert Opin. Ther. Targets* 26 (5) (2022) 427–444.
- [36] B. Griffiths, C.A. Lewis, K. Bensaad, S. Ros, Q. Zhang, E.C. Ferber, et al., Sterol regulatory element binding protein-dependent regulation of lipid synthesis supports cell survival and tumor growth, *Cancer Metab.* 1 (1) (2013) 3.
- [37] F. Shi, C. Wang, L. Wang, X. Song, H. Yang, Q. Fu, et al., Preparative isolation and purification of steroidal glycoalkaloid from the ripe berries of *Solanum nigram* L. by preparative HPLC-MS and UHPLC-TOF-MS/MS and its anti-non-small cell lung tumors effects in vitro and in vivo, *J. Sep. Sci.* 42 (15) (2019) 2471–2481.
- [38] H. Orita, J. Coulier, C. Lemmon, E. Tully, A. Vadlamudi, S.M. Medghalchi, et al., Selective inhibition of fatty acid synthase for lung cancer treatment, *Clin. Cancer Res.* 13 (23) (2007) 7139–7145.
- [39] J. Relat, A. Blancafort, G. Oliveras, S. Cuff, D. Haro, P.F. Marrero, et al., Different fatty acid metabolism effects of (–)-Epigallocatechin-3-Gallate and C75 in Adenocarcinoma lung cancer, *BMC Cancer* 12 (2012) 280.
- [40] A. Giro-Perafita, S. Palomerias, D.H. Lum, A. Blancafort, G. Viñas, G. Oliveras, et al., Preclinical evaluation of fatty acid synthase and EGFR inhibition in triple-negative breast cancer, *Clin. Cancer Res.* 22 (18) (2016) 4687–4697.
- [41] M.J. Sanad, S. Razi, A. Pourboghri-Sigaroodi, D. Bashah, The PI3K/Akt/mTOR pathway in lung cancer; oncogenic alterations, therapeutic opportunities, challenges, and a glance at the application of nanoparticles, *Transl. Oncol.* 18 (2022) 101364.
- [42] T. Ninomiya, N. Takigawa, E. Ichihara, N. Ochi, T. Murakami, Y. Honda, et al., Afatinib prolongs survival compared with gefitinib in an epidermal growth factor receptor-driven lung cancer model, *Mol. Cancer Ther.* 12 (5) (2013) 589–597.
- [43] H.Y. Lin, S.C. Hou, S.C. Chen, M.C. Kao, C.C. Yu, S. Funayama, et al., (–)-Epigallocatechin gallate induces Fas/CD95-mediated apoptosis through inhibiting constitutive and IL-6-induced JAK/STAT3 signaling in head and neck squamous cell carcinoma cells, *J. Agric. Food Chem.* 60 (10) (2012) 2480–2489.
- [44] S.N. Tang, J. Fu, S. Shankar, R.K. Srivastava, EGCG enhances the therapeutic potential of gemcitabine and CP690550 by inhibiting STAT3 signaling pathway in human pancreatic cancer, *PLoS One* 7 (2) (2012) e31967.
- [45] Y. Geng, Y. Zhou, S. Wu, Y. Hu, K. Liu, Y. Wang, et al., Sulforaphane induced apoptosis via promotion of mitochondrial fusion and ERK1/2-mediated 26S proteasome degradation of novel pro-survival bax and upregulation of bax in human non-small cell lung cancer cells, *J. Cancer* 8 (13) (2017) 2456.
- [46] X. Wu, L. Qin, V. Fako, J.T. Zhang, Molecular mechanisms of fatty acid synthase (FASN)-mediated resistance to anti-cancer treatments, *Adv. Biol. Regul.* 54 (1) (2014) 214–221.
- [47] B.M. Ky, J.Y. Heo, J. Kim, J.M. sun, S.H. Lee, J.S. Ahn, et al., ERK inhibitor ASN007 effectively overcomes acquired resistance to EGFR inhibitor in non-small cell lung cancer, *Invest New Drugs* 40 (2) (2022) 265–273.
- [48] W. Khan, D. Augustine, R. Rao, S. Patil, K. Awari, S. Sowmya, et al., Lipid metabolism in cancer: a systematic review, *J. Carcinog.* 20 (1) (2021) 4.
- [49] A. Giro-Perafita, M. Rabionet, M. Planas, L. Feliu, J. Giurana, S. Ruiz-Martínez, et al., EGCG-derivative G28 shows high efficacy inhibiting the mammosphere-forming capacity of sensitive and resistant TNBC models, *Molecules* 24 (6) (2019) 1–15.
- [50] M. Rabionet, E. Polonio-Alcalá, J. Relat, M. Yeste, J. Sims-Mouratada, A.M. Kloxin, et al., Fatty acid synthase as a feasible biomarker for triple negative breast cancer stem cell subpopulation cultured on electrospray scaffolds, *Mater. Today Bio* 12 (2021), 100155.
- [51] L. Li, C.C. Liu, X. Chen, S. Xu, S.H. Cortes-Manno, S.H. Cheng, Mechanistic study of bakuchiol-induced anti-breast cancer stem cell and in vivo anti-metastasis effects, *Front. Pharmacol.* 8 (2017) 746.
- [52] M.T.E. Montales, R.C.M. Simmen, E.S. Ferreira, V.A. Neves, F.A. Simmen, Metformin and soybean-derived bioactive molecules attenuate the expansion of stem cell-like epithelial subpopulation and confer apoptotic sensitivity in human colon cancer cells, *Genes Nutr* 10 (6) (2015) 49.
- [53] H. Dianat-Moghadam, M. Khalili, M. Keshavarz, M. Azizi, H. Hamishehkar, R. Rabbarghazi, et al., Modulation of LXR signaling altered the dynamic activity of human colon adenocarcinoma cancer stem cells in vitro, *Cancer Cell Int* 21 (1) (2021) 100.
- [54] L. Yang, P. Shi, G. Zhao, J. Xu, W. Peng, J. Zhang, et al., Targeting cancer stem cell pathways for cancer therapy, *Signal Transduct. Target Ther.* 5 (1) (2020) 8.
- [55] R. Rosell, T. Moran, C. Queralt, R. Porta, F. Cardenal, C. Camps, et al., Screening of epidermal growth factor receptor mutation in lung cancer, *N. Engl. J. Med.* 361 (2009) 958–967.
- [56] H. Orita, J. Coulier, E. Tully, F.P. Kuhajda, E. Gabrielson, Inhibiting fatty acid synthase for chemoprevention of chemically induced lung tumors, *Clin. Cancer Res.* 14 (8) (2008) 2458–2464.
- [57] P. Visca, V. Sebastiani, C. Botti, M.G. Diiodoro, R.P. Lasagni, F. Romagnoli, et al., Fatty Acid Synthase (FAS) is a marker of increased risk of recurrence in lung carcinoma, *Anticancer Res.* 24 (6) (2004) 4169–4173.
- [58] Y. Wang, X. Zhang, W. Tan, J. Fu, W. Zhang, Significance of fatty acid synthase expression in non-small cell lung cancer, *Zhonghua Zhong Liu Za Zhi* 3 (24) (2002) 271–273.
- [59] D. Cerne, I. Prodan Zljinik, M. Sok, Increased fatty acid synthase activity in non-small cell lung cancer tissue is a weaker predictor of shorter patient survival than increased lipoprotein lipase activity, *Arch. Med. Res.* 41 (6) (2010) 405–409.
- [60] L.R. Bollu, R.R. Katreddy, A.M. Blessing, N. Pham, B. Zheng, X. Wu, et al., Intracellular activation of EGFR by fatty acid synthase dependent palmitoylation, *Oncotarget* 6 (33) (2015) 34992–35003.

Discussion

1. Evaluation of poly(lactic acid) (PLA) scaffolds for 3D cell culture of breast CSC (BCSC)

CSCs are a small subpopulation of tumor cells responsible for carcinogenesis, tumor recurrence and progression, and metastasis. This malignant group of cells has specific characteristics such as self-renewal, pluripotency, and resistance to therapy [167–170]. Hence, the eradication of CSCs is necessary for effective anti-cancer treatment.

TNBC does not have a therapeutic target because it lacks ER, PR, and HER2 expression [127], and the only treatment available for these patients is chemotherapy [132,154,157]. Furthermore, patients with TNBC have a poor prognosis because the disease arises in young women, with high mortality and metastasis rates [128,146,147]. Thus, BCSCs may be a potential therapeutic target for this aggressive subtype of breast cancer. Unfortunately, no standard treatment is available for this malignant population.

Additionally, the majority of studies do not consider the microenvironment of CSCs because they are isolated [254] or cultured on flat surfaces such as Petri plates, which results in changes in cell behavior, either in cell proliferation or in gene and/or protein expression [257,263,276]. Two-dimensional (2D) cell culture also induces CSC differentiation [330,331], making it impossible to investigate them *in vitro*. Consequently, culture systems that allow their study are required so that researchers can find novel therapeutic strategies for CSCs.

Among the technologies that exist to manufacture 3D structures for cell culture purposes, the FFF and ES stand out for their simplicity and cost-effectiveness [257,278,287,288]. In addition, PLA is extensively used for biomedical applications due to its characteristics, such as biodegradability, biocompatibility, and safety [320,324–326]. However, only PLA scaffolds mixed with other materials, but not as sole material, have been tested for cancer cell culture using these two additive manufacturing techniques [328,329]. Therefore, the use of PLA for the manufacturing of FFF- and ES-scaffolds was evaluated in this section. Specifically, the ability of the scaffolds to culture a TNBC cell model, MDA-MB-231, and their capacity to enrich the CSC population were analyzed.

First, 27 scaffold models were designed considering five 3D printing parameters (*layer height, infill density, infill pattern, infill direction, and flow*) according to the Taguchi

Discussion

experimental design. Subsequently, they were manufactured using the BCN3D Sigma R17 3D printer. Pore areas of PLA-FFF structures were very distinct among the configurations. For example, some of the produced PLA-FFF structures were less than 0.1 mm^2 , while others were larger than 1 mm^2 . Furthermore, some PLA-FFF matrices had irregular pores, for instance, designs 15 and 27. Pore size is essential because it is directly related to cell growth and migration, nutrient and gases exchange, and remission of various molecules into the surrounding medium [400,401]. Although all PLA-FFF platforms had a similar filament diameter, fibers were slightly thicker when the flow increased because more material was extruded [402].

The influence of the 3D printing parameters on cell adhesion and proliferation was assessed by culturing MDA-MB-231 cells into PLA-FFF structures for 3 days. TNBC cells seeded on PLA-FFF matrices showed a cell growth ranging from approximately 5 to 25% compared to monolayer. Scaffolds with larger pores exhibited low cell proliferation, whereas PLA-FFF platforms with smaller pores exhibited higher cell proliferation. These results are directly related to the quantity of material available for cells to adhere to it, which is in agreement with the literature. Guerra *et al.* demonstrated that the smaller the pore area and the more material available, the higher the cell proliferation using cardiac stents printed using the FFF technique [403].

These data were analyzed using the Quantum XL software. The parameters *infill density* and *infill direction* had a significant influence on cell proliferation, with optimal values of 70% and 45° , respectively. These findings suggest that cell attachment and proliferation increase when more material and corners are available; thus, cells can communicate easily and grow faster. Several studies have shown that the scaffold geometry affects cell adhesion and proliferation. The orientation, layout, and stepped filaments are relevant parameters that affect cell behavior and must be considered. In addition, the researchers highlighted the importance of optimizing scaffold geometry for each cell type [404,405]. In fact, our research group observed that MCF-7 breast cancer cells displayed higher cell proliferation in scaffolds with an infill direction of 60° , whereas NIH/3T3 fibroblasts preferred scaffolds with an infill direction of 90° [313]. Hence, the PLA-FFF structure with the optimal theoretical values, SS1, was manufactured. The SS1 scaffold showed the highest cell proliferation in this study,

approximately 24% compared to 2D, including the initial 27 PLA-FFF matrices, validating the Taguchi experimental design applied. Moreover, the SS1 scaffolds exhibited the second lowest pore area of the study, concretely 0.054 mm^2 . As previously observed, the PLA-FFF platforms with the lowest pore areas demonstrated the highest cell proliferation.

Regarding PLA-ES scaffolds, two 3D structures were manufactured by preparing solutions with different polymer concentrations: 12% and 15%. The 12%-PLA solution was chosen because lower concentrations resulted in electrospray. The electrospray technique is similar to ES, usually involving more dilute polymer solutions, and it is used to create polymeric particles that have been employed in the biomedical field to encapsulate other molecules, such as drugs or proteins [406,407]. Thus, the 12%-PLA solution was the lowest amount of polymer that allowed electrospinning. In contrast, solutions with concentrations greater than 15% were excessively viscous and difficult to manufacture. Both PLA-ES matrices had fibers with an average diameter of $7 \text{ }\mu\text{m}$ and pore areas of approximately $0.3 \text{ }\mu\text{m}^2$. However, the 12%-PLA platforms had another population of thinner filaments, with an average diameter of 385 nm, and non-filamentary elements (called beads), which are normally observed in low-concentration solutions [408]. The PLA-ES fibers also exhibited surface roughness. In contrast, a study reported that 15%-PLA-ES scaffolds had filaments with a diameter of $4.5 \text{ }\mu\text{m}$, and a second population of thinner fibers was present [409]. Additionally, the use of chloroform as a dissolvent to prepare the polymeric solution directly influenced the filament diameter. For example, Chi and colleagues manufactured 40%-PLA-ES fibers with a diameter of $0.4 \text{ }\mu\text{m}$ because the solvent used was trifluoroacetic acid [410].

MDA-MB-231 cells were seeded on PLA-ES matrices for 3 and 6 days and cell adhesion and proliferation were analyzed. TNBC cells exhibited a high proliferation rate of approximately 70% compared to 2D-cultured cells, which might be attributed to the roughness of the filaments. This feature enhances the initial cell attachment and, consequently, cell growth [411]. Slight differences in the microarchitecture between both 3D platforms did not affect either cell adhesion or proliferation because similar proliferation values were obtained at both culture times tested. Although cell growth was slightly lower after 6 days, no significant changes were observed between the two culture periods.

Discussion

Comparing both methodologies, PLA-FFF scaffolds had approximately 60 times thicker fibers than PLA-ES ones. Consequently, the pore area of PLA-FFF matrices was around 6 million times larger than that of the PLA-ES scaffolds. The pore area plays a fundamental role in cell culture, as it directly influences the infiltration of cells into the scaffold [412]. The diameter of most human cells is approximately 20-50 μm (except for some cases, such as adipocytes and oocytes) [413]. On this basis, the results suggest that PLA-FFF pores were so large that many cells were lost through them at the time of seeding, and thus, they did not adhere to the scaffold. Moreover, cell-cell and cell-matrix communications, which play a relevant function in cell behavior [414], are facilitated when fibers and pores are smaller. Therefore, PLA-ES scaffolds exhibited higher cell adhesion and proliferation than PLA-FFF ones, even considering the configuration SS1, which had the optimal 3D printing parameters obtained by the Taguchi experimental design. Lombardo and coworkers reported the direct influence of pore sizes on cell adhesion and the resulting morphology of the MDA-MB-231 cells cultured on PLA scaffolds produced by thermally induced phase separation (TIPS) [415]. Besides, both types of 3D structures showed inferior cell proliferation than monolayer culture because 3D cell culture slows down cell growth, migration through pores, and proliferation among layers [315,416].

In addition to evaluating the ability of PLA scaffolds as a 3D cell culture system, it was assessed whether MDA-MB-231 cells seeded on these 3D platforms showed CSC enrichment.

Regarding PLA-FFF matrices, the ALDH activity was quantified to verify whether the BCSC population had increased in TNBC cells cultured on PLA-FFF scaffolds for 3 and 6 days. Elevated ALDH activity has been used as a biomarker for CSC [202–204]. Three different configurations were tested, but only the SS1 design significantly enhanced the ALDH+ population after 3 days of culture. The other configurations and days evaluated did not show any significant changes. Hence, the design SS1 allows for higher proliferation and expansion of BCSCs at short culture times. To the best of our knowledge, this is the first time PLA-FFF scaffolds have been employed to culture and expand this malignant subpopulation. Similar results were described by Rabionet *et al.*, who reported that MCF-7 breast carcinoma cells seeded on PCL-FFF platforms significantly increased the mammosphere formation index

(MFI) [314], an ability characteristic of CSCs to grow as spheres under anchorage-independent conditions [173,174].

Concerning PLA-ES structures, MDA-MB-231 cells cultured on 15%-PLA platforms showed a significant *SOX2* upregulation after 3 days and STAT3 activation after 3 and 6 days of culture. These markers have been associated with BCSCs, and thus could indicate an increase in this malignant population [221,417]. However, a significant *SOX2* decrease after 6 days of 3D cell culture and no significant variations in MFI were observed between cells seeded on 2D and 15%-PLA-ES scaffolds. Although a trend was noted, significant changes in genes related to the EMT process, such as *SNAIL*, *CDH1* (E-cadherin), and *VIM* (Vimentin), were neither displayed. The EMT process allows CSCs to invade other areas of the body and create metastases [213,215,216]. Additionally, a reduction of phosphorylated EGFR levels was observed in TNBC cells cultured on 15%-PLA-ES matrices. These results were surprising, as EGFR signaling is involved in cell proliferation, differentiation, and survival [38]. Nevertheless, Ekert and colleagues declared that, in contrast to 3D-cultured cells, 2D-cultured cells are directly exposed to medium' growth factors that induce EGFR expression and activation [418]. Previous investigations using the same cell model cultured in 15%-PCL-ES scaffolds showed a significant increase in MFI and ALDH activity [312], upregulation of EMT- and stemness-related genes, and resistance to chemotherapy treatment [392]. Moreover, Li and coworkers compared the behavior of breast cancer cells on different types of scaffolds. Although cells seeded on PLA scaffolds had superior proliferation compared to decellularized lung and chitosan/gelatin scaffolds, they did not exhibit the same tumorigenic capacity as the other two types [419]. Researchers also found different applications for PLA structures concerning stem cells. On the one hand, Islami *et al.* reported that PLA matrices coated with fibronectin and collagen, two ECM proteins, were suitable for the *in vitro* expansion of stem cells from umbilical cord blood [332]. On the other hand, Enderami and colleagues demonstrated that PLA/PVA platforms promoted the differentiation of human induced pluripotent stem cells (iPSCs) [420].

Considering these findings, PLA scaffolds are a suitable 3D cell culture system. Comparing both manufacturing techniques, FFF structures are more economical and user-friendly, whereas ES matrices are more expensive because of the purchase price of the ES machine

Discussion

[257,278,287,288]. However, PLA-ES scaffolds are preferable because they more closely resemble the ECM and allow better cell-cell and cell-matrix communications than PLA-FFF platforms. Similar results were also observed with PCL scaffolds [312,314]. Regarding BCSC population expansion, PLA scaffolds did not expand this malignant population as effectively as PCL ones [312,314,392]. One reason for these differences between the two materials could be their stiffness. PLA is stiffer than PCL [421]. It is described that adequate stiffness is essential for cell adhesion, morphology, cell growth, and cell differentiation [422]. It is also known that changes in cell morphology affect gene and protein expression [423,424]. Another hypothesis could be that the cell morphology of MDA-MB-231 cells cultured on PCL structures is more similar to that *in vivo*, thus allowing the increase of BCSCs, than cells seeded on PLA ones. In fact, TNBC cells cultured on PCL matrices were more elongated than 2D-cultured cells. However, the morphology of the MDA-MB-231 cells seeded on PLA matrices should be studied to confirm this hypothesis.

Therefore, PCL-ES scaffolds were selected for further investigation with another aggressive cancer, non-small cell lung cancer.

2. Evaluation of polycaprolactone (PCL) scaffolds manufactured by ES technology for 3D cell culture of lung CSCs (LCSC)

The identification of mutations in the *EGFR* gene revolutionized the treatment of patients with EGFRm NSCLC, allowing the introduction of several EGFR-TKIs [49,62]. Nevertheless, the therapeutic efficacy of these drugs is limited because most patients develop resistance to them [72]. At this point, chemotherapy is the most frequently used therapeutic modality. Additionally, most patients with NSCLC are diagnosed at advanced stages of the illness when treatment is unsuccessful [19]. NSCLC is also prone to drug toxicity, resistance, and malignant migration [20]. Hence, the removal of LCSCs may be a therapeutic strategy to avoid treatment resistance, relapse, and metastasis.

The importance of establishing a 3D culture system for the expansion of this malignant population has been discussed in the previous chapter. The results indicated that PCL-ES scaffolds were the best option for increasing the BCSC niche compared to other 3D

structures [312,392]. PCL is an inexpensive biocompatible polymer widely used in biomedical applications and approved by FDA [305–307]. Therefore, in this section, the ability of PCL-ES matrices to culture the LCSC population was evaluated in sensitive and resistant EGFRm NSCLC cell models. Two polymer concentrations were employed to fabricate these 3D platforms: 10% and 15%.

First, thermal characterization of the PCL-ES scaffolds was performed by TGA, DSC, and DMA analysis. The TGA and DSC results were consistent with those found in the literature [425,426], and no differences were observed between the 10%- and 15%-PCL-ES structures. The stiffness was measured using DMA. As previously mentioned, suitable stiffness of 3D platforms is critical for cell attachment, morphology, proliferation, and differentiation [422]. PCL-ES scaffolds (4.52-5.40 MPa) proved to be softer than polystyrene surfaces (2100 MPa), but stiffer than healthy lung tissue (1.40 kPa) [427,428], which is in agreement with other studies [392].

Visualization of the microarchitecture of the PCL-ES matrices revealed that the 15%-PCL-ES structures had significantly higher fiber diameter, porosity, and pore area than the 10%-PCL-ES ones. The results obtained depend largely on the solvent used for the solutions' preparation, which in this case was acetone. The use of the same amount of polymer dissolved in other solvents resulted in a change in the filament diameter [429]. Besides, a porosity of 82% was achieved in the 15%-PCL-ES matrices, similar to the recommended value (~90%) to provide adequate space for cell adhesion, migration, and ingrowth into the scaffold, as well as optimal nutrient exchange and metabolic elimination [430]. Another difference observed was that only 10%-PCL-ES platforms exhibited beads, which reduced cell attachment and growth kinetics [431]. Comparing 15%-PLA- and 15%-PCL-ES structures, the average filament diameter of PLA-ES scaffolds was approximately four times greater than that of PCL-ES ones, but the pore area of PCL-ES was 2.3 times larger than that of PLA-ES platforms.

PCL-ES scaffolds were sterilized by overnight ethanol 70% and UV light for 30 minutes. This process resulted in a significant increase of approximately 5% in the weight of the PCL-ES structures. It has demonstrated that neither of these methodologies individually affects nanofiber morphology, molecular weight, or thermal properties [432]. However, Horakova

Discussion

et al. only evaluated ethanol exposure for 30 minutes, whereas the exposure time was overnight and both approaches were employed in our study. In contrast, soaking the 3D meshes in the medium for 28 days did not cause any variation in their weight.

PC9 and PC9-GR3 cells were cultured on PCL-ES matrices for 3 and 6 days, and cell attachment, proliferation, and morphology were analyzed. EGFR^m NSCLC cell models exhibited higher cell viability on 15%-PCL-ES platforms than on 10%-PCL-ES ones, probably because of the presence of beads [431], and also after 3 days of culture than after 6 days. Protein adsorption influences cell-scaffold interactions, which determine cell adhesion and proliferation [433], and might be related to these findings. Interestingly, the 3D meshes showed significantly greater protein adsorption after 3 days than after 6 days. Moreover, the 15%-PCL-ES scaffolds had slightly higher adsorption than the 10%-PCL-ES ones. Although different cell models were employed, the cell proliferation of PLA-ES structure-cultured MDA-MB-231 cells was considerably higher than that observed in PCL-ES mesh-cultured EGFR^m NSCLC cells, with the maximum value obtained after 3 days of culture being approximately 50% in PC9 cells seeded on 15%-PCL-ES platforms. These results could be explained by the fact that PCL fibers do not display roughness, whereas PLA filaments do. Fiber roughness improves cell adhesion and proliferation [411] and is critical for the protein adsorption capacity, as it increases the surface area for protein binding [434,435]. As mentioned in the previous chapter, another reason why cell proliferation in PLA-ES scaffolds is higher is the pore area, which is smaller than that of PCL-ES structures.

In addition, the nucleus and cytoplasm of PC9 cells and the nucleus of PC9-GR3 cells cultured on 15%-PCL-ES scaffolds were significantly more elongated than those of the 2D-seeded cells. As previously mentioned, changes in cell morphology affect gene and protein expression [423,424]. In fact, PC9 cells cultured on 3D structures for 6 days showed lower levels of β -actin and γ -tubulin. In PC9-GR3 cells, α - and β -tubulin expression after 3 days of culture and γ -tubulin after 6 days increased their expression. These alterations have been related to a motile phenotype, tumorigenic activity, chemoresistance, and lower survival in patients with NSCLC. Concerning the EGFR status of sensitive and resistant EGFR^m NSCLC cells seeded on PCL-ES matrices, total EGFR protein expression decreased compared to monolayer-cultured cells, which is in concordance with the literature [418]. Nevertheless,

EGFR activation remained unchanged, presumably to preserve LCSC characteristics like self-renewal and pluripotency [436,437].

Several LCSC markers were investigated to validate whether PCL-ES platforms allow the enrichment of the LCSC niche. Both cell models cultured on PCL-ES scaffolds demonstrated higher EGFR-TKI resistance, upregulation of different genes and proteins related to the EMT process, stemness, and surface markers, and activation of the Hedgehog pathway. Hence, the identification of more than three stem cell markers (88) confirmed the expansion of this malignant subpopulation in sensitive and resistant EGFR^m NSCLC cell models seeded on these 3D structures.

Concretely, PC9 and PC9-GR3 cells cultured on PCL-ES matrices exhibited significantly higher resistance to osimertinib, caused by the LCSC population [223], and enhanced levels of the multi-drug efflux pump *ABCB1*, which is associated with poor response to therapy [438,439]. Regarding the EMT process, there was upregulation of Vimentin, *SNAIL*, and *TWIST* and downregulation of E-cadherin. EMT activation induces resistance to treatment in cancer cells through the upregulation of ATP-binding cassette transporters such as *ABCB1* [218]. Additionally, NSCLC cancer cells can change their dependence from EGFR to AXL receptor owing to the EMT process, producing resistance to EGFR-TKIs [440]. *SNAIL* is responsible for generating CSCs and initiating metastasis in breast cancer [441]. Both cell models seeded on PCL-ES platforms displayed increased levels of *SOX2* and Oct-4A and activation of Sox2. Although Sox2 has been described as a regulator of self-renewal and pluripotency independent of Oct-4 and Nanog [442] and has been associated with EGFR-TKI resistance [222], Oct-4 can cause gefitinib resistance by modulating CSC properties in EGFR^m NSCLC cells [443]. Guo *et al.* reported that Snail regulates the promotion of the EMT process and cancer stemness [444]. PCL-ES-cultured cells also demonstrated activation of the Hedgehog pathway, which supports the EMT process and drug resistance [445,446]. EGFR and the Hedgehog pathway can co-stimulate several LCSC markers, such as Sox2 [447]. Concerning surface markers, there was upregulation of CD166 and decreased CD133 protein expression. Different studies reported that CD166⁺ cells overexpressed Sox2 and Oct-4A, communicated with the Hedgehog pathway [198], and increased Vimentin, Snail, and Twist in NSCLC cells [448]. Regarding CD133, different researchers have obtained contradictory results, and

Discussion

some have reported no difference between CD133+ and CD133- cells [192,193,195,449–451]. However, none of these studies considered the mutational status of oncogenes. Therefore, this variability in the results could be due to the inherent heterogeneity of NSCLC.

Although both 3D platforms allowed the expansion of LCSCs, the 15%-PCL-ES scaffolds were a better 3D cell culture system than the 10%-PCL-ES ones, which is in agreement with previous findings using breast cancer cells [312]. The 15%-PCL-ES matrices were bead-free, exhibited higher cell adhesion, elongation, and proliferation, and some LCSC markers were upregulated only in the 15%-PCL-ES structures. Moreover, changes due to 3D culture, mainly in the EMT process and stemness and pluripotency abilities, were observed in PC9-GR3 cells after 6 days of culture, whereas in PC9 cells, these variations were already visible after 3 days. EGFR-TKI resistance has been associated with the EMT process and the abilities of stemness and pluripotency. Hence, resistant EGFRm NSCLC cells may already have a baseline overexpression of these characteristics, and additional days are required to visualize the differences between 2D- and 3D-culture.

In addition, vimentin and CD133 expression were analyzed in tumor biopsies from 36 patients with EGFRm NSCLC. Patients with vimentin expression tended to have low PFS, which is in agreement with other studies [452,453]. In contrast, patients with CD133 non-expression had low OS, disease progression, distant metastasis, and a poor degree of histological differentiation. To the best of our knowledge, basal CD133 expression levels in patients with EGFRm NSCLC have not been explored previously. Similar to the *in vitro* results, different investigations found contradictory results in the use of CD133 as a prognostic marker for patients with NSCLC [454–457]. Thus, our study highlights the importance of reviewing LCSC biomarkers because the mutational status has been shown to determine the presence of these markers.

Therefore, the results observed in the patients' biopsies reinforce the PCL-ES scaffolds as a suitable 3D culture system for culturing sensitive and resistant EGFRm NSCLC cells, which is consistent with the *in vitro* findings. In addition to expanding LCSCs, these 3D structures allow the cells to behave similarly to the physiological environment; therefore, the findings made, whether it is the testing of a new drug or the discovery of a new biomarker, will have higher reliability.

3. Inhibition of FASN as a new therapeutic strategy for the treatment of EGFRm NSCLC

The deregulation of cellular energy metabolism has been established as a hallmark of cancer [6]. In cancer, lipids are involved in multiple processes, such as tumorigenesis, cell survival, proliferation, migration, invasion, and metastasis, and they play a key role in the post-translational modification of proteins [340,341]. FASN is a fundamental enzyme for *de novo* lipogenesis [338], and its overexpression and/or hyperactivation have been reported as a resistance mechanism in cancer cells [339]. Additionally, the upregulation of FASN has been related to the ability to grow in anchorage-independent conditions [458], a trait associated with the CSC population [173,174]. Although there are many unresolved questions about the relationship between EGFRm and FASN, Ali *et al.* reported that palmitoylation of EGFRm was essential for the survival of resistant EGFRm NSCLC cells [373]. As mentioned previously, the efficacy of EGFR-TKIs is limited because most patients develop resistance to treatment [72]. CSCs are responsible for tumor relapse, progression, metastasis, and therapy resistance [167–170]. Hence, the inhibition of FASN, alone or in combination with EGFR-TKIs, may be a therapeutic approach for sensitive and resistant EGFRm NSCLC cells and the removal of LCSCs.

Specifically in this chapter, in addition to the sensitive model — PC9 cells —, three PC9-derived resistant cell models — PC9-GR1, PC9-GR3, and PC9-GR4 cells — were used. PC9-GR1 and PC9-GR4 exhibit resistance to gefitinib treatment. Both cell models harbor the secondary T790M mutation and show EphA2 activation. Moreover, PC9-GR1 possesses Axl overexpression, whereas PC9-GR4 demonstrates MET activation. In contrast, PC9-GR3 cells are resistant to treatment with gefitinib and osimertinib, but the cell model does not harbor the T790M mutation and possesses Bcl-2 overexpression [106].

First, gene and protein levels of FASN were determined in sensitive and resistant EGFRm NSCLC cell models. Resistant cells exhibited significantly higher FASN protein expression than sensitive cells, which is in agreement with the literature [373]. These findings suggest the contribution of FASN in the acquisition of EGFR-TKI resistance.

Discussion

Previous studies observed that other FASN inhibitors, such as cerulenin or TVB-3166, caused cytotoxic effects in sensitive and cisplatin-resistant NSCLC cells [377,459]. Thus, the cytotoxicity of three different compounds — EGCG, G28, and AZ12756122 — was analyzed in sensitive and resistant EGFRm NSCLC cell models. The compounds displayed cytotoxic effects in all cell models. Concretely, the IC₅₀ values of the natural polyphenolic compound EGCG ranged from 75 to 90 μM; its derivative G28 oscillated from 12 to 18 μM; and the synthetic compound AZ12756122 fluctuated from 45 to 77 μM. Hence, G28 demonstrated a more potent cytotoxic effect than the other compounds, as lower concentrations were needed to produce the same cytotoxicity. Regarding the G28 compound, PC9-GR3 cells were significantly more resistant to the treatment than the other cell models, probably because of the Bcl-2 overexpression showed only by PC9-GR3 cells. Schroeder and coworkers revealed that FASN inhibition elevated levels of pro-death proteins, but did not decrease the high expression of Bcl-2, a pro-survival protein, in breast cancer cells [460]. Pro-death protein levels must be higher than pro-survival proteins for cells to enter apoptosis. This would explain why higher concentrations of G28 were required to cause cytotoxic effects on PC9-GR3 cells. In contrast, the AZ12756122 IC₅₀ value of PC9-GR3 cells was significantly lower compared to PC9-GR1 and PC9-GR4 cells. The T790M+ cell models displayed EphA2 activation, which lead to lipogenesis, lipid accumulation, and tumor growth [461]. These results suggest that the response of FASN inhibitors was influenced by the distinct cellular resistance mechanisms, but was not determinative. Furthermore, G28 treatment barely provoked PARP cleavage in any cell model, whereas EGCG and AZ12756122 compounds induced apoptosis only in PC9, PC9-GR1, and PC9-GR3. These findings suggest that the treatment with G28 in all cell models and the treatment with EGCG or AZ12756122 in PC9-GR4 cells caused suppression of cell viability in an apoptosis-independent manner, as observed in NSCLC cells treated with low doses of resveratrol, which inhibited cell growth by overexpression of p53 and p21, ROS levels, or double-stranded DNA breaks [462].

The ability to inhibit the FASN activity of the three compounds was also tested. Previous investigations reported that Orlistat suppressed FASN activity in H1975 cells, but not in H3255 and PC14, suggesting that this drug was only useful in cells harboring the secondary T790M mutation [463]. In contrast, G28 and AZ12756122 decreased the activity in both

sensitive and resistant EGFRm NSCLC cell models, independently from the presence of the T790M mutation. A higher FASN suppression was obtained with G28 than with AZ12756122, particularly in PC9-GR3 cells. However, EGCG was able to reduce FASN activity only in PC9 cells. The capacity of the natural compound to inhibit the enzyme was 5.5 times less effective than its derivative. Thus, the anti-tumor effect of EGCG is independent of FASN inhibition in GR models. Previous studies demonstrated that EGCG could suppress FASN activity in wild-type EGFR NSCLC cells [381]. Nevertheless, EGCG has multiple targets and is involved in many signaling pathways, including TK receptors, among others [464]. For example, Ma and colleagues described that the anti-cancer effect of EGCG was due to the inhibition of EGFR signaling in NSCLC cells [465].

The molecular effect caused by the compounds on FASN, EGFR, and STAT3 was investigated in sensitive and resistant EGFRm NSCLC cells. AZ12751622 treatment reduced FASN protein expression in all cell models, while G28 and EGCG only decreased FASN levels in T790M+ cell models. Orita *et al.* observed that the inhibition of FASN activity did not result in a reduction of its protein levels [361]. Hence, FASN inhibition does not imply the reduction of its protein levels. Interestingly, gefitinib treatment diminished gene and protein expression of FASN in PC9 cells, which is in concordance with the literature [373].

A previous study demonstrated that EGCG reduced FASN and EGFR protein levels in wild-type EGFR NSCLC cells [381]. Nonetheless, our findings revealed that EGCG slightly increased phosphorylated and total EGFR levels in sensitive cells, while in T790M+ cell models, phosphorylated and total levels were decreased. Thus, these results indicate that the resistance mechanisms influence the molecular action of EGCG. In contrast, G28 elevated EGFR activation in PC9 cells, but no changes were observed in GR cell models. These data suggest that PC9 cells enhanced EGFR activation as a strategy to overcome FASN inhibition. AZ12751622 treatment upregulated EGFR protein expression in T790M+ cells, but diminished EGFR activation in all cell models. In fact, AZ12756122 and EGCG similarly decreased EGFR activation compared to EGFR-TKIs in GR cell models. Ali and coworkers reported that EGFR silencing significantly reduced FASN in sensitive and resistant EGFRm NSCLC cells [373]. Taken together, these data suggest that EGFRm is directly involved in FASN

Discussion

regulation. Moreover, FASN inhibitors may also affect EGFR as an off-target effect; however, resistance mechanisms have a relevant role in this regard, as previously mentioned.

The persistent STAT3 activation shown as a response to EGFR-TKI therapy, which is in agreement with the literature [99], has been reported as a mechanism of resistance [95]. Overall, phosphorylated levels of STAT3 remain unchanged in GR cell models after the treatment with FASN inhibitors, so it would not be a strategy used by cancer cells to mitigate the treatment with the compounds. However, EGCG reduced STAT3 activation only in PC9 cells. Previous studies described EGCG as a STAT3 inhibitor in colorectal carcinoma [466], pancreatic cancer [467], and head and neck carcinomas [468]. In contrast, the expression of FASN, EGFR, and STAT3 remained unchanged in PC9-GR3 cells. Hence, the cytotoxic effect observed by EGCG treatment could be a consequence of the inhibition of Axl [469], a protein that is overexpressed in this cell model.

In addition, the molecular effects of AZ12756122 on the AKT/PRAS40 and MAPK signaling pathways were studied. AZ12756122 decreased the activation of AKT and PRAS40 in all cell models. Similar findings were displayed using other FASN inhibitors, such as EGCG [381,465], C75 [381], or TVB-3166 [459], in NSCLC cells. Therefore, the diminishment in EGFR activation led to the suppression of the AKT/mTOR signaling pathway, resulting in the downregulation of SREBP-1c, a primary regulator of FASN [470]. Consequently, FASN levels also decreased. MAPK signaling was reduced after all treatments only in the PC9-GR3 cells. No changes were found in the other cell models. These results may also explain why PC9-GR3 cells are more sensitive to treatment with AZ12756122 than T790M+ cells. Contradictory results have been demonstrated in the literature [106,381,471] since FASN inhibition does not always result in the suppression of this signaling pathway. Nevertheless, constant activation of MAPK has been related to the induction of apoptosis in NSCLC cells [472].

The increased production of palmitate has been associated with the survival of EGFR-TKI resistant EGFRm NSCLC cells [373] and variations in the responsiveness of anti-cancer therapies [473]. The combination of treatments is a well-established approach to overcoming the resistance to the EGFR-TKIs [471]. Hence, EGCG, G28, or AZ12756122 were combined with gefitinib in T790M+ cell models and with gefitinib and osimertinib in PC9-GR3 cells. Previous investigations revealed that EGCG and its derivative exhibited synergism

with drugs against the ErbB family, such as cetuximab or pertuzumab, in breast cancer cell lines [390,391]. Although synergistic interactions were obtained with combinations of G28 with EGFR-TKIs and AZ12756122 with osimertinib, their molecular action in PC9-GR3 cells did not inhibit STAT3 activation. Nonetheless, the reduction of AKT, PRAS40, and MAPK was achieved with the combinatorial treatment of AZ12756122 and osimertinib. Jacobsen and colleagues found a synergistic effect combining EGFR-TKIs and AKT inhibitors in resistant EGFRm NSCLC cells, however, sustained AKT and MAPK activation were observed with the combinatorial treatment [106]. Therefore, combining FASN and EGFR inhibition may be a suitable approach to suppress the activation of these signaling pathways, which are crucial in EGFR-TKI resistance.

Although multiple novel therapies against LCSCs have been assessed [474,475], there is no approved treatment for this malignant population. The G28 compound demonstrated the capacity to decrease the CSC niche in sensitive and resistant TNBC cells [393]. Thus, FASN inhibition was evaluated as a therapeutic strategy against the LCSC population in sensitive and resistant EGFRm NSCLC cell models. The treatment with AZ12756122 compound resulted in a significant reduction of sphere and colony formation index, two common features of LCSCs [173–175]. Other researchers reported that FASN inhibition diminished the migration and invasion abilities [471], and clonogenicity [459] in NSCLC cells. Tiong *et al.* described that the inhibition of SREBP-1, the major regulator of FASN, led to a reduction of the CSC niche in cisplatin-resistant NSCLC cells [459]. As previously mentioned, treatment with AZ12756122 decreased the activation of the EGFR/AKT/mTOR signaling pathway, which is related to this malignant subpopulation [167,392]. Therefore, the results lead to the hypothesis that FASN inhibition and the suppression of this signaling pathway cause the death of LCSCs.

To confirm *in vitro* findings, FASN expression of tumor samples from patients with NSCLC harboring *EGFR*-sensitizing mutations was assessed. Several researchers reported that FASN expression was greater in lung tumor tissues than in normal bronchus and adjacent tissues [361,362,476]. Nonetheless, the mutational status of oncogenes, such as *EGFR*, was not considered. Thus, FASN expression from samples of lung adenocarcinoma showed high variability between studies, oscillating from approximately 22% to 81% [354,361,363]. To

Discussion

the best of our knowledge, this is the first research to provide standard levels of FASN tumor expression from patients with EGFRm NSCLC. The findings obtained revealed that patients with FASN expression tended to respond better to first-generation EGFR-TKIs and exhibited a longer mPFS. Furthermore, FASN expression was significantly associated with longer mPFS in patients who responded to the treatment with first-generation EGFR-TKIs. These results imply that FASN expression at baseline may play a key role in a better outcome in patients with NSCLC harboring *EGFR*-activating mutations. Our findings and other investigations [373] have indicated that the treatment with gefitinib reduced mRNA and protein expression of FASN exclusively in the sensitive cell model, i.e., PC9 cells. Different studies have demonstrated that (1) EGFRm regulates FASN expression to palmitoylate the receptor and localizes it in the cell membrane of PC9 cells [373,477], and (2) the inhibition of FASN leads to EGFR ubiquitination [373]. All together suggests that first-generation EGFR-TKI treatment exhibits a dual effect: suppressing EGFR activation and downregulating FASN expression. For this reason, the response to EGFR-TKI therapy, median PFS, and median PFS in relation to the response to EGFR-TKI treatment were superior in tumor samples from biopsies of patients with FASN+ NSCLC harboring *EGFR*-sensitizing mutations.

Therefore, FASN inhibition is an encouraging approach for the treatment of sensitive and resistant EGFRm NSCLC. Additionally, the combination of FASN and EGFR suppression arises as a therapeutic strategy to overcome resistance to EGFR-TKIs. Patients with NSCLC with EGFR-sensitizing mutations and FASN expression showed a better response to first-generation EGFR-TKIs. Hence, FASN expression should be evaluated before deciding the treatment line for these patients. Nonetheless, further studies are needed to confirm the efficacy of FASN inhibition in the treatment of patients with EGFRm NSCLC, either alone or in combination with EGFR-TKIs.

4. Concluding remarks

New strategies for the study and treatment of aggressive cancers, such as TNBC and EGFRm NSCLC, were explored in this study. Specifically, it has explored (1) 3D culture for CSC

expansion and (2) FASN inhibition as a therapy against this malignant population responsible for therapy resistance, tumor relapse, and metastasis.

First, PLA scaffolds were established as a suitable 3D cell culture system, especially those manufactured by electrospinning, because of their fibers, which were similar to those of the ECM, and because they allowed rapid cell proliferation. Nevertheless, the PLA-ES structures did not expand BCSCs. Hence, PCL-ES meshes were explored for LCSC enrichment in sensitive and resistant EGFRm NSCLC cell models. These 3D supports proved to be a useful tool to expand LCSCs, showing an increase in multiple markers related to this population, such as higher EGFR-TKI resistance and upregulation of different genes and proteins related to the EMT process, stemness, and surface markers, and activation of the Hedgehog pathway. Additionally, the results observed in the tumor samples from patients reinforced the use of PCL-ES scaffolds as a trustworthy 3D cell culture platform.

Second, FASN inhibition proved to be a promising approach for the treatment of sensitive and resistant EGFRm NSCLC cells. Treatment with the compounds produced similar cytotoxic effects in all cell models, regardless of their resistance to EGFR-TKIs. However, only G28 and AZ12751622 suppressed FASN activity, highlighting the off-target cytotoxic effects of EGCG independent of FASN inhibition. Moreover, the combination of G28 or AZ12751622 with EGFR-TKIs in resistant cell models resulted in synergistic interactions, overcoming resistance to EGFR-TKIs, and even inhibiting the EGFR/AKT/mTOR signaling pathway. Finally, FASN suppression caused a reduction in the LCSCs population. Interestingly, *in vitro* and patient sample-derived results revealed that NSCLC tumors with *EGFR*-sensitizing mutations and FASN expression showed a better response to first-generation EGFR-TKIs. Hence, first-generation EGFR-TKI treatment could have a dual effect: inhibition of EGFR activation and downregulation of FASN expression.

In addition, this investigation highlights the importance of the mutational status of oncogenes, such as *EGFR*, as it influences the behavior of cancer cells. For example, the need to reassess surface markers related to LCSCs, such as CD133, or FASN expression in tumor samples, has been raised.

Thus, this research provides a tool for *in vitro* research to study LCSCs and a biomarker to eliminate this malignant population. Furthermore, FASN inhibition has been introduced as a therapeutic strategy in sensitive and resistant EGFRm NSCLC.

5. Limitations of the study

There are some limitations inherent to a thesis, such as the time and material resources available or the possibility of performing certain techniques. There are also those specific to the study, such as the scarce literature on lung cancer metabolism that considers the mutational state of the cells. However, there were other limitations derived from the experimental design.

One of the most complex points is the choice of cell lines. In the first chapter, only the MDA-MB-231 cell line, which has a mesenchymal phenotype, was used. Therefore, it is advisable to perform the same experiment using other TNBC lines with a basal phenotype, such as the MDA-MB-468 cell model, to correctly evaluate whether PLA is a good material for expanding BCSCs. In the second and third chapters, only the PC9 cell line and derived resistant lines were used. Thus, other cell lines, such as NCI-H1650 or NCI-H1975, should be used to understand more precisely what is happening and draw more relevant conclusions.

The extrapolation of results from breast cancer to lung cancer is another critical point. The behavior and needs of each cell type are different, and it could be that PLA scaffolds may be useful for expanding the LCSC population or conversely, that they are not even a suitable tool for 3D culture, as has been observed in TNBC.

Another limitation is the selection of scaffolds. Other parameters could have been tested for the FFF structures, such as nozzle diameter, or other values of the parameters already selected to design the different configurations. Moreover, for ES meshes, screening of the solvents used to prepare the polymer solution should be performed because it directly influences the fiber diameter and filament roughness. Therefore, changing the solvent can modify the obtained results.

Another issue is the method of scaffold sterilization. In the second chapter, it was shown that sterilization increased the weight of the 3D structure. Therefore, other methodologies for sterilizing 3D supports should be investigated further.

Furthermore, additional experiments should be to obtain more robust conclusions, such as the use of another technique to analyze the CSC population, including the identification of CSC markers by flow cytometry, or the implantation of scaffolds in mice to determine their tumorigenic capacity. It is necessary to elucidate the mechanism of action of EGCG and G28, to complement the *in vitro* results with *in vivo* experiments, and to compare our FASN inhibitors with known inhibitors such as C75 or Orlistat.

Finally, regarding patient tumor samples, the population sample should be increased. This study had some limitations that may have influenced the results. First, it was a retrospective investigation, with the biases that this entails. Second, the number of samples with sufficient tissue for IHC was lower than that expected. Third, some tumor samples were relatively old, which may have influenced IHC results.

6. Future perspectives

The findings obtained in this thesis lead to the proposal of future research to study 3D culture for the expansion of LCSCs and the inhibition of FASN as a therapeutic target in sensitive and resistant EGFRm NSCLC tumors as well as in the LCSC population.

Future investigations should focus on exploring the activity and expression of FASN and its related signaling pathways in 3D-cultured cells. Thus, FASN inhibition could be studied to reduce the expansion of LCSCs achieved with 3D culture if FASN upregulation is found.

As previously mentioned, the results obtained from breast cancer were extrapolated to lung cancer. Thus, it is possible that the fabrication of 3D structures using other materials or techniques could allow for a higher enrichment of LCSCs.

The mechanism of action of G28 also needs to be further elucidated, as the findings obtained were very promising. Therefore, different signaling pathways, such as PI3K/AKT/mTOR or MAPK, should be investigated for their effects in different cell models and related to

Discussion

resistance mechanisms. Pharmacological interactions with other EGFR-TKIs widely used in the clinic, such as erlotinib or afatinib, should also be explored.

Finally, the cohort of patients should be expanded to verify the results. Furthermore, it would be interesting to examine the role of FASN before and after treatment with EGFR-TKIs, since its elevated expression has been related to treatment resistance.

Conclusions

I. Evaluation of poly(lactic acid) (PLA) scaffolds for 3D cell culture of breast CSC (BCSC)

- a) PLA scaffolds are suitable 3D cell culture systems for MDA-MB-231 TNBC cells.
- b) MDA-MB-231 TNBC cells cultured on PLA-FFF scaffolds with small pores exhibited higher cell proliferation values.
- c) The parameters infill density and infill direction had a significant influence on cell proliferation, with optimal values of 70% and 45°, respectively.
- d) The PLA-FFF scaffold with the optimal theoretical values, SS1, showed the highest cell proliferation compared to the initial 27 PLA-FFF matrices and SS2, validating the Taguchi experimental design.
- e) MDA-MB-231 TNBC cells cultured on the SS1 scaffold significantly increased BCSCs at short culture times.
- f) ES scaffolds from 12% and 15% PLA solutions showed similar microarchitecture, and consequently, MDA-MB-231 cells cultured on both PLA-ES scaffolds for 3 and 6 days exhibited similar cell proliferation rates.
- g) MDA-MB-231 cells cultured on 15%-PLA platforms did not show changes in most of the BCSC markers analyzed, including EMT markers and mammosphere formation capacity.
- h) PLA-FFF scaffolds had approximately 60 times thicker fibers and around 180 million times larger pore area than PLA-ES scaffolds.
- i) MDA-MB-231 cells cultured on PLA-FFF scaffolds exhibited a lower cell proliferation than those cultured on PLA-ES structures. PLA-ES scaffolds exhibited higher cell adhesion and proliferation than PLA-FFF matrices, even considering the SS1 PLA-FFF scaffold design.
- j) PLA scaffolds did not expand the BCSC population as effectively as PCL structures.

II. Evaluation of polycaprolactone (PCL) scaffolds manufactured by ES technology for 3D cell culture of lung CSCs (LCSC)

- a) PCL-ES scaffolds are suitable 3D cell culture systems for sensitive and resistant EGFRm NSCLC cells, specifically the PC9 and PC9-GR3 cell models.
- b) PCL-ES structures were stiffer than healthy lung tissue, but softer than polystyrene surfaces.
- c) The 15%-PCL-ES scaffolds had a significantly higher fiber diameter, porosity, and pore area than the 10%-PCL-ES ones. Moreover, only 10%-PCL-ES platforms exhibited beads.
- d) The sterilization process using overnight ethanol 70% and UV light for 30 minutes resulted in a significant increase of approximately 5% in the weight of the PCL-ES scaffolds. However, soaking the 3D meshes in the medium for 28 days did not cause any variation in their weight.
- e) PC9 and PC9-GR3 cell models exhibited higher cell viability and greater elongation on 15%-PCL-ES scaffolds than on 10%-PCL-ES ones.
- f) PC9 and PC9-GR3 cells cultured on PCL-ES matrices showed reduced levels of total EGFR expression, but phosphorylated levels remained unchanged, presumably contributing to the preservation of LCSC features.
- g) PC9 and PC9-GR3 cells seeded on PCL-ES scaffolds demonstrated enrichment of LCSCs. Specifically, higher EGFR-TKI resistance, upregulation of different genes and proteins related to the EMT process, stemness, and surface markers, and activation of the Hedgehog pathway.
- h) The 15%-PCL-ES scaffolds were a better 3D cell culture system than the 10%-PCL-ES ones.
- i) The resistant cell model required more time on 3D culture to expand its LCSC population than the sensitive one.
- j) The non-expression of CD133 surface marker was related to lower OS, disease progression, distant metastasis, and a poor degree of histological differentiation, traits directly associated with the LCSC niche.
- k) Mutational status of oncogenes determines the presence of LCSC markers.

- l) In addition to expanding LCSCs, PCL-ES scaffolds allow EGFRm NSCLC cells to behave similarly to the physiological environment.

III. Inhibition of FASN as a new therapeutic strategy for the treatment of EGFRm NSCLC

- a) FASN inhibition is a promising therapeutic approach for the treatment of patients with EGFRm NSCLC, both sensitive and resistant to the EGFR-TKIs.
- b) EGFR-TKI resistant cells exhibited significantly higher FASN protein expression than sensitive cells.
- c) G28 demonstrated a more potent cytotoxic effect than the other compounds, as lower concentrations were needed to produce the same cytotoxicity
- d) FASN inhibitors did not always cause cell death by apoptosis, but in some cell models occurs a suppression of cell viability in an apoptosis-independent manner.
- e) G28 and AZ12756122 decreased the activity in both sensitive and resistant EGFRm NSCLC cell models. However, the anti-cancer effect of EGCG is independent of FASN inhibition in GR models, since it was able to reduce it only in PC9 cells.
- f) FASN inhibitors may also affect EGFR as an off-target effect.
- g) The resistance mechanisms found in the GR cell models influence the molecular action of the compounds, particularly EGCG.
- h) AZ12756122 compound decreased EGFR activation leading to the suppression of the AKT/mTOR signaling pathway, resulting in the downregulation of FASN. Hence, EGFRm seems to be directly involved in the regulation of FASN.
- i) Synergistic interactions were obtained with combinations of G28 with EGFR-TKIs and AZ12756122 with osimertinib.
- j) The double inhibition of FASN and EGFR may be a suitable approach to suppress the activation of AKT/mTOR and MAPK signaling pathways.
- k) FASN inhibition reduced the LCSC population in sensitive and resistant EGFRm NSCLC cells.

Conclusions

- l) Patients with FASN expression tended to respond better to EGFR-TKIs and exhibited a longer mPFS. Furthermore, FASN expression was significantly associated with longer mPFS in patients who responded to the treatment with EGFR-TKIs.

References

1. World Health Organization - Cancer Available online: <https://www.who.int/news-room/fact-sheets/detail/cancer> (accessed on 25 March 2022).
2. National Cancer Institute - Understanding Cancer Available online: <https://www.cancer.gov/about-cancer/understanding> (accessed on 25 March 2022).
3. Sung, H.; Ferlay, J.; Siegel, R.L.; Laversanne, M.; Soerjomataram, I.; Jemal, A.; Bray, F. Global Cancer Statistics 2020: GLOBOCAN Estimates of Incidence and Mortality Worldwide for 36 Cancers in 185 Countries. *CA Cancer J Clin* **2021**, *71*, 209–249, doi:10.3322/CAAC.21660.
4. Cancer Today Available online: <https://gco.iarc.fr/today/home> (accessed on 26 March 2022).
5. Hanahan, D.; Weinberg, R.A. The Hallmarks of Cancer. *Cell* **2000**, *100*, 57–70.
6. Hanahan, D.; Weinberg, R.A. Hallmarks of Cancer: The next Generation. *Cell* **2011**, *144*, 646–674, doi:10.1016/j.cell.2011.02.013.
7. Hanahan, D. Hallmarks of Cancer: New Dimensions. *Cancer Discov* **2022**, *12*, 31–46, doi:10.1158/2159-8290.CD-21-1059.
8. Siegel, R.L.; Miller, K.D.; Fuchs, H.E.; Jemal, A. Cancer Statistics, 2022. *CA Cancer J Clin* **2022**, *72*, 7–33, doi:10.3322/caac.21708.
9. Torre, L.A.; Siegel, R.L.; Jemal, A. Lung Cancer Statistics. *Adv Exp Med Biol* **2016**, *893*, 1–19, doi:10.1007/978-3-319-24223-1_1.
10. Rami-Porta, R.; Call, S.; Doooms, C.; Obiols, C.; Sánchez, M.; Travis, W.D.; Vollmer, I. Lung Cancer Staging: A Concise Update. *Eur Respir J* **2018**, *51*, doi:10.1183/13993003.00190-2018.
11. Jones, G.S.; Baldwin, D.R. Recent Advances in the Management of Lung Cancer. *Clinical Medicine* **2018**, *18*, s41, doi:10.7861/CLINMEDICINE.18-2S-S41.
12. Minguet, J.; Smith, K.H.; Bramlage, P. Targeted Therapies for Treatment of Non-Small Cell Lung Cancer--Recent Advances and Future Perspectives. *Int J Cancer* **2016**, *138*, 2549–2561, doi:10.1002/IJC.29915.
13. Malhotra, J.; Jabbour, S.K.; Aisner, J. Current State of Immunotherapy for Non-Small Cell Lung Cancer. *Transl Lung Cancer Res* **2017**, *6*, 196–211, doi:10.21037/TLCR.2017.03.01.
14. Siegel, D.A.; Fedewa, S.A.; Henley, S.J.; Pollack, L.A.; Jemal, A. Proportion of Never Smokers Among Men and Women With Lung Cancer in 7 US States. *JAMA Oncol* **2021**, *7*, 302–304, doi:10.1001/JAMAONCOL.2020.6362.

References

15. Bade, B.C.; dela Cruz, C.S. Lung Cancer 2020: Epidemiology, Etiology, and Prevention. *Clin Chest Med* **2020**, *41*, 1–24, doi:10.1016/j.ccm.2019.10.001.
16. Types of Lung Cancer | Cancer Research UK Available online: <https://www.cancerresearchuk.org/about-cancer/lung-cancer/stages-types-grades/types> (accessed on 30 November 2022).
17. What Is Lung Cancer? | Types of Lung Cancer Available online: <https://www.cancer.org/cancer/lung-cancer/about/what-is.html> (accessed on 30 November 2022).
18. Yao, Y.; Fareed, R.; Zafar, A.; Saleem, K.; Huang, T.; Duan, Y.; Rehman, M.U. State-of-the-Art Combination Treatment Strategies for Advanced Stage Non–Small Cell Lung Cancer. *Front Oncol* **2022**, *12*.
19. Allemani, C.; Matsuda, T.; di Carlo, V.; Harewood, R.; Matz, M.; Nikšić, M.; Bonaventure, A.; Valkov, M.; Johnson, C.J.; Estève, J.; et al. Global Surveillance of Trends in Cancer Survival 2000–14 (CONCORD-3): Analysis of Individual Records for 37 513 025 Patients Diagnosed with One of 18 Cancers from 322 Population-Based Registries in 71 Countries. *Lancet* **2018**, *391*, 1023–1075, doi:10.1016/S0140-6736(17)33326-3.
20. Marino, F.Z.; Bianco, R.; Accardo, M.; Ronchi, A.; Cozzolino, I.; Morgillo, F.; Rossi, G.; Franco, R. Molecular Heterogeneity in Lung Cancer: From Mechanisms of Origin to Clinical Implications. *Int J Med Sci* **2019**, *16*, 981–989, doi:10.7150/IJMS.34739.
21. Yang, T.; Xiong, Y.; Zeng, Y.; Wang, Y.; Zeng, J.; Liu, J.; Xu, S.; Li, L.S. Current Status of Immunotherapy for Non-Small Cell Lung Cancer. *Front Pharmacol* **2022**, *13*.
22. Barta, J.A.; Powell, C.A.; Wisnivesky, J.P. Global Epidemiology of Lung Cancer. *Ann Glob Health* **2019**, *85*, doi:10.5334/AOGH.2419.
23. Lemjabbar-Alaoui, H.; Hassan, O.U.I.; Yang, Y.W.; Buchanan, P. Lung Cancer: Biology and Treatment Options. *Biochim Biophys Acta Rev Cancer* **2015**, *1856*, 189–210, doi:10.1016/J.BBCAN.2015.08.002.
24. Sequist, L. v.; Heist, R.S.; Shaw, A.T.; Fidias, P.; Rosovsky, R.; Temel, J.S.; Lennes, I.T.; Digumarthy, S.; Waltman, B.A.; Bast, E.; et al. Implementing Multiplexed Genotyping of Non-Small-Cell Lung Cancers into Routine Clinical Practice. *Ann Oncol* **2011**, *22*, 2616–2624, doi:10.1093/ANNONC/MDR489.
25. Collisson, E.A.; Campbell, J.D.; Brooks, A.N.; Berger, A.H.; Lee, W.; Chmielecki, J.; Beer, D.G.; Cope, L.; Creighton, C.J.; Danilova, L.; et al. Comprehensive Molecular Profiling of Lung Adenocarcinoma. *Nature* **2014**, *511*, 543–550, doi:10.1038/nature13385.

26. Testa, U.; Castelli, G.; Pelosi, E. Lung Cancers: Molecular Characterization, Clonal Heterogeneity and Evolution, and Cancer Stem Cells. *Cancers (Basel)* **2018**, *10*.
27. Hammerman, P.S.; Voet, D.; Lawrence, M.S.; Voet, D.; Jing, R.; Cibulskis, K.; Sivachenko, A.; Stojanov, P.; McKenna, A.; Lander, E.S.; et al. Comprehensive Genomic Characterization of Squamous Cell Lung Cancers. *Nature* **2012**, *489*:7417 **2012**, *489*, 519–525, doi:10.1038/nature11404.
28. Ruiz-Cordero, R.; Devine, W.P. Targeted Therapy and Checkpoint Immunotherapy in Lung Cancer. *Surg Pathol Clin* **2020**, *13*, 17–33.
29. Chan, A.W.; Chau, S.L.; Tong, J.H.; Chow, C.; Kwan, J.S.H.; Chung, L.Y.; Lung, R.W.; Tong, C.Y.; Tin, E.K.; Law, P.P.; et al. The Landscape of Actionable Molecular Alterations in Immunomarker-Defined Large-Cell Carcinoma of the Lung. *J Thorac Oncol* **2019**, *14*, 1213–1222, doi:10.1016/J.JTHO.2019.03.021.
30. Pelosi, G.; Fabbri, A.; Papotti, M.; Rossi, G.; Cavazza, A.; Righi, L.; Tamborini, E.; Perrone, F.; Settanni, G.; Busico, A.; et al. Dissecting Pulmonary Large-Cell Carcinoma by Targeted Next Generation Sequencing of Several Cancer Genes Pushes Genotypic-Phenotypic Correlations to Emerge. *J Thorac Oncol* **2015**, *10*, 1560–1569, doi:10.1097/JTO.0000000000000658.
31. Caliman, E.; Fancelli, S.; Petroni, G.; Gatta Michelet, M.R.; Cosso, F.; Ottanelli, C.; Mazzoni, F.; Voltolini, L.; Pillozzi, S.; Antonuzzo, L. Challenges in the Treatment of Small Cell Lung Cancer in the Era of Immunotherapy and Molecular Classification. *Lung cancer* **2022**, *175*, 88–100, doi:10.1016/J.LUNGCAN.2022.11.014.
32. Detterbeck, F.C.; Boffa, D.J.; Kim, A.W.; Tanoue, L.T. The Eighth Edition Lung Cancer Stage Classification. *Chest* **2017**, *151*, 193–203.
33. Petrella, F.; Rizzo, S.; Casiraghi, M.; Bardoni, C.; Mohamed, S.; Musso, V.; Simonini, E.; Spaggiari, L. State of the Art and New Perspectives in Surgical Treatment of Lung Cancer: A Narrative Review. *Transl Cancer Res* **2022**, *11*, 3869–3875, doi:10.21037/TCR-22-1491.
34. Oken, M.; Creech, R.; Tormey, D.; Horton, J.; Davis, T.; McFadden, E.; Carbone, P. Toxicity and Response Criteria of the Eastern Cooperative Oncology Group - PubMed. *Am J Clin Oncol* **1982**, *5*, 649–655.
35. Rosenkranz, A.A.; Slastnikova, T.A. Epidermal Growth Factor Receptor: Key to Selective Intracellular Delivery. *Biochemistry (Mosc)* **2020**, *85*, 967–993, doi:10.1134/S0006297920090011.
36. Liu, X.; Wang, P.; Zhang, C.; Ma, Z. Epidermal Growth Factor Receptor (EGFR): A Rising Star in the Era of Precision Medicine of Lung Cancer. *Oncotarget* **2017**, *8*, 50209–50220, doi:10.18632/ONCOTARGET.16854.

References

37. Campbell, J.M.; Lockwood, W.W.; Buys, T.P.H.; Chari, R.; Coe, B.P.; Lam, S.; Lam, W.L. Integrative Genomic and Gene Expression Analysis of Chromosome 7 Identified Novel Oncogene Loci in Non-Small Cell Lung Cancer. *Genome* **2008**, *51*, 1032–1039, doi:10.1139/G08-086.
38. Abbasian, M.H.; Ardekani, A.M.; Sobhani, N.; Roudi, R. The Role of Genomics and Proteomics in Lung Cancer Early Detection and Treatment. *Cancers (Basel)* **2022**, *14*, 5144, doi:10.3390/CANCERS14205144.
39. Zhuang, X.; Zhao, C.; Li, J.; Su, C.; Chen, X.; Ren, S.; Li, X.; Zhou, C. Clinical Features and Therapeutic Options in Non-small Cell Lung Cancer Patients with Concomitant Mutations of EGFR, ALK, ROS1, KRAS or BRAF. *Cancer Med* **2019**, *8*, 2858, doi:10.1002/CAM4.2183.
40. Kris, M.G.; Johnson, B.E.; Berry, L.D.; Kwiatkowski, D.J.; Iafrate, A.J.; Wistuba, I.I.; Varella-Garcia, M.; Franklin, W.A.; Aronson, S.L.; Su, P.-F.; et al. Using Multiplexed Assays of Oncogenic Drivers in Lung Cancers to Select Targeted Drugs. *JAMA : the journal of the American Medical Association* **2014**, *311*, 1998, doi:10.1001/JAMA.2014.3741.
41. Arrieta, O.; Cardona, A.F.; Martín, C.; Más-López, L.; Corrales-Rodríguez, L.; Bramuglia, G.; Castillo-Fernandez, O.; Meyerson, M.; Amieva-Rivera, E.; Campos-Parra, A.D.; et al. Updated Frequency of EGFR and KRAS Mutations in NonSmall-Cell Lung Cancer in Latin America: The Latin-American Consortium for the Investigation of Lung Cancer (CLICaP). *J Thorac Oncol* **2015**, *10*, 838–843, doi:10.1097/JTO.0000000000000481.
42. Shi, Y.; Au, J.S.K.; Thongprasert, S.; Srinivasan, S.; Tsai, C.M.; Khoa, M.T.; Heeroma, K.; Itoh, Y.; Cornelio, G.; Yang, P.C. A Prospective, Molecular Epidemiology Study of EGFR Mutations in Asian Patients with Advanced Non-Small-Cell Lung Cancer of Adenocarcinoma Histology (PIONEER). *J Thorac Oncol* **2014**, *9*, 154–162, doi:10.1097/JTO.0000000000000033.
43. Paez, J.G.; Jänne, P.A.; Lee, J.C.; Tracy, S.; Greulich, H.; Gabriel, S.; Herman, P.; Kaye, F.J.; Lindeman, N.; Boggon, T.J.; et al. EGFR Mutations in Lung Cancer: Correlation with Clinical Response to Gefitinib Therapy. *Science* **2004**, *304*, 1497–1500, doi:10.1126/SCIENCE.1099314.
44. Kosaka, T.; Yatabe, Y.; Endoh, H.; Yoshida, K.; Hida, T.; Tsuboi, M.; Tada, H.; Kuwano, H.; Mitsudomi, T. Analysis of Epidermal Growth Factor Receptor Gene Mutation in Patients with Non–Small Cell Lung Cancer and Acquired Resistance to Gefitinib. *Clinical Cancer Research* **2006**, *12*, 5764–5769, doi:10.1158/1078-0432.CCR-06-0714.
45. Balak, M.N.; Gong, Y.; Riely, G.J.; Somwar, R.; Li, A.R.; Zakowski, M.F.; Chiang, A.; Yang, G.; Ouerfelli, O.; Kris, M.G.; et al. Novel D761Y and Common Secondary T790M

- Mutations in Epidermal Growth Factor Receptor–Mutant Lung Adenocarcinomas with Acquired Resistance to Kinase Inhibitors. *Clinical Cancer Research* **2006**, *12*, 6494–6501, doi:10.1158/1078-0432.CCR-06-1570.
46. Wu, S.G.; Liu, Y.N.; Tsai, M.F.; Chang, Y.L.; Yu, C.J.; Yang, P.C.; Yang, J.C.H.; Wen, Y.F.; Shih, J.Y. The Mechanism of Acquired Resistance to Irreversible EGFR Tyrosine Kinase Inhibitor-Afatinib in Lung Adenocarcinoma Patients. *Oncotarget* **2016**, *7*, 12404–12413, doi:10.18632/ONCOTARGET.7189.
47. Romero, D. Amivantamab Is Effective in NSCLC Harboring EGFR Exon 20 Insertions. *Nature Reviews Clinical Oncology* *2021* **18:10** **2021**, *18*, 604–604, doi:10.1038/s41571-021-00551-8.
48. Cho, J.H.; Lim, S.H.; An, H.J.; Kim, K.H.; Park, K.U.; Kang, E.J.; Choi, Y.H.; Ahn, M.S.; Lee, M.H.; Sun, J.M.; et al. Osimertinib for Patients With Non-Small-Cell Lung Cancer Harboring Uncommon EGFR Mutations: A Multicenter, Open-Label, Phase II Trial (KCSG-LU15-09). *J Clin Oncol* **2020**, *38*, 488–495, doi:10.1200/JCO.19.00931.
49. Culy, C.R.; Faulds, D. Gefitinib. *Drugs* **2002**, *62*, 2237–2248, doi:10.2165/00003495-200262150-00008/FIGURES/4.
50. Mitsudomi, T.; Morita, S.; Yatabe, Y.; Negoro, S.; Okamoto, I.; Tsurutani, J.; Seto, T.; Satouchi, M.; Tada, H.; Hirashima, T.; et al. Gefitinib versus Cisplatin plus Docetaxel in Patients with Non-Small-Cell Lung Cancer Harboring Mutations of the Epidermal Growth Factor Receptor (WJTOG3405): An Open Label, Randomised Phase 3 Trial. *Lancet Oncol* **2010**, *11*, 121–128, doi:10.1016/S1470-2045(09)70364-X.
51. Maemondo, M.; Inoue, A.; Kobayashi, K.; Sugawara, S.; Oizumi, S.; Isobe, H.; Gemma, A.; Harada, M.; Yoshizawa, H.; Kinoshita, I.; et al. Gefitinib or Chemotherapy for Non-Small-Cell Lung Cancer with Mutated EGFR. *N Engl J Med* **2010**, *362*, 2380–2388, doi:10.1056/NEJMOA0909530.
52. Rosell, R.; Carcereny, E.; Gervais, R.; Vergnenegre, A.; Massuti, B.; Felip, E.; Palmero, R.; Garcia-Gomez, R.; Pallares, C.; Sanchez, J.M.; et al. Erlotinib versus Standard Chemotherapy as First-Line Treatment for European Patients with Advanced EGFR Mutation-Positive Non-Small-Cell Lung Cancer (EURTAC): A Multicentre, Open-Label, Randomised Phase 3 Trial. *Lancet Oncol* **2012**, *13*, 239–246, doi:10.1016/S1470-2045(11)70393-X.
53. Shi, Y.K.; Wang, L.; Han, B.H.; Li, W.; Yu, P.; Liu, Y.P.; Ding, C.M.; Song, X.; Ma, Z.Y.; Ren, X.L.; et al. First-Line Icotinib versus Cisplatin/Pemetrexed plus Pemetrexed Maintenance Therapy for Patients with Advanced EGFR Mutation-Positive Lung Adenocarcinoma (CONVINCE): A Phase 3, Open-Label, Randomized Study. *Ann Oncol* **2017**, *28*, 2443–2450, doi:10.1093/ANNONC/MDX359.

References

54. Westover, D.; Zugazagoitia, J.; Cho, B.C.; Lovly, C.M.; Paz-Ares, L. Mechanisms of Acquired Resistance to First- and Second-Generation EGFR Tyrosine Kinase Inhibitors. *Annals of Oncology* **2018**, *29*, i10, doi:10.1093/ANNONC/MDX703.
55. Sequist, L. v.; Yang, J.C.H.; Yamamoto, N.; O'Byrne, K.; Hirsh, V.; Mok, T.; Geater, S.L.; Orlov, S.; Tsai, C.M.; Boyer, M.; et al. Phase III Study of Afatinib or Cisplatin plus Pemetrexed in Patients with Metastatic Lung Adenocarcinoma with EGFR Mutations. *J Clin Oncol* **2013**, *31*, 3327–3334, doi:10.1200/JCO.2012.44.2806.
56. Wu, Y.L.; Zhou, C.; Hu, C.P.; Feng, J.; Lu, S.; Huang, Y.; Li, W.; Hou, M.; Shi, J.H.; Lee, K.Y.; et al. Afatinib versus Cisplatin plus Gemcitabine for First-Line Treatment of Asian Patients with Advanced Non-Small-Cell Lung Cancer Harboring EGFR Mutations (LUX-Lung 6): An Open-Label, Randomised Phase 3 Trial. *Lancet Oncol* **2014**, *15*, 213–222, doi:10.1016/S1470-2045(13)70604-1.
57. Yang, J.C.H.; Wu, Y.L.; Schuler, M.; Sebastian, M.; Popat, S.; Yamamoto, N.; Zhou, C.; Hu, C.P.; O'Byrne, K.; Feng, J.; et al. Afatinib versus Cisplatin-Based Chemotherapy for EGFR Mutation-Positive Lung Adenocarcinoma (LUX-Lung 3 and LUX-Lung 6): Analysis of Overall Survival Data from Two Randomised, Phase 3 Trials. *Lancet Oncol* **2015**, *16*, 141–151, doi:10.1016/S1470-2045(14)71173-8.
58. Park, K.; Tan, E.H.; O'Byrne, K.; Zhang, L.; Boyer, M.; Mok, T.; Hirsh, V.; Yang, J.C.H.; Lee, K.H.; Lu, S.; et al. Afatinib versus Gefitinib as First-Line Treatment of Patients with EGFR Mutation-Positive Non-Small-Cell Lung Cancer (LUX-Lung 7): A Phase 2B, Open-Label, Randomised Controlled Trial. *Lancet Oncol* **2016**, *17*, 577–589, doi:10.1016/S1470-2045(16)30033-X.
59. Wu, Y.L.; Cheng, Y.; Zhou, X.; Lee, K.H.; Nakagawa, K.; Niho, S.; Tsuji, F.; Linke, R.; Rosell, R.; Corral, J.; et al. Dacomitinib versus Gefitinib as First-Line Treatment for Patients with EGFR-Mutation-Positive Non-Small-Cell Lung Cancer (ARCHER 1050): A Randomised, Open-Label, Phase 3 Trial. *Lancet Oncol* **2017**, *18*, 1454–1466, doi:10.1016/S1470-2045(17)30608-3.
60. Mok, T.S.; Cheng, Y.; Zhou, X.; Lee, K.H.; Nakagawa, K.; Niho, S.; Lee, M.; Linke, R.; Rosell, R.; Corral, J.; et al. Improvement in Overall Survival in a Randomized Study That Compared Dacomitinib With Gefitinib in Patients With Advanced Non-Small-Cell Lung Cancer and EGFR-Activating Mutations. *J Clin Oncol* **2018**, *36*, 2244–2250, doi:10.1200/JCO.2018.78.7994.
61. Schuler, M.; Paz-Ares, L.; Sequist, L. v.; Hirsh, V.; Lee, K.H.; Wu, Y.L.; Lu, S.; Zhou, C.; Feng, J.; Ellis, S.H.; et al. First-Line Afatinib for Advanced EGFRm+ NSCLC: Analysis of Long-Term Responders in the LUX-Lung 3, 6, and 7 Trials. *Lung Cancer* **2019**, *133*, 10–19, doi:10.1016/J.LUNGCAN.2019.04.006.
62. Greig, S.L. Osimertinib: First Global Approval. *Drugs* **2015** *76:2* **2016**, *76*, 263–273, doi:10.1007/S40265-015-0533-4.

63. Mok, T.S.; Wu, Y.-L.; Ahn, M.-J.; Garassino, M.C.; Kim, H.R.; Ramalingam, S.S.; Shepherd, F.A.; He, Y.; Akamatsu, H.; Theelen, W.S.M.E.; et al. Osimertinib or Platinum–Pemetrexed in EGFR T790M–Positive Lung Cancer . *New England Journal of Medicine* **2017**, *376*, 629–640, doi:10.1056/NEJMOA1612674/SUPPL_FILE/NEJMOA1612674_DISCLOSURES.PDF.
64. Soria, J.-C.; Ohe, Y.; Vansteenkiste, J.; Reungwetwattana, T.; Chewaskulyong, B.; Lee, K.H.; Dechaphunkul, A.; Imamura, F.; Nogami, N.; Kurata, T.; et al. Osimertinib in Untreated EGFR -Mutated Advanced Non–Small-Cell Lung Cancer . *New England Journal of Medicine* **2018**, *378*, 113–125, doi:10.1056/NEJMOA1713137/SUPPL_FILE/NEJMOA1713137_DISCLOSURES.PDF.
65. Ramalingam, S.S.; Yang, J.C.H.; Lee, C.K.; Kurata, T.; Kim, D.W.; John, T.; Nogami, N.; Ohe, Y.; Mann, H.; Rukazenkov, Y.; et al. Osimertinib As First-Line Treatment of EGFR Mutation-Positive Advanced Non-Small-Cell Lung Cancer. *J Clin Oncol* **2018**, *36*, 841–849, doi:10.1200/JCO.2017.74.7576.
66. Ito, K.; Morise, M.; Wakuda, K.; Hataji, O.; Shimokawaji, T.; Takahashi, K.; Furuya, N.; Takeyama, Y.; Goto, Y.; Abe, T.; et al. A Multicenter Cohort Study of Osimertinib Compared with Afatinib as First-Line Treatment for EGFR-Mutated Non-Small-Cell Lung Cancer from Practical Dataset: CJLSG1903. *ESMO Open* **2021**, *6*, doi:10.1016/J.ESMOOP.2021.100115.
67. Wu, Y.-L.; Tsuboi, M.; He, J.; John, T.; Grohe, C.; Majem, M.; Goldman, J.W.; Laktionov, K.; Kim, S.-W.; Kato, T.; et al. Osimertinib in Resected EGFR-Mutated Non-Small-Cell Lung Cancer. *N Engl J Med* **2020**, *383*, 1711–1723, doi:10.1056/NEJMOA2027071.
68. Wu, Y.L.; John, T.; Grohe, C.; Majem, M.; Goldman, J.W.; Kim, S.W.; Kato, T.; Laktionov, K.; Vu, H.V.; Wang, Z.; et al. Postoperative Chemotherapy Use and Outcomes From ADAURA: Osimertinib as Adjuvant Therapy for Resected EGFR-Mutated NSCLC. *J Thorac Oncol* **2022**, *17*, 423–433, doi:10.1016/J.JTHO.2021.10.014.
69. Lu, S.; Wang, Q.; Zhang, G.; Dong, X.; Yang, C.T.; Song, Y.; Chang, G.C.; Lu, Y.; Pan, H.; Chiu, C.H.; et al. Efficacy of Aumolertinib (HS-10296) in Patients With Advanced EGFR T790M+ NSCLC: Updated Post-National Medical Products Administration Approval Results From the APOLLO Registrational Trial. *J Thorac Oncol* **2022**, *17*, 411–422, doi:10.1016/J.JTHO.2021.10.024.
70. Deeks, E.D. Furmonertinib: First Approval. *Drugs* **2021**, *81*, 1775–1780, doi:10.1007/S40265-021-01588-W.
71. Dhillon, S. Lazertinib: First Approval. *Drugs* **2021**, *81*, 1107–1113, doi:10.1007/S40265-021-01533-X.

References

72. Fu, K.; Xie, F.; Fu, L. Therapeutic Strategies for EGFR-Mutated Non-Small Cell Lung Cancer Patients with Osimertinib Resistance. *J Hematol Oncol* **2020**, *15*, 173, doi:10.1186/s13045-022-01391-4.
73. Lee, C.K.; Man, J.; Lord, S.; Cooper, W.; Links, M.; GebSKI, V.; Herbst, R.S.; Gralla, R.J.; Mok, T.; Yang, J.C.H. Clinical and Molecular Characteristics Associated With Survival Among Patients Treated With Checkpoint Inhibitors for Advanced Non-Small Cell Lung Carcinoma: A Systematic Review and Meta-Analysis. *JAMA Oncol* **2018**, *4*, 210, doi:10.1001/JAMAONCOL.2017.4427.
74. Liang, H.; Pan, Z.; Wang, W.; Guo, C.; Chen, D.; Zhang, J.; Zhang, Y.; Tang, S.; He, J.; Liang, W. The Alteration of T790M between 19 Del and L858R in NSCLC in the Course of EGFR-TKIs Therapy: A Literature-Based Pooled Analysis. *J Thorac Dis* **2018**, *10*, 2311–2320, doi:10.21037/JTD.2018.03.150.
75. Costa, D.B.; Schumer, S.T.; Tenen, D.G.; Kobayashi, S. Differential Responses to Erlotinib in Epidermal Growth Factor Receptor (EGFR)-Mutated Lung Cancers with Acquired Resistance to Gefitinib Carrying the L747S or T790M Secondary Mutations. *J Clin Oncol* **2008**, *26*, 1182–1184, doi:10.1200/JCO.2007.14.9039.
76. Bean, J.; Riely, G.J.; Balak, M.; Marks, J.L.; Ladanyi, M.; Miller, V.A.; Pao, W. Acquired Resistance to Epidermal Growth Factor Receptor Kinase Inhibitors Associated with a Novel T854A Mutation in a Patient with EGFR-Mutant Lung Adenocarcinoma. *Clin Cancer Res* **2008**, *14*, 7519–7525, doi:10.1158/1078-0432.CCR-08-0151.
77. Ramalingam, S.S.; Cheng, Y.; Zhou, C.; Ohe, Y.; Imamura, F.; Cho, B.C.; Lin, M.-C.; Majem, M.; Shah, R.; Rukazenzov, Y.; et al. Mechanisms of Acquired Resistance to First-Line Osimertinib: Preliminary Data from the Phase III FLAURA Study. *Annals of Oncology* **2018**, *29*, viii740, doi:10.1093/annonc/mdy424.063.
78. Papadimitrakopoulou, V.A.; Wu, Y.-L.; Han, J.-Y.; Ahn, M.-J.; Ramalingam, S.S.; John, T.; Okamoto, I.; Yang, J.C.-H.; Bulusu, K.C.; Laus, G.; et al. Analysis of Resistance Mechanisms to Osimertinib in Patients with EGFR T790M Advanced NSCLC from the AURA3 Study. *Annals of Oncology* **2018**, *29*, viii741, doi:10.1093/annonc/mdy424.064.
79. Mu, Y.; Hao, X.; Xing, P.; Hu, X.; Wang, Y.; Li, T.; Zhang, J.; Xu, Z.; Li, J. Acquired Resistance to Osimertinib in Patients with Non-Small-Cell Lung Cancer: Mechanisms and Clinical Outcomes. *J Cancer Res Clin Oncol* **2020**, *146*, 2427–2433, doi:10.1007/S00432-020-03239-1.
80. Yang, Z.; Yang, N.; Ou, Q.; Xiang, Y.; Jiang, T.; Wu, X.; Bao, H.; Tong, X.; Wang, X.; Shao, Y.W.; et al. Investigating Novel Resistance Mechanisms to Third-Generation EGFR Tyrosine Kinase Inhibitor Osimertinib in Non-Small Cell Lung Cancer Patients. *Clin Cancer Res* **2018**, *24*, 3097–3107, doi:10.1158/1078-0432.CCR-17-2310.

81. Nukaga, S.; Yasuda, H.; Tsuchihara, K.; Hamamoto, J.; Masuzawa, K.; Kawada, I.; Naoki, K.; Matsumoto, S.; Mimaki, S.; Ikemura, S.; et al. Amplification of EGFR Wild-Type Alleles in Non-Small Cell Lung Cancer Cells Confers Acquired Resistance to Mutation-Selective EGFR Tyrosine Kinase Inhibitors. *Cancer Res* **2017**, *77*, 2078–2089, doi:10.1158/0008-5472.CAN-16-2359.
82. Sun, R.; Hou, Z.; Zhang, Y.; Jiang, B. Drug Resistance Mechanisms and Progress in the Treatment of EGFR-mutated Lung Adenocarcinoma (Review). *Oncol Lett* **2022**, *24*, doi:10.3892/ol.2022.13528.
83. Castañeda-González, J.P.; Chaves, J.J.; Parra-Medina, R. Multiple Mutations in the EGFR Gene in Lung Cancer: A Systematic Review. *Transl Lung Cancer Res* **2022**, *11*, 2148–2163, doi:10.21037/TLCR-22-235.
84. Pasquini, G.; Giaccone, G. C-MET Inhibitors for Advanced Non-Small Cell Lung Cancer. *Expert Opin Investig Drugs* **2018**, *27*, 363–375, doi:10.1080/13543784.2018.1462336.
85. Engelman, J.A.; Zejnullahu, K.; Mitsudomi, T.; Song, Y.; Hyland, C.; Joon, O.P.; Lindeman, N.; Gale, C.M.; Zhao, X.; Christensen, J.; et al. MET Amplification Leads to Gefitinib Resistance in Lung Cancer by Activating ERBB3 Signaling. *Science* **2007**, *316*, 1039–1043, doi:10.1126/SCIENCE.1141478.
86. Sequist, L. v.; Waltman, B.A.; Dias-Santagata, D.; Digumarthy, S.; Turke, A.B.; Fidias, P.; Bergethon, K.; Shaw, A.T.; Gettinger, S.; Cospser, A.K.; et al. Genotypic and Histological Evolution of Lung Cancers Acquiring Resistance to EGFR Inhibitors. *Sci Transl Med* **2011**, *3*, 75ra26, doi:10.1126/SCITRANSLMED.3002003.
87. Oxnard, G.R.; Hu, Y.; Mileham, K.F.; Husain, H.; Costa, D.B.; Tracy, P.; Feeney, N.; Sholl, L.M.; Dahlberg, S.E.; Redig, A.J.; et al. Assessment of Resistance Mechanisms and Clinical Implications in Patients With EGFR T790M-Positive Lung Cancer and Acquired Resistance to Osimertinib. *JAMA Oncol* **2018**, *4*, 1527–1534, doi:10.1001/JAMAONCOL.2018.2969.
88. Riudavets, M.; Sullivan, I.; Abdayem, P.; Planchard, D. Targeting HER2 in Non-Small-Cell Lung Cancer (NSCLC): A Glimpse of Hope? An Updated Review on Therapeutic Strategies in NSCLC Harboring HER2 Alterations. *ESMO Open* **2021**, *6*, doi:10.1016/J.ESMOOP.2021.100260.
89. Yu, H.A.; Arcila, M.E.; Rekhtman, N.; Sima, C.S.; Zakowski, M.F.; Pao, W.; Kris, M.G.; Miller, V.A.; Ladanyi, M.; Riely, G.J. Analysis of Tumor Specimens at the Time of Acquired Resistance to EGFR-TKI Therapy in 155 Patients with EGFR-Mutant Lung Cancers. *Clin Cancer Res* **2013**, *19*, 2240–2247, doi:10.1158/1078-0432.CCR-12-2246.

References

90. Alqahtani, A.; Ayes, H.S.K.; Halawani, H. PIK3CA Gene Mutations in Solid Malignancies: Association with Clinicopathological Parameters and Prognosis. *Cancers (Basel)* **2019**, *12*, doi:10.3390/CANCERS12010093.
91. Lee, J.; Kim, H.S.; Lee, B.; Kim, H.K.; Sun, J.M.; Ahn, J.S.; Ahn, M.J.; Park, K.; Lee, S.H. Genomic Landscape of Acquired Resistance to Third-Generation EGFR Tyrosine Kinase Inhibitors in EGFR T790M-Mutant Non-Small Cell Lung Cancer. *Cancer* **2020**, *126*, 2704–2712, doi:10.1002/CNCR.32809.
92. Aggarwal, B.B.; Kunnumakkara, A.B.; Harikumar, K.B.; Gupta, S.R.; Tharakan, S.T.; Koca, C.; Dey, S.; Sung, B. Signal Transducer and Activator of Transcription-3, Inflammation, and Cancer: How Intimate Is the Relationship?. *Ann N Y Acad Sci* **2009**, *1171*, 59–76, doi:10.1111/j.1749-6632.2009.04911.x.
93. Frank, D.A. STAT3 as a Central Mediator of Neoplastic Cellular Transformation. *Cancer Lett* **2007**, *251*, 199–210, doi:10.1016/J.CANLET.2006.10.017.
94. Germain, D.; Frank, D.A. Targeting the Cytoplasmic and Nuclear Functions of Signal Transducers and Activators of Transcription 3 for Cancer Therapy. *Clin Cancer Res* **2007**, *13*, 5665–5669, doi:10.1158/1078-0432.CCR-06-2491.
95. Zulkifli, A.A.; Tan, F.H.; Putoczki, T.L.; Stylli, S.S.; Luwor, R.B. STAT3 Signaling Mediates Tumour Resistance to EGFR Targeted Therapeutics. *Mol Cell Endocrinol* **2017**, *451*, 15–23, doi:10.1016/j.mce.2017.01.010.
96. Yu, Y.; Zhao, Q.; Wang, Z.; Liu, X.Y. Activated STAT3 Correlates with Prognosis of Non-Small Cell Lung Cancer and Indicates New Anticancer Strategies. *Cancer Chemother Pharmacol* **2015**, *75*, 917–922, doi:10.1007/s00280-015-2710-2.
97. Xu, Y.H.; Lu, S. A Meta-Analysis of STAT3 and Phospho-STAT3 Expression and Survival of Patients with Non-Small-Cell Lung Cancer. *European Journal of Surgical Oncology (EJSO)* **2014**, *40*, 311–317, doi:10.1016/j.ejso.2013.11.012.
98. Lee, H.J.; Zhuang, G.; Cao, Y.; Du, P.; Kim, H.J.; Settleman, J. Drug Resistance via Feedback Activation of Stat3 in Oncogene-Addicted Cancer Cells. *Cancer Cell* **2014**, *26*, 207–221, doi:10.1016/j.ccr.2014.05.019.
99. Ninomiya, T.; Takigawa, N.; Ichihara, E.; Ochi, N.; Murakami, T.; Honda, Y.; Kubo, T.; Minami, D.; Kudo, K.; Tanimoto, M.; et al. Afatinib Prolongs Survival Compared with Gefitinib in an Epidermal Growth Factor Receptor-Driven Lung Cancer Model. *Mol Cancer Ther* **2013**, *12*, 589–597, doi:10.1158/1535-7163.MCT-12-0885.
100. Roca, E.; Pozzari, M.; Vermi, W.; Tovazzi, V.; Baggi, A.; Amoroso, V.; Nonnis, D.; Intagliata, S.; Berruti, A. Outcome of EGFR-Mutated Adenocarcinoma NSCLC Patients with Changed Phenotype to Squamous Cell Carcinoma after Tyrosine Kinase Inhibitors: A Pooled Analysis with an Additional Case. *Lung Cancer* **2019**, *127*, 12–18, doi:10.1016/J.LUNGCAN.2018.11.016.

101. Zhu, X.; Chen, L.; Liu, L.; Niu, X. EMT-Mediated Acquired EGFR-TKI Resistance in NSCLC: Mechanisms and Strategies. *Front Oncol* **2019**, *9*, doi:10.3389/FONC.2019.01044.
102. Ohashi, K.; Sequist, L. v.; Arcila, M.E.; Moran, T.; Chmielecki, J.; Lin, Y.L.; Pan, Y.; Wang, L.; de Stanchina, E.; Shien, K.; et al. Lung Cancers with Acquired Resistance to EGFR Inhibitors Occasionally Harbor BRAF Gene Mutations but Lack Mutations in KRAS, NRAS, or MEK1. *Proc Natl Acad Sci U S A* **2012**, *109*, doi:10.1073/PNAS.1203530109.
103. Wu, Z.; Bai, F.; Fan, L.; Pang, W.; Han, R.; Wang, J.; Liu, Y.; Yan, X.; Duan, H.; Xing, L. Coexpression of Receptor Tyrosine Kinase AXL and EGFR in Human Primary Lung Adenocarcinomas. *Hum Pathol* **2015**, *46*, 1935–1944, doi:10.1016/J.HUMPATH.2015.08.014.
104. Hayakawa, D.; Takahashi, F.; Mitsuishi, Y.; Tajima, K.; Hidayat, M.; Winardi, W.; Ihara, H.; Kanamori, K.; Matsumoto, N.; Asao, T.; et al. Activation of Insulin-like Growth Factor-1 Receptor Confers Acquired Resistance to Osimertinib in Non-Small Cell Lung Cancer with EGFR T790M Mutation. *Thorac Cancer* **2020**, *11*, 140–149, doi:10.1111/1759-7714.13255.
105. Ferrara, M.G.; Martini, M.; D'Argento, E.; Forcella, C.; Vita, E.; di Noia, V.; Sperduti, I.; Bilotta, M.; Ribelli, M.; Damiano, P.; et al. PTEN Loss as a Predictor of Tumor Heterogeneity and Poor Prognosis in Patients With EGFR-Mutant Advanced Non-Small-Cell Lung Cancer Receiving Tyrosine Kinase Inhibitors. *Clin Lung Cancer* **2021**, *22*, 351–360, doi:10.1016/J.CLLC.2020.12.008.
106. Jacobsen, K.; Bertran-Alamillo, J.; Molina, M.A.; Teixidó, C.; Karachaliou, N.; Pedersen, M.H.; Castellví, J.; Garzón, M.; Codony-Servat, C.; Codony-Servat, J.; et al. Convergent Akt Activation Drives Acquired EGFR Inhibitor Resistance in Lung Cancer. *Nat Commun* **2017**, *8*, doi:10.1038/s41467-017-00450-6.
107. Koch, H.; Busto, M.E.D.C.; Kramer, K.; Médard, G.; Kuster, B. Chemical Proteomics Uncovers EPHA2 as a Mechanism of Acquired Resistance to Small Molecule EGFR Kinase Inhibition. *J Proteome Res* **2015**, *14*, 2617–2625, doi:10.1021/ACS.JPROTEOME.5B00161.
108. Jia, Y.; Yun, C.H.; Park, E.; Ercan, D.; Manuia, M.; Juarez, J.; Xu, C.; Rhee, K.; Chen, T.; Zhang, H.; et al. Overcoming EGFR(T790M) and EGFR(C797S) Resistance with Mutant-Selective Allosteric Inhibitors. *Nature* **2016**, *534*, 129–132, doi:10.1038/nature17960.
109. To, C.; Jang, J.; Chen, T.; Park, E.; Mushajiang, M.; de Clercq, D.J.H.; Xu, M.; Wang, S.; Cameron, M.D.; Heppner, D.E.; et al. Single and Dual Targeting of Mutant EGFR with an Allosteric Inhibitor. *Cancer Discov* **2019**, *9*, 926–943, doi:10.1158/2159-8290.CD-18-0903.

References

110. Tripathi, S.K.; Biswal, B.K. Allosteric Mutant-Selective Fourth-Generation EGFR Inhibitors as an Efficient Combination Therapeutic in the Treatment of Non-Small Cell Lung Carcinoma. *Drug Discov Today* **2021**, *26*, 1466–1472, doi:10.1016/J.DRUDIS.2021.02.005.
111. Liu, X.; Zhang, X.; Yang, L.; Tian, X.; Dong, T.; Ding, C.Z.; Hu, L.; Wu, L.; Zhao, L.; Mao, J.; et al. Abstract 1320: Preclinical Evaluation of TQB3804, a Potent EGFR C797S Inhibitor. *Cancer Res* **2019**, *79*, 1320–1320, doi:10.1158/1538-7445.AM2019-1320.
112. Park, K.; Haura, E.B.; Leighl, N.B.; Mitchell, P.; Shu, C.A.; Girard, N.; Viteri, S.; Han, J.Y.; Kim, S.W.; Lee, C.K.; et al. Amivantamab in EGFR Exon 20 Insertion-Mutated Non-Small-Cell Lung Cancer Progressing on Platinum Chemotherapy: Initial Results From the CHRYSALIS Phase I Study. *J Clin Oncol* **2021**, *39*, 3391–3402, doi:10.1200/JCO.21.00662.
113. Cho, B.C.; Lee, K.H.; Cho, E.K.; Kim, D.-W.; Lee, J.-S.; Han, J.-Y.; Kim, S.-W.; Spira, A.; Haura, E.B.; Sabari, J.K.; et al. 12580 Amivantamab (JNJ-61186372), an EGFR-MET Bispecific Antibody, in Combination with Lazertinib, a 3rd-Generation Tyrosine Kinase Inhibitor (TKI), in Advanced EGFR NSCLC. *Annals of Oncology* **2020**, *31*, S813, doi:10.1016/j.annonc.2020.08.1572.
114. Yu, H.; Johnson, M.; Steuer, C.; Vigliotti, M.; Chen, S.; Kamai, Y.; Yu, C.; Jänne, P. MA21.06 Preliminary Phase 1 Results of U3-1402 — A Novel HER3-Targeted Antibody–Drug Conjugate—in EGFR TKI-Resistant, EGFR-Mutant NSCLC. *Journal of Thoracic Oncology* **2019**, *14*, S336–S337, doi:10.1016/j.jtho.2019.08.677.
115. Cui, Q.; Hu, Y.; Cui, Q.; Wu, D.; Mao, Y.; Ma, D.; Liu, H. Osimertinib Rechallenge With Bevacizumab vs. Chemotherapy Plus Bevacizumab in EGFR-Mutant NSCLC Patients With Osimertinib Resistance. *Front Pharmacol* **2022**, *12*, doi:10.3389/FPHAR.2021.746707.
116. Lu, S.; Wu, L.; Jian, H.; Cheng, Y.; Wang, Q.; Fang, J.; Wang, Z.; Hu, Y.; Sun, M.; Han, L.; et al. VP9-2021: ORIENT-31: Phase III Study of Sintilimab with or without IBI305 plus Chemotherapy in Patients with EGFR Mutated Nonsquamous NSCLC Who Progressed after EGFR-TKI Therapy. *Annals of Oncology* **2022**, *33*, 112–113, doi:10.1016/j.annonc.2021.10.007.
117. Reeves, G.K.; Pirie, K.; Green, J.; Bull, D.; Beral, V. Reproductive Factors and Specific Histological Types of Breast Cancer: Prospective Study and Meta-Analysis. *Br J Cancer* **2009**, *100*, 538–544, doi:10.1038/SJ.BJC.6604853.
118. Howell, A.; Anderson, A.S.; Clarke, R.B.; Duffy, S.W.; Evans, D.G.; Garcia-Closas, M.; Gescher, A.J.; Key, T.J.; Saxton, J.M.; Harvie, M.N. Risk Determination and Prevention of Breast Cancer. *Breast Cancer Res* **2014**, *16*, doi:10.1186/S13058-014-0446-2.

119. Miller, K.D.; Nogueira, L.; Mariotto, A.B.; Rowland, J.H.; Yabroff, K.R.; Alfano, C.M.; Jemal, A.; Kramer, J.L.; Siegel, R.L. Cancer Treatment and Survivorship Statistics, 2019. *CA Cancer J Clin* **2019**, *69*, 363–385, doi:10.3322/CAAC.21565.
120. Sotiriou, C.; Pusztai, L. Gene-Expression Signatures in Breast Cancer. *N Engl J Med* **2009**, *360*, 790–800, doi:10.1056/NEJMRA0801289.
121. Carey, L.A.; Perou, C.M.; Livasy, C.A.; Dressler, L.G.; Cowan, D.; Conway, K.; Karaca, G.; Troester, M.A.; Chiu, K.T.; Edmiston, S.; et al. Race, Breast Cancer Subtypes, and Survival in the Carolina Breast Cancer Study. *JAMA* **2006**, *295*, 2492–2502, doi:10.1001/JAMA.295.21.2492.
122. Abe, O.; Abe, R.; Enomoto, K.; Kikuchi, K.; Koyama, H.; Masuda, H.; Nomura, Y.; Ohashi, Y.; Sakai, K.; Sugimachi, K.; et al. Relevance of Breast Cancer Hormone Receptors and Other Factors to the Efficacy of Adjuvant Tamoxifen: Patient-Level Meta-Analysis of Randomised Trials. *Lancet* **2011**, *378*, 771–784, doi:10.1016/S0140-6736(11)60993-8.
123. F, L.; DA, S.; SM, B. Current Medical Treatment of Estrogen Receptor-Positive Breast Cancer. *World J Biol Chem* **2015**, *6*, 231, doi:10.4331/WJBC.V6.I3.231.
124. Slamon, D.J.; Clark, G.M.; Wong, S.G.; Levin, W.J.; Ullrich, A.; McGuire, W.L. Human Breast Cancer: Correlation of Relapse and Survival with Amplification of the HER-2/Neu Oncogene. *Science* **1987**, *235*, 182–191, doi:10.1126/SCIENCE.3798106.
125. Witton, C.J.; Reeves, J.R.; Going, J.J.; Cooke, T.G.; Barlett, J.M.S. Expression of the HER1-4 Family of Receptor Tyrosine Kinases in Breast Cancer. *J Pathol* **2003**, *200*, 290–297, doi:10.1002/PATH.1370.
126. Arteaga, C.L.; Sliwkowski, M.X.; Osborne, C.K.; Perez, E.A.; Puglisi, F.; Gianni, L. Treatment of HER2-Positive Breast Cancer: Current Status and Future Perspectives. *Nat Rev Clin Oncol* **2011**, *9*, 16–32, doi:10.1038/NRCLINONC.2011.177.
127. Bauer, K.R.; Brown, M.; Cress, R.D.; Parise, C.A.; Caggiano, V. Descriptive Analysis of Estrogen Receptor (ER)-Negative, Progesterone Receptor (PR)-Negative, and HER2-Negative Invasive Breast Cancer, the so-Called Triple-Negative Phenotype: A Population-Based Study from the California Cancer Registry. *Cancer* **2007**, *109*, 1721–1728, doi:10.1002/CNCR.22618.
128. Dent, R.; Trudeau, M.; Pritchard, K.I.; Hanna, W.M.; Kahn, H.K.; Sawka, C.A.; Lickley, L.A.; Rawlinson, E.; Sun, P.; Narod, S.A. Triple-Negative Breast Cancer: Clinical Features and Patterns of Recurrence. *Clin Cancer Res* **2007**, *13*, 4429–4434, doi:10.1158/1078-0432.CCR-06-3045.
129. Voduc, K.D.; Cheang, M.C.U.; Tyldesley, S.; Gelmon, K.; Nielsen, T.O.; Kennecke, H. Breast Cancer Subtypes and the Risk of Local and Regional Relapse. *J Clin Oncol* **2010**, *28*, 1684–1691, doi:10.1200/JCO.2009.24.9284.

References

130. Montagna, E.; Bagnardi, V.; Rotmensz, N.; Viale, G.; Renne, G.; Canello, G.; Balduzzi, A.; Scarano, E.; Veronesi, P.; Luini, A.; et al. Breast Cancer Subtypes and Outcome after Local and Regional Relapse. *Ann Oncol* **2012**, *23*, 324–331, doi:10.1093/ANNONC/MDR129.
131. Griffiths, C.L.; Olin, J.L. Triple Negative Breast Cancer: A Brief Review of Its Characteristics and Treatment Options. *J Pharm Pract* **2012**, *25*, 319–323, doi:10.1177/0897190012442062.
132. Carey, L.A.; Dees, E.C.; Sawyer, L.; Gatti, L.; Moore, D.T.; Collichio, F.; Ollila, D.W.; Sartor, C.I.; Graham, M.L.; Perou, C.M. The Triple Negative Paradox: Primary Tumor Chemosensitivity of Breast Cancer Subtypes. *Clin Cancer Res* **2007**, *13*, 2329–2334, doi:10.1158/1078-0432.CCR-06-1109.
133. Perou, C.M.; Sørli, T.; Eisen, M.B.; van de Rijn, M.; Jeffrey, S.S.; Rees, C. a; Pollack, J.R.; Ross, D.T.; Johnsen, H.; Akslen, L. a; et al. Molecular Portraits of Human Breast Tumours. *Nature* **2000**, *406*, 747–752, doi:10.1038/35021093.
134. Sørli, T.; Perou, C.M.; Tibshirani, R.; Aas, T.; Geisler, S.; Johnsen, H.; Hastie, T.; Eisen, M.B.; van de Rijn, M.; Jeffrey, S.S.; et al. Gene Expression Patterns of Breast Carcinomas Distinguish Tumor Subclasses with Clinical Implications. *Proc Natl Acad Sci U S A* **2001**, *98*, 10869–10874, doi:10.1073/PNAS.191367098.
135. Prat, A.; Parker, J.S.; Karginova, O.; Fan, C.; Livasy, C.; Herschkowitz, J.I.; He, X.; Perou, C.M. Phenotypic and Molecular Characterization of the Claudin-Low Intrinsic Subtype of Breast Cancer. *Breast Cancer Res* **2010**, *12*, doi:10.1186/BCR2635.
136. Perou, C.M.; Borresen-Dale, A.L. Systems Biology and Genomics of Breast Cancer. *Cold Spring Harb Perspect Biol* **2011**, *3*, 1–17, doi:10.1101/CSHPERSPECT.A003293.
137. Bertucci, F.; Finetti, P.; Birnbaum, D. Basal Breast Cancer: A Complex and Deadly Molecular Subtype. *Curr Mol Med* **2012**, *12*, 96–110, doi:10.2174/156652412798376134.
138. Cheang, M.C.U.; Voduc, D.; Bajdik, C.; Leung, S.; McKinney, S.; Chia, S.K.; Perou, C.M.; Nielsen, T.O. Basal-like Breast Cancer Defined by Five Biomarkers Has Superior Prognostic Value than Triple-Negative Phenotype. *Clin Cancer Res* **2008**, *14*, 1368–1376, doi:10.1158/1078-0432.CCR-07-1658.
139. Perou, C.M. Molecular Stratification of Triple-Negative Breast Cancers. *Oncologist* **2011**, *16*, 61–70, doi:10.1634/theoncologist.2011-S1-61.
140. Krishnamurthy, S.; Poornima, R.; Challa, V.R.; Goud, Y.G.B. Triple Negative Breast Cancer - Our Experience and Review. *Indian J Surg Oncol* **2012**, *3*, 12–16, doi:10.1007/S13193-012-0138-2.

141. Prat, A.; Perou, C.M. Deconstructing the Molecular Portraits of Breast Cancer. *Mol Oncol* **2011**, *5*, 5–23, doi:10.1016/J.MOLONC.2010.11.003.
142. BD, L.; JA, B.; X, C.; ME, S.; AB, C.; Y, S.; JA, P. Identification of Human Triple-Negative Breast Cancer Subtypes and Preclinical Models for Selection of Targeted Therapies. *J Clin Invest* **2011**, *121*, 2750–2767, doi:10.1172/JCI45014.
143. Morris, G.J.; Naidu, S.; Topham, A.K.; Guiles, F.; Xu, Y.; McCue, P.; Schwartz, G.F.; Park, P.K.; Rosenberg, A.L.; Brill, K.; et al. Differences in Breast Carcinoma Characteristics in Newly Diagnosed African-American and Caucasian Patients: A Single-Institution Compilation Compared with the National Cancer Institute’s Surveillance, Epidemiology, and End Results Database. *Cancer* **2007**, *110*, 876–884, doi:10.1002/CNCR.22836.
144. Aapro, M.; Wildiers, H. Triple-Negative Breast Cancer in the Older Population. *Ann Oncol* **2012**, *23 Suppl 6*, doi:10.1093/ANNONC/MDS189.
145. Millikan, R.C.; Newman, B.; Tse, C.K.; Moorman, P.G.; Conway, K.; Smith, L. v.; Labbok, M.H.; Geradts, J.; Bensen, J.T.; Jackson, S.; et al. Epidemiology of Basal-like Breast Cancer. *Breast Cancer Res Treat* **2008**, *109*, 123–139, doi:10.1007/S10549-007-9632-6.
146. Kumar, P.; Aggarwal, R. An Overview of Triple-Negative Breast Cancer. *Arch Gynecol Obstet* **2016**, *293*, 247–269, doi:10.1007/S00404-015-3859-Y.
147. Lin, N.U.; Claus, E.; Sohl, J.; Razzak, A.R.; Arnaout, A.; Winer, E.P. Sites of Distant Recurrence and Clinical Outcomes in Patients with Metastatic Triple-Negative Breast Cancer: High Incidence of Central Nervous System Metastases. *Cancer* **2008**, *113*, 2638–2645, doi:10.1002/CNCR.23930.
148. Smid, M.; Wang, Y.; Zhang, Y.; Sieuwerts, A.M.; Yu, J.; Klijn, J.G.M.; Foekens, J.A.; Martens, J.W.M. Subtypes of Breast Cancer Show Preferential Site of Relapse. *Cancer Res* **2008**, *68*, 3108–3114, doi:10.1158/0008-5472.CAN-07-5644.
149. Kennecke, H.; Yerushalmi, R.; Woods, R.; Cheang, M.C.U.; Voduc, D.; Speers, C.H.; Nielsen, T.O.; Gelmon, K. Metastatic Behavior of Breast Cancer Subtypes. *J Clin Oncol* **2010**, *28*, 3271–3277, doi:10.1200/JCO.2009.25.9820.
150. Nielsen, T.O.; Hsu, F.D.; Jensen, K.; Cheang, M.; Karaca, G.; Hu, Z.; Hernandez-Boussard, T.; Livasy, C.; Cowan, D.; Dressler, L.; et al. Immunohistochemical and Clinical Characterization of the Basal-like Subtype of Invasive Breast Carcinoma. *Clin Cancer Res* **2004**, *10*, 5367–5374, doi:10.1158/1078-0432.CCR-04-0220.
151. Yamamoto, Y.; Ibusuki, M.; Nakano, M.; Kawasoe, T.; Hiki, R.; Iwase, H. Clinical Significance of Basal-like Subtype in Triple-Negative Breast Cancer. *Breast Cancer* **2009**, *16*, 260–267, doi:10.1007/S12282-009-0150-8.

References

152. Gerhard, R.; Ricardo, S.; Albergaria, A.; Gomes, M.; Silva, A.R.; Logullo, Â.F.; Cameselle-Teijeiro, J.F.; Paredes, J.; Schmitt, F. Immunohistochemical Features of Claudin-Low Intrinsic Subtype in Metaplastic Breast Carcinomas. *Breast* **2012**, *21*, 354–360, doi:10.1016/J.BREAST.2012.03.001.
153. Choi, J.; Jung, W.H.; Koo, J.S. Clinicopathologic Features of Molecular Subtypes of Triple Negative Breast Cancer Based on Immunohistochemical Markers. *Histol Histopathol* **2012**, *27*, 1481–1493, doi:10.14670/HH-27.1481.
154. Liedtke, C.; Mazouni, C.; Hess, K.R.; André, F.; Tordai, A.; Mejia, J.A.; Symmans, W.F.; Gonzalez-Angulo, A.M.; Hennessy, B.; Green, M.; et al. Response to Neoadjuvant Therapy and Long-Term Survival in Patients with Triple-Negative Breast Cancer. *J Clin Oncol* **2008**, *26*, 1275–1281, doi:10.1200/JCO.2007.14.4147.
155. Senkus, E.; Kyriakides, S.; Ohno, S.; Penault-Llorca, F.; Poortmans, P.; Rutgers, E.; Zackrisson, S.; Cardoso, F. Primary Breast Cancer: ESMO Clinical Practice Guidelines for Diagnosis, Treatment and Follow-Up. *Ann Oncol* **2015**, *26 Suppl 5*, v8–v30, doi:10.1093/ANNONC/MDV298.
156. Gradishar, W.J.; Anderson, B.O.; Abraham, J.; Aft, R.; Agnese, D.; Allison, K.H.; Blair, S.L.; Burstein, H.J.; Dang, C.; Elias, A.D.; et al. Breast Cancer, Version 3.2020, NCCN Clinical Practice Guidelines in Oncology. *J Natl Compr Canc Netw* **2020**, *18*, 452–478, doi:10.6004/JNCCN.2020.0016.
157. Straver, M.E.; Glas, A.M.; Hannemann, J.; Wesseling, J.; van de Vijver, M.J.; Rutgers, E.J.T.; Vrancken Peeters, M.J.T.F.D.; van Tinteren, H.; Van'T Veer, L.J.; Rodenhuis, S. The 70-Gene Signature as a Response Predictor for Neoadjuvant Chemotherapy in Breast Cancer. *Breast Cancer Res Treat* **2010**, *119*, 551–558, doi:10.1007/S10549-009-0333-1.
158. Berry, D.A.; Cirincione, C.; Henderson, I.C.; Citron, M.L.; Budman, D.R.; Goldstein, L.J.; Martino, S.; Perez, E.A.; Muss, H.B.; Norton, L.; et al. Estrogen-Receptor Status and Outcomes of Modern Chemotherapy for Patients with Node-Positive Breast Cancer. *JAMA* **2006**, *295*, 1658–1667, doi:10.1001/JAMA.295.14.1658.
159. M, C.; AS, C.; SC, D.; C, D.; RD, G.; J, G.; A, G.; R, G.; R, P.; KI, P.; et al. Adjuvant Chemotherapy in Oestrogen-Receptor-Poor Breast Cancer: Patient-Level Meta-Analysis of Randomised Trials. *Lancet* **2008**, *371*, 29–40, doi:10.1016/S0140-6736(08)60069-0.
160. Bauer, J.A.; Chakravarthy, A.B.; Rosenbluth, J.M.; Mi, D.; Seeley, E.H.; Granja-Ingram, N.D.M.; Olivares, M.G.; Kelley, M.C.; Mayer, I.A.; Meszoely, I.M.; et al. Identification of Markers of Taxane Sensitivity Using Proteomic and Genomic Analyses of Breast Tumors from Patients Receiving Neoadjuvant Paclitaxel and Radiation. *Clin Cancer Res* **2010**, *16*, 681–690, doi:10.1158/1078-0432.CCR-09-1091.

161. Abe, O.; Abe, R.; Enomoto, K.; Kikuchi, K.; Koyama, H.; Masuda, H.; Nomura, Y.; Sakai, K.; Sugimachi, K.; Tominaga, T.; et al. Effects of Chemotherapy and Hormonal Therapy for Early Breast Cancer on Recurrence and 15-Year Survival: An Overview of the Randomised Trials. *Lancet* **2005**, *365*, 1687–1717, doi:10.1016/S0140-6736(05)66544-0.
162. Nakatsukasa, K.; Koyama, H.; Oouchi, Y.; Imanishi, S.; Mizuta, N.; Sakaguchi, K.; Fujita, Y.; Fujiwara, I.; Kotani, T.; Matsuda, T.; et al. Docetaxel and Cyclophosphamide as Neoadjuvant Chemotherapy in HER2-Negative Primary Breast Cancer. *Breast Cancer* **2017**, *24*, 63–68, doi:10.1007/S12282-016-0666-7.
163. Zhang, J.; Wang, Z.; Hu, X.; Wang, B.; Wang, L.; Yang, W.; Liu, Y.; Liu, G.; Di, G.; Hu, Z.; et al. Cisplatin and Gemcitabine as the First Line Therapy in Metastatic Triple Negative Breast Cancer. *Int J Cancer* **2015**, *136*, 204–211, doi:10.1002/IJC.28966.
164. Jovanovic, B.; Mayer, I.A.; Mayer, E.L.; Abramson, V.G.; Bardia, A.; Sanders, M.E.; Kuba, M.G.; Estrada, M. v.; Beeler, J.S.; Shaver, T.M.; et al. A Randomized Phase II Neoadjuvant Study of Cisplatin, Paclitaxel With or Without Everolimus in Patients with Stage II/III Triple-Negative Breast Cancer (TNBC): Responses and Long-Term Outcome Correlated with Increased Frequency of DNA Damage Response Gene Mutations, TNBC Subtype, AR Status, and Ki67. *Clin Cancer Res* **2017**, *23*, 4035–4045, doi:10.1158/1078-0432.CCR-16-3055.
165. Li, Q.; Li, Q.; Zhang, P.; Yuan, P.; Wang, J.; Ma, F.; Luo, Y.; Fan, Y.; Cai, R.; Xu, B. A Phase II Study of Capecitabine plus Cisplatin in Metastatic Triple-Negative Breast Cancer Patients Pretreated with Anthracyclines and Taxanes. *Cancer Biol Ther* **2015**, *16*, 1746–1753, doi:10.1080/15384047.2015.1095400.
166. Amir, E.; Miller, N.; Geddie, W.; Freedman, O.; Kassam, F.; Simmons, C.; Oldfield, M.; Dranitsaris, G.; Tomlinson, G.; Laupacis, A.; et al. Prospective Study Evaluating the Impact of Tissue Confirmation of Metastatic Disease in Patients with Breast Cancer. *J Clin Oncol* **2012**, *30*, 587–592, doi:10.1200/JCO.2010.33.5232.
167. Yang, L.; Shi, P.; Zhao, G.; Xu, J.; Peng, W.; Zhang, J.; Zhang, G.; Wang, X.; Dong, Z.; Chen, F.; et al. Targeting Cancer Stem Cell Pathways for Cancer Therapy. *Signal Transduct Target Ther* **2020**, *5*, 8, doi:10.1038/S41392-020-0110-5.
168. Najafi, M.; Mortezaee, K.; Majidpoor, J. Cancer Stem Cell (CSC) Resistance Drivers. *Life Sci* **2019**, *234*, 116781, doi:10.1016/J.LFS.2019.116781.
169. Huang, T.; Song, X.; Xu, D.; Tiek, D.; Goenka, A.; Wu, B.; Sastry, N.; Hu, B.; Cheng, S.Y. Stem Cell Programs in Cancer Initiation, Progression, and Therapy Resistance. *Theranostics* **2020**, *10*, 8721–8743, doi:10.7150/THNO.41648.

References

170. Lim, J.R.; Mouawad, J.; Gorton, O.K.; Bubb, W.A.; Kwan, A.H. Cancer Stem Cell Characteristics and Their Potential as Therapeutic Targets. *Med Oncol* **2021**, *38*, doi:10.1007/S12032-021-01524-8.
171. Furth, J.; Kahn, M.C. The Transmission of Leukemia of Mice with a Single Cell. *Am J Cancer* **1937**, *31*, 276–282, doi:10.1158/AJC.1937.276.
172. Bonnet, D.; Dick, J.E. Human Acute Myeloid Leukemia Is Organized as a Hierarchy That Originates from a Primitive Hematopoietic Cell. *Nat Med* **1997**, *3*, 730–737, doi:10.1038/NM0797-730.
173. Reynolds, B.A.; Weiss, S. Clonal and Population Analyses Demonstrate That an EGF-Responsive Mammalian Embryonic CNS Precursor Is a Stem Cell. *Dev Biol* **1996**, *175*, 1–13, doi:10.1006/DBIO.1996.0090.
174. Dontu, G.; Abdallah, W.M.; Foley, J.M.; Jackson, K.W.; Clarke, M.F.; Kawamura, M.J.; Wicha, M.S. In Vitro Propagation and Transcriptional Profiling of Human Mammary Stem/Progenitor Cells. *Genes Dev* **2003**, *17*, 1253–1270, doi:10.1101/GAD.1061803.
175. Fang, D.; Nguyen, T.K.; Leishear, K.; Finko, R.; Kulp, A.N.; Hotz, S.; van Belle, P.A.; Xu, X.; Elder, D.E.; Herlyn, M. A Tumorigenic Subpopulation with Stem Cell Properties in Melanomas. *Cancer Res* **2005**, *65*, 9328–9337, doi:10.1158/0008-5472.CAN-05-1343.
176. Atashzar, M.R.; Baharlou, R.; Karami, J.; Abdollahi, H.; Rezaei, R.; Pourramezan, F.; Zoljalali Moghaddam, S.H. Cancer Stem Cells: A Review from Origin to Therapeutic Implications. *J Cell Physiol* **2020**, *235*, 790–803, doi:10.1002/jcp.29044.
177. Tomasetti, C.; Vogelstein, B. Variation in Cancer Risk among Tissues Can Be Explained by the Number of Stem Cell Divisions. *Science* **2015**, *347*, 78, doi:10.1126/SCIENCE.1260825.
178. Lagasse, E. Cancer Stem Cells with Genetic Instability: The Best Vehicle with the Best Engine for Cancer. *Gene Ther* **2008**, *15*, 136–142, doi:10.1038/SJ.GT.3303068.
179. Bergsmedh, A.; Szeles, A.; Spetz, A.-L.; Holmgren, L. Loss of the P21 Cip1/Waf1 Cyclin Kinase Inhibitor Results in Propagation of Horizontally Transferred DNA 1. *Cancer Res* **2002**, *15*, 575–579.
180. Bergsmedh, A.; Szeles, A.; Henriksson, M.; Bratt, A.; Folkman, M.J.; Spetz, A.L.; Holmgren, L. Horizontal Transfer of Oncogenes by Uptake of Apoptotic Bodies. *Proc Natl Acad Sci U S A* **2001**, *98*, 6407–6411, doi:10.1073/PNAS.101129998/ASSET/DD0F1F72-99AA-455B-9F86-E4E7CA1AF19F/ASSETS/GRAPHIC/PQ1011299004.JPEG.

181. Bjerkvig, R.; Tysnes, B.B.; Aboody, K.S.; Najbauer, J.; Terzis, A.J.A. The Origin of the Cancer Stem Cell: Current Controversies and New Insights. *Nature Reviews Cancer* **2005**, *5*, 899–904, doi:10.1038/nrc1740.
182. Tokar, E.J.; Diwan, B.A.; Waalkes, M.P. Arsenic Exposure Transforms Human Epithelial Stem/Progenitor Cells into a Cancer Stem-like Phenotype. *Environ Health Perspect* **2010**, *118*, 108–115, doi:10.1289/EHP.0901059.
183. Rachkovsky, M.; Sodi, S.; Chakraborty, A.; Avissar, Y.; Bolognia, J.; McNiff, J.M.; Platt, J.; Bermudes, D.; Pawelek, J. Melanoma x Macrophage Hybrids with Enhanced Metastatic Potential. *Clin Exp Metastasis* **1998**, *16*, 299–312, doi:10.1023/A:1006557228604.
184. Folmes, C.D.L.; Nelson, T.J.; Martinez-Fernandez, A.; Arrell, D.K.; Lindor, J.Z.; Dzeja, P.P.; Ikeda, Y.; Perez-Terzic, C.; Terzic, A. Somatic Oxidative Bioenergetics Transitions into Pluripotency-Dependent Glycolysis to Facilitate Nuclear Reprogramming. *Cell Metab* **2011**, *14*, 264–271, doi:10.1016/J.CMET.2011.06.011.
185. Altevogt, P.; Sammar, M.; Hüser, L.; Kristiansen, G. Novel Insights into the Function of CD24: A Driving Force in Cancer. *Int J Cancer* **2020**, *148*, 546–559, doi:10.1002/ijc.33249.
186. Al-Hajj, M.; Wicha, M.S.; Benito-Hernandez, A.; Morrison, S.J.; Clarke, M.F. Prospective Identification of Tumorigenic Breast Cancer Cells. *Proc Natl Acad Sci U S A* **2003**, *100*, 3983–3988, doi:10.1073/PNAS.0530291100.
187. Baumann, P.; Cremers, N.; Kroese, F.; Orend, G.; Chiquet-Ehrismann, R.; Uede, T.; Yagita, H.; Sleeman, J.P. CD24 Expression Causes the Acquisition of Multiple Cellular Properties Associated with Tumor Growth and Metastasis. *Cancer Res* **2005**, *65*, 10783–10793, doi:10.1158/0008-5472.CAN-05-0619.
188. Yin, A.H.; Miraglia, S.; Zanjani, E.D.; Almeida-Porada, G.; Ogawa, M.; Leary, A.G.; Olweus, J.; Kearney, J.; Buck, D.W. AC133, a Novel Marker for Human Hematopoietic Stem and Progenitor Cells. *Blood* **1997**, *90*, 5002–5012, doi:10.1182/BLOOD.V90.12.5002.
189. Miraglia, S.; Godfrey, W.; Yin, A.H.; Atkins, K.; Warnke, R.; Holden, J.T.; Bray, R.A.; Waller, E.K.; Buck, D.W. A Novel Five-Transmembrane Hematopoietic Stem Cell Antigen: Isolation, Characterization, and Molecular Cloning. *Blood* **1997**, *90*, 5013–5021, doi:10.1182/BLOOD.V90.12.5013.
190. Ricci-Vitiani, L.; Lombardi, D.G.; Pilozzi, E.; Biffoni, M.; Todaro, M.; Peschle, C.; de Maria, R. Identification and Expansion of Human Colon-Cancer-Initiating Cells. *Nature* **2007**, *445*, 111–115, doi:10.1038/NATURE05384.
191. Hermann, P.C.; Huber, S.L.; Herrler, T.; Aicher, A.; Ellwart, J.W.; Guba, M.; Bruns, C.J.; Heeschen, C. Distinct Populations of Cancer Stem Cells Determine Tumor Growth

References

- and Metastatic Activity in Human Pancreatic Cancer. *Cell Stem Cell* **2007**, *1*, 313–323, doi:10.1016/J.STEM.2007.06.002.
192. Eramo, A.; Lotti, F.; Sette, G.; Pilozzi, E.; Biffoni, M.; di Virgilio, A.; Conticello, C.; Ruco, L.; Peschle, C.; de Maria, R. Identification and Expansion of the Tumorigenic Lung Cancer Stem Cell Population. *Cell Death Differ* **2008**, *15*, 504–514, doi:10.1038/sj.cdd.4402283.
193. Bertolini, G.; Roz, L.; Perego, P.; Tortoreto, M.; Fontanella, E.; Gatti, L.; Pratesi, G.; Fabbri, A.; Andriani, F.; Tinelli, S.; et al. Highly Tumorigenic Lung Cancer CD133+ Cells Display Stem-like Features and Are Spared by Cisplatin Treatment. *Proc Natl Acad Sci U S A* **2009**, *106*, 16281–16286, doi:10.1073/pnas.0905653106.
194. Arai, F.; Ohneda, O.; Miyamoto, T.; Zhang, X.Q.; Suda, T. Mesenchymal Stem Cells in Perichondrium Express Activated Leukocyte Cell Adhesion Molecule and Participate in Bone Marrow Formation. *J Exp Med* **2002**, *195*, 1549–1563, doi:10.1084/JEM.20011700.
195. Zhang, W.C.; Ng, S.C.; Yang, H.; Rai, A.; Umashankar, S.; Ma, S.; Soh, B.S.; Sun, L.L.; Tai, B.C.; Nga, M.E.; et al. Glycine Decarboxylase Activity Drives Non-Small Cell Lung Cancer Tumor-Initiating Cells and Tumorigenesis. *Cell* **2012**, *148*, 259–272, doi:10.1016/j.cell.2011.11.050.
196. Zhao, Y.; Zhang, W.; Guo, Z.; Ma, F.; Wu, Y.; Bai, Y.; Gong, W.; Chen, Y.; Cheng, T.; Zhi, F.; et al. Inhibition of the Transcription Factor Sp1 Suppresses Colon Cancer Stem Cell Growth and Induces Apoptosis in Vitro and in Nude Mouse Xenografts. *Oncol Rep* **2013**, *30*, 1782–1792, doi:10.3892/OR.2013.2627/HTML.
197. Yan, M.; Yang, X.; Wang, L.; Clark, D.; Zuo, H.; Ye, D.; Chen, W.; Zhang, P. Plasma Membrane Proteomics of Tumor Spheres Identify CD166 as a Novel Marker for Cancer Stem-like Cells in Head and Neck Squamous Cell Carcinoma. *Molecular and Cellular Proteomics* **2013**, *12*, 3271–3284, doi:10.1074/MCP.M112.025460/ATTACHMENT/DDBC8730-0D76-480B-93D6-8105624A5C41/MMC1.ZIP.
198. Zakaria, N.; Yusoff, N.M.; Zakaria, Z.; Lim, M.N.; Baharuddin, P.J.N.; Fakiruddin, K.S.; Yahaya, B. Human Non-Small Cell Lung Cancer Expresses Putative Cancer Stem Cell Markers and Exhibits the Transcriptomic Profile of Multipotent Cells. *BMC Cancer* **2015**, *15*, 84, doi:10.1186/s12885-015-1086-3.
199. Duester, G. Families of Retinoid Dehydrogenases Regulating Vitamin A Function: Production of Visual Pigment and Retinoic Acid. *Eur J Biochem* **2000**, *267*, 4315–4324, doi:10.1046/J.1432-1327.2000.01497.X.

200. Vasiliou, V.; Pappa, A. Polymorphisms of Human Aldehyde Dehydrogenases. Consequences for Drug Metabolism and Disease. *Pharmacology* **2000**, *61*, 192–198, doi:10.1159/000028400.
201. Chute, J.P.; Muramoto, G.G.; Whitesides, J.; Colvin, M.; Safi, R.; Chao, N.J.; McDonnell, D.P. Inhibition of Aldehyde Dehydrogenase and Retinoid Signaling Induces the Expansion of Human Hematopoietic Stem Cells. *Proc Natl Acad Sci U S A* **2006**, *103*, 11707–11712, doi:10.1073/PNAS.0603806103.
202. Liu, S.; Cong, Y.; Wang, D.; Sun, Y.; Deng, L.; Liu, Y.; Martin-Trevino, R.; Shang, L.; McDermott, S.P.; Landis, M.D.; et al. Breast Cancer Stem Cells Transition between Epithelial and Mesenchymal States Reflective of Their Normal Counterparts. *Stem Cell Reports* **2013**, *2*, 78–91, doi:10.1016/J.STEMCR.2013.11.009.
203. Ginestier, C.; Hur, M.H.; Charafe-Jauffret, E.; Monville, F.; Dutcher, J.; Brown, M.; Jacquemier, J.; Viens, P.; Kleer, C.G.; Liu, S.; et al. ALDH1 Is a Marker of Normal and Malignant Human Mammary Stem Cells and a Predictor of Poor Clinical Outcome. *Cell Stem Cell* **2007**, *1*, 555–567, doi:10.1016/J.STEM.2007.08.014.
204. Chefetz, I.; Grimley, E.; Yang, K.; Hong, L.; Vinogradova, E. v.; Suciu, R.; Kovalenko, I.; Karnak, D.; Morgan, C.A.; Chtcherbinine, M.; et al. A Pan-ALDH1A Inhibitor Induces Necroptosis in Ovarian Cancer Stem-like Cells. *Cell Rep* **2019**, *26*, 3061-3075.e6, doi:10.1016/J.CELREP.2019.02.032.
205. Lehmann, B.D.; Bauer, J.A.; Chen, X.; Sanders, M.E.; Chakravarthy, A.B.; Shyr, Y.; Pietenpol, J.A. Identification of Human Triple-Negative Breast Cancer Subtypes and Preclinical Models for Selection of Targeted Therapies. *Journal of Clinical Investigation* **2011**, *121*, 2750–2767, doi:10.1172/JCI45014.
206. Zhang, Y.; Weinberg, R.A. Epithelial-to-Mesenchymal Transition in Cancer: Complexity and Opportunities. *Front Med* **2018**, *12*, 361–373, doi:10.1007/s11684-018-0656-6.
207. Polyak, K.; Weinberg, R.A. Transitions between Epithelial and Mesenchymal States: Acquisition of Malignant and Stem Cell Traits. *Nat Rev Cancer* **2009**, *9*, 265–273, doi:10.1038/NRC2620.
208. Stemmler, M.P.; Eccles, R.L.; Brabletz, S.; Brabletz, T. Non-Redundant Functions of EMT Transcription Factors. *Nature Cell Biology* **2019**, *21*, 102–112, doi:10.1038/s41556-018-0196-y.
209. Wilson, M.M.; Weinberg, R.A.; Lees, J.A.; Guen, V.J. Emerging Mechanisms by Which EMT Programs Control Stemness. *Trends Cancer* **2020**, *6*, 775–780.
210. Frixen, U.H.; Behrens, J.; Sachs, M.; Eberle, G.; Voss, B.; Warda, A.; Lochner, D.; Birchmeier, W. E-Cadherin-Mediated Cell-Cell Adhesion Prevents Invasiveness of Human Carcinoma Cells. *J Cell Biol* **1991**, *113*, 173–185, doi:10.1083/JCB.113.1.173.

References

211. Roy, S.; Sunkara, R.R.; Parmar, M.Y.; Shaikh, S.; Waghmare, S.K. EMT Imparts Cancer Stemness and Plasticity: New Perspectives and Therapeutic Potential. *Front Biosci (Landmark Ed)* **2021**, *26*, 238–265, doi:10.2741/4893.
212. Shibue, T.; Weinberg, R.A. EMT, CSCs, and Drug Resistance: The Mechanistic Link and Clinical Implications. *Nat Rev Clin Oncol* **2017**, *14*, 611–629, doi:10.1038/NRCLINONC.2017.44.
213. Lambert, A.W.; Pattabiraman, D.R.; Weinberg, R.A. Emerging Biological Principles of Metastasis. *Cell* **2017**, *168*, 670–691, doi:10.1016/J.CELL.2016.11.037.
214. Tsai, J.H.; Yang, J. Epithelial-Mesenchymal Plasticity in Carcinoma Metastasis. *Genes Dev* **2013**, *27*, 2192–2206, doi:10.1101/GAD.225334.113.
215. Chaffer, C.L.; Brueckmann, I.; Scheel, C.; Kaestli, A.J.; Wiggins, P.A.; Rodrigues, L.O.; Brooks, M.; Reinhardt, F.; Suc, Y.; Polyak, K.; et al. Normal and Neoplastic Nonstem Cells Can Spontaneously Convert to a Stem-like State. *Proc Natl Acad Sci U S A* **2011**, *108*, 7950–7955, doi:10.1073/PNAS.1102454108/-/DCSUPPLEMENTAL/PNAS.201102454SI.PDF.
216. Chaffer, C.L.; Marjanovic, N.D.; Lee, T.; Bell, G.; Kleer, C.G.; Reinhardt, F.; D'Alessio, A.C.; Young, R.A.; Weinberg, R.A. Poised Chromatin at the ZEB1 Promoter Enables Breast Cancer Cell Plasticity and Enhances Tumorigenicity. *Cell* **2013**, *154*, 61, doi:10.1016/J.CELL.2013.06.005.
217. Vega, S.; Morales, A. v.; Ocaña, O.H.; Valdés, F.; Fabregat, I.; Nieto, M.A. Snail Blocks the Cell Cycle and Confers Resistance to Cell Death. *Genes Dev* **2004**, *18*, 1131–1143, doi:10.1101/GAD.294104.
218. Saxena, M.; Stephens, M.A.; Pathak, H.; Rangarajan, A. Transcription Factors That Mediate Epithelial-Mesenchymal Transition Lead to Multidrug Resistance by Upregulating ABC Transporters. *Cell Death Dis* **2011**, *2*, doi:10.1038/CDDIS.2011.61.
219. Hadjimichael, C.; Chanoumidou, K.; Papadopoulou, N.; Arampatzi, P.; Papamatheakis, J.; Kretsovali, A. Common Stemness Regulators of Embryonic and Cancer Stem Cells. *World J Stem Cells* **2015**, *7*, 1150–1184, doi:10.4252/WJSC.V7.I9.1150.
220. Pouremamali, F.; Vahedian, V.; Hassani, N.; Mirzaei, S.; Pouremamali, A.; Kazemzadeh, H.; Faridvand, Y.; Jafari-gharabaghlo, D.; Nouri, M.; Maroufi, N.F. The Role of SOX Family in Cancer Stem Cell Maintenance: With a Focus on SOX2. *Pathol Res Pract* **2022**, *231*.
221. Rodriguez-Pinilla, S.M.; Sarrio, D.; Moreno-Bueno, G.; Rodriguez-Gil, Y.; Martinez, M.A.; Hernandez, L.; Hardisson, D.; Reis-Filho, J.S.; Palacios, J. Sox2: A Possible Driver of the Basal-like Phenotype in Sporadic Breast Cancer. *Mod Pathol* **2007**, *20*, 474–481, doi:10.1038/MODPATHOL.3800760.

222. Murakami, A.; Takahashi, F.; Nurwidya, F.; Kobayashi, I.; Minakata, K.; Hashimoto, M.; Nara, T.; Kato, M.; Tajima, K.; Shimada, N.; et al. Hypoxia Increases Gefitinib-Resistant Lung Cancer Stem Cells through the Activation of Insulin-like Growth Factor 1 Receptor. *PLoS One* **2014**, *9*, doi:10.1371/journal.pone.0086459.
223. Wang, L.; Liu, X.; Ren, Y.; Zhang, J.; Chen, J.; Zhou, W.; Guo, W.; Wang, X.; Chen, H.; Li, M.; et al. Cisplatin-Enriching Cancer Stem Cells Confer Multidrug Resistance in Non-Small Cell Lung Cancer via Enhancing TRIB1/HDAC Activity. *Cell Death Dis* **2017**, *8*, doi:10.1038/cddis.2016.409.
224. Choe, C.; Kim, H.; Min, S.; Park, S.; Seo, J.; Roh, S. SOX2, a Stemness Gene, Induces Progression of NSCLC A549 Cells toward Anchorage-Independent Growth and Chemoresistance to Vinblastine. *Onco Targets Ther* **2018**, *11*, 6197–6207, doi:10.2147/OTT.S175810.
225. Zhou, R.-T.; Ni, Y.-R.; Zeng, F.-J. The Roles of Long Noncoding RNAs in the Regulation of OCT4 Expression. *Stem Cell Res Ther* **2022**, *13*, 383, doi:10.1186/s13287-022-03059-9.
226. Nichols, J.; Zevnik, B.; Anastassiadis, K.; Niwa, H.; Klewe-Nebenius, D.; Chambers, I.; Schöler, H.; Smith, A. Formation of Pluripotent Stem Cells in the Mammalian Embryo Depends on the POU Transcription Factor Oct4. *Cell* **1998**, *95*, 379–391, doi:10.1016/S0092-8674(00)81769-9.
227. Zhang, J.M.; Wei, K.; Jiang, M. OCT4 but Not SOX2 Expression Correlates with Worse Prognosis in Surgical Patients with Triple-Negative Breast Cancer. *Breast Cancer* **2018**, *25*, 447–455, doi:10.1007/S12282-018-0844-X.
228. Li, S.J.; Huang, J.; Zhou, X.D.; Zhang, W.B.; Lai, Y.T.; Che, G.W. Clinicopathological and Prognostic Significance of Oct-4 Expression in Patients with Non-Small Cell Lung Cancer: A Systematic Review and Meta-Analysis. *J Thorac Dis* **2016**, *8*, 1587–1600, doi:10.21037/JTD.2016.06.01.
229. Jen, J.; Tang, Y.A.; Lu, Y.H.; Lin, C.C.; Lai, W.W.; Wang, Y.C. Oct4 Transcriptionally Regulates the Expression of Long Non-Coding RNAs NEAT1 and MALAT1 to Promote Lung Cancer Progression. *Mol Cancer* **2017**, *16*, doi:10.1186/S12943-017-0674-Z.
230. Vasefifar, P.; Motafakkerazad, R.; Maleki, L.A.; Najafi, S.; Ghrobaninezhad, F.; Najafzadeh, B.; Alemohammad, H.; Amini, M.; Baghbanzadeh, A.; Baradaran, B. Nanog, as a Key Cancer Stem Cell Marker in Tumor Progression. *Gene* **2022**, *827*.
231. Wang, D.; Lu, P.; Zhang, H.; Luo, M.; Zhang, X.; Wei, X.; Gao, J.; Zhao, Z.; Liu, C. Oct-4 and Nanog Promote the Epithelial-Mesenchymal Transition of Breast Cancer Stem Cells and Are Associated with Poor Prognosis in Breast Cancer Patients. *Oncotarget* **2014**, *5*, 10803, doi:10.18632/ONCOTARGET.2506.

References

232. Guo, T.; Kong, J.; Liu, Y.; Li, Z.; Xia, J.; Zhang, Y.; Zhao, S.; Li, F.; Li, J.; Gu, C. Transcriptional Activation of NANOG by YBX1 Promotes Lung Cancer Stem-like Properties and Metastasis. *Biochem Biophys Res Commun* **2017**, *487*, 153–159, doi:10.1016/J.BBRC.2017.04.033.
233. Venkatesh, V.; Nataraj, R.; Thangaraj, G.S.; Karthikeyan, M.; Gnanasekaran, A.; Kagineelli, S.B.; Kuppanna, G.; Kallappa, C.G.; Basalingappa, K.M. Targeting Notch Signalling Pathway of Cancer Stem Cells. *Stem Cell Investig* **2018**, *5*, doi:10.21037/sci.2018.02.02.
234. Yamamoto, M.; Taguchi, Y.; Ito-Kureha, T.; Semba, K.; Yamaguchi, N.; Inoue, J.I. NF-KB Non-Cell-Autonomously Regulates Cancer Stem Cell Populations in the Basal-like Breast Cancer Subtype. *Nat Commun* **2013**, *4*, doi:10.1038/NCOMMS3299.
235. Westhoff, B.; Colaluca, I.N.; D'Ario, G.; Donzelli, M.; Tosoni, D.; Volorio, S.; Pelosi, G.; Spaggiari, L.; Mazzarol, G.; Viale, G.; et al. Alterations of the Notch Pathway in Lung Cancer. *Proc Natl Acad Sci U S A* **2009**, *106*, 22293–22298, doi:10.1073/PNAS.0907781106/SUPPL_FILE/0907781106SI.PDF.
236. Reedijk, M.; Odorcic, S.; Zhang, H.; Chetty, R.; Tennert, C.; Dickson, B.C.; Lockwood, G.; Gallinger, S.; Egan, S.E. Activation of Notch Signaling in Human Colon Adenocarcinoma. *Int J Oncol* **2008**, *33*, 1223, doi:10.3892/IJO_00000112.
237. Majumder, S.; Crabtree, J.S.; Golde, T.E.; Minter, L.M.; Osborne, B.A.; Miele, L. Targeting Notch in Oncology: The Path Forward. *Nat Rev Drug Discov* **2021**, *20*, 125–144, doi:10.1038/s41573-020-00091-3.
238. Salaritabar, A.; Berindan-Neagoe, I.; Darvish, B.; Hadjiakhoondi, F.; Manayi, A.; Devi, K.P.; Barreca, D.; Orhan, I.E.; Süntar, I.; Farooqi, A.A.; et al. Targeting Hedgehog Signaling Pathway: Paving the Road for Cancer Therapy. *Pharmacol Res* **2019**, *141*, 466–480, doi:10.1016/J.PHRS.2019.01.014.
239. Xin, M.; Ji, X.; de La Cruz, L.K.; Thareja, S.; Wang, B. Strategies to Target the Hedgehog Signaling Pathway for Cancer Therapy. *Med Res Rev* **2018**, *38*, 870–913, doi:10.1002/MED.21482.
240. Liu, J.; Wang, X.; Li, J.; Wang, H.; Wei, G.; Yan, J. Reconstruction of the Gene Regulatory Network Involved in the Sonic Hedgehog Pathway with a Potential Role in Early Development of the Mouse Brain. *PLoS Comput Biol* **2014**, *10*, e1003884, doi:10.1371/JOURNAL.PCBI.1003884.
241. Ma, J.; Zhou, C.; Chen, X. MiR-636 Inhibits EMT, Cell Proliferation and Cell Cycle of Ovarian Cancer by Directly Targeting Transcription Factor Gli2 Involved in Hedgehog Pathway. *Cancer Cell Int* **2021**, *21*, doi:10.1186/S12935-020-01725-7.

242. Bermudez, O.; Hennen, E.; Koch, I.; Lindner, M.; Eickelberg, O. Gli1 Mediates Lung Cancer Cell Proliferation and Sonic Hedgehog-Dependent Mesenchymal Cell Activation. *PLoS One* **2013**, *8*, doi:10.1371/JOURNAL.PONE.0063226.
243. Souzaki, M.; Kubo, M.; Kai, M.; Kameda, C.; Tanaka, H.; Taguchi, T.; Tanaka, M.; Onishi, H.; Katano, M. Hedgehog Signaling Pathway Mediates the Progression of Non-Invasive Breast Cancer to Invasive Breast Cancer. *Cancer Sci* **2011**, *102*, 373–381, doi:10.1111/J.1349-7006.2010.01779.X.
244. Krishnamurthy, N.; Kurzrock, R. Targeting the Wnt/Beta-Catenin Pathway in Cancer: Update on Effectors and Inhibitors Graphical Abstract. *Cancer Treatments Review* **2018**, *62*, 50–60, doi:10.1016/j.ctrv.2017.11.002.
245. Taciak, B.; Pruszyńska, I.; Kiraga, L.; Białasek, M.; Krol, M. Wnt Signaling Pathway in Development and Cancer. *J Physiol Pharmacol* **2018**, *69*, 185–196, doi:10.26402/JPP.2018.2.07.
246. Moon, H.G.; Zheng, Y.; An, C.H.; Kim, Y.K.; Jin, Y. CCN1 Secretion Induced by Cigarette Smoking Extracts Augments IL-8 Release from Bronchial Epithelial Cells. *PLoS One* **2013**, *8*, e68199, doi:10.1371/JOURNAL.PONE.0068199.
247. Zhang, L.; Luga, V.; Armitage, S.K.; Musiol, M.; Won, A.; Yip, C.M.; Plotnikov, S. v.; Wrana, J.L. A Lateral Signalling Pathway Coordinates Shape Volatility during Cell Migration. *Nat Commun* **2016**, *7*, doi:10.1038/NCOMMS11714.
248. Daulat, A.M.; Bertucci, F.; Audebert, S.; Sergé, A.; Finetti, P.; Josselin, E.; Castellano, R.; Birnbaum, D.; Angers, S.; Borg, J.P. PRICKLE1 Contributes to Cancer Cell Dissemination through Its Interaction with MTORC2. *Dev Cell* **2016**, *37*, 311–325, doi:10.1016/J.DEVCEL.2016.04.011.
249. Fan, G.; Ye, D.; Zhu, S.; Xi, J.; Guo, X.; Qiao, J.; Wu, Y.; Jia, W.; Wang, G.; Fan, G.; et al. RTL1 Promotes Melanoma Proliferation by Regulating Wnt/ β -Catenin Signalling. *Oncotarget* **2017**, *8*, 106026–106037, doi:10.18632/ONCOTARGET.22523.
250. Boni, V.; Burris III, H.A.; Liu, J.F.; Spira, A.I.; Arkenau, H.-T.; Fidler, M.J.; Rosen, L.S.; Sweis, R.F.; Uboha, N.V.; Sanborn, R.E.; et al. CX-2009, a CD166-Directed Probody Drug Conjugate (PDC): Results from the First-in-Human Study in Patients (Pts) with Advanced Cancer Including Breast Cancer (BC). *Journal of Clinical Oncology* **2020**, *38*, 526–526, doi:10.1200/JCO.2020.38.15_suppl.526.
251. Brancaccio, G.; Pea, F.; Moscarella, E.; Argenziano, G. Sonidegib for the Treatment of Advanced Basal Cell Carcinoma. *Front Oncol* **2020**, *10*, doi:10.3389/FONC.2020.582866.
252. Pietanza, M.C.; Litvak, A.M.; Varghese, A.M.; Krug, L.M.; Fleisher, M.; Teitcher, J.B.; Holodny, A.I.; Sima, C.S.; Woo, K.M.; Ng, K.K.; et al. A Phase I Trial of the Hedgehog Inhibitor, Sonidegib (LDE225), in Combination with Etoposide and Cisplatin for the

References

- Initial Treatment of Extensive Stage Small Cell Lung Cancer. *Lung Cancer* **2016**, *99*, 23–30, doi:10.1016/J.LUNGCAN.2016.04.014.
253. Bao, B.; Ahmad, A.; Azmi, A.S.; Ali, S.; Sarkar, F.H. Overview of Cancer Stem Cells (CSCs) and Mechanisms of Their Regulation: Implications for Cancer Therapy. *Curr Protoc Pharmacol* **2013**, *Chapter 14*, doi:10.1002/0471141755.PH1425S61.
254. Plaks, V.; Kong, N.; Werb, Z. The Cancer Stem Cell Niche: How Essential Is the Niche in Regulating Stemness of Tumor Cells? *Cell Stem Cell* **2015**, *16*, 225, doi:10.1016/J.STEM.2015.02.015.
255. Wainwright, E.N.; Scaffidi, P. Epigenetics and Cancer Stem Cells: Unleashing, Hijacking, and Restricting Cellular Plasticity. *Trends Cancer* **2017**, *3*, 372–386, doi:10.1016/J.TRECAN.2017.04.004.
256. Sancho, P.; Barneda, D.; Heeschen, C. Hallmarks of Cancer Stem Cell Metabolism. *Br J Cancer* **2016**, *114*, 1305–1312, doi:10.1038/BJC.2016.152.
257. Polonio-Alcalá, E.; Rabionet, M.; Ruiz-Martínez, S.; Ciurana, J.; Puig, T. Three-Dimensional Manufactured Supports for Breast Cancer Stem Cell Population Characterization. *Curr Drug Targets* **2018**, *20*, 839–851, doi:10.2174/1389450120666181122113300.
258. Ringer, S. Concerning the Influence Exerted by Each of the Constituents of the Blood on the Contraction of the Ventricle. *J Physiol* **1882**, *3*, 380–393, doi:10.1113/JPHYSIOL.1882.SP000111.
259. Ringer, S. A Further Contribution Regarding the Influence of the Different Constituents of the Blood on the Contraction of the Heart. *J Physiol* **1883**, *4*, 29–42, doi:10.1113/JPHYSIOL.1883.SP000120.
260. Harrison, R.G.; Greenman, M.J.; Mall, F.P.; Jackson, C.M. Observations of the Living Developing Nerve Fiber. *Anat Rec* **1907**, *1*, 116–128, doi:10.1002/AR.1090010503.
261. Earle, W.R.; Schilling, E.L.; Stark, T.H.; Straus, N.P.; Brown, M.F.; Shelton, E. Production of Malignancy in Vitro. IV. The Mouse Fibroblast Cultures and Changes Seen in the Living Cells. *JNCI: Journal of the National Cancer Institute* **1943**, *4*, 165–212, doi:10.1093/JNCI/4.2.165.
262. Gey, G.; Coffman, W.; Kubicek, M. Tissue Culture Studies of the Proliferative Capacity of Cervical Carcinoma and Normal Epithelium. *Cancer Res* **1952**, *12*, 264–265.
263. Chaicharoenaudomrung, N.; Kunhorm, P.; Noisa, P. Three-Dimensional Cell Culture Systems as an in Vitro Platform for Cancer and Stem Cell Modeling. *World J Stem Cells* **2019**, *11*, 1065–1083, doi:10.4252/wjsc.v11.i12.1065.

264. Frantz, C.; Stewart, K.M.; Weaver, V.M. The Extracellular Matrix at a Glance. *J Cell Sci* **2010**, *123*, 4195–4200, doi:10.1242/jcs.023820.
265. Theocharis, A.D.; Skandalis, S.S.; Gialeli, C.; Karamanos, N.K. Extracellular Matrix Structure. *Adv Drug Deliv Rev* **2016**, *97*, 4–27, doi:10.1016/j.addr.2015.11.001.
266. Winkler, J.; Abisoye-Ogunniyan, A.; Metcalf, K.J.; Werb, Z. Concepts of Extracellular Matrix Remodelling in Tumour Progression and Metastasis. *Nature Communications* **2020**, *11*, 1–19, doi:10.1038/s41467-020-18794-x.
267. Boucherit, N.; Gorvel, L.; Olive, D. 3D Tumor Models and Their Use for the Testing of Immunotherapies. *Front Immunol* **2020**, *11*, 603640, doi:10.3389/fimmu.2020.603640.
268. Mak, I.W.; Evaniew, N.; Ghert, M. *Lost in Translation: Animal Models and Clinical Trials in Cancer Treatment*; 2014; Vol. 6;.
269. Westhouse, R.A. Safety Assessment Considerations and Strategies for Targeted Small Molecule Cancer Therapeutics in Drug Discovery. *Toxicol Pathol* **2010**, *38*, 165–168, doi:10.1177/0192623309354341.
270. Burdett, E.; Kasper, F.K.; Mikos, A.G.; Ludwig, J.A. Engineering Tumors: A Tissue Engineering Perspective in Cancer Biology. *Tissue Eng Part B Rev* **2010**, *16*, 351–359, doi:10.1089/TEN.TEB.2009.0676.
271. Nakamura, H.; Sugano, M.; Miyashita, T.; Hashimoto, H.; Ochiai, A.; Suzuki, K.; Tsuboi, M.; Ishii, G. Organoid Culture Containing Cancer Cells and Stromal Cells Reveals That Podoplanin-Positive Cancer-Associated Fibroblasts Enhance Proliferation of Lung Cancer Cells. *Lung Cancer* **2019**, *134*, 100–107, doi:10.1016/j.lungcan.2019.04.007.
272. Sachs, N.; Paspaspyropoulos, A.; Zomer-van Ommen, D.D.; Heo, I.; Böttinger, L.; Klay, D.; Weeber, F.; Huelsz-Prince, G.; Iakobachvili, N.; Amatngalim, G.D.; et al. Long-term Expanding Human Airway Organoids for Disease Modeling. *EMBO J* **2019**, *38*, e100300, doi:10.15252/embj.2018100300.
273. Godugu, C.; Patel, A.R.; Desai, U.; Andey, T.; Sams, A.; Singh, M. AlgiMatrix™ Based 3D Cell Culture System as an In-Vitro Tumor Model for Anticancer Studies. *PLoS One* **2013**, *8*, e53708, doi:10.1371/journal.pone.0053708.
274. Yao, K.; Li, W.; Li, K.; Wu, Q.; Gu, Y.; Zhao, L.; Zhang, Y.; Gao, X. Simple Fabrication of Multicomponent Heterogeneous Fibers for Cell Co-Culture via Microfluidic Spinning. *Macromol Biosci* **2020**, *20*, e1900395, doi:10.1002/mabi.201900395.
275. Giró-Perafita, A.; Rabionet, M.; Puig, T.; Ciurana, J. Optimization of Poli(ε-Caprolactone) Scaffolds Suitable for 3D Cancer Cell Culture. *Procedia CIRP* **2016**, *49*, 61–66, doi:10.1016/j.procir.2015.07.031.

References

276. Costard, L.S.; Hosn, R.R.; Ramanayake, H.; O'Brien, b,c, F.J.; Curtin, C.M. Influences of the 3D Microenvironment on Cancer Cell Behaviour and Treatment Responsiveness: A Recent Update on Lung, Breast and Prostate Cancer Models. *Acta Biomater* **2021**, doi:10.1016/j.actbio.2021.01.023.
277. Hu, S.; Dasbiswas, K.; Guo, Z.; Tee, Y.H.; Thiagarajan, V.; Hersen, P.; Chew, T.L.; Safran, S.A.; Zaidel-Bar, R.; Bershadsky, A.D. Long-Range Self-Organization of Cytoskeletal Myosin II Filament Stacks. *Nat Cell Biol* **2017**, *19*, 133–141, doi:10.1038/ncb3466.
278. Wu, Y.; Lu, Y.; Zhao, M.; Bosiakov, S.; Li, L. A Critical Review of Additive Manufacturing Techniques and Associated Biomaterials Used in Bone Tissue Engineering. *Polymers (Basel)* **2022**, *14*, doi:10.3390/POLYM14102117.
279. Crump, S. Fast, Precise, Safe Prototypes with FDM. *ASME, PED* **1991**, *50*, 53–60.
280. Grivet-Brancot, A.; Boffito, M.; Ciardelli, G. Use of Polyesters in Fused Deposition Modeling for Biomedical Applications. *Macromol Biosci* **2022**, doi:10.1002/MABI.202200039.
281. Auriemma, G.; Tommasino, C.; Falcone, G.; Esposito, T.; Sardo, C.; Aquino, R.P. Additive Manufacturing Strategies for Personalized Drug Delivery Systems and Medical Devices: Fused Filament Fabrication and Semi Solid Extrusion. *Molecules* **2022**, *27*, 2784, doi:10.3390/molecules27092784.
282. Ragelle, H.; Rahimian, S.; Guzzi, E.A.; Westenskow, P.D.; Tibbitt, M.W.; Schwach, G.; Langer, R. Additive Manufacturing in Drug Delivery: Innovative Drug Product Design and Opportunities for Industrial Application. *Adv Drug Deliv Rev* **2021**, *178*, doi:10.1016/J.ADDR.2021.113990.
283. Skylar-Scott, M.A.; Mueller, J.; Visser, C.W.; Lewis, J.A. Voxeled Soft Matter via Multimaterial Multinozzle 3D Printing. *Nature* **2019**, *575*, 330–335, doi:10.1038/s41586-019-1736-8.
284. Tan, L.J.; Zhu, W.; Zhou, K. Recent Progress on Polymer Materials for Additive Manufacturing. *Adv Funct Mater* **2020**, *30*, 2003062, doi:10.1002/ADFM.202003062.
285. Pantermehl, S.; Emmert, S.; Foth, A.; Grabow, N.; Alkildani, S.; Bader, R.; Barbeck, M.; Jung, O. 3D Printing for Soft Tissue Regeneration and Applications in Medicine. *Biomedicines* **2021**, *9*, 336, doi:10.3390/biomedicines9040336.
286. Li, R.; Ting, Y.-H.; Youssef, S.H.; Song, Y.; Garg, S.; López-Castellano, A.; Rodilla, V. Three-Dimensional Printing for Cancer Applications: Research Landscape and Technologies. *Pharmaceuticals* **2021**, *14*, 787, doi:10.3390/ph14080787.
287. Reneker, D.H.; Yarin, A.L. Electrospinning Jets and Polymer Nanofibers. *Polymer (Guildf)* **2008**, *49*, 2387–2425, doi:10.1016/J.POLYMER.2008.02.002.

288. Cavo, M.; Serio, F.; Kale, N.R.; D'amone, E.; Gigli, G.; del Mercato, L.L. Electrospun Nanofibers in Cancer Research: From Engineering of in Vitro 3D Cancer Models to Therapy. *Biomater Sci* **2020**, *8*, 4887, doi:10.1039/d0bm00390e.
289. Zong, H.; Xia, X.; Liang, Y.; Dai, S.; Alsaedi, A.; Hayat, T.; Kong, F.; Pan, J.H. Designing Function-Oriented Artificial Nanomaterials and Membranes via Electrospinning and Electro spraying Techniques. *Mater Sci Eng C Mater Biol Appl* **2018**, *92*, 1075–1091, doi:10.1016/J.MSEC.2017.11.007.
290. Yan, B.; Zhang, Y.; Li, Z.; Zhou, P.; Mao, Y. Electrospun Nanofibrous Membrane for Biomedical Application. *SN Appl Sci* **2022**, *4*, doi:10.1007/S42452-022-05056-2.
291. Deshawar, D.; Chokshi, P. Stability Analysis of an Electrospinning Jet of Polymeric Fluids. *Polymer (Guildf)* **2017**, *131*, 34–49, doi:10.1016/J.POLYMER.2017.10.019.
292. Liu, W.; Thomopoulos, S.; Xia, Y. Electrospun Nanofibers for Regenerative Medicine. *Adv Healthc Mater* **2012**, *1*, 10–25, doi:10.1002/ADHM.201100021.
293. Han, S.; Nie, K.; Li, J.; Sun, Q.; Wang, X.; Li, X.; Li, Q. 3D Electrospun Nanofiber-Based Scaffolds: From Preparations and Properties to Tissue Regeneration Applications. *Stem Cells Int* **2021**, *2021*, 8790143, doi:10.1155/2021/8790143.
294. Yan, X.; Yu, M.; Ramakrishna, S.; Russell, S.J.; Long, Y.Z. Advances in Portable Electrospinning Devices for in Situ Delivery of Personalized Wound Care. *Nanoscale* **2019**, *11*, 19166–19178, doi:10.1039/C9NR02802A.
295. Ferraris, S.; Spriano, S.; Scalia, A.C.; Cochis, A.; Rimondini, L.; Cruz-Maya, I.; Guarino, V.; Varesano, A.; Vineis, C. Topographical and Biomechanical Guidance of Electrospun Fibers for Biomedical Applications. *Polymers (Basel)* **2020**, *12*, 1–32, doi:10.3390/POLYM12122896.
296. Okutan, N.; Terzi, P.; Altay, F. Affecting Parameters on Electrospinning Process and Characterization of Electrospun Gelatin Nanofibers. *Food Hydrocoll* **2014**, *39*, 19–26, doi:10.1016/J.FOODHYD.2013.12.022.
297. Wu, X.F.; Salkovskiy, Y.; Dzenis, Y.A. Modeling of Solvent Evaporation from Polymer Jets in Electrospinning. *Appl Phys Lett* **2011**, *98*, 223108, doi:10.1063/1.3585148.
298. Yördem, O.S.; Papila, M.; Menceloğlu, Y.Z. Effects of Electrospinning Parameters on Polyacrylonitrile Nanofiber Diameter: An Investigation by Response Surface Methodology. *Mater Des* **2008**, *29*, 34–44, doi:10.1016/J.MATDES.2006.12.013.
299. Yang, Q.; Zhenyu, L.I.; Hong, Y.; Zhao, Y.; Qiu, S.; Wang, C.E.; Wei, Y. Influence of Solvents on the Formation of Ultrathin Uniform Poly(Vinyl Pyrrolidone) Nanofibers with Electrospinning. *J Polym Sci B Polym Phys* **2004**, *42*, 3721–3726, doi:10.1002/POLB.20222.

References

300. Malikmammadov, E.; Tanir, T.E.; Kiziltay, A.; Hasirci, V.; Hasirci, N. PCL and PCL-Based Materials in Biomedical Applications. *J Biomater Sci Polym Ed* **2018**, *29*, 863–893, doi:10.1080/09205063.2017.1394711.
301. Hoskins, J.N.; Grayson, S.M. Synthesis and Degradation Behavior of Cyclic Poly(ϵ -Caprolactone). *Macromolecules* **2009**, *42*, 6406–6413, doi:10.1021/MA9011076/SUPPL_FILE/MA9011076_SI_001.PDF.
302. Woodruff, M.A.; Hutmacher, D.W. The Return of a Forgotten Polymer—Polycaprolactone in the 21st Century. *Prog Polym Sci* **2010**, *35*, 1217–1256, doi:10.1016/J.PROGPOLYMSCI.2010.04.002.
303. Huang, Y.T.; Wang, W.C.; Hsu, C.P.; Lu, W.Y.; Chuang, W.J.; Chiang, M.Y.; Lai, Y.C.; Chen, H.Y. The Ring-Opening Polymerization of ϵ -Caprolactone and L-Lactide Using Aluminum Complexes Bearing Benzothiazole Ligands as Catalysts. *Polym Chem* **2016**, *7*, 4367–4377, doi:10.1039/C6PY00569A.
304. Sabzi, F.; Boushehri, A. Sorption Phenomena of Organic Solvents in Polymers: Part I. *Eur Polym J* **2005**, *41*, 974–983, doi:10.1016/J.EURPOLYMJ.2004.11.035.
305. Nair, L.S.; Laurencin, C.T. Biodegradable Polymers as Biomaterials. *Prog Polym Sci* **2007**, *32*, 762–798, doi:10.1016/J.PROGPOLYMSCI.2007.05.017.
306. Abedalwafa, M.; Wang, F.; Li, C. Bbiodegradable Poly-Epsilon-Caprolactone (PCL) for Tissue Engineering Applications: A Review. *Rev. Adv. Mater. Sci* **2013**, *34*, 123–140.
307. Teoh, S.H.; Goh, B.T.; Lim, J. Three-Dimensional Printed Polycaprolactone Scaffolds for Bone Regeneration Success and Future Perspective. *Tissue Eng Part A* **2019**, *25*, 931–935, doi:10.1089/TEN.TEA.2019.0102.
308. Gleadall, A.; Pan, J.; Krufft, M.A.; Kellomäki, M. Degradation Mechanisms of Bioresorbable Polyesters. Part 1. Effects of Random Scission, End Scission and Autocatalysis. *Acta Biomater* **2014**, *10*, 2223–2232, doi:10.1016/J.ACTBIO.2013.12.039.
309. Hernández, A.R.; Contreras, O.C.; Acevedo, J.C.; Moreno, L.G.N. Poly(ϵ -Caprolactone) Degradation Under Acidic and Alkaline Conditions. *American Journal of Polymer Science* **2013**, *3*, 70–75, doi:10.5923/J.AJPS.20130304.02.
310. Domingos, M.; Intranuovo, F.; Russo, T.; Santis, R. de; Gloria, A.; Ambrosio, L.; Ciurana, J.; Bartolo, P. The First Systematic Analysis of 3D Rapid Prototyped Poly(ϵ -Caprolactone) Scaffolds Manufactured through BioCell Printing: The Effect of Pore Size and Geometry on Compressive Mechanical Behaviour and in Vitro HMSC Viability. *Biofabrication* **2013**, *5*, 045004, doi:10.1088/1758-5082/5/4/045004.

311. Saha, S.; Duan, X.; Wu, L.; Lo, P.-K.; Chen, H.; Wang, Q. Electrospun Fibrous Scaffolds Promote Breast Cancer Cell Alignment and Epithelial–Mesenchymal Transition. *Langmuir* **2012**, *28*, 2028–2034, doi:10.1021/la203846w.
312. Rabionet, M.; Yeste, M.; Puig, T.; Ciurana, J. Electrospinning PCL Scaffolds Manufacture for Three-Dimensional Breast Cancer Cell Culture. *Polymers (Basel)* **2017**, *9*, 328, doi:10.3390/polym9080328.
313. Rabionet, M.; Polonio, E.; Guerra, A.J.; Martin, J.; Puig, T.; Ciurana, J. Design of a Scaffold Parameter Selection System with Additive Manufacturing for a Biomedical Cell Culture. *Materials* **2018**, *11*, 1–14, doi:10.3390/ma11081427.
314. Palomeras, S.; Rabionet, M.; Ferrer, I.; Sarrats, A.; Garcia-Romeu, M.; Puig, T.; Ciurana, J.; Palomeras, S.; Rabionet, M.; Ferrer, I.; et al. Breast Cancer Stem Cell Culture and Enrichment Using Poly(ϵ -Caprolactone) Scaffolds. *Molecules* **2016**, *21*, 537, doi:10.3390/molecules21040537.
315. Feng, S.; Duan, X.; Lo, P.-K.; Liu, S.; Liu, X.; Chen, H.; Wang, Q. Expansion of Breast Cancer Stem Cells with Fibrous Scaffolds. *Integrative Biology* **2013**, *5*, 768, doi:10.1039/c3ib20255k.
316. Adsul, M.G.; Varma, A.J.; Gokhale, D. v. Lactic Acid Production from Waste Sugarcane Bagasse Derived Cellulose. *Green Chemistry* **2007**, *9*, 58–62, doi:10.1039/B605839F.
317. Singhvi, M.; Joshi, D.; Adsul, M.; Varma, A.; Gokhale, D. D-(–)-Lactic Acid Production from Cellobiose and Cellulose by *Lactobacillus Lactis* Mutant RM2-24. *Green Chemistry* **2010**, *12*, 1106–1109, doi:10.1039/B925975A.
318. Shunmugasundaram, M.; Ali baig, M.A.; Ajay Kumar, M. A Review of Bio-Degradable Materials for Fused Deposition Modeling Machine. *Mater Today Proc* **2020**, *27*, 1596–1600, doi:10.1016/J.MATPR.2020.03.267.
319. Saini, P.; Arora, M.; Kumar, M.N.V.R. Poly(Lactic Acid) Blends in Biomedical Applications. *Adv Drug Deliv Rev* **2016**, *107*, 47–59, doi:10.1016/j.addr.2016.06.014.
320. Nofar, M.; Sacligil, D.; Carreau, P.J.; Kamal, M.R.; Heuzey, M. Poly (Lactic Acid) Blends : Processing , Properties and Applications. *Int J Biol Macromol* **2019**, *125*, 307–360, doi:10.1016/j.ijbiomac.2018.12.002.
321. Tsuji, H. Poly(Lactide) Stereocomplexes: Formation, Structure, Properties, Degradation, and Applications. *Macromol Biosci* **2005**, *5*, 569–597, doi:10.1002/MABI.200500062.
322. Chiulan, I.; Frone, A.N.; Brandabur, C.; Panaitescu, D.M. Recent Advances in 3D Printing of Aliphatic Polyesters. *Bioengineering 2018, Vol. 5, Page 2* **2017**, *5*, 2, doi:10.3390/BIOENGINEERING5010002.

References

323. Li, G.; Zhao, M.; Xu, F.; Yang, B.; Li, X.; Meng, X.; Teng, L.; Sun, F.; Li, Y. Synthesis and Biological Application of Polylactic Acid. *Molecules* **2020**, *25*, doi:10.3390/MOLECULES25215023.
324. Coudane, J.; Berghe, H. van den; Mouton, J.; Garric, X.; Nottelet, B. Poly(Lactic Acid)-Based Graft Copolymers: Syntheses Strategies and Improvement of Properties for Biomedical and Environmentally Friendly Applications: A Review. *Molecules* **2022**, *27*, 4135, doi:10.3390/MOLECULES27134135.
325. DeStefano, V.; Khan, S.; Tabada, A. Applications of PLA in Modern Medicine. *Engineered Regeneration* **2020**, *1*, 76–87, doi:10.1016/J.ENGREG.2020.08.002.
326. Tyler, B.; Gullotti, D.; Mangraviti, A.; Utsuki, T.; Brem, H. Polylactic Acid (PLA) Controlled Delivery Carriers for Biomedical Applications. *Adv Drug Deliv Rev* **2016**, *107*, 163–175, doi:10.1016/J.ADDR.2016.06.018.
327. Grémare, A.; Guduric, V.; Bareille, R.; Heroguez, V.; Latour, S.; L'heureux, N.; Fricain, J.C.; Catros, S.; le Nihouannen, D. Characterization of Printed PLA Scaffolds for Bone Tissue Engineering. *J Biomed Mater Res A* **2018**, *106*, 887–894, doi:10.1002/JBM.A.36289.
328. Wang, Y.; Qian, J.; Liu, T.; Xu, W.; Zhao, N.; Suo, A. Electrospun PBLG/PLA Nanofiber Membrane for Constructing in Vitro 3D Model of Melanoma. *Materials Science and Engineering C* **2017**, *76*, 313–318, doi:10.1016/J.MSEC.2017.03.098.
329. Girard, Y.K.; Wang, C.; Ravi, S.; Howell, M.C.; Mallela, J.; Alibrahim, M.; Green, R.; Hellermann, G.; Mohapatra, S.S.; Mohapatra, S. A 3D Fibrous Scaffold Inducing Tumoroids: A Platform for Anticancer Drug Development. *PLoS One* **2013**, *8*, e75345, doi:10.1371/journal.pone.0075345.
330. Chitcholtan, K.; Asselin, E.; Parent, S.; Sykes, P.H.; Evans, J.J. Differences in Growth Properties of Endometrial Cancer in Three Dimensional (3D) Culture and 2D Cell Monolayer. *Exp Cell Res* **2013**, *319*, 75–87, doi:10.1016/j.yexcr.2012.09.012.
331. Sims-Mourtada, J.; Niamat, R.A.; Samuel, S.; Eskridge, C.; Kmiec, E.B. Enrichment of Breast Cancer Stem-like Cells by Growth on Electrospun Polycaprolactone-Chitosan Nanofiber Scaffolds. *Int J Nanomedicine* **2014**, *9*, 995–1003, doi:10.2147/IJN.S55720.
332. Islami, M.; Mortazavi, Y.; Soleimani, M.; Nadri, S. In Vitro Expansion of CD 133+ Cells Derived from Umbilical Cord Blood in Poly-L-Lactic Acid (PLLA) Scaffold Coated with Fibronectin and Collagen. *Artif Cells Nanomed Biotechnol* **2018**, *46*, 1025–1033, doi:10.1080/21691401.2017.1358733.
333. Boroughs, L.K.; Deberardinis, R.J. Metabolic Pathways Promoting Cancer Cell Survival and Growth. *Nat Cell Biol* **2015**, *17*, 351, doi:10.1038/NCB3124.

334. Warburg, O. On Respiratory Impairment in Cancer Cells. *Science (1979)* **1956**, *124*, 267–272, doi:10.1126/science.124.3215.267.
335. Warburg, O. On the Origin of Cancer Cells. *Science* **1956**, *123*, 309–314, doi:10.1126/SCIENCE.123.3191.309.
336. V.R., P. The Biochemical Approach to the Cancer Problem. *Fed Proc* **1958**, *17*, 691–697.
337. Heiden, M.G.V.; Cantley, L.C.; Thompson, C.B. Understanding the Warburg Effect: The Metabolic Requirements of Cell Proliferation. *Science* **2009**, *324*, 1029–1033, doi:10.1126/SCIENCE.1160809.
338. Merino Salvador, M.; Gómez de Cedrón, M.; Merino Rubio, J.; Falagán Martínez, S.; Sánchez Martínez, R.; Casado, E.; Ramírez de Molina, A.; Sereno, M. Lipid Metabolism and Lung Cancer. *Crit Rev Oncol Hematol* **2017**, *112*, 31–40, doi:10.1016/j.critrevonc.2017.02.001.
339. Montesdeoca, N.; López, M.; Ariza, X.; Herrero, L.; Makowski, K. Inhibitors of Lipogenic Enzymes as a Potential Therapy against Cancer. *The FASEB Journal* **2020**, *34*, 11355–11381, doi:10.1096/FJ.202000705R.
340. S, B.-D.; S, V.; F, G. Lipid Metabolic Reprogramming in Cancer Cells. *Oncogenesis* **2016**, *5*, e189–e189, doi:10.1038/ONCSIS.2015.49.
341. Baenke, F.; Peck, B.; Miess, H.; Schulze, A. Hooked on Fat: The Role of Lipid Synthesis in Cancer Metabolism and Tumour Development. *Dis Model Mech* **2013**, *6*, 1353–1363, doi:10.1242/DMM.011338.
342. Wymann, M.P.; Schneider, R. Lipid Signalling in Disease. *Nature Reviews Molecular Cell Biology* **2008**, *9*, 162–176, doi:10.1038/nrm2335.
343. Dall'Armi, C.; Devereaux, K.A.; di Paolo, G. The Role of Lipids in the Control of Autophagy. *Curr Biol* **2013**, *23*, doi:10.1016/J.CUB.2012.10.041.
344. Fhu, C.W.; Ali, A. Fatty Acid Synthase: An Emerging Target in Cancer. *Molecules* **2020**, *25*, doi:10.3390/MOLECULES25173935.
345. Chirala, S.S.; Wakil, S.J. Structure and Function of Animal Fatty Acid Synthase. *Lipids* **2004**, *39*, 1045–1053, doi:10.1007/S11745-004-1329-9.
346. Smith, S.; Tsai, S.C. The Type I Fatty Acid and Polyketide Synthases: A Tale of Two Megasyntases. *Nat Prod Rep* **2007**, *24*, 1041–1072, doi:10.1039/B603600G.
347. Semenkovich, C.F.; Coleman, T.; Fiedorek, F.T. Human Fatty Acid Synthase MRNA: Tissue Distribution, Genetic Mapping, and Kinetics of Decay after Glucose Deprivation. *J Lipid Res* **1995**, *36*, 1507–1521, doi:10.1016/S0022-2275(20)39738-8.

References

348. Pizer, E.S.; Kurman, R.J.; Pasternack, G.R.; Kuhajda, F.P. Expression of Fatty Acid Synthase Is Closely Linked to Proliferation and Stromal Decidualization in Cycling Endometrium. *Int J Gynecol Pathol* **1997**, *16*, 45–51, doi:10.1097/00004347-199701000-00008.
349. Dhanasekaran, S.M.; Dash, A.; Yu, J.; Maine, I.P.; Laxman, B.; Tomlins, S.A.; Creighton, C.J.; Menon, A.; Rubin, M.A.; Chinnaiyan, A.M. Molecular Profiling of Human Prostate Tissues: Insights into Gene Expression Patterns of Prostate Development during Puberty. *FASEB J* **2005**, *19*, 1–23, doi:10.1096/FJ.04-2415FJE.
350. Kusakabe, T.; Maeda, M.; Hoshi, N.; Sugino, T.; Watanabe, K.; Fukuda, T.; Suzuki, T. Fatty Acid Synthase Is Expressed Mainly in Adult Hormone-Sensitive Cells or Cells with High Lipid Metabolism and in Proliferating Fetal Cells. *The journal of histochemistry and cytochemistry* **2000**, *48*, 613–622, doi:10.1177/002215540004800505.
351. Bowers, M.; Liang, T.; Gonzalez-Bohorquez, D.; Zocher, S.; Jaeger, B.N.; Kovacs, W.J.; Röhrl, C.; Cramb, K.M.L.; Winterer, J.; Kruse, M.; et al. FASN-Dependent Lipid Metabolism Links Neurogenic Stem/Progenitor Cell Activity to Learning and Memory Deficits. *Cell Stem Cell* **2020**, *27*, 98-109.e11, doi:10.1016/J.STEM.2020.04.002/ATTACHMENT/36F6F416-F5B1-4A59-90C3-CB03D65F73C9/MMC4.XLSX.
352. Chirala, S.S.; Chang, H.; Matzuk, M.; Abu-Elheiga, L.; Mao, J.; Mahon, K.; Finegold, M.; Wakil, S.J. Fatty Acid Synthase Is Essential in Embryonic Development: Fatty Acid Synthase Null Mutants and Most of the Heterozygotes Die in Utero. *Proc Natl Acad Sci U S A* **2003**, *100*, 6358–6363, doi:10.1073/PNAS.0931394100/ASSET/D754B8F0-2C10-45B1-8072-982382C959B2/ASSETS/GRAPHIC/PQ0931394005.JPEG.
353. Rudolph, M.C.; McManaman, J.L.; Phang, T.L.; Russell, T.; Kominsky, D.J.; Serkova, N.J.; Stein, T.; Anderson, S.M.; Neville, M.C. Metabolic Regulation in the Lactating Mammary Gland: A Lipid Synthesizing Machine. *Physiol Genomics* **2007**, *28*, 323–336, doi:10.1152/PHYSIOLGENOMICS.00020.2006/SUPPL_FILE/TABLE_S6.PDF.
354. Visca, P.; Sebastiani, V.; Botti, C.; Diodoro, M.G.; Lasagni, R.P.; Romagnoli, F.; Brenna, A.; de Joannon, B.C.; Donnorso, R.P.; Lombardi, G.; et al. Fatty Acid Synthase (FAS) Is a Marker of Increased Risk of Recurrence in Lung Carcinoma. *Anticancer Res* **2004**, *24*, 4169–4173.
355. Giró-Perafita, A.; Sarrats, A.; Pérez-Bueno, F.; Oliveras, G.; Buxó, M.; Brunet, J.; Viñas, G.; Miquel, T.P. Fatty Acid Synthase Expression and Its Association with Clinico-Histopathological Features in Triple-Negative Breast Cancer. *Oncotarget* **2017**, *8*, 74391–74405, doi:10.18632/oncotarget.20152.
356. Corominas-Faja, B.; Vellon, L.; Cuyàs, E.; Buxó, M.; Martin-Castillo, B.; Serra, D.; García, J.; Menendez, J.A.; Lupu, R. Clinical and Therapeutic Relevance of the

- Metabolic Oncogene Fatty Acid Synthase in HER2+ Breast Cancer. *Histol Histopathol* **2017**, *32*, 687, doi:10.14670/HH-11-830.
357. Rashid, A.; Pizer, E.S.; Moga, M.; Milgraum, L.Z.; Zahurak, M.; Pasternack, G.R.; Kuhajda, F.P.; Hamilton, S.R. Elevated Expression of Fatty Acid Synthase and Fatty Acid Synthetic Activity in Colorectal Neoplasia. *Am J Pathol* **1997**, *150*, 201.
358. Tsuji, T.; Yoshinaga, M.; Togami, S.; Douchi, T.; Nagata, Y. Fatty Acid Synthase Expression and Clinicopathological Findings in Endometrial Cancer. *Acta Obstet Gynecol Scand* **2004**, *83*, 586–590, doi:10.1111/J.0001-6349.2004.00511.X.
359. Rossi, S.; Graner, E.; Febbo, P.; Weinstein, L.; Bhattacharya, N.; Onody, T.; Bubley, G.; Balk, S.; Loda, M. Fatty Acid Synthase Expression Defines Distinct Molecular Signatures in Prostate Cancer. *Molecular Cancer Research* **2003**, *1*, 707–715.
360. Cerne, D.; Prodan Zitnik, I.; Sok, M. Increased Fatty Acid Synthase Activity in Non-Small Cell Lung Cancer Tissue Is a Weaker Predictor of Shorter Patient Survival than Increased Lipoprotein Lipase Activity. *Arch Med Res* **2010**, *41*, 405–409, doi:10.1016/j.arcmed.2010.08.007.
361. Orita, H.; Coulter, J.; Lemmon, C.; Tully, E.; Vadlamudi, A.; Medghalchi, S.M.; Kuhajda, F.P.; Gabrielson, E. Selective Inhibition of Fatty Acid Synthase for Lung Cancer Treatment. *Clinical Cancer Research* **2007**, *13*, 7139–7145, doi:10.1158/1078-0432.CCR-07-1186.
362. Yan, Y.; Zhou, Y.; Li, J.; Zheng, Z.; Hu, Y.; Li, L.; Wu, W. Sulforaphane Downregulated Fatty Acid Synthase and Inhibited Microtubule-Mediated Mitophagy Leading to Apoptosis. *Cell Death Dis* **2021**, *12*, 917, doi:10.1038/S41419-021-04198-2.
363. Wang, Y.; Zhang, X.; Tan, W.; Fu, J.; Zhang, W. Significance of Fatty Acid Synthase Expression in Non-Small Cell Lung Cancer. *Chinese Journal of Oncology* **2002**, *3*, 271–273.
364. Guo, D.; Bell, E.; Mischel, P.; Chakravarti, A. Targeting SREBP-1-Driven Lipid Metabolism to Treat Cancer. *Curr Pharm Des* **2015**, *20*, 2619–2626, doi:10.2174/13816128113199990486.
365. Horton, J.D.; Bashmakov, Y.; Shimomura, I.; Shimano, H. Regulation of Sterol Regulatory Element Binding Proteins in Livers of Fasted and Refed Mice. *Proc Natl Acad Sci U S A* **1998**, *95*, 5987–5992, doi:10.1073/PNAS.95.11.5987/ASSET/19481A1D-0A6B-4D8B-ABD3-E4CCE991D813/ASSETS/GRAPHIC/PQ1080890006.JPEG.
366. Shimomura, I.; Bashmakov, Y.; Ikemoto, S.; Horton, J.D.; Brown, M.S.; Goldstein, J.L. Insulin Selectively Increases SREBP-1C MRNA in the Livers of Rats with Streptozotocin-Induced Diabetes. *Proc Natl Acad Sci U S A* **1999**, *96*, 13656–13661,

References

- doi:10.1073/PNAS.96.24.13656/ASSET/F4C82927-A669-40BD-9626-6246986C2FA7/ASSETS/GRAPHIC/PQ2293675004.JPEG.
367. Gu, L.; Zhu, Y.; Lin, X.; Tan, X.; Lu, B.; Li, Y. Stabilization of FASN by ACAT1-Mediated GNPAT Acetylation Promotes Lipid Metabolism and Hepatocarcinogenesis. *Oncogene* 2020 39:11 **2020**, 39, 2437–2449, doi:10.1038/s41388-020-1156-0.
368. Floris, A.; Mazarei, M.; Yang, X.; Robinson, A.E.; Zhou, J.; Barberis, A.; D'hallewin, G.; Azara, E.; Spissu, Y.; Iglesias-Ara, A.; et al. SUMOylation Protects FASN Against Proteasomal Degradation in Breast Cancer Cells Treated with Grape Leaf Extract. *Biomolecules* 2020, Vol. 10, Page 529 **2020**, 10, 529, doi:10.3390/BIOM10040529.
369. Lin, H.P.; Cheng, Z.L.; He, R.Y.; Song, L.; Tian, M.X.; Zhou, L.S.; Groh, B.S.; Liu, W.R.; Ji, M.B.; Ding, C.; et al. Destabilization of Fatty Acid Synthase by Acetylation Inhibits De Novo Lipogenesis and Tumor Cell Growth. *Cancer Res* **2016**, 76, 6924–6936, doi:10.1158/0008-5472.CAN-16-1597.
370. Ishii, S.; Iizuka, K.; Miller, B.C.; Uyeda, K. Carbohydrate Response Element Binding Protein Directly Promotes Lipogenic Enzyme Gene Transcription. *Proc Natl Acad Sci U S A* **2004**, 101, 15597, doi:10.1073/PNAS.0405238101.
371. Shih, I.M.; Ueda, S.M.; Yap, K.L.; Davidson, B.; Tian, Y.; Murthy, V.; Wang, T.L.; Visvanathan, K.; Kuhajda, F.P.; Bristow, R.E.; et al. Expression of Fatty Acid Synthase Depends on NAC1 and Is Associated with Recurrent Ovarian Serous Carcinomas. *J Oncol* **2010**, 2010, doi:10.1155/2010/285191.
372. Gang, X.; Yang, Y.; Zhong, J.; Jiang, K.; Pan, Y.; Jeffrey Karnes, R.; Zhang, J.; Xu, W.; Wang, G.; Huang, H. P300 Acetyltransferase Regulates Fatty Acid Synthase Expression, Lipid Metabolism and Prostate Cancer Growth. *Oncotarget* **2016**, 7, 15135, doi:10.18632/ONCOTARGET.7715.
373. Ali, A.; Levantini, E.; Teo, J.T.; Goggi, J.; Clohessy, J.G.; Wu, C.S.; Chen, L.; Yang, H.; Krishnan, I.; Kocher, O.; et al. Fatty Acid Synthase Mediates EGFR Palmitoylation in EGFR Mutated Non-small Cell Lung Cancer. *EMBO Mol Med* **2018**, 10, 1–19, doi:10.15252/emmm.201708313.
374. Lupu, R.; Menendez, J. Pharmacological Inhibitors of Fatty Acid Synthase (FASN)--Catalyzed Endogenous Fatty Acid Biogenesis: A New Family of Anti-Cancer Agents? *Curr Pharm Biotechnol* **2006**, 7, 483–494, doi:10.2174/138920106779116928.
375. Pizer, E.S.; Wood, F.D.; Heine, H.S.; Romantsev, F.E.; Pasternack, G.R.; Kuhajda, F.P. Inhibition of Fatty Acid Synthesis Delays Disease Progression in a Xenograft Model of Ovarian Cancer. *Cancer Res* **1996**, 56, 1189–1193.
376. Pizer, E.S.; Jackisch, C.; Wood, F.D.; Pasternack, G.R.; Davidson, N.E.; Kuhajda, F.P. Inhibition of Fatty Acid Synthesis Induces Programmed Cell Death in Human Breast Cancer Cells. *Cancer Res* **1996**, 56, 2745–2747.

377. Yang, L.; Zhang, F.; Wang, X.; Tsai, Y.; Chuang, K.-H.; Keng, P.C.; Lee, S.O.; Chen, Y. A FASN-TGF- β 1-FASN Regulatory Loop Contributes to High EMT/ Metastatic Potential of Cisplatin-Resistant Non-Small Cell Lung Cancer. *Oncotarget* **2016**, *7*, 55543–55554.
378. Kuhajda, F.P.; Pizer, E.S.; Li, J.N.; Mani, N.S.; Frehywot, G.L.; Townsend, C.A. Synthesis and Antitumor Activity of an Inhibitor of Fatty Acid Synthase. *Proc Natl Acad Sci U S A* **2000**, *97*, 3450–3454, doi:10.1073/PNAS.97.7.3450.
379. Pizer, E.S.; Chrest, F.J.; Diggiuseppe, J.A.; Han, W.F. Pharmacological Inhibitors of Mammalian Fatty Acid Synthase Suppress DNA Replication and Induce Apoptosis in Tumor Cell Lines. *Cancer Res* **1998**, *58*, 4611–4615.
380. Loftus, T.M.; Jaworsky, D.E.; Frehywot, C.L.; Townsend, C.A.; Ronnett, G. v.; Daniel Lane, M.; Kuhajda, F.P. Reduced Food Intake and Body Weight in Mice Treated with Fatty Acid Synthase Inhibitors. *Science (1979)* **2000**, *288*, 2379–2381, doi:10.1126/SCIENCE.288.5475.2379/SUPPL_FILE/1050858S5_THUMB.GIF.
381. Relat, J.; Blancafort, A.; Oliveras, G.; Cufí, S.; Haro, D.; Marrero, P.F.; Puig, T. Different Fatty Acid Metabolism Effects of (–)-Epigallocatechin-3-Gallate and C75 in Adenocarcinoma Lung Cancer. *BMC Cancer* **2012**, *12*, 280, doi:10.1186/1471-2407-12-280.
382. Puig, T.; Vázquez-Martín, A.; Relat, J.; Pétriz, J.; Menéndez, J.A.; Porta, R.; Casals, G.; Marrero, P.F.; Haro, D.; Brunet, J.; et al. Fatty Acid Metabolism in Breast Cancer Cells: Differential Inhibitory Effects of Epigallocatechin Gallate (EGCG) and C75. *Breast Cancer Res Treat* **2008**, *109*, 471–479, doi:10.1007/s10549-007-9678-5.
383. Heck, A.M.; Yanovski, J.A.; Calis, K.A. Orlistat, a New Lipase Inhibitor for the Management of Obesity. *Pharmacotherapy* **2000**, *20*, 270, doi:10.1592/PHCO.20.4.270.34882.
384. Pemble IV, C.W.; Johnson, L.C.; Kridel, S.J.; Lowther, W.T. Crystal Structure of the Thioesterase Domain of Human Fatty Acid Synthase Inhibited by Orlistat. *Nature Structural & Molecular Biology* **2007**, *14*:8 **2007**, *14*, 704–709, doi:10.1038/nsmb1265.
385. Kridel, S.J.; Axelrod, F.; Rozenkrantz, N.; Smith, J.W. Orlistat Is a Novel Inhibitor of Fatty Acid Synthase with Antitumor Activity. *Cancer Res* **2004**, *64*, 2070–2075, doi:10.1158/0008-5472.CAN-03-3645.
386. Zhi, J.; Melia, A.T.; Eggers, H.; Joly, R.; Patel, I.H. Review of Limited Systemic Absorption of Orlistat, a Lipase Inhibitor, in Healthy Human Volunteers. *The Journal of Clinical Pharmacology* **1995**, *35*, 1103–1108, doi:10.1002/J.1552-4604.1995.TB04034.X.

References

387. Falchook, G.; Infante, J.; Arkenau, H.T.; Patel, M.R.; Dean, E.; Borazanci, E.; Brenner, A.; Cook, N.; Lopez, J.; Pant, S.; et al. First-in-Human Study of the Safety, Pharmacokinetics, and Pharmacodynamics of First-in-Class Fatty Acid Synthase Inhibitor TVB-2640 Alone and with a Taxane in Advanced Tumors. *EclinicalMedicine* **2021**, *34*, 100797, doi:10.1016/J.ECLINM.2021.100797.
388. Wang, X.; Tian, W. Green Tea Epigallocatechin Gallate: A Natural Inhibitor of Fatty-Acid Synthase. *Biochem Biophys Res Commun* **2001**, *288*, 1200–1206, doi:10.1006/BBRC.2001.5923.
389. Zhou, D.H.; Wang, X.; Feng, Q. EGCG Enhances the Efficacy of Cisplatin by Downregulating Hsa-MiR-98-5p in NSCLC A549 Cells. *Nutr Cancer* **2014**, *66*, 636–644, doi:10.1080/01635581.2014.894101/SUPPL_FILE/HNUC_A_894101_SM1347.XLS.
390. Giró-Perafita, A.; Palomeras, S.; Lum, D.H.; Blancafort, A.; Viñas, G.; Oliveras, G.; Pérez-Bueno, F.; Sarrats, A.; Welm, A.L.; Puig, T. Preclinical Evaluation of Fatty Acid Synthase and EGFR Inhibition in Triple-Negative Breast Cancer. *Clinical Cancer Research* **2016**, *22*, 4687–4697, doi:10.1158/1078-0432.CCR-15-3133.
391. Blancafort, A.; Giró-Perafita, A.; Oliveras, G.; Palomeras, S.; Turrado, C.; Campuzano, Ò.; Carrión-Salip, D.; Massaguer, A.; Brugada, R.; Palafox, M.; et al. Dual Fatty Acid Synthase and HER2 Signaling Blockade Shows Marked Antitumor Activity against Breast Cancer Models Resistant to Anti-HER2 Drugs. *PLoS One* **2015**, *10*, e0131241, doi:10.1371/journal.pone.0131241.
392. Rabionet, M.; Polonio-Alcalá, E.; Relat, J.; Yeste, M.; Sims-Mourtada, J.; Kloxin, A.M.; Planas, M.; Feliu, L.; Ciurana, J.; Puig, T. Fatty Acid Synthase as a Feasible Biomarker for Triple Negative Breast Cancer Stem Cell Subpopulation Cultured on Electrospun Scaffolds. *Mater Today Bio* **2021**, *12*, 100155, doi:10.1016/j.mtbio.2021.100155.
393. Giró-Perafita, A.; Rabionet, M.; Planas, M.; Feliu, L.; Ciurana, J.; Ruiz-Martínez, S.; Puig, T. EGCG-Derivative G28 Shows High Efficacy Inhibiting the Mammosphere-Forming Capacity of Sensitive and Resistant TNBC Models. *Molecules* **2019**, *24*, 1–15, doi:10.3390/molecules24061027.
394. Deng, P.B.; Hu, C.P.; Xiong, Z.; Yang, H.P.; Li, Y.Y. Treatment with EGCG in NSCLC Leads to Decreasing Interstitial Fluid Pressure and Hypoxia to Improve Chemotherapy Efficacy through Rebalance of Ang-1 and Ang-2. *Chin J Nat Med* **2013**, *11*, 245–253, doi:10.1016/S1875-5364(13)60023-0.
395. Puig, T.; Relat, J.; Marrero, P.F.; Haro, D.; Brunet, J.; Colomer, R. Green Tea Catechin Inhibits Fatty Acid Synthase without Stimulating Carnitine Palmitoyltransferase-1 or Inducing Weight Loss in Experimental Animals. *Anticancer Res* **2008**, *28*.
396. Puig, T.; Turrado, C.; Benhamú, B.; Aguilar, H.; Relat, J.; Ortega-Gutiérrez, S.; Casals, G.; Marrero, P.F.; Urruticoechea, A.; Haro, D.; et al. Novel Inhibitors of Fatty Acid

- Synthase with Anticancer Activity. *Clinical Cancer Research* **2009**, *15*, 7608–7615, doi:10.1158/1078-0432.CCR-09-0856.
397. Turrado, C.; Puig, T.; García-Ca, J.; Artola, M.; Benhamu, B.; Ortega-Gutie, S.; Relat, J.; Oliveras, G.; Blancafort, A.; Haro, D.; et al. New Synthetic Inhibitors of Fatty Acid Synthase with Anticancer Activity. *J Med Chem* **2012**, *55*, 5013–5023, doi:10.1021/jm2016045.
398. Crous-Masó, J.; Palomeras, S.; Relat, J.; Camó, C.; Martínez-Garza, Ú.; Planas, M.; Feliu, L.; Puig, T. (-)-Epigallocatechin 3-Gallate Synthetic Analogues Inhibit Fatty Acid Synthase and Show Anticancer Activity in Triple Negative Breast Cancer. *Molecules* **2018**, *23*, 1160, doi:10.3390/molecules23051160.
399. Puig, T.; Aguilar, H.; Cufí, S.; Oliveras, G.; Turrado, C.; Ortega-Gutiérrez, S.; Benhamú, B.; López-Rodríguez, M.L.; Urruticoechea, A.; Colomer, R. A Novel Inhibitor of Fatty Acid Synthase Shows Activity against HER2+ Breast Cancer Xenografts and Is Active in Anti-HER2 Drug-Resistant Cell Lines. *Breast Cancer Res* **2011**, *13*, doi:10.1186/BCR3077.
400. O'Bryan, C.S.; Bhattacharjee, T.; Hart, S.; Kabb, C.P.; Schulze, K.D.; Chilakala, I.; Sumerlin, B.S.; Sawyer, W.G.; Angelini, T.E. Self-Assembled Micro-Organogels for 3D Printing Silicone Structures. *Sci Adv* **2017**, *3*, doi:10.1126/SCIADV.1602800.
401. Xiong, G.; Luo, H.; Zhu, Y.; Raman, S.; Wan, Y. Creation of Macropores in Three-Dimensional Bacterial Cellulose Scaffold for Potential Cancer Cell Culture. *Carbohydr Polym* **2014**, *114*, 553–557, doi:10.1016/J.CARBPOL.2014.08.073.
402. Guerra, A.J.; Ciurana, J. 3D-Printed Bioabsorbable Polycaprolactone Stent: The Effect of Process Parameters on Its Physical Features. *Mater Des* **2018**, *137*, 430–437, doi:10.1016/j.matdes.2017.10.045.
403. Guerra, A.J.; Cano, P.; Rabionet, M.; Puig, T.; Ciurana, J. 3D-Printed PCL/PLA Composite Stents: Towards a New Solution to Cardiovascular Problems. *Materials (Basel)* **2018**, *11*, doi:10.3390/MA11091679.
404. Gleadall, A.; Visscher, D.; Yang, J.; Thomas, D.; Segal, J. Review of Additive Manufactured Tissue Engineering Scaffolds: Relationship between Geometry and Performance. *Burns Trauma* **2018**, *6*, 19, doi:10.1186/s41038-018-0121-4.
405. Sobral, J.M.; Caridade, S.G.; Sousa, R.A.; Mano, J.F.; Reis, R.L. Three-Dimensional Plotted Scaffolds with Controlled Pore Size Gradients: Effect of Scaffold Geometry on Mechanical Performance and Cell Seeding Efficiency. *Acta Biomater* **2011**, *7*, 1009–1018, doi:10.1016/J.ACTBIO.2010.11.003.
406. He, T.; Jokerst, J. v. Structured Micro/Nano Materials Synthesized via Electrospray: A Review. *Biomater Sci* **2020**, *8*, 5555–5573, doi:10.1039/D0BM01313G.

References

407. Steipel, R.T.; Gallovic, M.D.; Batty, C.J.; Bachelder, E.M.; Ainslie, K.M. Electrospray for Generation of Drug Delivery and Vaccine Particles Applied in Vitro and in Vivo. *Materials Science and Engineering: C* **2019**, *105*, 110070, doi:10.1016/J.MSEC.2019.110070.
408. Fong, H.; Chun, I.; Reneker, D.H. Beaded Nanofibers Formed during Electrospinning. *Polymer (Guildf)* **1999**, *40*, 4585–4592, doi:10.1016/S0032-3861(99)00068-3.
409. Damanik, F.F.R.; Spadolini, G.; Rotmans, J.; Farè, S.; Moroni, L. Biological Activity of Human Mesenchymal Stromal Cells on Polymeric Electrospun Scaffolds. *Biomater Sci* **2019**, *7*, 1088, doi:10.1039/c8bm00693h.
410. Chi, H.Y.; Chan, V.; Li, C.; Hsieh, J.H.; Lin, P.H.; Tsai, Y.-H.; Chen, Y. Fabrication of Polylactic Acid/Paclitaxel Nano Fibers by Electrospinning for Cancer Therapeutics. *Chemistry (Easton)* **2020**, *14*, 63, doi:10.1186/s13065-020-00711-4.
411. Abadi, F.J.H.; Tehran, M.A.; Zamani, F.; Nematollahi, M.; Mobarakeh, L.G.; Nasr-Esfahani, M.H. Effect of Nanoporous Fibers on Growth and Proliferation of Cells on Electrospun Poly (ϵ -Caprolactone) Scaffolds. *International Journal of Polymeric Materials and Polymeric Biomaterials* **2013**, *63*, 57–64, doi:10.1080/00914037.2013.769248.
412. Bolbasov, E.; Goreninskii, S.; Tverdokhlebov, S.; Mishanin, A.; Viknianshchuk, A.; Bezuidenhout, D.; Golovkin, A. Comparative Study of the Physical, Topographical and Biological Properties of Electrospinning PCL, PLLA, Their Blend and Copolymer Scaffolds. *IOP Conf Ser Mater Sci Eng* **2018**, *350*, 012012, doi:10.1088/1757-899X/350/1/012012.
413. Ginzberg, M.B.; Kafri, R.; Kirschner, M. On Being the Right (Cell) Size. *Science (1979)* **2015**, *348*, doi:10.1126/SCIENCE.1245075/ASSET/6F6F0D07-A330-483B-BC8C-61053A5A3D20/ASSETS/GRAPHIC/348_1245075_FA.JPEG.
414. Habanjar, O.; Diab-Assaf, M.; Caldefie-Chezet, F.; Delort, L. 3D Cell Culture Systems: Tumor Application, Advantages, and Disadvantages. *Int J Mol Sci* **2021**, *22*, 12200, doi:10.3390/ijms222212200.
415. Lombardo, M.E.; Carfi Pavia, F.; Vitrano, I.; Gherzi, G.; Brucato, V.; Rosei, F.; la Carrubba, V. PLLA Scaffolds with Controlled Architecture as Potential Microenvironment for in Vitro Tumor Model. *Tissue Cell* **2019**, *58*, 33–41, doi:10.1016/J.TICE.2019.04.004.
416. Rijal, G.; Bathula, C.; Li, W. Application of Synthetic Polymeric Scaffolds in Breast Cancer 3D Tissue Cultures and Animal Tumor Models. *Int J Biomater* **2017**, *2017*, 8074890, doi:10.1155/2017/8074890.
417. Thiagarajan, P.S.; Zheng, Q.; Bhagrath, M.; Mulkearns-Hubert, E.E.; Myers, M.G.; Lathia, J.D.; Reizes, O. STAT3 Activation by Leptin Receptor Is Essential for TNBC Stem

- Cell Maintenance. *Endocr Relat Cancer* **2017**, *24*, 415–426, doi:10.1530/ERC-16-0349.
418. Ekert, J.E.; Johnson, K.; Strake, B.; Pardinias, J.; Jarantow, S.; Perkinson, R.; Colter, D.C. Three-Dimensional Lung Tumor Microenvironment Modulates Therapeutic Compound Responsiveness in Vitro--Implication for Drug Development. *PLoS One* **2014**, *9*, e92248, doi:10.1371/journal.pone.0092248.
419. Li, W.; Hu, X.; Wang, S.; Xing, Y.; Wang, H.; Nie, Y.; Liu, T.; Song, K. Multiple Comparisons of Three Different Sources of Biomaterials in the Application of Tumor Tissue Engineering in Vitro and in Vivo. *Int J Biol Macromol* **2019**, *130*, 166–176, doi:10.1016/J.IJBIOMAC.2019.02.136.
420. Enderami, S.E.; Kehtari, M.; Abazari, M.F.; Ghoraieian, P.; Nouri Aleagha, M.; Soleimanifar, F.; Soleimani, M.; Mortazavi, Y.; Nadri, S.; Mostafavi, H.; et al. Generation of Insulin-Producing Cells from Human Induced Pluripotent Stem Cells on PLLA/PVA Nanofiber Scaffold. *Artif Cells Nanomed Biotechnol* **2018**, *46*, 1062–1069, doi:10.1080/21691401.2018.1443466.
421. Fortelny, I.; Ujcic, A.; Fambri, L.; Slouf, M. Phase Structure, Compatibility, and Toughness of PLA/PCL Blends: A Review. *Front Mater* **2019**, *6*, 206, doi:10.3389/FMATS.2019.00206/BIBTEX.
422. Balgude, A.P.; Yu, X.; Szymanski, A.; Bellamkonda, R. v. Agarose Gel Stiffness Determines Rate of DRG Neurite Extension in 3D Cultures. *Biomaterials* **2001**, *22*, 1077–1084, doi:10.1016/S0142-9612(00)00350-1.
423. Thomas, C.H.; Collier, J.H.; Sfeir, C.S.; Healy, K.E. Engineering Gene Expression and Protein Synthesis by Modulation of Nuclear Shape. *Proc Natl Acad Sci U S A* **2002**, *99*, 1972–1977, doi:10.1073/pnas.032668799.
424. Vergani, L.; Grattarola, M.; Nicolini, C. Modifications of Chromatin Structure and Gene Expression Following Induced Alterations of Cellular Shape. *International Journal of Biochemistry and Cell Biology* **2004**, *36*, 1447–1461, doi:10.1016/j.biocel.2003.11.015.
425. Mohamed, A.; Gordon, S.H.; Biresaw, G. Polycaprolactone/Polystyrene Bioblends Characterized by Thermogravimetry, Modulated Differential Scanning Calorimetry and Infrared Photoacoustic Spectroscopy. *Polym Degrad Stab* **2007**, *92*, 1177–1185, doi:10.1016/j.polymdegradstab.2007.04.012.
426. Wang, Y.; Rodriguez-Perez, M.A.; Reis, R.L.; Mano, J.F. Thermal and Thermomechanical Behaviour of Polycaprolactone and Starch/Polycaprolactone Blends for Biomedical Applications. *Macromol Mater Eng* **2005**, *290*, 792–801, doi:10.1002/mame.200500003.

References

427. Singh, D.; Zo, S.M.; Kumar, A.; Han, S.S. Engineering Three-Dimensional Macroporous Hydroxyethyl Methacrylate- Alginate-Gelatin Cryogel for Growth and Proliferation of Lung Epithelial Cells. *J Biomater Sci Polym Ed* **2013**, *24*, 1343–1359, doi:10.1080/09205063.2012.759505.
428. Russo, P.; Acierno, D.; Corradi, A.; Leonelli, C. Dynamic-Mechanical Behavior and Morphology of Polystyrene/Perovskite Composites: Effects of Filler Size. In Proceedings of the Procedia Engineering; Elsevier Ltd, 2011; Vol. 10, pp. 1017–1022.
429. Qin, X.; Wu, D. Effect of Different Solvents on Poly(Caprolactone)(PCL) Electrospun Nonwoven Membranes. *J Therm Anal Calorim* **2012**, *107*, 1007–1013, doi:10.1007/s10973-011-1640-4.
430. Lawrence, B.J.; Madihally, S. v. Cell Colonization in Degradable 3D Porous Matrices. *Cell Adh Migr* **2008**, *2*, 9–16, doi:10.4161/cam.2.1.5884.
431. Chen, M.; Patra, P.K.; Warner, S.B.; Bhowmick, S. Role of Fiber Diameter in Adhesion and Proliferation of NIH 3T3 Fibroblast on Electrospun Polycaprolactone Scaffolds. *Tissue Eng* **2007**, *13*, 579–587, doi:10.1089/ten.2006.0205.
432. Horakova, J.; Klicova, M.; Erben, J.; Klapstova, A.; Novotny, V.; Behalek, L.; Chvojka, J. Impact of Various Sterilization and Disinfection Techniques on Electrospun Poly-ε-Caprolactone. **2020**, doi:10.1021/acsomega.0c00503.
433. Kumar, N.; Parajuli, O.; Gupta, A.; Hahm, J.I. Elucidation of Protein Adsorption Behavior on Polymeric Surfaces: Toward High-Density, High-Payload Protein Templates. *Langmuir* **2008**, *24*, 2688–2694, doi:10.1021/la7022456.
434. Nandakumar, A.; Tahmasebi Birgani, Z.; Santos, D.; Mentink, A.; Auffermann, N.; van der Werf, K.; Bennink, M.; Moroni, L.; van Blitterswijk, C.; Habibovic, P. Surface Modification of Electrospun Fibre Meshes by Oxygen Plasma for Bone Regeneration. *Biofabrication* **2013**, *5*, doi:10.1088/1758-5082/5/1/015006.
435. Santos, M.I.; Pashkuleva, I.; Alves, C.M.; Gomes, M.E.; Fuchs, S.; Unger, R.E.; Reis, R.L.; Kirkpatrick, C.J. Surface-Modified 3D Starch-Based Scaffold for Improved Endothelialization for Bone Tissue Engineering. *J Mater Chem* **2009**, *19*, 4091–4101, doi:10.1039/b819089e.
436. Du, W.; Ni, L.; Liu, B.; Wei, Y.; Lv, Y.; Qiang, S.; Dong, J.; Liu, X. Upregulation of SALL4 by EGFR Activation Regulates the Stemness of CD44-Positive Lung Cancer. *Oncogenesis* **2018**, *7*, doi:10.1038/s41389-018-0045-7.
437. Singh, S.; Trevino, J.; Bora-Singhal, N.; Coppola, D.; Haura, E.; Altiok, S.; Chellappan, S.P. EGFR/Src/Akt Signaling Modulates Sox2 Expression and Self-Renewal of Stem-like Side-Population Cells in Non-Small Cell Lung Cancer. *Mol Cancer* **2012**, *11*, doi:10.1186/1476-4598-11-73.

438. Goldstein, L.J.; Galski, H.; Fojo, A.; Willingham, M.; Lai, S.L.; Gazdar, A.; Pirker, R.; Green, A.; Crist, W.; Brodeur, G.M.; et al. Expression of Multidrug Resistance Gene in Human Cancers. *J Natl Cancer Inst* **1989**, *81*, 116–124, doi:10.1093/jnci/81.2.116.
439. Liu, B.; Guo, Z.; Dong, H.; Daofeng, T.; Cai, Q.; Ji, B.; Zhang, S.; Wu, L.; Wang, J.; Wang, L.; et al. LRIG1, Human EGFR Inhibitor, Reverses Multidrug Resistance through Modulation of ABCB1 and ABCG2. *Brain Res* **2015**, *1611*, 93–100, doi:10.1016/j.brainres.2015.03.023.
440. Byers, L.A.; Diao, L.; Wang, J.; Saintigny, P.; Girard, L.; Peyton, M.; Shen, L.; Fan, Y.; Giri, U.; Tumula, P.K.; et al. An Epithelial-Mesenchymal Transition Gene Signature Predicts Resistance to EGFR and PI3K Inhibitors and Identifies Axl as a Therapeutic Target for Overcoming EGFR Inhibitor Resistance. *Clin Cancer Res* **2013**, *19*, 279–290, doi:10.1158/1078-0432.CCR-12-1558.
441. Ye, X.; Tam, W.L.; Shibue, T.; Kaygusuz, Y.; Reinhardt, F.; Ng Eaton, E.; Weinberg, R.A. Distinct EMT Programs Control Normal Mammary Stem Cells and Tumour-Initiating Cells. *Nature* **2015**, *525*, 256–260, doi:10.1038/NATURE14897.
442. Singh, S.; Chellappan, S. Lung Cancer Stem Cells: Molecular Features and Therapeutic Targets. *Mol Aspects Med* **2014**, *39*, 50–60, doi:10.1016/j.mam.2013.08.003.
443. Kobayashi, I.; Takahashi, F.; Nurwidya, F.; Nara, T.; Hashimoto, M.; Murakami, A.; Yagishita, S.; Tajima, K.; Hidayat, M.; Shimada, N.; et al. Oct4 Plays a Crucial Role in the Maintenance of Gefitinib-Resistant Lung Cancer Stem Cells. *Biochem Biophys Res Commun* **2016**, *473*, 125–132, doi:10.1016/J.BBRC.2016.03.064.
444. Guo, L.; Sun, C.; Xu, S.; Xu, Y.; Dong, Q.; Zhang, L.; Li, W.; Wang, X.; Ying, G.; Guo, F. Knockdown of Long Non-Coding RNA Linc-ITGB1 Inhibits Cancer Stemness and Epithelial-Mesenchymal Transition by Reducing the Expression of Snail in Non-Small Cell Lung Cancer. *Thorac Cancer* **2019**, *10*, 128–136, doi:10.1111/1759-7714.12911.
445. Li, H.; Yue, D.; Jin, J.Q.; Woodard, G.A.; Tolani, B.; Luh, T.M.; Giroux-Leprieur, E.; Mo, M.; Chen, Z.; Che, J.; et al. Gli Promotes Epithelial-Mesenchymal Transition in Human Lung Adenocarcinomas. *Oncotarget* **2016**, *7*, 80415–80425, doi:10.18632/oncotarget.11246.
446. della Corte, C.M.; Malapelle, U.; Vigliar, E.; Pepe, F.; Troncione, G.; Ciaramella, V.; Troiani, T.; Martinelli, E.; Belli, V.; Ciardiello, F.; et al. Efficacy of Continuous EGFR-Inhibition and Role of Hedgehog in EGFR Acquired Resistance in Human Lung Cancer Cells with Activating Mutation of EGFR. *Oncotarget* **2017**, *8*, 23020–23032, doi:10.18632/oncotarget.15479.
447. Bora-Singhal, N.; Perumal, D.; Nguyen, J.; Chellappan, S. Gli1-Mediated Regulation of Sox2 Facilitates Self-Renewal of Stem-Like Cells and Confers Resistance to EGFR

References

- Inhibitors in Non-Small Cell Lung Cancer. *Neoplasia (United States)* **2015**, *17*, 538–551, doi:10.1016/j.neo.2015.07.001.
448. Gomez-Casal, R.; Bhattacharya, C.; Ganesh, N.; Bailey, L.; Basse, P.; Gibson, M.; Epperly, M.; Levina, V. Non-Small Cell Lung Cancer Cells Survived Ionizing Radiation Treatment Display Cancer Stem Cell and Epithelial-Mesenchymal Transition Phenotypes. *Mol Cancer* **2013**, *12*, doi:10.1186/1476-4598-12-94.
449. Zhang, Y.; Xu, W.; Guo, H.; Zhang, Y.; He, Y.; Lee, S.H.; Song, X.; Li, X.; Guo, Y.; Zhao, Y.; et al. NOTCH1 Signaling Regulates Self-Renewal and Platinum Chemoresistance of Cancer Stem-like Cells in Human Non-Small Cell Lung Cancer. *Cancer Res* **2017**, *77*, 3082–3091, doi:10.1158/0008-5472.CAN-16-1633.
450. Meng, X.; Wang, X.; Wang, Y. More than 45% of A549 and H446 Cells Are Cancer Initiating Cells: Evidence from Cloning and Tumorigenic Analyses. *Oncol Rep* **2009**, *21*, 995–1000, doi:10.3892/or_00000314.
451. Alama, A.; Gangemi, R.; Ferrini, S.; Barisione, G.; Orengo, A.M.; Truini, M.; Bello, M.G.D.; Grossi, F. CD133-Positive Cells from Non-Small Cell Lung Cancer Show Distinct Sensitivity to Cisplatin and Afatinib. *Arch Immunol Ther Exp (Warsz)* **2015**, *63*, 207–214, doi:10.1007/s00005-015-0330-5.
452. Teocharoen, R.; Ruangritchankul, K.; Vinayanuwattikun, C.; Sriuranpong, V.; Sitthideatphaiboon, P. Vimentin Expression Status Is a Potential Biomarker for Brain Metastasis Development in EGFR-Mutant NSCLC Patients. *Transl Lung Cancer Res* **2021**, *10*, 790–801, doi:10.21037/tlcr-20-1020.
453. Richardson, F.; Young, G.D.; Sennello, R.; Wolf, J.; Argast, G.M.; Mercado, P.; Davies, A.; Epstein, D.M.; Wacker, B. The Evaluation of E-Cadherin and Vimentin as Biomarkers of Clinical Outcomes Among Patients with Non-Small Cell Lung Cancer Treated with Erlotinib as Second- or Third-Line Therapy. *Anticancer Res* **2012**, *32*, 537–552.
454. Janikova, M.; Skarda, J.; Dziechciarkova, M.; Radova, L.; Chmelova, J.; Krejci, V.; Sedlakova, E.; Zapletalova, J.; Langova, K.; Klein, J.; et al. *Identification of CD133+/Nestin+ Putative Cancer Stem Cells in Non-Small Cell Lung Cancer*; 2010; Vol. 154;.
455. Herpel, E.; Jensen, K.; Muley, T.; Warth, A.; Schnabel, P.A.; Meister, M.; Herth, F.J.F.; Dienemann, H.; Thomas, M.; Gottschling, S. The Cancer Stem Cell Antigens CD133, BCRP1/ABCG2 and CD117/c-KIT Are Not Associated with Prognosis in Resected Early-Stage Non-Small Cell Lung Cancer. *Anticancer Res* **2011**, *31*, 4491–4500.
456. Okudela, K.; Woo, T.; Mitsui, H.; Tajiri, M.; Masuda, M.; Ohashi, K. Expression of the Potential Cancer Stem Cell Markers, CD133, CD44, ALDH1, and β -Catenin, in Primary

- Lung Adenocarcinoma-Their Prognostic Significance. *Pathol Int* **2012**, *62*, 792–801, doi:10.1111/pin.12019.
457. Mizugaki, H.; Sakakibara-Konishi, J.; Kikuchi, J.; Moriya, J.; Hatanaka, K.C.; Kikuchi, E.; Kinoshita, I.; Oizumi, S.; Dosaka-Akita, H.; Matsuno, Y.; et al. CD133 Expression: A Potential Prognostic Marker for Non-Small Cell Lung Cancers. *Int J Clin Oncol* **2014**, *19*, 254–259, doi:10.1007/s10147-013-0541-x.
458. Bueno, M.J.; Jimenez-Renard, V.; Samino, S.; Capellades, J.; Junza, A.; López-Rodríguez, M.L.; Garcia-Carceles, J.; Lopez-Fabuel, I.; Bolaños, J.P.; Chandel, N.S.; et al. Essentiality of Fatty Acid Synthase in the 2D to Anchorage-Independent Growth Transition in Transforming Cells. *Nat Commun* **2019**, *10*, doi:10.1038/S41467-019-13028-1.
459. Ventura, R.; Mordec, K.; Waszczuk, J.; Wang, Z.; Lai, J.; Fridlib, M.; Buckley, D.; Kemble, G.; Heuer, T.S. Inhibition of de Novo Palmitate Synthesis by Fatty Acid Synthase Induces Apoptosis in Tumor Cells by Remodeling Cell Membranes, Inhibiting Signaling Pathways, and Reprogramming Gene Expression. *EBioMedicine* **2015**, *2*, 808, doi:10.1016/J.EBIOM.2015.06.020.
460. Schroeder, B.; vander Steen, T.; Espinoza, I.; Venkatapoorna, C.M.K.; Hu, Z.; Silva, F.M.; Regan, K.; Cuyàs, E.; Meng, X.W.; Verdura, S.; et al. Fatty Acid Synthase (FASN) Regulates the Mitochondrial Priming of Cancer Cells. *Cell Death Dis* **2021**, *12*, doi:10.1038/S41419-021-04262-X.
461. Youngblood, V.M.; Kim, L.C.; Edwards, D.N.; Hwang, Y.; Santapuram, P.R.; Stirdivant, S.M.; Lu, P.; Ye, F.; Brantley-Sieders, D.M.; Chen, J. The Ephrin-A1/EPHA2 Signaling Axis Regulates Glutamine Metabolism in HER2-Positive Breast Cancer. *Cancer Res* **2016**, *76*, 1825, doi:10.1158/0008-5472.CAN-15-0847.
462. Luo, H.; Yang, A.; Schulte, B.A.; Wargovich, M.J.; Wang, G.Y. Resveratrol Induces Premature Senescence in Lung Cancer Cells via ROS-Mediated DNA Damage. *PLoS One* **2013**, *8*, doi:10.1371/JOURNAL.PONE.0060065.
463. Sankaranarayananpillai, M.; Zhang, N.; Baggerly, K.A.; Gelovani, J.G. Metabolic Shifts Induced by Fatty Acid Synthase Inhibitor Orlistat in Non-Small Cell Lung Carcinoma Cells Provide Novel Pharmacodynamic Biomarkers for Positron Emission Tomography and Magnetic Resonance Spectroscopy. *Mol Imaging Biol* **2013**, *15*, 136–147, doi:10.1007/S11307-012-0587-6.
464. Colomer, R.; Sarrats, A.; Lupu, R.; Puig, T. Natural Polyphenols and Their Synthetic Analogs as Emerging Anticancer Agents. *Curr Drug Targets* **2017**, *18*, 147–159, doi:10.2174/1389450117666160112113930.

References

465. Ma, Y.C.; Li, C.; Gao, F.; Xu, Y.; Jiang, Z. bin; Liu, J.X.; Jin, L.Y. Epigallocatechin Gallate Inhibits the Growth of Human Lung Cancer by Directly Targeting the EGFR Signaling Pathway. *Oncol Rep* **2014**, *31*, 1343–1349, doi:10.3892/or.2013.2933.
466. Jin, G.; Yang, Y.; Liu, K.; Zhao, J.; Chen, X.; Liu, H.; Bai, R.; Li, X.; Jiang, Y.; Zhang, X.; et al. Combination Curcumin and (-)-Epigallocatechin-3-Gallate Inhibits Colorectal Carcinoma Microenvironment-Induced Angiogenesis by JAK/STAT3/IL-8 Pathway. *Oncogenesis* **2017**, *6*, e384–e384, doi:10.1038/oncsis.2017.84.
467. Tang, S.N.; Fu, J.; Shankar, S.; Srivastava, R.K. EGCG Enhances the Therapeutic Potential of Gemcitabine and CP690550 by Inhibiting STAT3 Signaling Pathway in Human Pancreatic Cancer. *PLoS One* **2012**, *7*, e31067, doi:10.1371/JOURNAL.PONE.0031067.
468. Lin, H.Y.; Hou, S.C.; Chen, S.C.; Kao, M.C.; Yu, C.C.; Funayama, S.; Ho, C.T.; Way, T. der (-)-Epigallocatechin Gallate Induces Fas/CD95-Mediated Apoptosis through Inhibiting Constitutive and IL-6-Induced JAK/STAT3 Signaling in Head and Neck Squamous Cell Carcinoma Cells. *J Agric Food Chem* **2012**, *60*, 2480–2489, doi:10.1021/JF204362N.
469. Kim, K.C.; Lee, C. Reversal of Cisplatin Resistance by Epigallocatechin Gallate Is Mediated by Downregulation of Axl and Tyro 3 Expression in Human Lung Cancer Cells. *Korean J Physiol Pharmacol* **2014**, *18*, 61–66, doi:10.4196/KJPP.2014.18.1.61.
470. Menendez, J.A.; Lupu, R. Fatty Acid Synthase: A Druggable Driver of Breast Cancer Brain Metastasis. *Expert Opin Ther Targets* **2022**, *26*, 427–444, doi:10.1080/14728222.2022.2077189.
471. Chang, L.; Fang, S.; Chen, Y.; Yang, Z.; Yuan, Y.; Zhang, J.; Ye, L.; Gu, W. Inhibition of FASN Suppresses the Malignant Biological Behavior of Non-Small Cell Lung Cancer Cells via Dereglulating Glucose Metabolism and AKT/ERK Pathway. *Lipids Health Dis* **2019**, *18*, 118, doi:10.1186/S12944-019-1058-8.
472. Geng, Y.; Zhou, Y.; Wu, S.; Hu, Y.; Lin, K.; Wang, Y.; Zheng, Z.; Wu, W. Sulforaphane Induced Apoptosis via Promotion of Mitochondrial Fusion and ERK1/2-Mediated 26S Proteasome Degradation of Novel Pro-Survival Bim and Upregulation of Bax in Human Non-Small Cell Lung Cancer Cells. *J Cancer* **2017**, *8*, 2456, doi:10.7150/JCA.19383.
473. Wu, X.; Qin, L.; Fako, V.; Zhang, J.T. Molecular Mechanisms of Fatty Acid Synthase (FASN)-Mediated Resistance to Anti-Cancer Treatments. *Adv Biol Regul* **2014**, *54*, 214–221, doi:10.1016/j.jbior.2013.09.004.
474. Cao, K.; Pan, Y.; Yu, L.; Shu, X.; Yang, J.; Sun, L.; Sun, L.; Yang, Z.; Ran, Y. Monoclonal Antibodies Targeting Non-Small Cell Lung Cancer Stem-like Cells by Multipotent

- Cancer Stem Cell Monoclonal Antibody Library. *Int J Oncol* **2017**, *50*, 587–596, doi:10.3892/IJO.2016.3818.
475. Zhang, M.; Tan, S.; Yu, D.; Zhao, Z.; Zhang, B.; Zhang, P.; Lv, C.; Zhou, Q.; Cao, Z. Triptonide Inhibits Lung Cancer Cell Tumorigenicity by Selectively Attenuating the Shh-Gli1 Signaling Pathway. *Toxicol Appl Pharmacol* **2019**, *365*, 1–8, doi:10.1016/J.TAAP.2019.01.002.
476. Orita, H.; Coulter, J.; Tully, E.; Kuhajda, F.P.; Gabrielson, E. Inhibiting Fatty Acid Synthase for Chemoprevention of Chemically Induced Lung Tumors. *Clinical Cancer Research* **2008**, *14*, 2458–2464, doi:10.1158/1078-0432.CCR-07-4177.
477. Bollu, L.R.; Katreddy, R.R.; Blessing, A.M.; Pham, N.; Zheng, B.; Wu, X.; Weihua, Z. Intracellular Activation of EGFR by Fatty Acid Synthase Dependent Palmitoylation. *Oncotarget* **2015**, *6*, 34992–35003, doi:10.18632/oncotarget.5252.